

Saccadic suppression by way of retinal image processing

Dissertation

zur Erlangung des Grades eines
Doktors der Naturwissenschaften

der Mathematisch-Naturwissenschaftlichen Fakultät

und

der Medizinischen Fakultät

der Eberhard-Karls-Universität Tübingen

vorgelegt

von

Saad Idrees

aus Lahore, Pakistan

September 2020

Tag der mündlichen Prüfung:23.11.2020.....

Stellv. Dekan der Math.-Nat. Fakultät: Prof. Dr. J. Fortágh

Dekan der Medizinischen Fakultät: Prof. Dr. B. Pichler

1. Berichterstatter: Prof. Dr. Ziad M. Hafed

2. Berichterstatter: Prof. Dr. Frank Schaeffel

Prüfungskommission: Prof. Dr. Ziad M. Hafed

Prof. Dr. Frank Schaeffel

Prof. Dr. Thomas Euler

Dr. Felix Franke

Erklärung / Declaration:

Ich erkläre, dass ich die zur Promotion eingereichte Arbeit mit dem Titel:

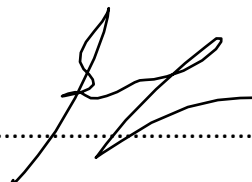
„Saccadic suppression by way of retinal image processing“

selbständig verfasst, nur die angegebenen Quellen und Hilfsmittel benutzt und wörtlich oder inhaltlich übernommene Stellen als solche gekennzeichnet habe. Ich versichere an Eides statt, dass diese Angaben wahr sind und dass ich nichts verschwiegen habe. Mir ist bekannt, dass die falsche Abgabe einer Versicherung an Eides statt mit Freiheitsstrafe bis zu drei Jahren oder mit Geldstrafe bestraft wird.

I hereby declare that I have produced the work entitled “Saccadic suppression by way of retinal image processing”, submitted for the award of a doctorate, on my own (without external help), have used only the sources and aids indicated and have marked passages included from other works, whether verbatim or in content, as such. I swear upon oath that these statements are true and that I have not concealed anything. I am aware that making a false declaration under oath is punishable by a term of imprisonment of up to three years or by a fine.

Tübingen, den02.12.2020.....

Datum



Unterschrift

**In the name of God
the Compassionate and Merciful**

Abstract

Humans make eye movements such as saccades four times every second. Saccades disrupt the visual flow on the retina; however, visual perception remains a stable and coherent process. This is a striking achievement of the visual system. Visual stability around the time of these eye movements is partially associated with a reduction in visual sensitivity, a phenomenon known as saccadic suppression. While saccadic suppression has been extensively characterized at the perceptual and neural levels, its underlying mechanisms remain elusive. According to the favored view, eye-movement related signals play a central role in the genesis of saccadic suppression. Despite extensive efforts to substantiate these claims, the neural origin of such signals has not been established.

In this dissertation, we challenge the dominant view that saccadic suppression is triggered by eye-movement related signals. Instead, using electrophysiology in mouse, pig, and macaque retina, 2-photon calcium imaging, computational modeling, and human psychophysics we show evidence that visual mechanisms starting at the retina account for perceptual saccadic suppression. Cellular and circuit level descriptions of these retinal mechanisms are presented in detail. Most notably, we find a novel retinal processing motif underlying retinal saccadic suppression, “dynamic reversal suppression”, which is triggered by sequential stimuli containing contrast reversals. This motif does not involve inhibition but relies on nonlinear transformation of the inherently slow responses of cone photoreceptors by downstream retinal pathways.

We also found that eye-movement related signals act to shorten the suppression resulting from visual mechanisms - a diametrically opposite involvement of eye movement signals than proposed in the literature.

Overall, our results establish a neural locus of saccadic suppression, and provide detailed mechanistic insights underlying it. These findings resolve a long-standing open question concerning the origin of saccadic suppression. Given that the retinal saccadic suppression is triggered by sequential visual stimulation, our results also describe retinal processing of dynamic stimuli.

Contents

Introduction	1
General organization of the visual system.....	1
The retina	3
Visual processing under dynamic conditions of natural vision.....	6
Mechanisms of saccadic suppression – past state of the art	7
Aim of the thesis	11
Key findings.....	12
Visual mechanisms alone can account for perceptual saccadic suppression.....	12
Saccadic suppression starts in the retina.....	13
Saccadic suppression is triggered by interactions between sequential stimuli	14
Mechanisms underlying retinal saccadic suppression	15
Retinal saccadic suppression in other animal models	16
Discussion	18
Summary of key findings.....	18
Retrospective analysis of the evidence supporting saccadic suppression by eye movement related signals	19
Does perceptual saccadic suppression in humans start in the retina?	21
Why does saccadic suppression occur?	22
Saccadic suppression, visual masking or neural adaptation?	23
Visual mechanisms of suppression downstream of the retina.....	24
Variability in retinal suppression.....	24
Implications for retinal signal processing.....	25
Role of global and surround components of retinal suppression in perceptual saccadic suppression	26
Scientific and technological impacts.....	28
References	29
List of publications and statement of contributions.....	39
Chapter 1	41
Chapter 2	74
Acknowledgements	167

Introduction

In natural vision, the flow of images across the retina is dominated by the consequences of ballistic eye movements called saccades. However, our visual perception is stable, with these frequent image shifts being discounted. Attempts to explain perceptual stability in the face of constant eye movements can be traced back to the 11th century, when mathematician and physicist Ibn al-Haytham¹ (Alhazen) suggested that our “sight” becomes accustomed to external world motion caused by eye movements. Later in the 19th century, Hermann von Helmholtz suggested the existence of an active brain mechanism warranting perceptual stability². Towards the end of the 19th century, Erdmann and Dodge reported failure in visual perception during eye movements^{3,4}, which was later termed “saccadic suppression”. In 1950, Sperry proposed that a copy of the eye movement motor command signal, a “corollary discharge”⁵, may modulate visual perception. From there on, saccadic suppression and other phenomena⁶ that are thought to contribute towards perceptual stability around the time of saccades, have been associated with such eye movement related signals. An assumption with intuitive appeal is that the “purpose” or “function” of suppression is to reduce vision disruption caused by rapid image-shifts across the retina. Irrespective of the specific mechanisms alluded, this suppression is described as an active phenomenon of central origin triggered around the time of saccades. Here, I challenge this dominant view by offering psychophysical and neurophysiological evidence that the perceptual suppression usually characterized as ‘saccadic’ results from image processing, starting already in the retina. I present mouse, pig, macaque and human data showing that these conclusions hold true across animal species. A general review of basic visual processing and retinal neurophysiology, given below, may be relevant to contextualize these findings.

General organization of the visual system

As you stare at a scene, the light reflected off different objects is guided by the optics of your eye, and focused to form an image on your retina – a thin neural structure at the back of the eye. The light focused onto the retina is captured by photoreceptors, the sensory cells of the retina. Photoreceptors transduce photons into electrical signals. Downstream, a network of

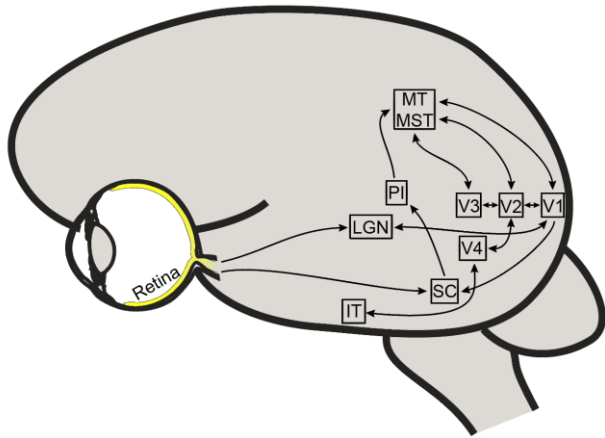


Figure 1. Schematic showing some of the key visual pathways in the brain. Retinal output is relayed to primary visual cortex (V1) via the lateral geniculate nucleus (LGN). Superior colliculus (SC) also receives input directly from the retina. SC superficial layers (visual) project to medial temporal (MT) and medial superior temporal (MST) regions of the visual pathway via the inferior pulvinar (PI). MT and MST also receive projections from other areas of the visual cortex, including V1, V2 and V3. V2 projects to V4 and from there to the inferior temporal cortex (IT) for processing complex visual features.

interneurons processes the transduced signals to extract multiple visual features, such as edges and color. These visual features, encoded in electrical signals, are carried to downstream brain areas by axons of ganglion cells, the output cells of the retina. In the brain, visual features go through organized levels of processing implemented in different areas to form perception of the scene you are looking at.

Two key brain areas receiving direct input signals from the retina are the lateral geniculate nucleus (LGN) in the thalamus and the superior colliculus (SC).

Traditionally, LGN was considered simply as a relay structure between the retina and the primary visual cortex (**Figure 1**). However, LGN has been recently shown to pre-process visual information before sending it to the primary visual cortex (V1). Specifically, LGN adjusts the gain and increases the signal-to-noise ratio of the retinal output while preserving the extracted visual features⁷. LGN output is sent to V1 and subsequently undergoes further processing in different brain areas. The entire visual system is organized as a layered topology, where higher levels combine information from lower levels to form complex features: from V1 neurons, encoding edges and orientation, to moderately complex features in the intermediate areas (such as contours), to complex features, such as faces, in higher visual areas like the inferior temporal cortex⁸⁻¹⁰. This functional hierarchical architecture is a hallmark of the organization of the visual system¹⁰⁻¹³.

The superior colliculus (SC) is a subcortical structure situated just below the thalamus (**Figure 1**). The superficial layers of the SC receive input from over 30 parallel visual feature streams in the

retina¹⁴, while deep layers receive input from other sensory modalities¹⁵. A population of motor neurons involved in generation of eye movements¹⁶, is also found in deep layers. The SC plays an important role in directing behavior by integrating information from different sensory modalities. For example, the SC likely alters the kinematics of eye movements according to the ongoing visual input^{17,18}.

The retina

Light is first captured by the photoreceptors. The photoreceptors are the visual sensory transducers, or light sensors, of the visual system. Two classes of photoreceptors, tuned to different visual properties, are present in a mammalian retina – rods and cones. Rods account for nearly 97% of the photoreceptors in the mouse retina¹⁹. Being able to detect single photons, they enable vision at very dim lights. They respond maximally to light with 508 nm wavelength. However, rods provide very poor spatial resolution. Cones, on the other hand, reliably encode information at brighter light levels despite a more noise membrane voltage. In the mouse retina, S- and M- cone pigments show maximal spectral sensitivity at 360 and 508 nm, respectively. The different response properties of rods and cones mainly arise from important differences in their phototransduction cascade. Since rods lose sensitivity in bright light, they were thought to contribute to vision only in low light conditions. A recent study from our lab, to which I have contributed, showed that rods progressively recover from saturation, enabling them to encode visual stimuli at arbitrarily bright light levels²⁰.

The retina is not merely an image sensor, but is also an image processor²¹. Different interneuron types arranged in layers (**Figure II**) simultaneously extract multiple features from a scene. Encoded features include edges, color and contrast, which are required by other visual and non-visual brain areas to construct a visual percept of the world.

Throughout the day, the amount of light falling on the photoreceptors gradually change by several orders of magnitude. More sudden changes occur when we move our eyes from a dark patch in a scene to a brighter patch. This wide operating range of the retina is partly achieved by the horizontal cells, that feedback onto the photoreceptors. Having a wide lateral spread,

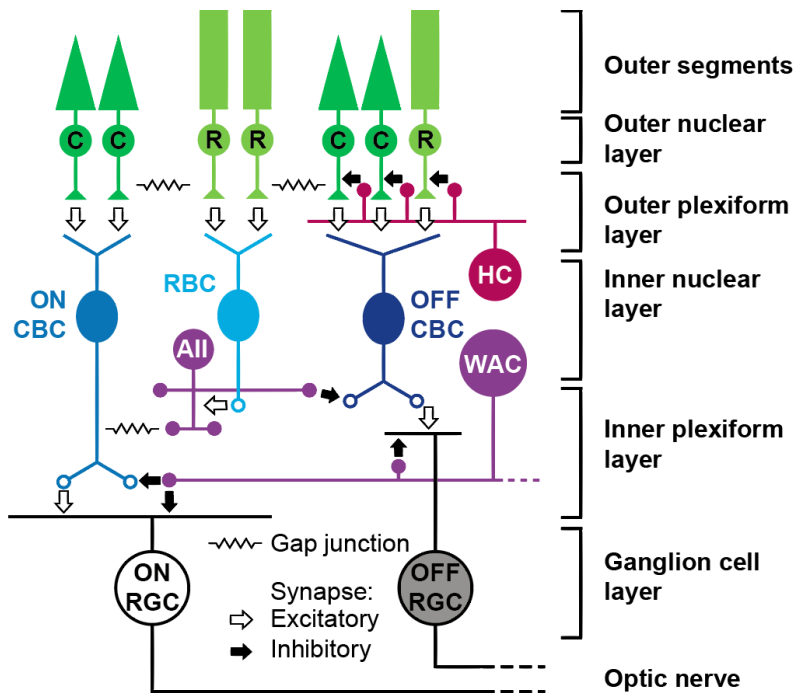


Figure II. Schematic of the retina showing the different cell classes and the typical signaling pathways. The direct central feedforward pathway is via cone (C) → cone bipolar cell (CBC) → retinal ganglion cell (RGC). Rods (R) also use this pathway by transmitting to cones via gap junctions. Another rod signaling pathway is via the rod bipolar cell (RBC) which connects to the narrow-field amacrine cell (All). From here the signal is transmitted to ON CBC → ON RGC via gap junction or to OFF CBC → OFF RGC via inhibitory synapse. Horizontal cells (HC) provide lateral inhibition to photoreceptors. Wide-field amacrine cells (WAC) provide lateral inhibition to bipolar cells or to ganglion cells directly.

horizontal cells measure the average light level falling on to the retina. A proportionate value to this average is then fed back to the photoreceptors, thus dynamically maintaining their output within an operating range. Horizontal cells also play an important role in shaping retinal circuit responses by modulating the cone²².

The photoreceptors contact different types of bipolar cells. There are at least 13 distinct bipolar cell types in the mouse retina²³. Distinct bipolar cell types differ in their morphology, the set of photoreceptors types they contact, the spatial extent of their dendritic fields, the types of glutamate receptors expressed on the dendrites and the distribution of ion channels²⁴. Functionally, these factors give rise to distinct parallel signal-processing streams, kick-starting the simultaneous extraction of multiple features at the very first synapse of the visual system. Bipolar cells can be broadly categorized into ON and the OFF types, respectively signaling increment and decrement of light intensities within the span of their dendritic fields. The expression of different glutamate receptors differentiates bipolar cell types: ON bipolar cell dendrites express metabotropic receptors, while OFF bipolar cell dendrites express ionotropic receptors. The temporal response profiles of bipolar cells are governed by two broad properties: the inactivation

kinetics of their specific glutamate receptors; and the inhibitory network in which they are embedded. This further splits the ON and OFF types into several subtypes. For example, transient bipolar cells have fast response kinetics and therefore can detect instantaneous changes in light across photoreceptors. In contrast, sustained bipolar cells with slower response kinetics encode more steady changes in light across photoreceptors. In short, different molecular makeup confers how the different bipolar cell types derive different light responses. In addition, their output is influenced by the amacrine cells connecting to them. Consequently, the output of bipolar cells feeding into the ganglion cells already includes the effects of these amacrine cells.

Amacrine cells are a class of inhibitory interneurons in the retina. They are perhaps the most complex retinal cell class, owing to their great structural diversity and complex processing capabilities. Morphologically, there are at least 40 different types of amacrine cells²⁵. Amacrine cells receive inputs from different bipolar parallel streams to compute simple and complex image features. Narrow-field amacrine cells typically perform local computation, often integrating information from different bipolar cells, whereas wide-field amacrine cells, whose processes can extend over 1mm on the retinal surface, are involved in more global computations. In addition to providing inhibition to bipolar cells, amacrine cells also directly connect to ganglion cells and other amacrine cells. Together, amacrine cells are part of intricate circuits that include feedforward and feedback inhibition, often serially stacked or recurrent, that can compute complex functions like detecting motion^{26,27}, motion direction^{28,29}, approach³⁰, and signaling peripheral changes³¹⁻³⁴.

Retinal ganglion cells (RGCs), the output cells of the retina, transmit the extracted visual information to downstream brain areas. While most cells in the retina encode the information with graded potentials, RGCs transmit information as action potentials, commonly known as spikes. RGCs inherit functional differences from the synaptic networks prior to it. The synaptic inputs are notably shaped by the intrinsic properties of specific ganglion cells³⁵, generating further variability in stimulus responses. In the end, there are over 32 functionally distinct ganglion cell types³⁶, each encoding a unique image feature in spikes and transmitting it via axons

to higher visual areas. Ganglion cells of each type cover the entire retina surface evenly, ensuring that every point is spatially sampled at least once by each type of ganglion cell.

In summary, from every region of a scene, the retina extracts more than 32 features that are sent to downstream visual areas for further processing.

Visual processing under dynamic conditions of natural vision

When you move your eyes to fixate on a new position in the visual scene, a new image is projected onto the retina. Interestingly, our visual perception is not blurred by the rapid-image shifts the retina experiences during eye movement, unlike a blurred image captured by a camera that shook while its shutter remained open. Feature extraction by the retina, and processing of the retinal output by downstream visual areas, somehow combine to create an effortless visual perception of the new scene.

Maintaining perceptual visual stability during dynamic conditions of natural vision, such as with eye movements or changes in ambient luminance, is a striking achievement of our visual system. The retina already compensates for some dynamic changes in its input, thereby enabling stable signaling to higher visual areas. At the same time, other changes in the environment, for example moderate alteration of ambient brightness, can lead to altered signaling from the retina to the brain³⁷. In short, our visual system is also highly dynamic, with different areas working in tandem with each other, to produce a stable visual percept across dynamic conditions.

Eye movements such as saccades are a prominent behavior of natural vision. On the one hand, saccades are important for efficiently sampling the visual world^{38–40}, especially in species where high visual resolution is limited to a small fraction of the overall visual space, such as the foveal region in primates. On the other hand, these ballistic eye movements cause rapid image shifts across the retina that could potentially lead to disruptive visual experience. Yet, we do not experience disrupted vision. This is because in our visual perception, these disruptive epochs are curtailed by reducing the sensitivity of the visual system around the time of saccades – a phenomenon known as **saccadic suppression**.

While saccadic suppression has been extensively characterized, its underlying mechanisms remain unknown. The core theme of my doctoral work is to understand the mechanisms of saccadic suppression. In the following section I review what was known about these mechanisms prior to my contributions.

Mechanisms of saccadic suppression – past state of the art

Suppression of our visual sensitivity starts ~50 ms prior to saccade onset and lasts for up to ~100 ms after it. At a perceptual level, this phenomenon has been characterized in great detail^{4,41–45}. However, its neural origins and the underlying mechanisms are not clear. Two opposing (but not necessarily exclusive) views have been proposed in the literature concerning the neural origins of saccadic suppression: active suppression triggered by eye-movement related signals; or suppression caused by visual mechanisms.

According to the first and dominant view, saccadic suppression is driven by some sort of internal knowledge of the planned eye movements. The involvement of eye movement related signals are a necessary prerequisite in this view^{41,46–49}. Specifically, a corollary discharge from (pre-) motor areas may directly or indirectly inhibit visual neurons and ultimately cause perceptual suppression. Several studies characterized the influence of eye movements on neural activity in different visual areas. In these experiments, saccadic suppression was observed as a reduction in neuronal responses to a test stimulus, like a flash, presented at different times relative to saccades. In an attempt to eliminate visual input during saccades, these experiments were typically made while the subject (usually a monkey) made saccades across a dark or a uniform background, on which also the test flashes were presented. The observed suppression of neural activity around saccades has been solely attributed to eye movement related signals in particular since suppression precedes the saccade. Early visual areas like the V1, have shown only weak suppression of neural responses around the time of saccades⁵⁰. In general, there is little evidence that suppression by an eye movement related signal occurs in the LGN-V1 pathway⁶. In fact, most studies reported enhanced activity in V1^{50,51} around the time of saccades. In higher visual cortical areas, on the other hand, like the medial temporal (MT) and medial superior temporal (MST) (**Figure I**), robust and strong suppression has been observed^{52,53}, which

is inherited from suppressed activity observed in superficial layers (visual) of the SC^{54–56}. Neurons in the deeper layers of SC, which are active immediately before saccade onset, could in principle provide the corollary discharge signal that suppresses the activity in the superficial layers of the SC⁵⁴. Hence, in the context of eye-movement triggered suppression, SC has been proposed as the most probable origin of saccadic suppression.

Visual mechanisms constitute the second proposed origin of saccadic suppression in the literature. This view is supported by the observation that a first stimulus can suppress response to a subsequent visual stimulus presented in close temporal proximity. This phenomenon, where response to a stimulus is suppressed or “masked” by another stimulus, is generally referred to as visual masking^{57–65}. While a direct link between visual masking and saccadic suppression has not been proved, the parallels between the two suppressive phenomena^{6,59–62,65–67}, suggest that there could be common underlying visual mechanisms. Unlike suppression by an eye-movement related signal, visual masking was observed in areas as early as the LGN⁶⁸ and V1^{69,70}. Visual masking can occur in two ways: forward visual masking whereby a first stimulus suppresses the response to a second stimulus, as described above; and backwards masking in which a second stimulus suppresses the response to a first stimulus. While both masking types have been characterized in great detail⁷¹, the precise underlying mechanisms remain elusive. A computational model⁷² proposes that forward masking occurs through feedforward processes. Here, the response to the second stimulus is caused by inhibition triggered by the first stimulus, either through center-surround antagonism in early visual areas or through long-lasting cortical inhibition⁷². The proposed mechanism underlying backward masking can be summarized as follows. The first stimulus elicits a response in V1 neurons that is purely stimulus driven, the stimulus-response. But there is also an after-response to the same stimulus, with a short latency after the stimulus-response. A second stimulus, presented just after the first one, suppresses the after-response of the first stimulus. Suppression of the after-response correlates with a lack of perception of the first stimulus⁶⁹, suggesting that both the stimulus-response and the after-response are necessary for conscious visual perception. The after-response appears to be generated by a cascade of reverberating loops of cortical activity, where a visual stimulus triggers a feedforward response (the stimulus-response) that passes through different cortical levels of

processing (V1, V2, V4 ...). Each level sends back a feedback signal (the after-response) to the prior area from which it received the feedforward signal⁷³. A suppression of this feedback signal, potentially by the stimulus-response of the second stimulus, would result in the suppression or “disappearance” of the after-response of the first stimulus which is correlated with its visibility or perceptual awareness. Such suppression has been narrowed down to occur in pathways between V1 and the fusiform gyrus⁷⁴, with strong indications that it occurs beyond V1/V2⁷⁵.

There have been suggestions of hybrid mechanisms in which saccades are detected as “visual events” by the retina and signaled to downstream visual areas for subsequent saccadic processing, including suppression. This suggestion was mainly based on cat optic tract recordings where a class of ganglion cells responded transiently to eye movements across a grating pattern⁷⁶. Another study⁷⁷ in tiger salamander retina reported that certain OFF-type retinal ganglion cells switch their polarity to ON-type after rapid-saccade like visual changes. The resulting brief balance in the number of ON-type and OFF-type ganglion cells, in the otherwise OFF-type biased salamander retina, is speculated to be important for signaling saccade-related changes to downstream visual areas. Several studies have reported modulation of ganglion cell activity during rapid saccade-like visual changes across the retina, which may or may not contribute towards saccadic suppression. For example, some ganglion cell types show suppressed responses to rapid saccade-like image shifts²⁷ or to visual changes in their periphery^{34,78–80}. Other ganglion cell types are sensitized following rapid global visual changes^{81,82}, and yet other types signal image recurrence across saccades⁸³. While these and several other studies^{26,28,30,32,37,84–86} have investigated retinal processing in the context of spatio-temporal visual dynamics that naturally occur during saccades, a direct retinal neural correlate of perceptual saccadic suppression was never observed or rather never investigated in a manner congruent with investigations in higher visual areas or perception.

Despite the parallels between saccadic suppression caused by eye movement related signals and by visual mechanisms^{6,59–62,65–67}, the view that saccadic suppression is caused by eye movement related signals dominates the literature. This is partially due to a classic study⁸⁷ demonstrating the selective suppression of low spatial frequencies grating flashed around the time of saccades.

Since the magnocellular pathway is selective to high-velocity stimuli of low spatial frequencies⁸⁸, the suppression of low spatial frequencies has been interpreted as a motor-related suppression of the magnocellular visual pathways^{47,48}, even though recent studies have argued against the selectivity of the magnocellular pathway for low spatial frequencies⁸⁹. Maybe the most convincing reason for suppression by eye movement related signals is that saccadic suppression starts prior to saccade onset. (Pre-)motor areas have knowledge about the imminent saccade, while visual areas have not yet experienced the effect of the saccade^{6,44,47,90}. Moreover, such an active (motor-related) mechanism of central origin has the intuitive appeal that the purpose of suppression is to reduce visual disruption around the time of saccades, and hence contribute towards perceptual stability.

Aim of the thesis

The neural mechanisms of saccadic suppression and its neural loci still remain controversial after decades of research on this topic. This suggests a need for a ‘reset’ in this field. In most experiments, saccadic suppression was observed while subjects made saccades on dark or uniform backgrounds. A key assumption was that such backgrounds do not induce visual change across the retina during saccades. Consequently, the resulting suppression has purely been associated with eye movement related signals. From a visual processing perspective, this assumption is rather naïve, as under typical laboratory settings eliminating visual input entirely is not straightforward. Even small changes in peripheral vision by the sweeping edge of a display device during saccades can trigger strong visual responses in the retina^{27,34,78}, starting a cascade of visual processing that could ultimately lead to saccadic suppression. Hence, it is conceivable that visual mechanisms contributed to saccadic suppression even in such experiments.

The aim of my doctoral work was to investigate the role and contribution of visual mechanisms in saccadic suppression, locate its neural loci and probe the underlying mechanisms. For these investigations, I used a combination of experimental approaches across multiple species and also computational modeling. The key findings have been presented in two publications. **Publication 1** details the contribution of visual mechanisms towards perceptual saccadic suppression, and identifies the retina as one of the neural loci of perceptual saccadic suppression. These investigations were done in close collaboration with the lab of Ziad Hafed at the University of Tübingen. **Publication 2** describes the detailed retinal mechanisms underlying saccadic suppression.

Key findings

Visual mechanisms alone can account for perceptual saccadic suppression

Together with the Haged Lab, we first investigated whether visual mechanisms play a role in saccadic suppression at all. We hypothesized that if visual mechanisms do contribute towards saccadic suppression, then visual input during saccades can modulate perceptual saccadic suppression. To test this hypothesis, we asked human subjects' to localize a flash while they made saccades on coarse and fine textured backgrounds as opposed to dark or uniform backgrounds (**Publication 1: Fig. 1**). Their ability to localize the flash diminished for flashes presented between 50 ms before and 100 ms after saccade onset, reflecting saccadic suppression. While this result is consistent with previous studies, we showed that saccadic suppression depended on the textured background. Suppression was stronger and lasted longer for saccades across coarse textures than across fine textures. This proved that visual experience during saccades, and thus visual mechanisms, play a role in saccadic suppression.

These experiments however did not show the strength of the contribution by visual mechanisms. Perhaps visual mechanisms merely modulated the suppression triggered by eye movement related signals. To understand the extent to which visual mechanisms were involved, we repeated the above experiments in the absence of saccades (**Publication 1: Fig. 6**). Here, instead of making real saccades over textured backgrounds, human subjects maintained saccade-free fixation while we induced saccade-like displacements of the textures across their eyes. This time, due to the absence of real saccades, eye movement related signals could not influence flash-induced neural responses and perception. Therefore, the observed effects, if any, can only be attributed to visual mechanisms. Perceptual suppression still occurred, with the same dependency on texture as with real saccades. Surprisingly, the resulting suppression was even stronger and longer lasting than with real saccades. Even pre-saccadic suppression occurred, which in the past has always been assumed to be caused by with eye movement related signals. Moreover, the pre-saccadic suppression caused by texture displacements started earlier than suppression observed with real saccades. These observations are key to two fundamental

findings. First, perceptual saccadic suppression can be caused by visual mechanisms alone, without the need for any eye movement related signals. Second, eye movement related signals are instead shortening the long-lasting saccadic suppression caused by visual mechanisms. These findings are further elaborated in **Publication 1**.

Saccadic suppression starts in the retina

Having established that visual mechanisms contribute to saccadic suppression, we characterized them at the neural level. Given its rich visual processing capabilities and its projection to LGN where visual masking has been observed, retina was a probable candidate⁶⁸.

We isolated mouse and pig retinæ and performed multi-electrode array recordings to record the spiking activity of retinal ganglion cells (RGCs). As in our human psychophysics experiments, each retina was exposed to coarse and fine textures. Here, I replicated the visual flow resulting from saccades by displacing the texture in a saccade-like manner over the retinæ. At different times relative to the texture displacements, I presented brief probe flashes to the retina. I then analyzed how the spiking responses to these probe flashes were influenced by the saccade, as compared to the flash presented in isolation (baseline response).

Most RGCs exhibited suppressed responses to flashes presented during or after saccades, with gradual recovery to baseline (**Publication 1: Fig. 3**). Interestingly, this suppression was more pronounced for coarse texture than for fine texture, in line with the dependency on the background texture properties of perceptual suppression. Moreover, retinal saccadic suppression was long-lasting with recovery time of almost 1 second after saccade onset. Taken together, these observations suggest that a large component of perceptual saccadic suppression, is caused by visual mechanisms starting already in the retina.

Pre-saccadic suppression, however, was not observed in the retina. We therefore concluded that it originates from visual mechanisms in downstream pathways, most likely those underlying backwards visual masking^{62,69,71}.

Saccadic suppression is triggered by interactions between sequential stimuli

Rapid global image-shifts across the retina naturally occur during saccades. We initially hypothesized that retinal saccadic suppression was triggered by specialized circuits that detect such shifts. To test this hypothesis, texture displacements used in previous experiments were replaced by a sudden texture jump (an infinite-speed saccade) (**Publication 1: Fig. 4**). The observed suppression was similar to texture displacement and still depended on texture properties, suggesting that suppression was triggered by visual transients across the retina, not specifically by motion, contrary to our hypothesis. To further confirm that this was the case, we characterized suppression evoked by sudden changes in uniform background luminance. Specifically, instead of a texture I showed a uniform background which changed in luminance (luminance step) and I characterized the suppression following a range of luminance step contrasts. Interestingly, suppression after high- and low-contrast luminance steps was qualitatively and quantitatively similar to suppression after coarse and fine texture displacements, respectively, both in terms of strength and time course. Presumably, moving larger blobs of the coarse texture across the retina result in high-contrast changes within individual receptive fields (e.g., from a bright blob in a receptive field before texture displacement to a dark blob thereafter). In comparison, smaller blobs in the fine texture would be spatially averaged within receptive fields, resulting in low-contrast changes.

Taken together, the results of these experiments provide evidence that retinal saccadic suppression arises from generic retinal mechanisms triggered by visual transients; whether through texture displacements, texture jumps or luminance steps: each of these transients suppress responses to subsequent probe flashes. Such stimulus-stimulus retinal effects may be inherited deep into the brain's visual processing hierarchy, including cortical (frontal eye field) and subcortical (superior colliculus) areas⁹¹ that are implicated in saccadic suppression^{55,92–94}. In fact, these stimulus-stimulus retinal effects were preserved all the way till perception, which we discovered upon replicating the luminance step experiments in human psychophysics (**Publication 1: Fig. 5**). The fact that saccadic suppression can be evoked simply by visual transients suggest that saccadic suppression might not critically depend on the specific oculomotor behavior of a species. This concept is further elaborated in the discussion section.

Mechanisms underlying retinal saccadic suppression

The RGCs in our dataset showed diverse response properties (**Publication 1: Supplementary Fig. 6**), presumably belonging to several functionally different cell types. While most of these RGCs exhibited retinal saccadic suppression, the temporal profile of suppression, in particular its recovery, differed across ON and OFF RGC types (**Publication 2: Fig. 2**). OFF RGCs recovered by ~350 ms after saccade onset whereas ON RGCs recovered only by ~1 s. The longer suppression in ON RGCs was due to an additional component of suppression acting only in ON RGCs.

We identified 3 components contributing to retinal saccadic suppression (**Publication 2: Fig. 3**): global; surround; and central components. As I describe below, these components differed in their suppressive strength, temporal properties, spatial origins relative to a cell's receptive field center, and underlying mechanisms.

Global component

The global component of suppression acted only on ON RGCs. It had a fast onset, and recovered by 350 ms following saccade onset. This component originated from as far as the cell's far surround, mediated by GABAergic inhibition via the GABA_A receptors. Data underlying this component is shown in **Publication 2: Figs. 2b, S5**.

Surround component

Similar to the global component, the surround component of suppression acted only in ON RGCs. It had a delayed onset and lasted much longer (up to ~1 s). It most likely originated in the cell's immediate surround. This component did not depend on classical GABAergic or glycinergic pathways. However, the precise mechanisms of suppression underlying this component remain unknown. Possible mechanisms include feedback of horizontal cells onto the cones^{22,95}. Data underlying this component is shown in **Publication 2: Figs. 2f, S7e**.

Central component

The central component was the only source of suppression in OFF RGCs, and the dominant source in ON RGCs; making it the main contributing component of retinal saccadic suppression. This component was short-lived (~250 – 350 ms) and originated from a cell's receptive field center. It

was triggered by opposite-polarity sequential stimuli: responses to bright flashes in ON RGCs were predominantly suppressed when presented after a negative-contrast luminance step; responses to dark flashes in OFF RGCs were only suppressed when presented after positive-contrast luminance steps.

To investigate this central component, we recorded cone photoreceptor output (**Publication 2: Fig. 5**) under the luminance step paradigm (in collaboration with the lab of Katrin Franke) and parsed it through a phenomenological model²² of retinal processing (in collaboration with Felix Franke) (**Publication 2: Fig. 6**). This technique allowed us to analyze suppression in the central feedforward pathway, namely photoreceptors – bipolar cells – ganglion cell. We found that suppression resulted from the relatively slow kinetics of cone responses, combined with temporal properties and nonlinearities of downstream retinal pathways. This component therefore results from generic retinal signal processing of opposite-polarity sequential visual stimuli. It cannot be pinpointed to one specific site, but is an emergent property where the temporal dynamics of cones photoreceptors are the basis for subsequent non-linear processing. We call this novel processing motif “dynamic reversal suppression”: “dynamic” because of the necessarily tight temporal link between responses to the two consecutive stimuli; and “reversal” because the response to an event gets suppressed when it reverses the cone output triggered by the first stimulus.

Retinal saccadic suppression in other animal models

In addition to mouse retina, we characterized retinal saccadic suppression in ex vivo pig retinae (**Publication 2: Fig. S13**). Suppression properties, including dependency on background texture statistics was consistent with suppression in mouse RGCs. Similar to our findings in mice, ON RGCs in pig retinae also exhibited longer suppression, suggesting that multiple components of retinal saccadic suppression are present across animal species. In additional experiments, our collaborator Alexandra Kling at Stanford University recorded RGCs from an ex vivo macaque retina using the luminance step paradigm. Macaque RGCs also exhibited retinal saccadic suppression consistent with results from mouse RGC recordings (**Publication 2: Fig. 7**). Additional

data is required to characterize responses at the population level and to develop a dictionary of response modulations in macaque retina.

Discussion

Summary of key findings

1) Mechanisms underlying perceptual saccadic suppression: we demonstrated that visual mechanisms contribute to perceptual saccadic suppression in humans. First, in carefully designed psychophysical experiments, we showed that perceptual saccadic suppression is modulated by the visual properties of the background texture across which subjects made saccades. Specifically, suppression is stronger and longer lasting for coarse than for fine background textures. Second, suppression persists when saccades are replaced by rapid saccade-like displacements of the background texture across the subjects' eyes. Interestingly, the resulting suppression in the latter case is stronger and longer-lasting than with real saccades. Together, these findings suggest that visual mechanisms alone can account for saccadic suppression, without requiring the involvement of eye movement related signals. Instead, we offer evidence that eye movement related signals shorten this suppression.

2) Neural locus of perceptual saccadic suppression: I proved that saccadic suppression starts in the retina. Using ex vivo mouse retina electrophysiology, I showed that most ganglion cells exhibit suppressed responses to flashes presented after saccade-like displacements of a background texture. Moreover, retinal saccadic suppression has similar dependencies on the texture properties as the perceptual saccadic suppression: suppression is stronger with coarse than with fine textures. Both retinal and perceptual saccadic suppression are triggered by visual transients across the retina.

3) Mechanisms of saccadic suppression in the retina: I showed that in the retina, saccadic suppression is mediated by at least three components, differing in their spatial origins, temporal properties, suppression strength and underlying mechanisms. First, the central component, originating in the receptive field center of an RGC, is the only source of suppression in OFF RGCs, and the dominant source of suppression in ON RGCs for time points immediately after saccade-like image displacements. This component relies on a novel processing motif that we term

“dynamic reversal suppression”. It emerges by an interplay of the relatively slow cone dynamics and non-linear processing in bipolar pathways of the retina. This motif is very robust, triggered by local successive contrast reversals that naturally occur during saccades, and efficiently suppresses ganglion cell spiking by often over 50%. Second, the global component of suppression acts only on ON RGCs. It is mediated by GABAergic pathways and is carried to the RGC by wide-field amacrine cells from as far as the cell’s far surround. Third, the surround component, also acting only on ON RGCs, presumably arises from the immediate surround of a RGC’s receptive field. It does not depend on inhibitory neurotransmission, but its exact mechanisms remain to be explored.

4) Retinal saccadic suppression does not account for pre-saccadic suppression observed perceptually. Therefore, visual mechanisms of saccadic suppression must also exist downstream of the retina.

In the present doctoral work, I offer robust psychophysical and neurophysiological evidence that contradicts the standard account of saccadic suppression as driven by eye movement related signals, such as corollary discharge. Instead, I show that ‘saccadic’ suppression can be caused purely by visual mechanisms, starting in the retina. These findings radically affect the general view that saccadic suppression is an active mechanism evoked by the brain to maintain perceptual stability. Moreover, the retinal mechanisms underlying saccadic suppression are triggered not only by saccade-like image shifts, but in general by interactions between consecutive stimuli across the retina. Thus, these results not only describe the mechanisms underlying saccadic suppression, but more generally describe the processing of sequential visual stimuli which are ubiquitous in natural vision.

Retrospective analysis of the evidence supporting saccadic suppression by eye movement related signals

Undeniably, the past observations that perceptual saccadic suppression occurs selectively for low spatial frequency stimuli⁸⁷ and that it starts prior to saccade onset^{6,44,47,90} has generated the view

that suppression is caused by eye movement related signals. Given the new insights presented here, can visual mechanisms account for those results?

In the introduction, I reviewed the past study demonstrating that low spatial frequency are selectively suppressed⁸⁷ around the time of saccades. This was interpreted as an eye movement related influence on the magnocellular visual pathways^{47,48}. Together with the Hafed Lab, we analyzed this phenomenon from the perspective of visual flow across the retina. We found that the phenomenon of selective suppression of low spatial frequencies could be violated in two ways (**Publication 1: Fig. 8**). First, such selective suppression could be obtained simply by saccade-like texture displacements across the retina of human observers, in the absence of eye movements. Second, the suppression selectivity could be abolished with a simple change in background-texture statistics. Both observations reinforce our finding that visual mechanisms underlie saccadic suppression. In short, the observation that originally supported suppression by eye movement related signals, could in fact be replicated in the absence of eye movements, simply by mimicking the visual flow across the retina. Hence, selective suppression of low spatial frequencies⁸⁷ can no longer be interpreted as an eye movement related influence on the magnocellular visual pathways^{47,48}.

The other argument that has been used to support suppression by eye movement related signals is that suppression starts before saccade onset. This has been interpreted as an influence of eye movements on the neural activity prior to saccades, as eye movements, like all motor activities, involve a “planning phase” so that information about the upcoming saccade exists before the actual movement is carried out^{6,44,47,90}. However, as we show, pre-saccadic perceptual suppression occurs even in the absence of eye movements, simply from visual mechanisms triggered by visual transients across the retina of human observers (**Publication 1: Figs. 5, 6**). In fact, pre-saccadic suppression in the absence of saccades is stronger and begins earlier than with real saccades. This finding therefore suggests that eye movement related signals are not necessary for pre-saccadic suppression. It should be noted that pre-saccadic suppression in the absence of saccades was observed previously by Diamond et al, 2000⁴⁷, but has largely been neglected.

Taken together, our findings invalidate two key interpretations of observations supporting saccadic suppression by an eye movement related signal. Given the lack of further evidence and convincing neural mechanisms, it is conceivable that eye movement related mechanism of saccadic suppression does not exist. Still, this can only be verified through characterizing the effects of saccades on visual sensitivity in the absence of any visual input. Such experiments would be extremely difficult under standard laboratory settings but perhaps possible through a Ganzfeld device.

Does perceptual saccadic suppression in humans start in the retina?

Despite the similarities between perceptual saccadic suppression and mouse retinal saccadic suppression, these are two species with very different oculomotor behavior. Mice make saccade-like eye movements⁹⁶ to stabilize their gaze, whereas humans typically make saccades to bring an object-of-interest in their foveal region. Additionally, the kinetics and frequency of eye movements differ across species. Such differences in oculomotor behavior can challenge the validity of neural investigations in mice to elucidate saccadic suppression mechanisms in humans. However, this is a problem only when saccadic suppression arises from planned eye movements and their associated motor commands, or when the statistics of visual flow during saccades (such as acceleration, maximal velocity, and deceleration of the image moving across the retina) govern the suppressive effect. Both is not the case. We show that the major component of suppression (the central component) in mouse retina ultimately results from the slow response kinetics of cone photoreceptors, rather than being caused by specialized motion detection circuits. Such a generic visual processing motif, emerging from elementary response properties of photoreceptors, is likely to be conserved across species, given that many building blocks of photoreceptors are conserved across species⁹⁷. Consistently, suppression was also present in pig and macaque retinae.

In summary, this work offers evidence that: (1) Saccadic suppression in mouse retina emerges from generic visual processing of sequential stimuli; (2) Retinal saccadic suppression exists in mouse, pigs and monkeys; and (3) Suppression properties are congruent across the retina of these animals and human perception. From (1) and (2), it can be inferred that the mechanisms

of retinal saccadic suppression are likely conserved across species. Taken together with (3), it can be inferred that retinal saccadic suppression also exists in human retina. Nonetheless, these inferences are based on a high degree of correlation, which does not imply causation. Therefore, in order to draw these inferences causatively, one has to investigate the existence of saccadic suppression in human retina; and the mechanisms of saccadic suppression in retinae of different species.

Oculomotor differences across species may still play an important role, for example, in shortening the suppression caused by visual mechanisms, and therefore the time course of the resulting perceptual saccadic suppression might be different across species. Eye movements will also play an important role in governing the statistics of saccade-induced visual transients across the retina.

Why does saccadic suppression occur?

The general assumption in vision science is that the “purpose” or “function” of saccadic suppression is reducing the visual disruption caused by rapid image-shifts across the retina around the time of saccades. This assumption is largely based on the intuitive appeal that visual disruptions will otherwise mar our visual experience. Saccadic suppression is therefore one component contributing towards perceptual stability across saccades.

Our finding that suppression is caused by inherent properties of photoreceptors and downstream nonlinearities suggests that saccadic suppression is not “caused purposefully” by higher brain centers. Rather it is an inevitable consequence of general retinal visual processing. So much so, that the brain needs to compensate for this long-lasting suppression, as indicated by our human psychophysics experiments.

While retinal suppression is not “caused purposefully”, it nonetheless reduces the sensitivity to stimuli following it, which is one of the building blocks of perceptual stability around the time of saccades. Eye movement related signals form another building block as they are required to optimize the duration of this suppression. Thus, the time course of perceptual saccadic

suppression seems to be the result of efficient sensorimotor integration where suppression occurs as a result of visual mechanisms and compensation is achieved by the motor system.

It would be interesting to understand the origins and mechanisms of saccadic compensation. Perhaps it occurs in areas as early as the LGN, where disinhibition could occur as a result of activation of pretectal neurons projecting to it, thereby countering the suppression inherited by the LGN neurons^{98,99} from the retina. This could then also explain the increased excitability of V1 neurons towards the end of a saccade^{100,101}.

Saccadic suppression, visual masking or neural adaptation?

The phenomenon of reduced perceptual and neural responses to brief flashes presented around the time of saccades is termed “saccadic suppression”. Similarly, the phenomenon of reduced perceptual or neural response to a flash presented in close temporal proximity to a another stimulus (mask) is termed as “visual masking”⁷¹, and the phenomenon of reduced flash neural response when presented after another flash is termed “neural adaption”⁹¹. These phenomena are usually associated with different underlying mechanisms. However, the visual flow induced across the retina in paradigms underlying these phenomena, and their resulting effects are in fact similar: the response to a second stimulus (in these cases a flash) is suppressed by the first stimulus, be it a saccade (**Publication 1: Figs. 1-3; Publication 2: Figs. 1-2**), another stimulus referred to as mask (**Publication 1: Figs. 4-5; Publication 2: Figs. 4-8**), or a flash. The parallels between these suppressive effects and retinal saccadic suppression suggest that the retina is one of the neural substrates of these seemingly different types of suppression, thereby unifying their underlying mechanisms.

It would be pertinent to change “saccadic suppression” terminology to a more general term, like “visual suppression” that would encompass the suppression resulting from visual processing of sequential stimuli. “Saccadic compensation” could then be used to capture the shortening of this suppression during saccades.

Visual mechanisms of suppression downstream of the retina

Retinal saccadic suppression alone cannot explain all the perceptual suppressive effects we observed. Specifically, pre-saccadic suppression observed perceptually (**Publication 1: Figs. 1, 5, 6**), is not present in the retinal output (**Publication 1: Fig. 3**). Visual mechanisms of suppression must therefore exist downstream of the retina, perhaps even at multiple levels. For example, given the similarities in perceptual suppression prior to saccade-like texture displacements / luminance steps and backwards visual masking, it is likely that they share the same underlying mechanism. Similarly, other visual mechanisms might be present downstream of the retina that modulate and complement retinal saccadic suppression. This would not be surprising given that saccadic suppression is a consequence of rather generic visual processing and that other generic visual functions such as gain control occur at multiple sites throughout the visual system¹⁰².

Variability in retinal suppression

I observed suppression in most of the RGCs I recorded from ($N > 2000$ from ~ 50 retinae). These RGCs presumably belonged to several different functional cell types (**Publication 1: Supplementary Fig. 6**). The presence of suppression in most RGC types is not surprising, given that the central component of suppression ultimately results from inherent properties of cone photoreceptors, which are the first cells in the visual processing cascade. However, the duration and strength of suppression varies across RGCs (**Publication 2: Supplementary Figs. S3, S8, S13**). I identified at least two sources of suppression variation. First, the differences in the readout of cone output by different downstream retinal pathways can lead to variability in suppression at the RGC output. For example, RGCs that are driven more by the instantaneous changes in cone output (i.e. transient RGCs), are more strongly suppressed than cells that reflect more the absolute cone output (i.e. sustained RGCs) (**Publication 2: Fig. 6e, f**). Second, different ganglion cell types can be suppressed by different mechanisms. We found that ON RGCs get suppressed by at least three components of suppression, whereas OFF RGCs are suppressed by a single component (**Publication 2: Fig. 2**). The differences in suppression strength and time course across the different components can also explain the variability in suppression across RGC types.

Implications for retinal signal processing

Retinal saccadic suppression has several implications on retinal processing itself, in addition to its contribution towards perceptual saccadic suppression. Irrespective of the variability in retinal suppression (as stated above), most RGCs show suppressed response to a second stimulus in a sequence. Consequently, the retinal suppression may also contribute towards specialized visual motor tasks. For example, while threading a needle, microsaccades will jitter the needle and its background across the retina. RGCs exposed to the background will experience stronger visual transients than RGCs exposed to the needle. As a result, RGCs 'seeing' the background might show suppressed responses following microsaccades, perceptually blurring out the background. This relative enhancement of the fixated object by background suppression could be valuable for visual tasks such as object recognition.

Retinal suppression will also effect the extraction or processing of most visual features across any time-varying visual input will be affected. For example, some RGCs encode the presence of local edges in a scene. But what if this scene is brought into an RGC's receptive field through a saccade or external motion? How will retinal saccadic suppression influence the processing of these edges? Overall, retinal saccadic suppression, or rather sequential-stimuli suppression will modulate retinal output during natural vision. These modulations should be considered in any future investigations where dynamic visual stimuli are used.

Our study, together with several other studies^{27,76,77,79–82,103–105} that investigated retinal processing under dynamic conditions, demonstrate the complex image processing capabilities in the retina to facilitate downstream visual processing for the ultimate service of perception during natural vision. Future investigations of how retina extracts and processes visual features under dynamic conditions of natural vision and how it integrates information in such scenarios will advance our understanding of the complex image processing capabilities the retina possesses.

Role of global and surround components of retinal suppression in perceptual saccadic suppression

Both ON and OFF RGCs are suppressed by the central component of suppression, resulting from the nonlinear readout of inherently slow responses of cone photoreceptors. This component has a fast onset and recovers within ~250 ms. ON RGCs, are suppressed by two additional components: the global component that originates from the far surround of the receptive field and has a similar time course as the central component; and the surround component that presumably originates from the immediate surround of the receptive field, has a delayed onset and lasts much longer. The exact contribution of these two additional components to perceptual saccadic suppression is not so clear.

During saccades, the entire visual world shifts across the retina. Such image-shifts across the retina, concurrently activate the three components of suppression in ON RGCs. However, blocking the GABA_A mediated global component has a negligible effect on the total suppression, suggesting that the other components play a more dominant role in retinal suppression. The global component may play a role for example in perceptual modulations during pursuit eye movements⁴⁰. Here, the central component of suppression will not be triggered in RGCs whose receptive field centers are locked to the tracked object; but these RGCs could be suppressed by the global component. In such scenarios, the resulting suppression can be said to have originated from a specialized suppression circuit in the retina. This likely belongs to the same class of circuits that suppress ganglion cell responses to saccade-like image shifts themselves^{26,27}. These circuits were previously suggested to suppress motion awareness during saccades, a phenomenon known as saccadic omission. Our findings indicate that during specific conditions, such circuits may also contribute towards suppressing RGC sensitivity even after the motion is completed. The role of the surround component of suppression towards perceptual saccadic suppression also remains ambiguous as it suppresses ON RGC responses for up to 1 second whereas perceptual saccadic suppression only lasts for ~100 ms after saccade onset.

Irrespective of which components of retinal saccadic suppression contribute towards perceptual saccadic suppression, our results show that retinal responses to stimuli following visual transients

are modulated concurrently by several mechanisms. Additional mechanisms might exist under different stimulus conditions. From the perspective of retinal visual feature processing, this would be consistent with how multiple mechanisms concurrently process other visual features in the retina, such as motion³².

Scientific and technological impacts

The findings from my doctoral work contributes significantly to the area of visual neuroscience, specifically towards how our brain reduces the visual sensitivity in order to maintain visual stability under dynamic conditions of natural viewing. We now know that eye movement signals are not a prerequisite of saccadic suppression, but are rather necessary for shortening the long-lasting suppression caused by visual mechanisms. This insight will trigger research towards finding the neural correlates and underlying mechanisms of such saccadic compensation. We also now know the identity of at least one neural locus of saccadic suppression – the retina, which I consider as a huge leap considering that the search for such neural loci has been ongoing for over 5 decades. Moreover, studying the mechanisms of saccadic suppression in the retina led to several important insights into visual processing in dynamic conditions of natural vision. Firstly, suppression is a result of stimulus-stimulus interactions, which naturally occur during saccades, but also during many other forms of sequential visual stimulation. This finding unifies the mechanisms underlying several suppressive phenomena, such as saccadic suppression, visual masking and neural adaptation. Secondly, my results show novel disparities between the circuits underlying ON and OFF RGCs, which in future studies would aid in understanding how visual features are processed in dynamic conditions.

In addition to the scientific contributions, my doctoral work also has important technological impacts. The knowledge that suppression already starts in the retina would be extremely important in the development of future retinal prosthesis devices. In addition, the phenomena of retinal saccadic suppression could inspire improved stabilization techniques for cameras operating under highly dynamic visual condition, such as for autonomous vehicles.

References

1. Sabra, A. I. *The Optics of Ibn al-Haytham. Books I-III: On Direct Vision. With Translation, Introduction, Commentary, Glossaries.* London: The Warburg Institute, 1989. **1–3**, (1989).
2. Zimmermann, E. & Bremmer, F. Visual Neuroscience: The Puzzle of Perceptual Stability. *Curr. Biol.* **26**, R199–R201 (2016).
3. Dodge, R. Visual perception during eye movement. *Psychol. Rev.* **7**, 454–465 (1900).
4. Matin, E. Saccadic suppression: a review and an analysis. *Psychol. Bull.* **81**, 899–917 (1974).
5. Sperry, R. W. Neural basis of the spontaneous optokinetic response produced by visual inversion. *J. Comp. Physiol. Psychol.* **43**, 482–489 (1950).
6. Wurtz, R. H. Neuronal mechanisms of visual stability. *Vision Res.* **48**, 2070–2089 (2008).
7. Usrey, W. M. & Alitto, H. J. Visual Functions of the Thalamus. *Annu. Rev. Vis. Sci.* **1**, 351–371 (2015).
8. DiCarlo, J. J., Zoccolan, D. & Rust, N. C. How does the brain solve visual object recognition? *Neuron* **73**, 415–434 (2012).
9. DiCarlo, J. J. & Cox, D. D. Untangling invariant object recognition. *Trends Cogn. Sci.* **11**, 333–341 (2007).
10. Serre, T. Hierarchical Models of the Visual System. in *Encyclopedia of Computational Neuroscience* 1–12 (Springer New York, 2014). doi:10.1007/978-1-4614-7320-6_345-1
11. Heeger, D. J., Simoncelli, E. P. & Movshon, J. A. Computational models of cortical visual processing. *Proc. Natl. Acad. Sci.* **93**, 623–627 (1996).
12. Hubel, D. H. & Wiesel, T. N. Receptive fields and functional architecture of monkey striate cortex. *J. Physiol.* **195**, 215–243 (1968).

13. Van Essen, D. C. & Maunsell, J. H. R. Hierarchical organization and functional streams in the visual cortex. *Trends Neurosci.* **6**, 370–375 (1983).
14. Reinhard, K. *et al.* A projection specific logic to sampling visual inputs in mouse superior colliculus. *Elife* **8**, 272914 (2019).
15. Wallace, M. T., Meredith, M. A. & Stein, B. E. Multisensory integration in the superior colliculus of the alert cat. *J. Neurophysiol.* **80**, 1006–1010 (1998).
16. Gandhi, N. J. & Katnani, H. A. Motor Functions of the Superior Colliculus. *Annu. Rev. Neurosci.* **34**, 205–231 (2011).
17. Buonocore, A. *et al.* Alteration of the microsaccadic velocity-amplitude main sequence relationship after visual transients : implications for models of saccade control. 1894–1910 (2017). doi:10.1152/jn.00811.2016
18. Buonocore, A., Baumann, M. P. & Hafed, Z. M. Instantaneous movement-unrelated midbrain activity modifies ongoing eye movements. *bioRxiv* 1–46 (2020). doi:10.1101/2020.05.31.126359
19. Fu, Y. & Yau, K.-W. Phototransduction in mouse rods and cones. *Pflügers Arch. - Eur. J. Physiol.* **454**, 805–819 (2007).
20. Tikidji-Hamburyan, A. *et al.* Rods progressively escape saturation to drive visual responses in daylight conditions. *Nat. Commun.* **8**, (2017).
21. Münch, T. A. Information Processing : Ganglion Cells. *Encycl. Eye* 355–362 (2010).
22. Drinnenberg, A. *et al.* How Diverse Retinal Functions Arise from Feedback at the First Visual Synapse. *Neuron* 1–18 (2018). doi:10.1016/j.neuron.2018.06.001
23. Ghosh, K. K., Bujan, S., Haverkamp, S., Feigenspan, A. & Wässle, H. Types of Bipolar Cells in the Mouse Retina. *J. Comp. Neurol.* **469**, 70–82 (2004).

24. Euler, T., Haverkamp, S., Schubert, T. & Baden, T. Retinal bipolar cells: elementary building blocks of vision. *Nat. Rev. Neurosci.* **15**, 507–519 (2014).
25. Kolb, H. *Roles of Amacrine Cells. Webvision: The Organization of the Retina and Visual System* (University of Utah Health Sciences Center, 1995).
26. Baccus, S. A., Olveczky, B. P., Manu, M. & Meister, M. A Retinal Circuit That Computes Object Motion. *J. Neurosci.* **28**, 6807–6817 (2008).
27. Roska, B. & Werblin, F. Rapid global shifts in natural scenes block spiking in specific ganglion cell types. *Nat. Neurosci.* **6**, 600–608 (2003).
28. Fried, S., Münch, T. & Werblin, F. Mechanisms and circuitry underlying directional selectivity in the retina. *Nature* 411–414 (2002).
29. Fried, S., Münch, T. & Werblin, F. Directional selectivity is formed at multiple levels by laterally offset inhibition in the rabbit retina. *Neuron* **46**, 117–27 (2005).
30. Münch, T. A. *et al.* Approach sensitivity in the retina processed by a multifunctional neural circuit. *Nat. Neurosci.* **12**, 1308–1316 (2009).
31. Werblin, F. Six different roles for crossover inhibition in the retina: correcting the nonlinearities of synaptic transmission. *Vis. Neurosci.* **27**, 1–8 (2010).
32. Wei, W. Neural mechanisms of motion processing in the mammalian retina. *Annu. Rev. Vis. Sci.* **4**, 165–192 (2018).
33. van Wyk, M., Taylor, W. R. & Vaney, D. I. Local Edge Detectors: A Substrate for Fine Spatial Vision at Low Temporal Frequencies in Rabbit Retina. *J. Neurosci.* **26**, 13250–13263 (2006).
34. Passaglia, C. L., Freeman, D. K. & Troy, J. B. Effects of remote stimulation on the modulated activity of cat retinal ganglion cells. *J. Neurosci.* **29**, 2467–2476 (2009).
35. O’Brien, B. J., Isayama, T., Richardson, R. & Berson, D. M. Intrinsic physiological properties

- of cat retinal ganglion cells. *J. Physiol.* **538**, 787–802 (2002).
36. Baden, T. *et al.* The functional diversity of mouse retinal ganglion cells. *Nature* **529**, 1–21 (2016).
 37. Tikidji-Hamburyan, A. *et al.* Retinal output changes qualitatively with every change in ambient illuminance. *Nat. Neurosci.* **18**, 66–74 (2015).
 38. Yarbus, A. L. *Eye Movements and Vision*. (Springer US, 1967). doi:10.1007/978-1-4899-5379-7
 39. Tatler, B. W., Wade, N. J., Kwan, H., Findlay, J. M. & Velichkovsky, B. M. Yarbus, Eye Movements, and Vision. *Perception*. **1**, 7–27 (2010).
 40. Schütz, A., Braun, D. & Gegenfurtner, K. Eye movements and perception: A selective review. *J. Vis.* **11**, 1–30 (2011).
 41. Zuber, B. L. & Stark, L. Saccadic suppression: Elevation of visual threshold associated with saccadic eye movements. *Exp. Neurol.* **16**, 65–79 (1966).
 42. Beeler, G. W. Visual threshold changes resulting from spontaneous saccadic eye movements. *Vision Res.* **7**, 769–775 (1967).
 43. Volkman, F. C. Human visual suppression. *Vision Res.* **26**, 1401–1416 (1986).
 44. Bremmer, F., Kubischik, M., Hoffmann, K. P. & Krekelberg, B. Neural dynamics of saccadic suppression. *J. Neurosci.* **29**, 12374–12383 (2009).
 45. Krekelberg, B. Saccadic suppression. *Curr. Biol.* **20**, R228–R229 (2010).
 46. Duffy, F. H. & Lombroso, C. T. Electrophysiological evidence for visual suppression prior to the onset of a voluntary saccadic eye movement. *Nature* **218**, 1074–1075 (1968).
 47. Diamond, M. R., Ross, J. & Morrone, M. C. Extraretinal control of saccadic suppression. *J. Neurosci.* **20**, 3449–3455 (2000).

48. Ross, J., Morrone, M. C., Goldberg, M. E. & Burr, D. C. Changes in visual perception at the time of saccades. *Trends Neurosci.* **24**, 113–121 (2001).
49. Gremmler, S. & Lappe, M. Saccadic suppression during voluntary versus reactive saccades. *J. Vis.* **17**, 1–10 (2017).
50. Kagan, I., Gur, M. & Snodderly, D. Saccades and drifts differentially modulate neuronal activity in V1: effects of retinal image motion, position, and extraretinal influences. *J. Vis.* **8**, 1–25 (2008).
51. Supèr, H., Van Der Togt, C., Spekreijse, H. & Lamme, V. A. F. Correspondence of presaccadic activity in the monkey primary visual cortex with saccadic eye movements. *Proc. Natl. Acad. Sci. U. S. A.* **101**, 3230–3235 (2004).
52. Thiele, A., Henning, P., Kubischik, M. & Hoffmann, K. P. Neural mechanisms of saccadic suppression. *Science (80-.)*. **295**, 2460–2462 (2002).
53. Ibbotson, M. R., Price, N. S. C., Crowder, N. A., Ono, S. & Mustari, M. J. Enhanced motion sensitivity follows saccadic suppression in the superior temporal sulcus of the macaque cortex. *Cereb. Cortex* **17**, 1129–38 (2007).
54. Berman, R. A., Cavanaugh, J., McAlonan, K. & Wurtz, R. H. A circuit for saccadic suppression in the primate brain. *J. Neurophysiol.* **117**, 1720–1735 (2017).
55. Robinson, D. L. & Wurtz, R. H. Use of an extraretinal signal by monkey superior colliculus neurons to distinguish real from self-induced stimulus movement. *J. Neurophysiol.* **39**, 852–870 (1976).
56. Hafed, Z. M. & Krauzlis, R. J. Microsaccadic suppression of visual bursts in the primate superior colliculus. *J. Neurosci.* **30**, 9542–9547 (2010).
57. MACKAY, D. M. Elevation of Visual Threshold by Displacement of Retinal Image. *Nature* **225**, 90–92 (1970).

58. García-Pérez, M. A. & Peli, E. Visual contrast processing is largely unaltered during saccades. *Front. Psychol.* **2**, 1–15 (2011).
59. Ilg, U. J. & Hoffmann, K. P. Motion perception during saccades. *Vision Res.* **33**, 211–220 (1993).
60. Campbell, F. W. & Wurtz, R. H. Saccadic omission: Why we do not see a grey-out during a saccadic eye movement. *Vision Res.* **18**, 1297–1303 (1978).
61. Mitrani, L., Mateeff, S. & Yakimoff, N. Is saccadic suppression really saccadic? *Vision Res.* **11**, 1157–1161 (1971).
62. Matin, E., Clymer, A. B. & Matin, L. Metacontrast and saccadic suppression. *Science* **178**, 179–182 (1972).
63. Mitrani, L., Yakimoff, N. & Mateeff, S. Saccadic suppression in the presence of structured background. *Vision Res.* **13**, 517–521 (1973).
64. Mateeff, S., Yakimoff, N. & Mitrani, L. Some characteristics of the visual masking by moving contours. *Vision Res.* **16**, 489–492 (1976).
65. Brooks, B. A., Impelman, D. M. K. & Lum, J. T. Backward and forward masking associated with saccadic eye movement. *Percept. Psychophys.* **30**, 62–70 (1981).
66. Castet, E., Jeanjean, S. & Masson, G. S. 'Saccadic suppression'- no need for an active extra-retinal mechanism. *Trends Neurosci.* **24**, 317–318 (2001).
67. Castet, E. Perception of intra-saccadic motion. in *Dynamics of visual motion processing* 141–160 (Springer US, 2010). doi:10.1007/978-1-4419-0781-3
68. Schiller, P. H. Single unit analysis of backward visual masking and metacontrast in the cat lateral geniculate nucleus. *Vision Res.* **8**, 855–866 (1968).
69. Macknik, S. L. & Livingstone, M. S. Neuronal correlates of visibility and invisibility in the

- primate visual system. *Nat. Neurosci.* **1**, 144–149 (1998).
70. Judge, S. J., Wurtz, R. H. & Richmond, B. J. Vision during saccadic eye movements. I. Visual interactions in striate cortex. *J. Neurophysiol.* **43**, 1133–1155 (1980).
71. Breitmeyer, B. Visual masking: Past accomplishments, present status, future developments. *Adv. Cogn. Psychol.* **3**, 9–20 (2007).
72. Breitmeyer, B. G. *et al.* Meta- and paracontrast reveal differences between contour- and brightness-processing mechanisms. *Vision Res.* **46**, 2645–2658 (2006).
73. Breitmeyer, B. G. Visual masking: past accomplishments, present status, future developments. *Adv. Cogn. Psychol.* **3**, 9–20 (2007).
74. Haynes, J. D., Driver, J. & Rees, G. Visibility reflects dynamic changes of effective connectivity between V1 and fusiform cortex. *Neuron* **46**, 811–821 (2005).
75. Tse, P. U., Martinez-Conde, S., Schlegel, A. A. & Macknik, S. L. Visibility, visual awareness, and visual masking of simple unattended targets are confined to areas in the occipital cortex beyond human V1/V2. *Proc. Natl. Acad. Sci. U. S. A.* **102**, 17178–17183 (2005).
76. Noda, H. & Adey, W. R. Retinal ganglion cells of the cat transfer information on saccadic eye movement and quick target motion. *Brain Res.* **70**, 340–345 (1974).
77. Geffen, M. N., De Vries, S. E. J. & Meister, M. Retinal ganglion cells can rapidly change polarity from off to on. *PLoS Biol.* **5**, 0640–0650 (2007).
78. Krueger, J. & Fischer, B. Strong periphery effect in cat retinal ganglion cells. Excitatory responses in ON- and OFF-center neurones to single grid displacements. *Exp. Brain Res.* **18**, 316–318 (1973).
79. Barlow, H. B., Derrington, A. M., Harris, L. R. & Lennie, P. The effects of remote retinal stimulation on the responses of cat retinal ganglion cells. *J. Physiol.* **269**, 177–194 (1977).

80. Enroth-Cugell, C. & Jakiela, H. G. Suppression of cat retinal ganglion cell responses by moving patterns. *J. Physiol.* **302**, 49–72 (1980).
81. Appleby, T. R. & Manookin, M. B. Neural sensitization improves encoding fidelity in the primate retina. *Nat. Commun.* **10**, 1–15 (2019).
82. Amthor, F. R., Tootle, J. S. & Gawne, T. J. Retinal ganglion cell coding in simulated active vision. *Vis. Neurosci.* **22**, 789–806 (2005).
83. Krishnamoorthy, V. Encoding of Saccadic Scene Changes in the Mouse Retina. (2012).
84. Garvert, M. M. & Gollisch, T. Local and global contrast adaptation in retinal ganglion cells. *Neuron* **77**, 915–28 (2013).
85. Zaghoul, K. A., Manookin, M. B., Borghuis, B. G., Boahen, K. & Demb, J. B. Functional circuitry for peripheral suppression in Mammalian Y-type retinal ganglion cells. *J Neurophysiol* **97**, 4327–4340 (2007).
86. Zhang, Y., Kim, I.-J., Sanes, J. R. & Meister, M. The most numerous ganglion cell type of the mouse retina is a selective feature detector. *Proc. Natl. Acad. Sci.* **109**, E2391–E2398 (2012).
87. Burr, D. D. C., Morrone, M. C. & Ross, J. Selective suppression of the magnocellular visual pathway during saccadic eye movements. *Nature* **371**, 511–513 (1994).
88. Merigan, W., Byrne, C. & Maunsell, J. Does primate motion perception depend on the magnocellular pathway? *J. Neurosci.* **11**, 3422–3429 (1991).
89. Skottun, B. C. On the use of spatial frequency to isolate contributions from the magnocellular and parvocellular systems and the dorsal and ventral cortical streams. *Neurosci. Biobehav. Rev.* **56**, 266–275 (2015).
90. Sommer, M. A. & Wurtz, R. H. Brain Circuits for the Internal Monitoring of Movements. *Annu. Rev. Neurosci.* **31**, 317–338 (2008).

91. Mayo, J. P. & Sommer, M. A. Neuronal Adaptation Caused by Sequential Visual Stimulation in the Frontal Eye Field. *J. Neurophysiol.* **100**, 1923–1935 (2008).
92. Chen, C.-Y. & Hafed, Z. M. A neural locus for spatial-frequency specific saccadic suppression in visual-motor neurons of the primate superior colliculus. *J. Neurophysiol.* **117**, 1657–1673 (2017).
93. Krock, R. M. & Moore, T. Visual sensitivity of frontal eye field neurons during the preparation of saccadic eye movements. *J. Neurophysiol.* **116**, 2882–2891 (2016).
94. Chen, C.-Y., Ignashchenkova, A., Thier, P. & Hafed, Z. M. Neuronal response gain enhancement prior to microsaccades. *Curr. Biol.* **25**, 2065–2074 (2015).
95. Kemmler, R., Schultz, K., Dedek, K., Euler, T. & Schubert, T. Differential regulation of cone calcium signals by different horizontal cell feedback mechanisms in the mouse retina. *J. Neurosci.* **34**, 11826–11843 (2014).
96. Sakatani, T. & Isa, T. Quantitative analysis of spontaneous saccade-like rapid eye movements in C57BL/6 mice. *Neurosci. Res.* **58**, 324–331 (2007).
97. Williams, D. L. Light and the evolution of vision. *Eye* **30**, 173–178 (2016).
98. Schmidt, M. Neurons in the cat pretectum that project to the dorsal lateral geniculate nucleus are activated during saccades. *J Neurophysiol* **76**, 2907–2918 (1996).
99. Cucchiaro, J. B., Uhlrich, D. J. & Sherman, S. M. Ultrastructure of synapses from the pretectum in the A-laminae of the cat's lateral geniculate nucleus. *J. Comp. Neurol.* **334**, 618–630 (1993).
100. Rajkai, C. *et al.* Transient cortical excitation at the onset of visual fixation. *Cereb. Cortex* **18**, 200–209 (2008).
101. Lee, D. & Malpeli, J. Effects of saccades on the activity of neurons in the cat lateral geniculate nucleus. *J. Neurophysiol.* 922–936 (1998).

102. Shapley, R. & Enroth-Cugell, C. Chapter 9 Visual adaptation and retinal gain controls. *Prog. Retin. Res.* **3**, 263–346 (1984).
103. Krishnamoorthy, V., Weick, M. & Gollisch, T. Sensitivity to image recurrence across eye-movement-like image transitions through local serial inhibition in the retina. *Elife* e22431 (2017). doi:10.7554/eLife.22431
104. Passaglia, C. L., Freeman, D. K. & Troy, J. B. Effects of remote stimulation on the modulated activity of cat retinal ganglion cells. *J. Neurosci.* **29**, 2467–2476 (2009).
105. Schreyer, H. M. & Gollisch, T. Nonlinearities in retinal bipolar cells shape the encoding of artificial and natural stimuli. *bioRxiv* 1–40 (2020). doi:10.1101/2020.06.10.144576

List of publications and statement of contributions

Publication 1

Saad Idrees*, Matthias P. Baumann*, Felix Franke, Thomas A. Münch, Ziad M. Hafed. Perceptual saccadic suppression starts in the retina. *Nature Communications*, 2020.

* Equal contributions

Framework: In this paper, we use human psychophysics to understand the visual mechanisms underlying perceptual saccadic suppression; and animal retina electrophysiology to show that the underlying visual mechanisms start already at the level of the retina.

Contributions: TAM and ZMH conceptualized the overall study. I together with MB, TAM, and ZMH, designed the overall study and the experiments. I performed the ex vivo retina electrophysiology experiments and analyzed its data together with FF and TAM. MB performed the human psychophysics experiments and analyzed it together with ZMH. I together with the other authors interpreted the data and wrote the manuscript.

Publication 2

Saad Idrees, Matthias P. Baumann, Maria M. Korympidou, Timm Schubert, Alexandra Kling, Katrin Franke, Ziad M. Hafed, Felix Franke, Thomas A. Münch. Suppression without inhibition: A novel mechanism in the retina accounts for saccadic suppression. *Submitted*.

<https://doi.org/10.1101/2020.08.21.261198>

Framework: In this paper, we describe the detailed mechanisms of retinal saccadic suppression using electrophysiology of ex vivo mouse, pig and macaque retinae 2-photon calcium imaging computational modeling and human psychophysics.

Contributions: TAM conceptualized the study. I designed the overall study together with TAM and under his supervision, designed the experimental paradigms for ex vivo retina electrophysiology and imaging. I performed ex vivo mouse and pig retinae electrophysiology

experiments using multielectrode arrays. I analyzed the electrophysiology data and also the imaging data which was collected by MK and KF. In addition, I implemented a computational model of retinal ganglion cells that was developed by FF. Together with other authors, I interpreted the data. I wrote the first version of the manuscript and produced all the figures.

KF helped in interpreting the imaging data and reviewing the overall manuscript. AK conducted macaque retina electrophysiology. MB and ZMH performed, analyzed and interpreted human psychophysics experiments. In addition, ZMH contributed to overall interpretation of the data and writing the manuscript. TS helped in analyzing and interpreting the data and reviewing the manuscript. FF contributed to design of the experiments, interpreting the data, supervision of computational modeling, and in writing the manuscript. TAM supervised the overall study and contributed to all aspects of this paper.

Chapter 1

Perceptual saccadic suppression starts in the retina

Saad Idrees, Matthias P. Baumann, Felix Franke, Thomas A. Münch, Ziad M. Hafed

Nature Communications | (2020) 11:1977

<https://doi.org/10.1038/s41467-020-15890-w>

ARTICLE




<https://doi.org/10.1038/s41467-020-15890-w>

OPEN

Perceptual saccadic suppression starts in the retina

Saad Idrees ^{1,5}, Matthias P. Baumann^{1,2,5}, Felix Franke³, Thomas A. Münch^{1,4}  & Ziad M. Hafed ^{1,2} 

Visual sensitivity, probed through perceptual detectability of very brief visual stimuli, is strongly impaired around the time of rapid eye movements. This robust perceptual phenomenon, called saccadic suppression, is frequently attributed to active suppressive signals that are directly derived from eye movement commands. Here we show instead that visual-only mechanisms, activated by saccade-induced image shifts, can account for all perceptual properties of saccadic suppression that we have investigated. Such mechanisms start at, but are not necessarily exclusive to, the very first stage of visual processing in the brain, the retina. Critically, neural suppression originating in the retina outlasts perceptual suppression around the time of saccades, suggesting that extra-retinal movement-related signals, rather than causing suppression, may instead act to shorten it. Our results demonstrate a far-reaching contribution of visual processing mechanisms to perceptual saccadic suppression, starting in the retina, without the need to invoke explicit motor-based suppression commands.

¹Werner Reichardt Centre for Integrative Neuroscience, Tübingen University, 72076 Tübingen, Germany. ²Hertie Institute for Clinical Brain Research, Tübingen University, 72076 Tübingen, Germany. ³Bio Engineering Laboratory, ETH Zürich, 4058 Basel, Switzerland. ⁴Institute for Ophthalmic Research, Tübingen University, 72076 Tübingen, Germany. ⁵These authors contributed equally: Saad Idrees, Matthias P. Baumann. email: thomas.muench@uni-tuebingen.de; ziad.m.hafed@cin.uni-tuebingen.de

Saccadic eye movements are a prominent feature of visual behavior; they allow successive sampling of information from the environment. However, from the perspective of visual information flow into the brain, these rapid eye movements constitute highly disruptive events, introducing spurious motions that should normally go perceptually unnoticed, or canceled. The question of how and why such perceptual cancellation takes place has intrigued philosophers and scientists for many decades^{1–4}. Indeed, sensitivity to brief peri-saccadic visual probes is strongly impaired, in a phenomenon known as saccadic suppression that has repeatedly been demonstrated in a multitude of experiments^{5–14}.

Despite the robustness of saccadic suppression as a perceptual phenomenon, the mechanisms behind it remain highly controversial. On the one hand, perceptual suppression may arise through internal knowledge of planned eye movements and their associated motor commands^{5,12,15–18}. According to this popular view, eye movement commands are a necessary prerequisite for saccadic suppression: a movement-related signal^{16,17}, such as corollary discharge from (pre-)motor areas, may act as a suppressive command for visual neurons to cause perceptual suppression, and maybe even in a pathway-selective manner¹⁰.

On the other hand, perceptual saccadic suppression could also arise as a result of the visual consequences of retinal image shifts^{2,19–30}. After all, the early visual system, including the retina, is a highly sensitive light sensing device, and can capture visual transients associated with saccade-induced retinal image shifts. Such early processing of visual transients could modulate the retinal output, jumpstarting an image processing cascade to mediate perceptual suppression.

In this study, rather than arguing either strictly for or against one of these seemingly contrasting hypotheses, we asked to what extent they might interact with and support each other to ultimately serve perception. We were specifically motivated by the fact that the very first visual processing stage in the brain, the retina, is not only sensitive to visual transients (such as saccade-induced image shifts), but it also possesses rich image processing circuitry that could regularize the visual disruptions^{31–35} caused by saccades. We therefore asked: how much of the characteristics of perceptual saccadic suppression can be explained by visual-only mechanisms? And, to the extent that there are visual-only mechanisms, would the first neural locus for them indeed be the very first stage of visual processing in the brain, the retina?

We used a multi-disciplinary approach in which we experimentally mimicked the visual consequences of saccades and recorded neural activity from *ex vivo* retinæ of different animal models. We also measured human perceptual reports using both real saccades and saccade-like image displacements to simulate the saccadic visual flow. We found a surprisingly far-reaching contribution of visual processing mechanisms to perceptual saccadic suppression, starting in the retina, without the need to invoke explicit motor-based suppression commands. Intriguingly, the role of motor-based commands seems to be the opposite of what has been proposed before. Rather than sending an explicit suppressive command to reduce visual system sensitivity, motor-based commands instead seem to minimize the duration of visually derived saccadic suppression.

Results

Perceptual saccadic suppression depends on image content. We first asked human subjects to generate saccades across textured backgrounds, akin to how saccades may be made in real life. Subjects viewed coarse or fine textures (Fig. 1a, Methods and Supplementary Fig. 1). Starting from one of four locations on the display, subjects made 4.8 deg saccades towards display center

(Fig. 1a, left). We varied saccade onset and endpoint locations, as well as texture images, across trials to avoid subjects remembering specific texture patterns. At a random time, a luminance pedestal (probe flash) was added to the texture background, for one display frame (~12 ms), at one of four locations relative to saccade endpoint (7 deg eccentricity; Fig. 1a, right). Subjects localized the probe flash (4-alternative-forced-choice paradigm), and we analyzed how well they did so. We ensured that the retinal region of flash location was stimulated with the background texture (rather than the edge of the monitor or the black surround of the dark laboratory) throughout any given trial, and that the probe flash was larger than the image blobs in the coarse texture, such that average luminance variation within each flash was matched across trials and textures. Coarse and fine textures had blobs that approximated the sizes of retinal ganglion cell (RGC) or retinal bipolar cell receptive fields, respectively, at the retinal flash locations³⁶ (Methods).

For both coarse and fine textures, subjects were strongly impaired in their ability to localize peri-saccadic flashes, thus experiencing strong perceptual saccadic suppression (Fig. 1b, c). Importantly, the suppression clearly depended on background visual images: it started earlier and recovered later with saccades across coarse rather than fine textures (Fig. 1d; the highlighted time intervals show significant differences between coarse and fine textures with $p < 0.001$, cluster-based random permutation test^{37,38}). Moreover, the peak amount of suppression was stronger with the coarse textures (Fig. 1d). However, for both types of textures, performance reached a floor effect, masking an even larger difference (addressed below and in Fig. 2). This dependence of perceptual saccadic suppression on background texture was robust across individual subjects (Supplementary Fig. 2a; also see Supplementary Fig. 4 for further individual subject effects).

To rule out the possibility that flashes might simply be easier to see over the fine texture, we performed a control experiment in which we collected full psychometric curves of perceptual performance during fixation. Without any saccades, probe flash visibility was identical over coarse and fine textures (Supplementary Fig. 3a, b). Therefore, the image dependence demonstrated in Fig. 1 was related to saccadic suppression itself and not to the baseline visibility of brief flashes over the different textures. Similarly, analyzing eye movement properties showed that the results of Fig. 1 were also not due to different saccade kinematics for the different textures (Supplementary Fig. 3c, d).

We next employed a more sensitive procedure to evaluate perceptual thresholds. We repeated the same experiment of Fig. 1 on five subjects (three being the same as in the earlier experiment). This time, however, we collected full psychometric curves (Methods; similar to Supplementary Fig. 3a, b). As collecting full psychometric curves for each texture and each time point relative to saccade onset would be a very data-intensive endeavor, we expedited data collection by implementing a real-time saccade detection algorithm, described by Chen and Hafed³⁹. This allowed us to present the probe flash at only four defined times after online saccade detection, strategically chosen to evaluate peak suppression (shortly after saccade onset), as well as the recovery time course after a saccade. We used an adaptive QUEST⁴⁰ procedure to estimate perceptual threshold per condition and flash time (Methods), with perceptual threshold (for the purposes of QUEST) being defined as the flash contrast value resulting in 62.5% correct performance. Besides the QUEST procedure, we also collected more trials showing different flash contrast levels relative to the estimated threshold, in order to obtain full psychometric curves. The results are shown in Fig. 2, and they match those of Fig. 1: relative to the baseline psychometric curves of flash visibility long after saccades (dashed

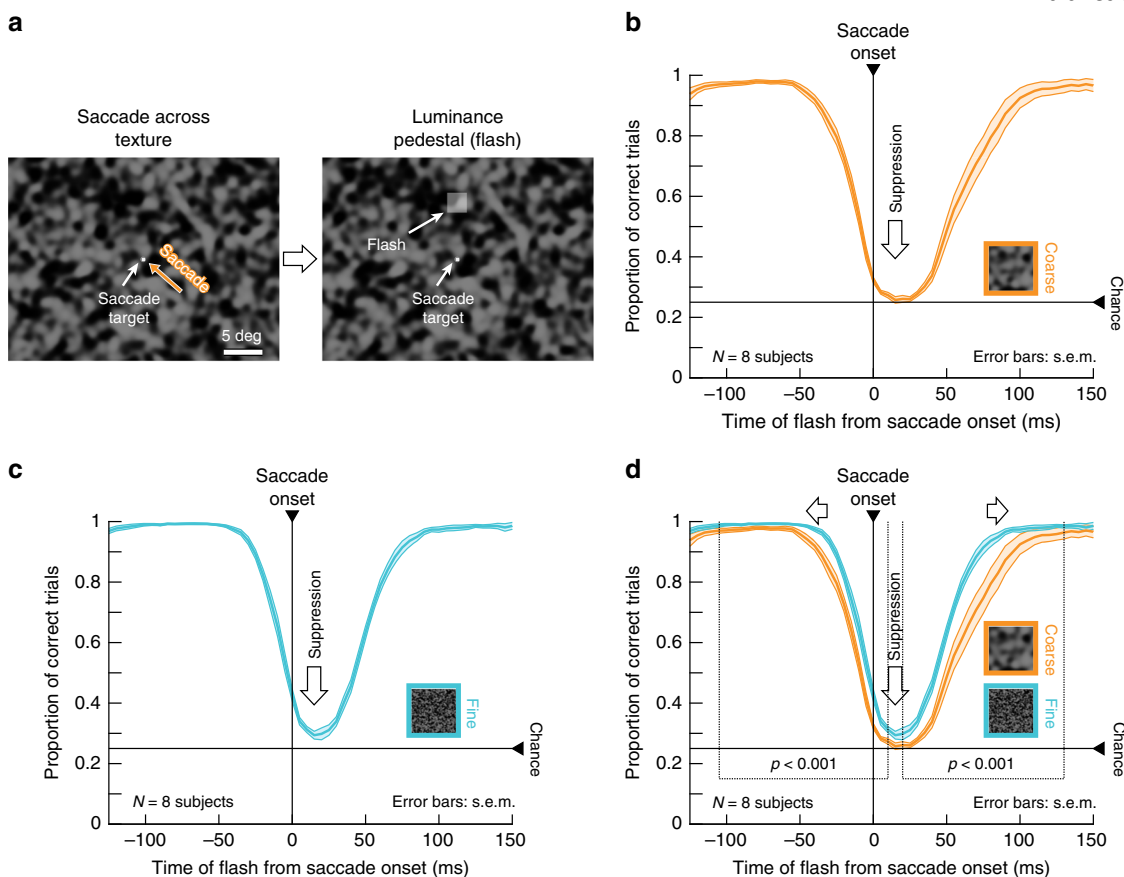


Fig. 1 Image dependence of perceptual saccadic suppression. **a** Human subjects generated saccades across a texture (here: coarse) from one of four diagonal locations towards display center (here: from the lower right). A luminance pedestal was flashed peri-saccadically at one of four locations around display center (right, left, up, or down; here: up). The insets in **c**, **d** show fine textures for comparison; also see Supplementary Fig. 1 and Methods. **b**, **c** Subjects failed to localize peri-saccadic flashes with both coarse (**b**) and fine (**c**) textures (perceptual reports were binned as a function of flash time from saccade onset using 50-ms bins moving in steps of 5 ms). **d** Perceptual suppression started earlier and lasted longer with a coarse background (also see Fig. 2). The highlighted times denote significantly different ($p < 0.001$, two-tailed random permutation test) time clusters between coarse and fine conditions (Methods). Curves show averages \pm s.e.m. of individual subjects' suppression curves ($N = 8$). Supplementary Figs. 2, 3 show individual subject results, as well as controls for flash visibility (in the absence of saccades) and saccade motor variability.

curves), peri-saccadic psychometric curves were clearly shifted towards higher thresholds (Fig. 2a–d), consistent with Fig. 1. Critically, the more sensitive approach of full psychometric curves revealed that perceptual saccadic suppression was much stronger for coarse than fine textures at peak suppression; that is, perceptual thresholds (defined as luminance increments required for a specific correct performance level; Methods) near peak suppression were higher for coarse than fine textures (Fig. 2e). Supplementary Fig. 4 shows the individual subject psychometric curves.

To summarize, perceptual saccadic suppression is associated with a visual component directly influencing its strength and time course: saccades across coarse textures are associated with both stronger and longer-lasting perceptual suppression than saccades across fine textures, even when eye movement kinematics (and thus underlying motor commands) are controlled for.

Perceptual saccadic suppression originates in the retina. To test if this visual component of perceptual saccadic suppression originates in the retina, we isolated mouse and pig retinae and performed multi-electrode array recordings (Methods). We continuously exposed each retina to coarse and fine textures, matched to ganglion and bipolar cell receptive field sizes in the recorded species (Supplementary Fig. 1). We rapidly translated

the textures to simulate saccade-like image displacements (Fig. 3a). Such displacements can robustly activate RGCs, as is evident from the example mouse RGC shown in Fig. 3b. In fact, most recorded RGCs (mouse: 83% of 1,423 cells, pig: 73% of 394 cells) responded to texture displacements, indicating that saccade-induced visual transients during active gaze behavior constitute strong signals to the retina. Next, at different times relative to texture displacements, we introduced a luminance pedestal (probe flash) to the entire texture for 16 or 33 ms, similar in principle to the perceptual experiments of Figs. 1 and 2. Such flashes, when presented in isolation (that is, temporally removed from texture displacements), elicited responses in a sizable fraction of RGCs (baseline response; mouse: 688 of 1423 RGCs; pig: 228 of 394 RGCs). This allowed us to evaluate the consequences of texture displacements on flash responses in these cells—conceptually similar to the experiments in Figs. 1 and 2 (in which we evaluated the consequences of saccades on flash perception). The same example RGC of Fig. 3b showed much suppressed neural responses to the flash when it was presented immediately after texture displacements compared to baseline (Fig. 3c, d). This suppression of flash-induced responses (Fig. 3d) looks remarkably similar to suppression of visual responses in, say, macaque superior colliculus for stimuli presented after real saccades^{13,14,41}. Thus, neuronally, there does exist “saccadic suppression” of visual sensitivity at the very first stage of visual processing, the retina,

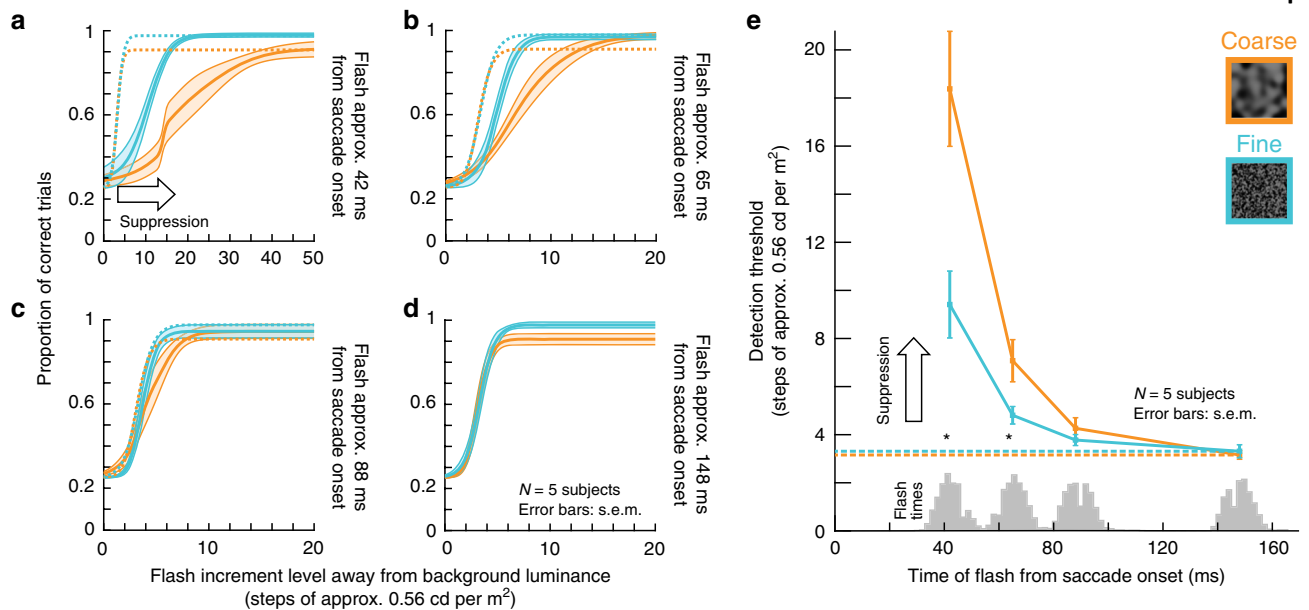


Fig. 2 Image-dependent elevation of perceptual thresholds across saccades. **a–d** Full psychometric curves of flash visibility with the paradigm like in Fig. 1. Solid curves: mean \pm s.e.m. of the individual psychometric curves of $N = 5$ subjects (individual results in Supplementary Fig. 4). Dashed curves: psychometric curves near recovery from suppression long after saccades (same data as in **d**). Orange and light-blue: data for coarse and fine textures, respectively. **a** For flashes approximately 42 ms from saccade onset, strong perceptual saccadic suppression occurred (compare solid with dashed curves), and coarse textures yielded stronger perceptual saccadic suppression than fine textures. **b** At approximately 65 ms after saccade onset, substantial recovery was visible (note the different x-axis scale from **a**), still with stronger suppression for coarse than fine textures. **c, d** Recovery of visibility continued at later times after saccade onset (88 ms, **c**, and 168 ms, **d**), consistent with Fig. 1. **e** Perceptual detection thresholds (i.e., flash luminance levels needed to achieve a certain correct performance rate; Methods) from **a–d** as a function of flash times from saccade onset. Since flash times were determined using online saccade detection, there was some variability of actual displayed flash times; the gray histograms on the x-axis show the actual distributions of flash times for each group of data from **a–d**. Asterisks denote significant ($p < 0.05$) differences between coarse and fine textures (two-tailed two-sample t -test). Exact p -values at each flash time: 42 ms ($p = 0.012$) and 65 ms ($p = 0.044$). The dashed horizontal lines show the detection thresholds at the longest flash times (**d**); note that these thresholds are also similar to those in the control experiments for visibility (Supplementary Fig. 3a, b).

and it looks qualitatively indistinguishable from saccadic suppression at downstream neural sites^{13,14,41} and, indeed, perception (Figs. 1 and 2).

Importantly, retinal “saccadic suppression” strongly depended on background texture (Fig. 3e), exactly like in perception (Figs. 1 and 2). Specifically, we quantified retinal “saccadic suppression” by calculating a neuronal modulation index, defined as $(r_d - r_b) / (r_d + r_b)$. r_d is the response strength to the probe flash presented with a delay d relative to the texture displacement onset, and r_b is the baseline response strength (Methods). The great majority of RGCs were strongly suppressed during and after texture displacements (indicated by negative modulation indices), with gradual recovery afterwards (Fig. 3e; Supplementary Fig. 5 shows the underlying population data), and suppression was more pronounced for coarse than fine textures (Fig. 3e and Supplementary Fig. 5). These results are consistent with the dependence of human perceptual saccadic suppression on background texture statistics (Figs. 1 and 2), suggesting that this dependence starts already in the retina.

We also found that retinal “saccadic suppression” was a robust phenomenon across many different RGCs with diverse properties (Supplementary Fig. 6). Further, it occurred both in mouse (Fig. 3e, left) and pig (Fig. 3e, right) retinæ, two mammalian species with different native oculomotor behavior, different lifestyles, and different eye sizes. Thus, our results so far suggest that perceptual saccadic suppression (Figs. 1 and 2), including its dependence on background texture statistics, most likely originates in the retina (Fig. 3), being the outcome of very general retinal-circuit mechanisms that are conserved across species.

Stimulus–stimulus interactions underlie retinal suppression.

To understand the underlying mechanisms for “saccadic suppression” in the retina in more detail, we explored its properties using different analyses and additional stimulus manipulations. First, we wondered about neural activity saturation, given that saccade-like texture displacements before flash onset could activate RGCs (e.g., Fig. 3b). Specifically, if RGC activity is elevated by the texture displacement, then any subsequent flash-induced response could have caused the cell to reach activity saturation. However, this was not sufficient to explain our results. For example, we observed that suppression often also occurred in RGCs that did not respond strongly to the texture displacements in the first place (Fig. 4a).

Second, we investigated whether retinal “saccadic suppression” critically depended on particular saccade-like speed profiles. In the original experiments (Fig. 3), we simulated saccade-induced image translation speeds to the best of our abilities (given display refresh rates; Methods). However, if we replaced the original translation over 100 ms with a sudden texture jump in one display update (an infinite-speed texture jump), then the same suppression took place, with similar dependence on texture statistics (Fig. 4b). Similarly, in yet another manipulation, we presented the probe flash before the texture displacement; the second response (now to the texture displacement) was suppressed (Fig. 4c). This suggests that retinal “saccadic suppression” can be explained by general stimulus–stimulus interaction effects. As a result, it is a phenomenon that is unlikely to critically depend (qualitatively) on the specific oculomotor repertoire of either mice, pigs, or humans.

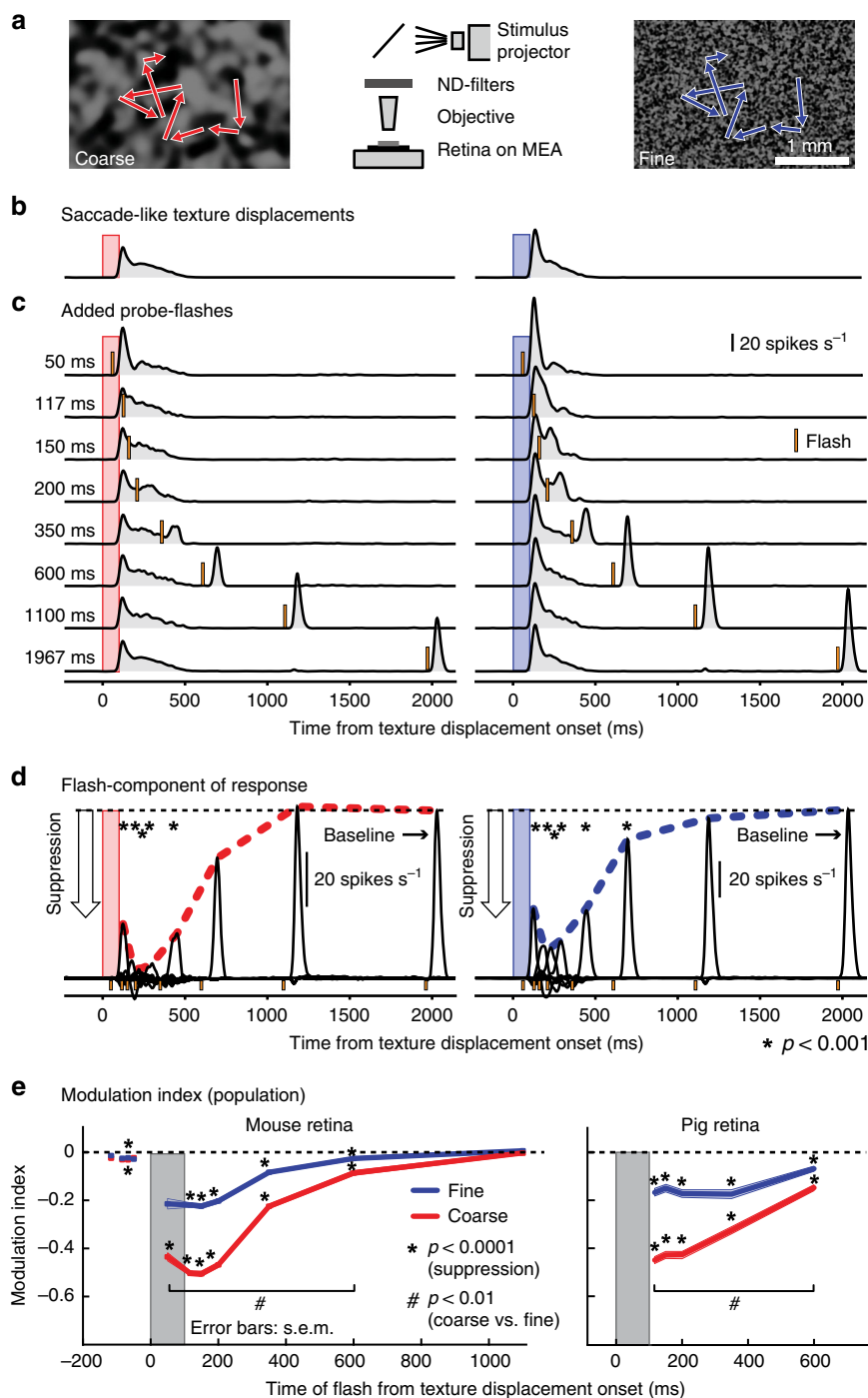


Fig. 3 “Saccadic suppression” in retina. **a** We recorded RGC activity from ex vivo retinæ placed on multi-electrode arrays (MEA). A coarse (left) or fine (right) texture was repeatedly translated in a saccade-like manner (red or blue scan paths), and we presented brief visual flashes at different times relative to “saccades” (similar to Fig. 1). **b, c** Average activity of an example RGC to 39 texture displacements alone (**b**) or followed by probe flashes at different time delays (**c**). Red and blue bars show the timings of the texture displacements; orange bars indicate probe flashes. Flash-induced responses were strongly suppressed immediately following saccade-like texture displacements. **d** Isolated flash responses of the same RGC obtained by subtracting responses in **b** from those in **c**. Dashed colored lines highlight the time courses of retinal “saccadic suppression” relative to baseline flash-induced responses. Asterisks indicate flash-induced responses that are significantly suppressed from baseline ($p < 0.001$, one-tailed sign test; Methods). **e** Population modulation index (mean \pm s.e.m.) across individual RGCs highlighting retinal “saccadic suppression” (Methods; negative values indicate suppressed flash-induced neural responses). Both mouse and pig retinæ showed strong suppression during and after texture displacements, which also depended on texture statistics (similar to perception; Figs. 1 and 2). Asterisks indicate statistically significant suppression ($p < 0.0001$, two-tailed Wilcoxon signed-rank test; Methods). Hash symbols indicate significant differences in suppression between coarse and fine textures ($p < 0.01$, two-tailed Wilcoxon signed-rank test; Methods). Exact p -values are indicated in Supplementary Fig. 5. The numbers of recorded cells at each flash time in **e** were: mouse RGCs: $N = 179$ (-177 ms, -84 ms, -50 ms), 161 (-67 ms), 136 (50 ms), 527 (117 ms), 520 (150 ms), 502 (200 ms, 600 ms), 688 (350 ms), 345 (1100 ms); pig RGCs: $N = 228$ for each time point. Supplementary Figs. 5 and 6 show the population data underlying panel **e**.

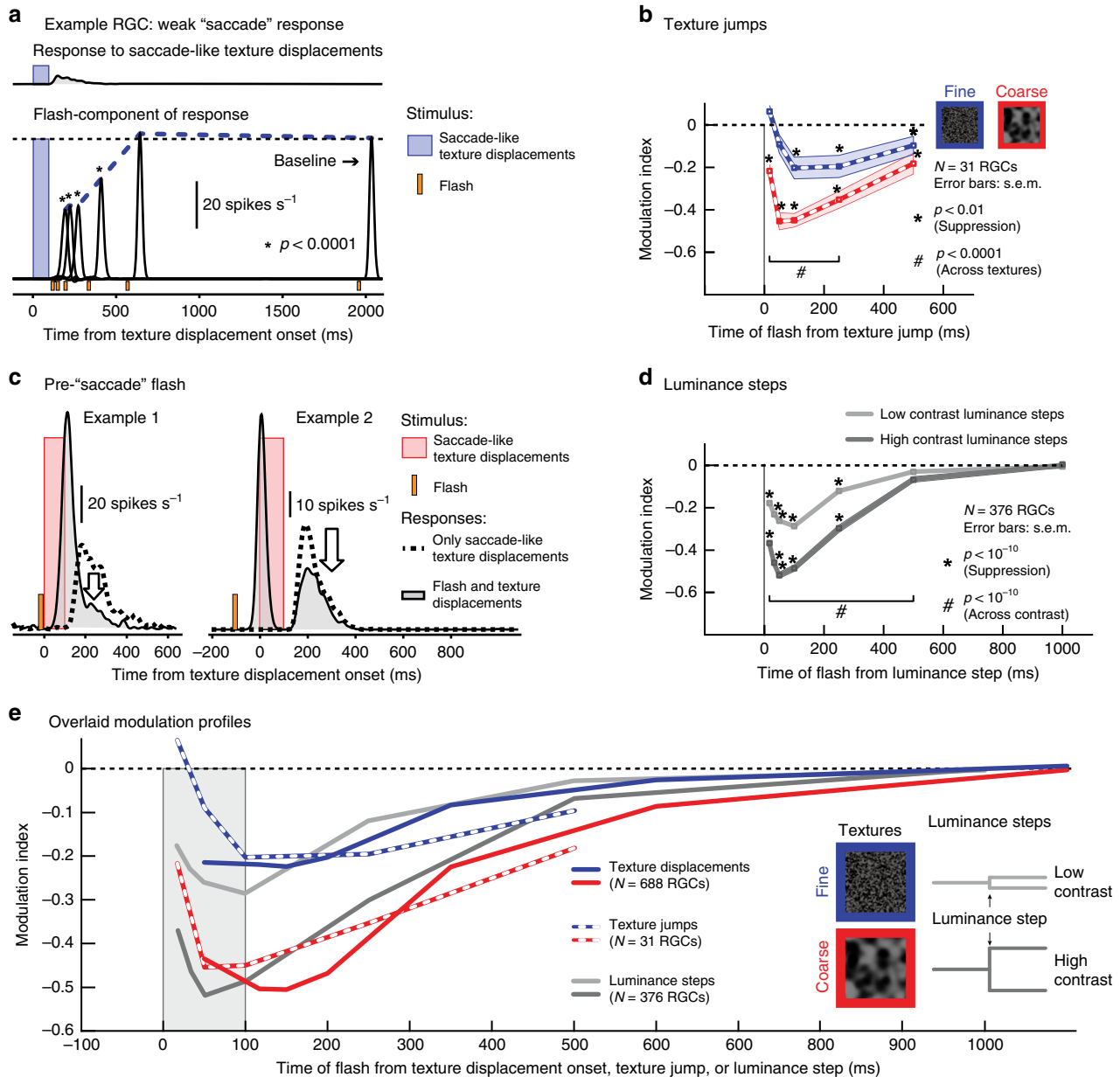


Fig. 4 Stimulus-stimulus interactions in retinal "saccadic suppression". **a** Example RGC responding only weakly to texture displacements (top), but nevertheless exhibiting strong suppression of flash-induced responses (bottom; curves plotted at the same scale). Asterisks indicate significantly suppressed flash-induced responses ($p < 0.0001$, one-tailed sign test, $N = 39$ independent observations; Methods). Exact p -values at each flash time: 117 ms ($p = 10^{-5}$), 150 ms (10^{-5}), 200 ms (10^{-6}), 350 ms (10^{-5}), and 600 ms (0.26). **b** Population modulation index (mean \pm s.e.m., $N = 31$ RGCs) when the textures jumped from their start to end positions instantaneously. Strong suppression (* $p < 0.01$, two-tailed Wilcoxon signed-rank test) and significant differences between coarse (red) and fine (blue) textures (# $p < 0.0001$, two-tailed Wilcoxon signed-rank test) still occurred. Exact p -values at each flash time (coarse, fine, across): 17 ms ($p = 10^{-6}$, $p = 0.027$, $p = 10^{-6}$), 50 ms (10^{-6} , 0.021, 10^{-6}), 100 ms (10^{-5} , 0.001, 10^{-6}), 250 ms (10^{-6} , 0.001, 10^{-4}), and 500 ms (0.002, 0.04, 0.06). **c** Two example RGCs showing that a flash before saccade-like texture displacements suppressed the response to the displacements, suggesting that stimulus-stimulus interactions drive retinal "saccadic suppression". **d** Population modulation index (mean \pm s.e.m., $N = 376$ RGCs) for a paradigm similar to **b**, but with textures replaced by spatially uniform backgrounds of different intensity (i.e., instantaneous luminance steps). Suppression of flash-induced responses was preserved (* $p < 10^{-10}$, two-tailed Wilcoxon signed-rank test), and differences between low-contrast (light gray) and high-contrast (dark gray) luminance steps (# $p < 10^{-10}$, two-tailed Wilcoxon signed-rank test) resembled the differences between fine and coarse texture jumps in **b**. Exact p -values at each flash time (high contrast, low contrast, across contrasts): 17 ms ($p = 10^{-48}$, $p = 10^{-32}$, $p = 10^{-43}$), 33 ms (10^{-55} , 10^{-41} , 10^{-48}), 50 ms (10^{-60} , 10^{-46} , 10^{-51}), 100 ms (10^{-57} , 10^{-50} , 10^{-42}), 250 ms (10^{-39} , 10^{-33} , 10^{-26}), 500 ms (10^{-8} , 0.02, 10^{-8}) and 1000 ms (0.9, 0.7, 0.8). **e** Overlaid modulation profiles from texture displacements (Fig. 3e), texture jumps (**b**), and contrast steps (**d**). Coarse texture displacements, coarse texture jumps, and high-contrast luminance steps had similar effects; and so did fine texture displacements, fine texture jumps, and low-contrast luminance steps.

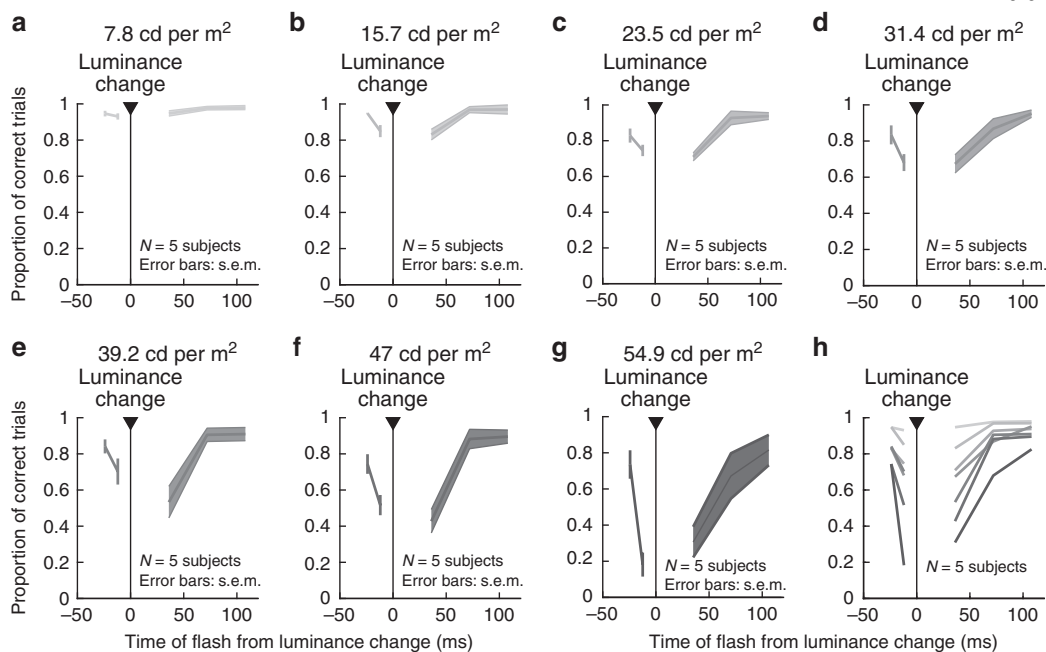


Fig. 5 Stimulus-stimulus interactions in perceptual suppression without saccades (similar experiment to the retinal paradigm of Fig. 4d). Subjects fixated and detected brief probe flashes as in the experiments of Figs. 1 and 2; here, the flashes happened around the time of a luminance step (i.e., a sudden change in background luminance) instead of a saccade. The title above each panel indicates the absolute value of the luminance change that took place. **a–g** Proportion of correct responses as a function of flash time from the time of background luminance step. There was progressively stronger perceptual suppression with increasing contrast of the luminance step, consistent with the retinal results of Fig. 4d. **h** Summary of panels **a–g**. Darker colors denote larger absolute values of background luminance changes. Since coarse textures (Figs. 1–4) presumably cause larger contrast variations over retinal receptive fields, this suggests that the image dependence of perceptual saccadic suppression (Figs. 1 and 2) is mediated by stimulus-stimulus interaction effects originating in the retina (Fig. 4d).

The most compelling evidence for stimulus-stimulus interactions underlying retinal “saccadic suppression” came from experiments replacing the texture displacements with structure-free luminance steps (Fig. 4d). Specifically, instead of a background texture that we displaced, we exposed the retina to a uniform gray background and introduced a sudden luminance increase or decrease as the visual transient. This luminance step was either of high (± 0.20 to ± 0.40 Michelson contrast) or low contrast (± 0.03 to ± 0.15 Michelson contrast, Methods). The probe flash then followed the luminance step as in the original experiments. Flash responses were indeed suppressed after luminance steps, and this suppression was stronger after high- than after low-contrast visual transients. Interestingly, suppression after high- and low-contrast luminance steps resembled suppression after coarse and fine texture displacements, respectively (e.g., Fig. 3), both in terms of time course and strength (Fig. 4e). Presumably, moving the larger blobs of a coarse texture across the retina would result in high-contrast changes within individual relevant retinal receptive fields (e.g., from a bright blob in a receptive field before texture displacement to a dark blob thereafter), while the smaller blobs in the fine texture would be spatially averaged within receptive fields, resulting in low-contrast changes.

When we next performed human psychophysical experiments mimicking the luminance step retinal experiments, we found remarkably congruent results (Fig. 5). Specifically, subjects maintained saccade-free fixation, and we changed the luminance of the homogenous background (Methods). At random times relative to the change, we presented brief probe flashes like in Fig. 1. All subjects experienced clear perceptual suppression around the luminance steps. Importantly, perceptual suppression depended on the contrast of the luminance change: with a small change in background luminance, suppression was minimal; with

a large change, suppression was strong and long lasting (Fig. 5). As we discuss below, we also observed perceptual suppression even for flashes before the background luminance changes; this matters for interpretations of pre-movement perceptual saccadic suppression (e.g., see Fig. 6 below).

Therefore, the most likely mechanism for retinal “saccadic suppression” is that it emerges as a result of retinal-circuit image processing that is initiated by visual transients; whether they be through texture displacements, infinite-speed texture jumps, or luminance steps (Fig. 4e). It is intriguing that such stimulus-stimulus retinal effects may be inherited deep into the brain’s visual processing hierarchy, including cortical (frontal eye field) and subcortical (superior colliculus) areas⁴² that are implicated in saccadic suppression^{14,41,43,44}.

Motor-related signals shorten visually derived suppression. In retina, we not only observed similarities to perceptual saccadic suppression (the presence of retinal suppression, and its dependence on texture statistics or luminance step contrast). We additionally noticed that retinal “saccadic suppression” was particularly long lasting (e.g., Fig. 3e). To explore the potential perceptual implications of this observation, we next asked our subjects to maintain fixation while we introduced saccade-like texture displacements in a manner similar to the retinal experiments of Fig. 3 (Fig. 6a); brief flashes occurred around the time of these “simulated saccades” like in Fig. 1. This time, due to the absence of real saccades (trials with microsaccades were excluded), non-visual (motor-related) components could not influence flash-induced neural responses and perception. Still, given the retinal results (Figs. 3 and 4), we had three hypotheses that we validated: (1) strong perceptual suppression still occurred regardless of texture details (Fig. 6b, c);

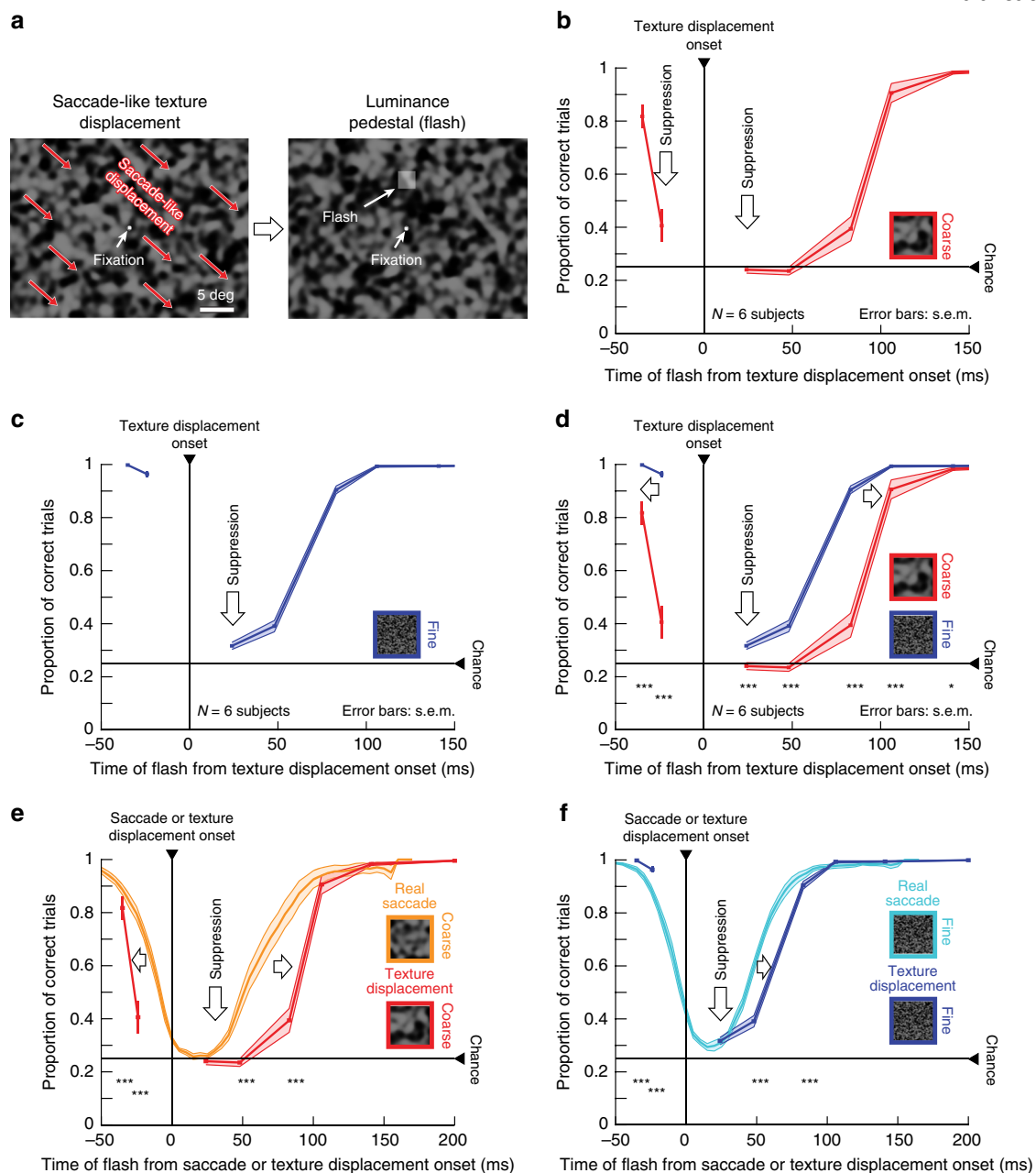


Fig. 6 Image dependence of perceptual suppression without saccades. **a** Rapid texture displacements simulating saccade-like image displacements, similar to the retina experiments (Fig. 3). We used the same flashes and simulated saccade directions as in Fig. 1. The example shows a coarse texture (fine textures shown in insets in **c**, **d**, and **f**). **b**, **c** Pre-, peri-, and post-displacement perceptual suppression (mean \pm s.e.m. over $N = 6$ individual subjects) occurred for both coarse (**b**) and fine (**c**) textures. **d** As with real saccades (Fig. 1), suppression started earlier and lasted longer with coarse textures (also compare to similar retinal effects in Fig. 3e). Notably, pre-displacement suppression depended on texture statistics, just like with real saccades (Fig. 1). **e**, **f** Simulated saccades were associated with significantly longer suppression than real saccades for both fine and coarse textures (e, which were most effective in causing suppression overall), flashes presented before the “saccade” event were suppressed earlier in the simulated saccade condition than in the real saccade condition (also see Fig. 7); thus, prolonged suppression with texture displacements was not restricted to post-displacement flashes only. Asterisks denote significant differences between coarse and fine textures (**d**) or between real and simulated saccades (**e**, **f**) at each indicated time point (χ^2 tests with Bonferroni corrections; * $p < 0.005$ in **d** and $p < 0.007$ in **e**, **f**; *** $p < 0.0001$ in **d** and $p < 0.00014$ in **e**, **f**). Supplementary Fig. 2 shows individual subject results.

(2) suppression strength and duration depended on texture statistics (Fig. 6d); and (3) suppression outlasted suppression with real saccades (Fig. 6e, f). This last point, in particular, suggests that motor-related saccadic signals may act to shorten the perceptual interruption resulting from visually induced saccadic suppression, while maintaining the putatively retinally determined (Figs. 3 and 4) dependence on image statistics. Note

also that the first and third points above are consistent with earlier observations by Diamond et al.¹⁶

In humans, we observed perceptual suppression also prior to saccade-like texture displacements^{19,26} (Fig. 6). This was again consistently dependent on texture statistics (Fig. 6b–d; also see Fig. 7 below for additional evidence). Further, like the suppression after saccade onset, this pre-saccadic perceptual suppression

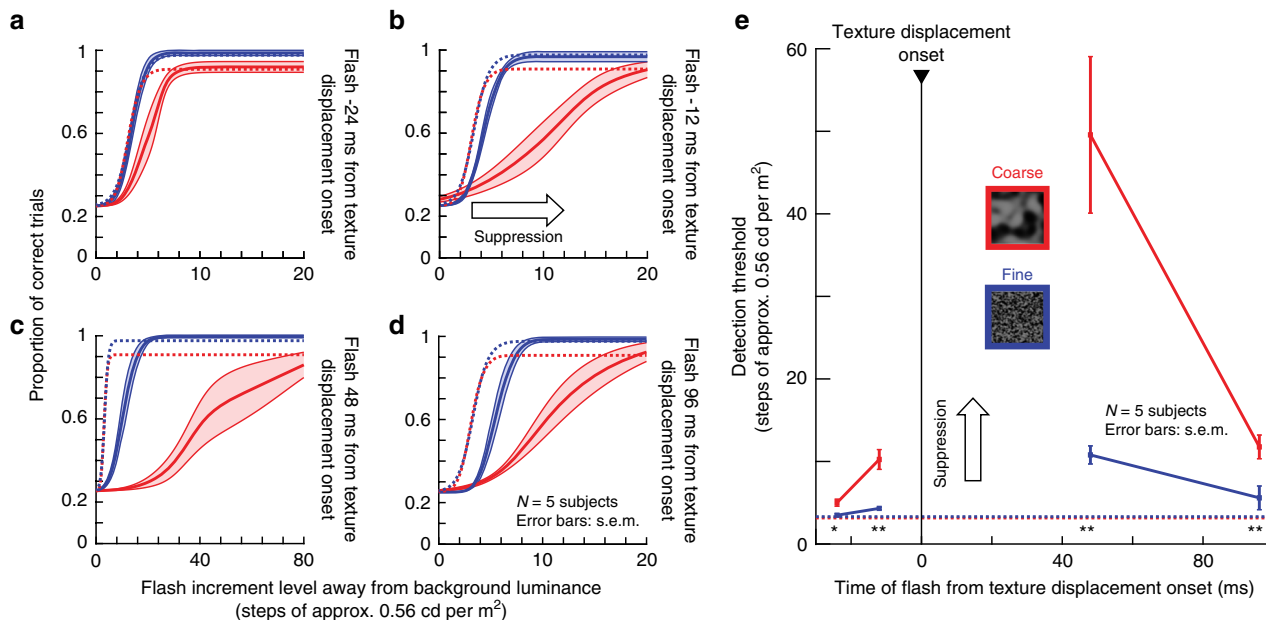


Fig. 7 Image-dependent elevation of perceptual thresholds without saccades. Full psychometric curves of flash visibility around the time of simulated saccades (similar to Fig. 2, paradigm similar to Fig. 6). **a–d** Solid curves: mean ± s.e.m. of individual psychometric curves of $N = 5$ subjects (individual subject results: Supplementary Fig. 7). Dashed curves: baseline data from the same subjects without simulated saccades and long after any real saccades (same data as in Fig. 2d; also similar to Supplementary Fig. 3a, b with additional subjects). Red and blue: data for coarse and fine textures, respectively. **a** Flash 24 ms before texture displacement onset: coarse texture (red) requires higher flash contrasts (that is, reduced sensitivity) relative to baseline. This effect was much weaker with fine textures (blue). **b** Flash 12 ms before displacement onset: both coarse and fine textures were associated with significant perceptual suppression relative to baseline, consistent with Fig. 6. Suppression was stronger for coarse than fine textures. **c** Perceptual suppression was the strongest (note the different x-axis scale from the other panels) immediately after texture displacement onset. **d** 96 ms after texture displacement onset, there was still significant perceptual suppression, again significantly stronger for coarse than fine textures. This result is consistent with Fig. 6 and highlights the longer-lasting suppression around simulated saccades compared to real saccades (Figs. 1 and 2). **e** Detection thresholds from **a–d** as a function of flash time from texture displacement onset. Pre- and post-displacement perceptual suppression occurred and was stronger with coarse textures. Asterisks: significant differences between coarse and fine textures (two-tailed two-sample t -test; $*p < 0.05$; $**p < 0.01$). Horizontal dashed lines: baseline detection thresholds from Fig. 2d, e. All other conventions are similar to Figs. 1, 2, 6.

was shorter during real saccades than during simulated saccades (due to later onset of suppression, Fig. 6e). Even in our retinal data, we found very slight “pre-saccadic” suppression. However, for retinal responses, the effect size before texture displacements was much smaller than after texture displacements: the strongest “pre-saccadic” retinal effect occurred at -67 ms with a median population modulation index of -0.024 ($p = 6 \times 10^{-8}$, Wilcoxon signed-rank test) compared to -0.55 ($p = 3 \times 10^{-82}$) for “post-saccadic” suppression at 150 ms delay (Fig. 3e and Supplementary Fig. 5b). It is therefore likely that this particular phenomenon, perceptual pre-saccadic suppression (Fig. 6b–f), arises from visual (not movement-command-related) processing further downstream of the retina, perhaps through backwards masking^{28,45}. This also holds true for our experiments with background luminance steps (Fig. 5), and it can also explain why peak suppression time in our retinal experiments (Figs. 3 and 4) appeared slightly different from peak suppression time with real saccades (Figs. 1 and 2).

Next, we determined explicit perceptual thresholds for the texture displacement paradigm introduced in Fig. 6, using the QUEST and full psychometric curve procedures described for Fig. 2. We again picked four specific time points relative to texture displacement onset, chosen strategically to highlight perceptual threshold elevations at maximal suppression, to characterize differences in recovery time between coarse and fine textures, and to fill the gap before texture displacement onset. The net conclusion (Fig. 7) was the same as that in Fig. 6. There was robust elevation of perceptual thresholds before, during, and after texture displacements. Most importantly, the elevation was much

stronger and longer-lasting (both before and after texture displacements) for coarse than for fine textures. The effect was also robust across individual subjects (Supplementary Fig. 7).

Therefore, our long-lasting RGC suppression effects (Figs. 3 and 4) were not an idiosyncrasy of our ex vivo electrophysiological procedures, but they were reflected in the longer duration of perceptual suppression after simulated saccades. Importantly, they were indicative of a potential shortening of visually derived suppression in association with real saccades.

Visually derived suppression underlies even more phenomena.

Our results so far suggest that visual contributions can go a long way in explaining perceptual properties of saccadic suppression (e.g., the presence of suppression, and the dependencies on image content), without the need for invoking mechanisms related to motor commands. We wondered whether visual contributions can also explain classic suppression phenomena in experiments when uniform, rather than textured, backgrounds are used. One such robust phenomenon has been the selective suppression of low spatial frequencies. In a classic study¹⁰, subjects viewed briefly flashed Gabor gratings over a uniform background. Around the time of saccades, visibility of low spatial frequency gratings was suppressed more strongly than of high-frequency gratings. This was interpreted as a motor-related influence on magnocellular pathways^{16,17}. Still, convincing neural mechanisms for this phenomenon remain elusive^{14,21,29,30,46–50}. Can the strong prominence of visual contributions to saccadic suppression revealed by our results also be extended to account for this

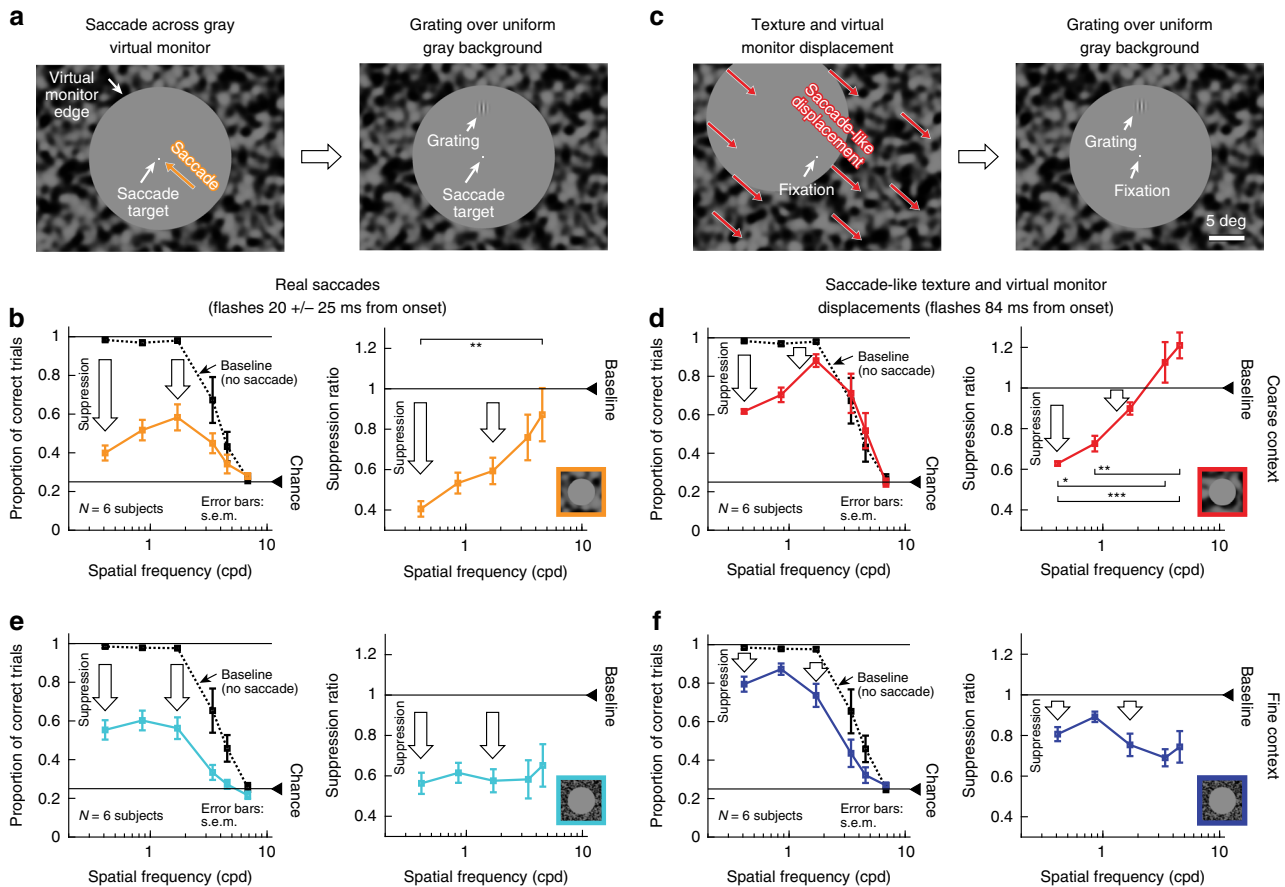


Fig. 8 Selective peri-saccadic suppression of low spatial frequencies¹⁰ is a visual phenomenon. **a** Left: subjects made saccades towards display center. Right: gratings were flashed peri-saccadically over a uniform gray background (circular “virtual monitor” surrounded by a coarse texture; saccade directions and flash locations: similar to Figs. 5 and 6). **b** Left: proportion of correct grating localizations with different spatial frequencies during fixation (“Baseline”; dashed curve) and for peri-saccadically flashed gratings (solid curve). Low spatial frequencies were associated with the strongest suppression relative to baseline. Right: ratio of peri-saccadic to baseline performance (highest spatial frequency not shown because it was at chance performance even in baseline). Suppression depended on grating spatial frequency ($\chi^2 = 13.46$, $p = 0.0092$, $df = 4$, Kruskal-Wallis test; $**p < 0.01$ for post-hoc pairwise comparisons between the lowest and highest spatial frequencies). **c** Left: simulated saccade-induced image displacements by translating the virtual monitor and surrounding texture from one corner towards display center. Right: gratings appeared as in **a**. **d** The same selective suppression of low spatial frequencies occurred as with real saccades (**b**). “Baseline” in this context means both no saccades and no virtual monitor and texture displacements. Suppression depended on spatial frequency ($\chi^2 = 25.33$, $p < 0.0001$, $df = 4$, Kruskal-Wallis test; $*p < 0.05$, $**p < 0.01$, $***p < 0.001$ for post-hoc pairwise comparisons between individual spatial frequencies). **e, f** With a fine surround texture, both real (**e**) and simulated (**f**) saccades were associated with suppression for all spatial frequencies; suppression selectivity¹⁰ was eliminated ($\chi^2 = 0.8$, $p = 0.938$, $df = 4$ for **e** and $\chi^2 = 7.74$, $p = 0.102$, $df = 4$ for **f**, Kruskal-Wallis test). Error bars: s.e.m. across individual subjects’ curves. Supplementary Figs. 8–10: full time courses and controls with black surrounds around the virtual monitor. Note that in **d, f**, we exploited the longer time course of visual suppression (Fig. 6 and Supplementary Figs. 8 and 9) to probe perception at a later time than in **b, e**. This also explains why suppression appeared quantitatively weaker in **d, f** than in **b, e**.

classic phenomenon? In other words, is peri-saccadic selective suppression of low spatial frequencies¹⁰ fundamentally a visual, rather than motor, phenomenon?

We considered this phenomenon from the perspective of visual input during such experiments: saccades across a uniform background invariably involve moving the image of the video monitor (or other form of display) in visual coordinates. Therefore, the image of any edge discontinuity associated with the display monitor (or with the surrounding cardboard paper around it¹⁰) will invariably move across the retina. This allows us to ask if one can replicate selective suppression of low spatial frequencies¹⁰ without any saccades at all, solely based on the visual flow during such experiments.

We first replicated the classic phenomenon itself (Methods). Subjects localized briefly flashed vertical Gabor gratings with different spatial frequencies; the flashes occurred peri-saccadically as in Fig. 1a. Here, however, the screen was homogeneous, like in

the classic experiment, with the exception of a surround region showing a stationary texture (the coarse texture used in our earlier experiments, Fig. 8a). We call the large homogeneous region (diameter: 20 deg) the “virtual monitor”. The outcome confirmed the classic findings: Fig. 8b (left) shows localization performance for flashed gratings around saccade onset, compared to flashes without saccades (and without any other display transients), and Fig. 8b (right) plots the ratio of those percepts. Perception of low spatial frequency gratings was selectively suppressed (relevant statistics are shown in Fig. 8; full time courses of these effects are shown in Supplementary Figs. 8 and 9). These results are consistent with the classic phenomenon¹⁰.

The presence of the textured surround allowed us to next isolate the effects of visual flow. In separate trials, subjects fixated, and we presented saccade-like image motion. For example, in order to simulate a real saccade from the lower right corner to display center (Fig. 8a), the virtual monitor moved together with

its textured surround from the top left corner towards display center (Fig. 8c). We then briefly presented the same Gabor gratings as in Fig. 8a, b. Relative to fixation position, this experiment was comparable to the situation with real saccades: there was a uniform background against which a brief Gabor grating was flashed. And, indeed, we observed the same selective suppression of low spatial frequencies despite the absence of saccades (Fig. 8d). Moreover, again consistent with our results from Figs. 1–7, the suppression lasted longer than with real saccades (robust selective suppression in Fig. 8d occurred even 84 ms after simulated saccades; Supplementary Figs. 8 and 9). Similar results were obtained with a uniform black surround around the virtual monitor, as might be the case in typical laboratory settings (Supplementary Fig. 10). Therefore, visual mechanisms account even for the results of Burr et al.¹⁰ and similar experiments¹⁴ using uniform backgrounds, without the need to invoke non-visual (motor-related) mechanisms.

Motivated by the differences between coarse and fine textures in Figs. 1–7, we next replaced the coarse texture around the virtual monitor (Fig. 8c) with a fine texture, and we repeated the experiments with simulated saccades (Fig. 8f). Surprisingly, we observed uniform suppression for all spatial frequencies (Fig. 8f). In other words, the specific suppression of low spatial frequencies (Fig. 8c, with saccade-like visual flow, but without eye movements) depended on the visual context containing a coarse texture in the visual surround. This led to a very strong prediction: if saccadic suppression properties do indeed rely on visual processing, then suppression during real saccades should depend mainly on visual context; one should be able to easily violate the classic phenomenon (namely, the specific suppression of low spatial frequencies¹⁰). This is exactly what we found (Fig. 8e): for real saccades across the virtual monitor, and with the surrounding visual context being a fine rather than coarse texture, we observed perceptual suppression for all gratings, abolishing suppression selectivity for low spatial frequencies. In all cases, the effects were not explained by motor variability across surround texture conditions (Supplementary Fig. 3e, f).

We further confirmed all these observations by collecting full psychometric curves (Methods), similar to Figs. 2 and 7 above: Fig. 9 shows results for real saccades, and Fig. 10 for simulated saccades. In both cases, with a coarse surround texture, perceptual threshold was elevated more strongly for low spatial frequency Gabor patches. With a fine surround texture, perceptual threshold was elevated non-specifically for all probe Gabor patches.

In summary, perceptual saccadic suppression occurred in all of our experiments, either with or without real saccades, simply as a function of visual flow (Figs. 1, 2, 6–10). Simple visual transients, without the need for saccade-like stimulus kinematics, were sufficient to elicit suppression in both retina and perception (Figs. 4 and 5). Such suppression quantitatively depended on scene statistics, both for full-field textures (Figs. 1, 2, 6, 7) in a manner predicted by retinal processing (Figs. 3–5), and for textures limited to the surround (Figs. 8–10). Even the suppression selectivity of low spatial frequency Gabor probes¹⁰ was determined by visual context (Figs. 8–10).

Discussion

We found that visual image processing accounts for a large component of classic perceptual demonstrations of saccadic suppression, and that such image processing occurs as early as in the very first stage of visual processing, the retina. In fact, we found remarkable congruence between the image dependence of three seemingly disparate phenomena: perceptual suppression with real saccades (Figs. 1 and 2), perceptual suppression with simulated saccades (Figs. 6 and 7), and neural suppression in

RGCs, which carry the retinal output (Figs. 3 and 4). In all cases, modifying the background texture statistics resulted in highly predictable changes in suppression profiles. This was further corroborated in both the retina (Fig. 4d) and perception (Fig. 5) when we replaced texture displacements with simple background luminance steps.

Key to all our observations is the single insight that, from the perspective of visual image processing, a saccade itself generates a potent visual stimulus. For example, our RGCs often responded vigorously to saccade-like image displacements (Fig. 3b). Therefore, when probing peri-saccadic perceptual sensitivity using brief flashes, as in classic studies of perceptual saccadic suppression, the visual system is not only responding to the externally provided flashes, but it is also responding to the self-induced visual flows caused by eyeball rotations. These saccade-induced retinal image shifts trigger visual mechanisms that can suppress the retinal response to subsequent stimulation. Such suppression is not exclusive to saccades. It instead occurs for any scenario that involves sequential visual stimulation, including visual masking^{2,27,28,45} and double-flash⁴² paradigms. It is, therefore, not surprising that the outcome is also comparable: the response to a second stimulus is suppressed by the presence of a first stimulus, be it a mask, a flash, or transients caused by saccades. Indeed, our own results demonstrate that simpler sequential visual stimulation with luminance steps plus probe flashes shows qualitatively similar perceptual (Fig. 5) and retinal (Fig. 4d) suppression profiles to those seen with simulated saccades. Therefore, classic saccadic suppression paradigms, employing brief peri-saccadic visual probes, are essentially stimulus–stimulus paradigms from the perspective of visual flow on the retina.

Additional support for the above sentiment emerges from the time courses of stimulus–stimulus neural adaptation effects in areas like the frontal eye field and superior colliculus⁴². These time courses are particularly intriguing because they agree with our observations that retinal (Figs. 3 and 4) and perceptual (Figs. 6 and 7) suppression with simulated saccades had longer suppression time courses than observed with real saccades (Figs. 1 and 2). Indeed, the time courses of the neural adaptation effects in the frontal eye field and superior colliculus⁴², and related brain areas, are similar to our observed perceptual time courses without real saccades. Given that both the frontal eye field and superior colliculus have previously been implicated in saccadic suppression^{14,41,43,44}, it is thus conceivable that suppression in these areas is inherited, at least partially, from the retina.

Looking forward, it is imperative to investigate the neural mechanisms behind visual masking in much more detail. In our perceptual experiments with simulated saccades (Figs. 6 and 7), we saw clear suppression even with probe flashes before texture displacement. That is, perceptual localization of the probes was masked, backwards in time, by the subsequent texture displacement. In the past, pre-saccadic suppression with real saccades (e.g., Fig. 1) was sometimes taken as evidence that perceptual saccadic suppression is fundamentally driven by motor-related signals like corollary discharge. However, our results (Figs. 6 and 7) show that a visual transient is sufficient. Even simple background luminance steps were associated with pre-step perceptual suppression (Fig. 5). These effects have been described as backwards visual masking⁴⁵, but what are the underlying neural mechanisms? Such backwards masking was not present in our retinal results, certainly not as clearly as in perception, so it must emerge through visual mechanisms in other brain structures.

One possibility could be related to the fact that priors strongly influence the perceptual interpretation of sensory evidence. In the case of global retinal image motion, which is caused by eye movements in most real-world scenarios, priors could influence the percept of a flash occurring before a saccade or texture

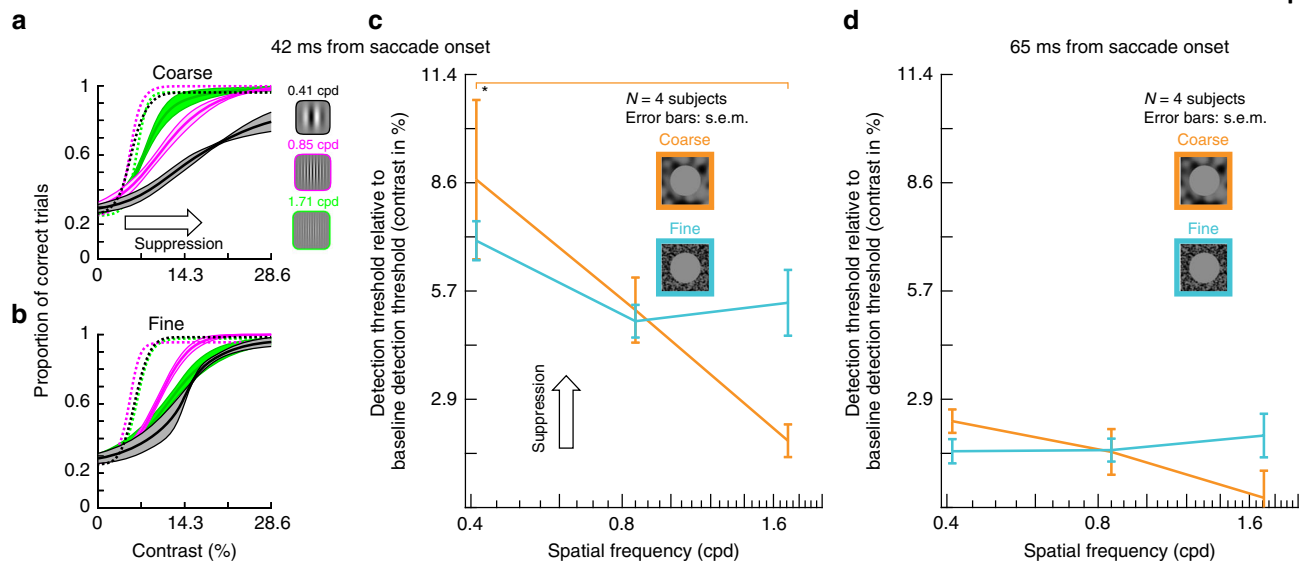


Fig. 9 Selective and unselective saccadic suppression measured using full psychometric curves. **a** We repeated the real saccade experiments of Fig. 8, and obtained full psychometric curves by using different Gabor grating contrasts (Methods). Different colors indicate different spatial frequencies of the flashed gratings. When the gratings were flashed -42 ms after saccade onset (Methods) and there was a coarse surround texture, perceptual suppression clearly depended on spatial frequency: detection thresholds were highest for the lowest spatial frequency, and they progressively decreased with increasing spatial frequency. Each curve shows mean \pm s.e.m. of four subjects' psychometric curves. Dashed psychometric curves show perceptual detectability without saccadic suppression (obtained similarly to Fig. 8). **b** When the surround context was fine, rather than coarse, perceptual suppression was not selective for low spatial frequencies (consistent with Fig. 8). **c** Detection thresholds from **a**, **b** as a function of grating spatial frequency for flashes -42 ms after saccade onset. With a coarse surround, detection thresholds were highest for low spatial frequencies and progressively decreased with increasing spatial frequency (1-way ANOVA, $p = 0.0168$, $F = 6.6608$; $p = 0.0133$ for post-hoc comparison between lowest and highest spatial frequency, indicated by *). With a fine surround, detection thresholds did not depend on spatial frequency. **d** Same as in **c** but now for grating flashes occurring -65 ms after saccade onset. For both surround textures, detection thresholds decreased, indicating perceptual recovery. There was still a trend for dependence of perception on spatial frequency in the coarse condition, consistent with **c**.

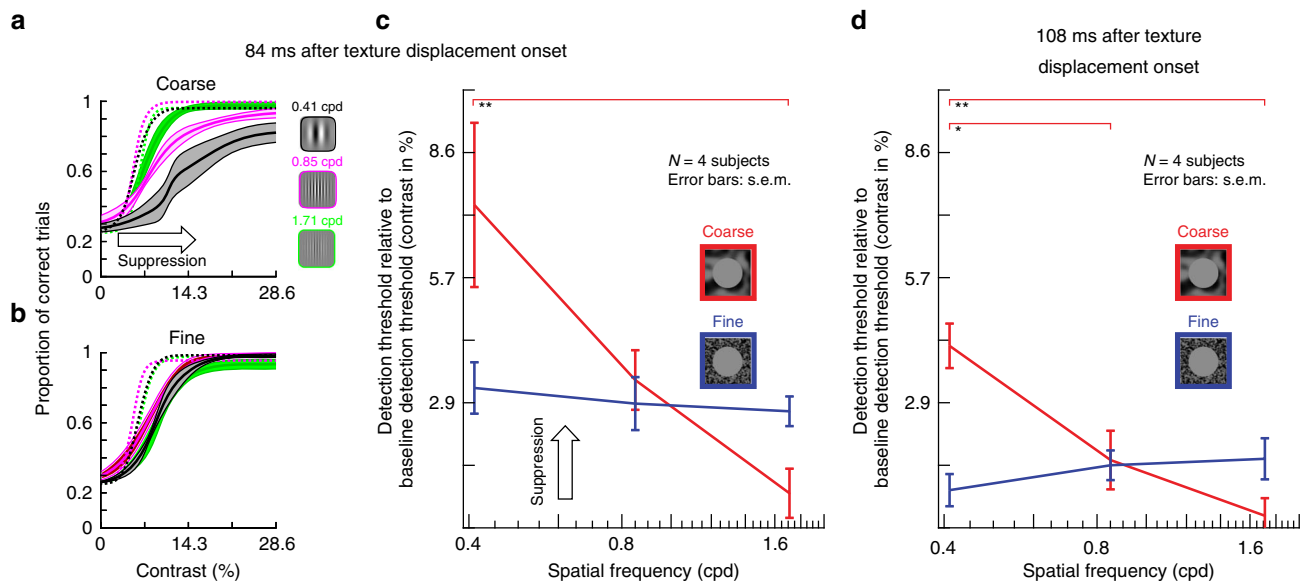


Fig. 10 Selective and unselective saccadic suppression without any saccades. This figure is identical to Fig. 9, except that real saccades were replaced (in the same subjects) with simulated saccades (exactly as in Fig. 8). All of the same conclusions were reached. There was selective suppression for low spatial frequencies when the texture surround was coarse (**a**); suppression was unselective for grating spatial frequency with a fine surround (**b**); and there was gradual recovery with time (**c**, **d**). In fact, perceptual suppression was clearer and longer lasting in this condition than with real saccades (also consistent with Figs. 1, 6, 8). All other conventions are as in Fig. 9. In **c**, the coarse texture surround showed a significant main effect of spatial frequency (1-way ANOVA, $p = 0.0113$, $F = 7.6878$; $p = 0.0092$ for post-hoc comparison between lowest and highest spatial frequency, indicated by **). In **d**, the coarse surround also showed a significant main effect of spatial frequency (1-way ANOVA, $p = 0.0019$, $F = 13.5276$; $p = 0.0017$ for post-hoc comparison between lowest and highest spatial frequency, and $p = 0.0186$ for post-hoc comparison between lowest and intermediate spatial frequency).

displacement. Specifically, such priors may cause perception to “omit” the pre-saccadic flash even though it evokes a strong retinal transient. This would happen exactly because of the pairing of the flash with a very likely occurrence of a saccade, interpreted as such due to the global image motion, even if its neural transient in the retina is weakened by the prior flash. This would result in a kind of credit assignment problem due to a strong prior association of global image motion with saccades.

More generally, our results suggest that visual flow is important in perceptual saccadic suppression, even in paradigms that have often been taken as indication for motor-related top-down suppression (Figs. 8–10). It would be interesting in the future to further test the generalizability of this notion. We were indeed greatly surprised when we found that selective suppression of low spatial frequencies¹⁰ can be violated in two important ways. First, the suppression selectivity can be abolished with a simple change of visual context. Second, the same selective suppression of low spatial frequencies can be obtained without saccades. Thus, with or without saccades, either selective or nonselective suppression could occur as a function of visual flow. In hindsight, this might shed light on a surprising recent finding in superior colliculus¹⁴. There, using essentially the same paradigms, only one type of superior colliculus visually responsive neurons (so-called visual-motor neurons) exhibited selective suppression of low spatial frequency sensitivity. The other type of visually responsive neurons (visual-only neurons) showed mild but, critically, non-selective suppression¹⁴. These two types of neurons occupy different superior colliculus laminae and have different patterns of lateral interactions from across this structure’s visual field representation⁵¹. It is now conceivable, considering our current results (Figs. 8–10), that both patterns of suppression (selective or not) may be embedded simultaneously in these different neuronal populations with specific circuitry and tuning for visual peripheral contexts.

Finally, motor-related mechanisms still likely play an important role in perceptual saccadic suppression. Such mechanisms appear to shorten suppression originating from visual processing (Fig. 6), and might therefore minimize the duration of saccade-induced disruptions. Indeed, a variety of cortical areas exhibit post-saccadic excitability enhancement^{52–54}. It would be interesting to further investigate how such enhancement may contribute to the shortened time courses of perceptual saccadic suppression that we observed (e.g., Fig. 6e, f). Furthermore, besides just suppression, saccades are also associated with “omission”, the lack of awareness of intra-saccadic background image motion^{22,55}. It would, therefore, also be interesting to study the neural mechanisms through which strong saccade-induced neural transients in the retina (Fig. 3b) are perceptually “omitted” to give the illusion of continuous perception across saccades. More intriguingly, saccades also cause spatial updating of visual reference frames (compensating the image shifts that they cause). Information contained in the motor command itself is likely critical for adjusting spatial receptive fields across saccades, as observed in some brain areas^{56,57}. Our findings leave open the possibility, however, that trans-saccadic image flow might play a role in this phenomenon as well.

Methods

Ethics approvals. We performed electrophysiological experiments on ex vivo mouse and pig retinae as well as non-invasive perceptual experiments on human subjects.

Animal use was in accordance with German and European regulations, and animal experiments were approved by the Regierungspräsidium Tübingen.

Human subjects provided written, informed consent, and they were paid 8–15 Euros per session of 45–90 min each. Depending on the experiment, each subject was measured for 2–10 sessions (detailed trial and session numbers are provided below). Human experiments were approved by ethics committees at the Medical

Faculty of Tübingen University, and they were in accordance with the Declaration of Helsinki.

Retina electrophysiology laboratory setup. We used retinae extracted from *PV-Cre x Thy-S-Y* mice (*B6;129P2-Pvalb^{tm1(cre)Arbr}/J × C57BL/6-tg (ThystopYFPJS)*), which are functionally wild type^{58–60}. Twenty-three retinae from seven male and fifteen female mice (3–12-months-old) were used. We also replicated experiments on pig retinae obtained from domestic female pigs after they had been sacrificed during independent studies at the Department of Experimental Surgery in our Medical Faculty. We used nine pig retinae.

We housed mice on a 12/12 h light/dark cycle in ambient temperature, ranging between 20–22 °C, and humidity levels of ~40%. Mice were dark adapted for 4–16 h before experiments. We then sacrificed them under dim red light, removed the eyes, and placed eyecups in Ringer solution (in mM: 110 NaCl, 2.5 KCl, 1 CaCl₂, 1.6 MgCl₂, 10 D-glucose, and 22 NaHCO₃) bubbled with 5% CO₂ and 95% O₂. We removed the retina from the pigment epithelium and sclera while in Ringer solution.

Pigs were anesthetized using atropine, azaperone, benzodiazepine (midazolam), and ketamine, and then sacrificed with embutramide (T61). Before embutramide administration, heparin was injected. The pigs were dark adapted for 15–20 min before sacrifice. Immediately after sacrifice, the eyes were enucleated under dim red light, and the cornea, lens, and vitreous were removed. Eyecups were kept in CO₂-independent culture medium (Gibco) and protected from light. We transported eyecups to our laboratory and cut pieces from mid-peripheral or peripheral retinae. Only those retinae that were healthy and showed ganglion cell responses to light stimuli were used in our experiments.

We recorded retinal ganglion cell (RGC) activity using either low- or high-density multi-electrode arrays (MEAs). The low-density setup consisted of a perforated 60-electrode MEA (60pMEA200/30ir-Ti-gt, Multichannel Systems, Reutlingen, Germany) having a square grid arrangement and 200 μm inter-electrode distance. We mounted an isolated retina on a nitrocellulose filter (Millipore) with a central 2 × 2 mm hole. The mounted retina was placed with the RGC-side down into the recording chamber, and good electrode contact was achieved by negative pressure through the MEA perforation. We superfused the tissue with Ringer solution at 30–34 °C during recordings, and we recorded extracellular activity at 25 kHz using a USB-MEA-system (USB-MEA 1060, Multichannel Systems) or a memory-card based system (MEA1060, Multichannel Systems). Data were acquired using MC Rack version 4.6.2 (Multichannel Systems). More details are provided in Reinhard et al.⁶¹.

The high-density MEA setup consisted of either a HiDens CMOS MEA⁶² (developed by the lab of Andreas Hierlemann, Basel, Switzerland) or a MaxOne system⁶³ (Maxwell Biosystems, Basel, Switzerland). The HiDens CMOS MEA featured 11,011 metal electrodes with inter-electrode (center-to-center) spacing of 18 μm placed in a honeycomb pattern over an area of 2 × 1.75 mm. Any combination of 126 electrodes could be selected for simultaneous recording. The MaxOne MEA featured 26,400 metal electrodes with center-to-center spacing of 17.5 μm over an area of 3.85 × 2.1 mm. In this system, up to 1024 electrodes could be selected for simultaneous recordings. For each experiment, a piece of isolated retina covering almost the entire electrode array was cut and placed RGC-side down in the recording chamber. We achieved good electrode contact by applying pressure on the photoreceptor side of the retina by carefully lowering a transparent permeable membrane (Corning Transwell polyester membrane, 10 μm thick, 0.4 μm pore diameter) with the aid of a micromanipulator. The membrane was drilled with 200 μm holes, with center-center distance of 400 μm, to improve access of the Ringer solution to the retina. We recorded extracellular activity at 20 kHz using FPGA signal processing hardware. In the case of the HiDens CMOS MEA, data were acquired using custom data acquisition software, called MEA 1k Scope (developed by the lab of Andreas Hierlemann, Basel, Switzerland). In the case of the MaxOne MEA, data were acquired using MaxLab software provided by Maxwell Biosystems, Basel, Switzerland.

In total, we performed 36 recordings, 24 from mouse and 12 from pig retina. Fifteen of the 36 recordings were done using low-density MEAs. Once a basic experimental protocol was established, we shifted to HiDens CMOS MEA providing much higher throughput. Twelve experiments were done using this setup. We upgraded to the MaxOne MEA for even higher throughput and did our final nine recordings using this setup.

We presented light stimuli to the retinal piece that was placed on the MEA using a DLP projector running at 60 Hz (Acer K11 for low-density MEA experiments and Lightcrafter 4500 for high-density MEA experiments). In all, 60 Hz is above the flicker fusion frequency of both mouse and pig retinae; therefore, the framerate of these projectors was adequate for our purposes. The Acer K11 projector had a resolution of 800 × 600 pixels covering 3 × 2.25 mm on the retinal surface. Lightcrafter 4500 had a resolution of 1280 × 800 pixels, extending 3.072 × 1.92 mm on the retinal surface. We focused images onto the photoreceptors using a condenser (low-density MEA recordings, illumination from below) or a 5x objective (high-density MEAs, illumination from above). In each case, the light path contained a shutter and two motorized filter wheels with a set of neutral density (ND) filters (Thorlabs NE10B-A to NE50B-A), having optical densities from 1 (ND1) to 5 (ND5). Light intensity was adjusted to be in the mesopic range.

We measured the spectral intensity profile (in $\mu\text{W cm}^{-2} \text{ nm}^{-1}$) of our light stimuli with a calibrated USB2000 + spectrophotometer (Ocean Optics) and converted the physical intensity into a biological equivalent of photoisomerizations per rod photoreceptor per second ($R^* \text{ rod}^{-1} \text{ s}^{-1}$), as described before⁶⁰. Light intensities of the projector output covered a range of 3 log units (i.e., 1,000-fold difference between black and white pixels, over an 8-bit range). We linearized the projector output, and we used only grayscale images of limited contrast, spanning at most the range from 0 to 120 in the 8-bit range of the projector (see stimulus description below for details). Absolute light intensities were set to the mesopic level, where a stimulus intensity of “30” in our 8-bit DLP projector scale (0–255) corresponded to 225 to 425 $R^* \text{ rod}^{-1} \text{ s}^{-1}$, depending on the experimental rig used for the experiment (i.e., different DLP projectors and MEAs). We pooled all data from the different rigs because separate individual analyses from the individual setups revealed no effects of recording conditions in the different setups.

Human psychophysics laboratory setup. We used a similar laboratory setup to our recent experiments^{38,64,65}. Briefly, subjects sat in a dark room 57 cm in front of a CRT monitor (85 Hz refresh rate; 41 pixels per deg resolution) spanning 34.1×25.6 deg (horizontal \times vertical). Head fixation was achieved with a custom head, forehead, and chin rest⁶⁴, and we tracked eye movements (of the left eye) at 1 kHz using a video-based eye tracker (EyeLink 1000, SR Research Ltd, Canada). Gray and texture backgrounds (e.g., Figs. 1, 6, 8–10) were always presented at an average luminance of 22.15 cd m^{-2} , and the monitor was linearized (8-bit resolution) such that equal luminance increments and decrements were possible around this average for textures and gratings. For the experiments in which we used luminance steps of the background as the visual transients replacing saccade-induced transients (Fig. 5), details of the luminances used are presented below with the experimental procedures.

Human Experiment 1 (Fig. 1) was performed by eight subjects (two female) who were 21–25-year-old. All subjects were naive to the purposes of the experiment, except for subject MB (an author). For Human Experiment 2, the “simulated saccade” version of Human Experiment 1 (Fig. 6), six of the same subjects participated. A control experiment for testing visibility of flashes without saccades and without saccade-like texture displacements (Supplementary Fig. 3a, b) was performed by six of the same subjects plus one non-naive subject, Z.H. (another author).

In the variants of Human Experiments 1 and 2 in which we collected full psychometric curves and perceptual thresholds (e.g., Figs. 2 and 7 and Supplementary Figs. 4 and 7), five subjects (24–29-year-old; one female) participated. Three of these subjects were the same as those who performed Human Experiments 1 and 2 above, confirming that both variants of the experiments (either with a fixed flash contrast or with full threshold calculations) allowed similar conclusions.

In the control experiment (Fig. 5) mimicking the retinal results of Fig. 4d, we collected data from five subjects (25–29-year-old; two female). Two of these subjects were the same as those who performed all experiments.

Human Experiment 3 tested suppression selectivity for low spatial frequencies (Fig. 8). Six subjects (three females, 23–25-year-old) participated, and only subject MB was non-naive. Three subjects had also participated in Human Experiments 1 and 2 and most of their control versions above. A control version of Human Experiment 3 was also performed with black surrounds (Supplementary Fig. 10). This control experiment was performed by the same subjects that participated in Human Experiment 3.

We also ran a variant of Human Experiment 3 describing full psychometric curves of perceptual detectability (Figs. 9 and 10). For each of the real (Fig. 9) or simulated (Fig. 10) variants, we ran four subjects (24–29-year-old; one female; three being the same as those who performed the experiments of Fig. 8).

Across all experiments, we ensured that the same subjects performed real and “simulated” saccade versions of a given paradigm so that we could make meaningful comparisons between these two eye movement conditions.

Coarse and fine textures. We created coarse and fine textures (Supplementary Fig. 1a) by convolving a random binary (i.e., white or black) pixel image with a two-dimensional Gaussian blurring filter⁶⁶ with the kernel

$$G(x, y) = e^{-\frac{(x^2+y^2)}{2\sigma^2}} \quad (1)$$

The parameter σ of the kernel influenced the amount of blurring. This resulted in textures having effectively low-pass spectral content (Supplementary Fig. 1b) with a cutoff frequency (f_c) depending on σ . As we describe below, we picked cutoff frequencies for coarse and fine textures that resulted in dark and bright image blobs approximating the receptive field sizes of RGCs (for coarse textures) and retinal bipolar cells (for fine textures). In other words, for a given species, coarse textures matched the resolution of RGCs, and fine textures matched the resolution of one processing stage earlier, the retinal bipolar cells.

For the ex vivo experiments with mouse and pig retinae, we assumed receptive field diameters for RGCs of at least $150 \mu\text{m}$ (Supplementary Fig. 1c; the parameter σ of the Gaussian blurring filter would be half that value), and diameters for bipolar cells of $25 \mu\text{m}$ (see Zhang et al.⁶⁷). For human psychophysics experiments, we estimated, from the literature³⁶, the sizes of human parasol RGC receptive fields at eccentricities >6 deg from the fovea (our flash eccentricities were 7 deg) to be

around $200 \mu\text{m}$. This translated into a cutoff frequency of ~ 0.68 cycles per deg (cpd) (Supplementary Fig. 1b). Bipolar cell receptive field sizes at this eccentricity were estimated to be $10 \mu\text{m}$ (corresponding to a cutoff frequency of ~ 13.7 cpd), based on sizes of human midget RGC receptive fields in the fovea³⁶. When calculating the textures, the actual value of the parameter σ (in pixel-dimensions) always incorporated the specific experimental magnification factor between the stimulation screen and the retinal projection of the image. Calculating power spectra for coarse and fine textures confirmed that cutoff frequencies for a given species were consistent with our aimed designs described above (Supplementary Fig. 1b).

For both retinal and perceptual experiments, we normalized pixel intensities in the textures to have uniform variations in luminance around a given mean. In the retinal experiments, we used pixel intensities (from our 8-bit resolution scale) ranging from 0 to 60 around a mean of 30, or ranging from 30 to 90 around a mean of 60 (see Retina electrophysiology experimental procedures below for when each paradigm was used). For the human experiments, textures had a mean luminance of 22.15 cd m^{-2} with undulations in luminance in the texture within the range of $7.5\text{--}35.5 \text{ cd m}^{-2}$.

As each texture, particularly when coarse, could have patterns of dark and bright blobs that human subjects can remember or interpret as potential shapes/objects/figures, we varied the displayed texture images from trial to trial. This was also necessary to avoid afterimages. We generated sets of 20 coarse and 20 fine textures, which we randomly interleaved across trials. Moreover, the textures themselves were designed to be larger than the viewable display area, allowing us to jitter the displayed sub-rectangle of each texture (within the viewable area of the display) from trial to trial (we jittered the displayed sub-rectangle within a range of 0.6×0.6 deg in steps of 0.024 deg). This way, even fine patterns at foveal fixation locations could not be memorized by the subjects across trials.

Retina electrophysiology experimental procedures. To simulate saccades in our ex vivo retina electrophysiology experiments, we displaced the texture across the retina in 6 display frames (100 ms at 60 Hz refresh rate). For easier readability, we sometimes refer to these saccade-like texture displacements as “saccades”. The textures were displaced in each frame by a constant distance along a linear trajectory. While each “saccade” lasted 100 ms, displacement direction was varied randomly for each “saccade” (uniformly distributed across all possible directions), and “saccade” amplitude could range from 310 to 930 μm (corresponding to a velocity range of $3100\text{--}9300 \mu\text{m s}^{-1}$ on the retinal surface). In visual degrees, this corresponds to a velocity range of $100\text{--}300 \text{ deg s}^{-1}$ and displacement range of $10\text{--}30$ deg in mice, well in the range of observed mouse saccade amplitudes⁶⁸. In fact, similar to primates, mice also have oculomotor behavior, even under cortical control⁶⁹. For example, they make, on average, 7.5 saccade-like rapid eye movements per minute when their head is fixed⁶⁸ (humans make several saccades per second). We used the same retinal displacement range of 310 to 930 μm for pig retinae. To the best of our knowledge, pig oculomotor behavior has not been documented in the literature. However, with their larger eyeball sizes, our translations of the retinal image would correspond to slower saccades (e.g., small saccades in humans and monkeys), which are also associated with saccadic suppression. Moreover, we showed (Fig. 4) that retinal “saccadic suppression” is not critically dependent on the details of movement kinematics.

Each “trial” consisted of 39 successive sequences that each combined a “saccade” with a probe flash, as follows: there was first a “pre-saccade” fixation of 2 s, then a 100 ms “saccade”, followed by “post-saccade” fixation. The background texture was switched on at the beginning of each trial and was translated across the retina during each “saccade”. At a certain time from “saccade” onset (delay d , range: -177 to 2100 ms), we presented a probe flash. In most cases, the probe flash had a duration of 1 frame (~ 16 ms). We used 2 frames (~ 33 ms) in a subset of experiments (mouse: 161 of 688 cells analyzed for “saccadic suppression”; pig: 112 of 228 cells). Results were pooled across these paradigms as they were indistinguishable. For sequences containing no probe flash, the next “saccade” happened 4 s after the previous one. The probe flash was a full-screen positive (“bright”) or negative (“dark”) stimulus transient. In different experiments, only a subset of possible delays was used within a given set of trials, depending on total recording time for a given retina (see below).

Bright or dark probe flashes could happen in two different ways across our experiments. The results were indistinguishable between the two ways, so we pooled results across them. Briefly, in one manipulation, the probe flash was a homogeneous bright (pixel intensity of 60 in our 8-bit projectors) or dark (pixel intensity of 0) full-screen rectangle replacing the background texture (in these experiments, the textures themselves had intensities ranging from 0 to 60 pixel intensity; see Coarse and fine textures above). This way, the flash contrast from the underlying background luminance was variable (e.g., a bright flash on a bright portion of a texture had lower contrast from the underlying texture than the same flash over a dark portion of the texture). In the second manipulation, the bright and dark flashes were simply luminance increments or decrements (by pixel values of 30 on our 8-bit projectors) over the existing textures (like in our human perceptual experiments). This way, local contrast relationships in the background textures were maintained. In these experiments, the textures themselves had a range of 30–90 pixel intensities and a mean pixel value of 60 (on our 8-bit projectors). Three-hundred thirty-two of 688 cells that we analyzed for “saccadic suppression”

experienced such probe flashes, whereas the rest (356 cells) experienced the homogenous probe flash. For pig retina recordings, we always used the homogenous framework. However, in the subset of pig experiments where the 2-frame probe flash was employed (112 of 228 RGCs), we used a high-contrast probe flash such that a bright flash would be achieved by first going completely dark in the first frame followed by the bright flash in the next frame and vice versa for a dark flash. Again, all data were pooled across these different paradigms because their outcomes were indistinguishable.

The number of trials required during a physiology experiment depended on the number of conditions that we ran on a specific day. For example, testing 7 different flash delays required 15 trials (7 with bright probe flashes, 7 with dark probe flashes, and 1 without probes). In a given experiment, we always interleaved all conditions; that is, in any one of the 15 necessary trials, each of the 39 “saccades” could be followed by a bright or a dark probe at any of the 7 delays, or no probe at all. Moreover, we repeated the total number of conditions (e.g., the interleaved 15 trials) four times per session, and we averaged responses across repetitions. Since one trial typically lasted for 2 min, the example of 15 trials repeated 4 times lasted for ~2 h. This was usually combined with additional conditions (e.g., other background textures), such that typical recordings lasted 10–12 h. If the combination of conditions would have required even longer recordings in a given session, we typically reduced the number of conditions (e.g., we presented flashes at fewer delays).

We sometimes replaced the 100 ms “saccade” with an instantaneous texture jump, to test the sensitivity of retinal “saccadic suppression” (Fig. 3) to the kinematic properties of saccade-like texture displacements (Fig. 4b). Here, the texture simply jumped, in one display frame, from the pre- to the post-displacement position. All other procedures were like described above. Thirty-one RGCs were recorded with this paradigm.

In the control experiments of Fig. 4d, we used no textures at all. The screen was always a homogenous gray field, and the visual event of a “saccade” was replaced by an instantaneous step to a different gray value. The gray backgrounds had intensities between 30 and 90 (on our 8-bit projector). This instantaneous change in intensity caused either a positive contrast step (+0.03 to +0.50 Michelson contrast) or a negative contrast step (−0.03 to −0.50 Michelson contrast). A “trial” consisted of either 57 or 157 successive sequences that each combined a contrast step with a probe flash, as follows: there was first a “pre-step” fixation of 2 s (analogous to “pre-saccade” fixation in texture displacements), then an instantaneous switch to “post-step” fixation. At a certain time from the contrast step (delay: 17, 33, 50, 100, 250, 500, 1000, or 2000 ms), we presented a 2-frame (~33 ms) probe flash. For sequences containing no probe flash, the next contrast step happened 4 s after the previous one. The probe flash was either a uniform negative step of −0.33 Michelson contrast (“dark”) or a uniform positive step of +0.33 Michelson contrast (“bright”).

Finally, we used other stimuli unrelated to the main experiments to help us characterize RGC types and other receptive field properties (e.g., response polarity, latency, transiency, and spatial receptive fields). These stimuli had the same mean intensities and intensity ranges as the textures used in each experiment. Below, we describe these stimuli for the condition in which the texture intensities ranged from 0 to 60 pixel intensity (represented as grayscale RGB values in the units of our 8-bit projects). In experiments in which the textures ranged in intensity from 30 to 90, all intensities reported below were shifted upward by 30. (1) Full-field contrast steps. ON steps: stepping from 0 to 30 (+1 Michelson contrast) and from 30 to 60 (+0.33) for 2 s. OFF steps: stepping from 60 to 30 (−0.33) and from 30 to 0 (−1) for 2 s. (2) Full-field Gaussian flicker, 1 min. Screen brightness was updated every frame and was drawn from a Gaussian distribution with mean 30 and standard deviation 9. This stimulus was used to calculate the linear receptive field filters of ganglion cells through reverse correlation (spike-triggered averaging of the stimulus history). (3) Binary checkerboard flicker, 10–15 min. The screen was divided into a checkerboard pattern; each checker either covered an area of 55 × 55 μm, 60 × 60 μm, or 65 × 65 μm depending on the recording rig. The intensity of each checker was updated independently from the other checkers and randomly switched between 10 and 50 or 0 and 120. This stimulus also allowed us to calculate the linear filters of cells’ receptive fields.

Human psychophysics experimental procedures. In Human Experiment 1, we presented a coarse or fine background texture (Fig. 1) for 800–1700 ms in every trial. Over the texture, a white fixation marker (square of 7.3 × 7.3 arcmin) surrounded by a uniform gray circle of 30 min arc radius was presented at one screen location in order to guide gaze fixation onto the marker. The fixation marker was always at 4.8 deg eccentricity from display center, but its specific location was varied from trial to trial (up-right, up-left, down-right, or down-left relative to display center; 45 deg direction from horizontal). After the end of the initial interval, the fixation marker jumped to display center, instructing subjects to generate a saccade.

At a random time from the saccade instruction (47, 94, 153, 200, 247, or 507 ms), a luminance pedestal (probe flash) was applied for one display frame (~12 ms) at one of four locations relative to display center (7 deg above, below, to the right of, or to the left of center). Note that because the display was rasterized (that is, drawn by the computer graphics board from the top left corner in rows of pixels), the actual exact flash time and duration depended on the location of the flash on

the display (but in a manner like other psychophysical experiments studying the same phenomenon, and also in a manner that is unlikely to affect our results). The luminance pedestal consisted of a square of 147.8 × 147.8 min arc in which we added or subtracted a value of 4.8 cd m^{−2} to the texture pattern. Therefore, local contrast within the luminance pedestal was the same as that without the pedestal. Since all of our analyses revealed identical results whether the pedestal was a luminance increment or decrement, we combined these conditions in all analyses. At the end of the trial, subjects had to report their perceived flash location by pressing one of four buttons, corresponding to the four possible flash locations, on a hand-held response box.

As saccadic reaction times were 156.9 ± 3.3 ms s.e.m. across subjects, our choice of flash times above meant that we could analyze trials in which flashes appeared before or after saccade onset, allowing us to obtain full time courses (e.g., Fig. 1). Also, because of the display geometry, the retinal region that experienced a flash before, during, or after a saccade was always a region that was visually stimulated by the texture before flash onset (rather than by the monitor edge or the black surround of the laboratory). Therefore, we maintained pre- and post-flash visual stimulation by texture background, as in the retinal experiments. We also ensured that flash locations were not coincident with saccade goal locations both retinotopically and also in display coordinates. We confirmed in separate analyses that similar effects of suppression (e.g., Fig. 1) occurred for each flash location separately.

We collected 576 trials per session in this experiment. Six subjects participated in six sessions each, and the remaining two participated in three or four sessions.

Human Experiment 2 (Fig. 6) was identical, except that the initial fixation marker was presented at display center and remained there for the entire duration of a trial. Instead of instructing a saccade 800–1700 ms after fixation marker onset, we translated the entire background texture (switched on at trial onset) rapidly to simulate a saccade-like image displacement. Texture displacement consisted of a 6-frame translation at a speed of 176 deg s^{−1}. Note that, because of our display refresh rate and geometry, this meant a slightly larger displacement (of 12.4 deg) when compared to the saccade sizes in Human Experiment 1. However, we chose this translation because it resulted in a sufficiently fast average speed of the displacement (average speed in the real saccades of Human Experiment 1 was 160 deg s^{−1}). This choice is not problematic because our retinal experiments revealed that visual mechanisms related to saccadic suppression were not sensitive to parameters of individual motion patterns (Fig. 4b).

In this experiment, the texture displacement happened in a diagonal direction to simulate the directions of saccadic displacements of Human Experiment 1 (and also to dissociate the direction of motion flow from the locations of the flashes, again as in Human Experiment 1). For example, the texture could move globally down-right, as might be expected (in terms of image motion) if subjects made upward-leftward saccades in Human Experiment 1. Also, flash times were chosen relative to the onset of texture displacement from among the following values: −35, −24, 24, 47, 84, 108, 141, 200, 259, 494 ms.

All subjects participated in ten sessions each in this experiment.

We also performed a control experiment, in which there was neither a real saccade (Human Experiment 1) nor a texture displacement (Human Experiment 2), but otherwise identical to these two experiments. Subjects simply fixated display center, and we presented (after 1200 to 2400 ms from trial onset) a luminance pedestal exactly as in Human Experiments 1 and 2. To obtain full psychometric curves, we varied the luminance increment from among six values (Supplementary Fig. 3a, b). Subjects performed two sessions each of this experiment (600 trials per session).

To explore perceptual thresholds in a more quantitative manner for Human Experiments 1 and 2, we also performed additional real or simulated saccade experiments collecting full psychometric curves (Figs. 2 and 7; and Supplementary Figs. 4 and 7). The logic of both additional experiments (real or simulated) was the same as that of Human Experiments 1 and 2, except that we varied the luminance of the probe flash from trial to trial (like in the above control experiment of flash visibility; Supplementary Fig. 3a, b). As this endeavor (allowing us to measure full psychometric curves) was very data intensive, we reduced the time samples relative to saccade onset or texture displacement onset at which we probed perceptual performance. For the experiment with real saccades, we used an automatic procedure to detect saccade onset in real-time based on eye velocity, as described by Chen and Hafed³⁹. We then presented the probe flash at 42, 65, 88, or 148 ms after saccade detection. These times were chosen because they covered intervals of maximum perceptual saccadic suppression as well as recovery, allowing us to get a time course of perceptual threshold elevation associated with saccadic suppression. In subsequent data analyses, we confirmed that these flash times were as planned (within the expected variability due to the asynchronous nature of saccade times relative to display update times; Fig. 2). For the experiment with simulated saccades, we presented the probe flash at −24, −12, 48, or 96 ms relative to the onset time of the texture displacement. In this case, we introduced a new negative time sample to the set (−12 ms) because the original Human Experiment 2 did not probe this particular time (e.g., Fig. 6). It was therefore important to clarify that the time course of perceptual suppression for simulated saccades was continuous and well-behaved, exactly like that for real saccades.

In order to also estimate perceptual thresholds online in these additional experiments, and therefore optimize the numbers of trials needed, we applied an adaptive QUEST procedure⁴⁰ on each randomly interleaved condition. Specifically,

the first 40 trials of each randomly interleaved condition (e.g., flash time -24 ms and coarse texture, or flash -12 ms time and fine texture, and so on) were part of the QUEST procedure. The remaining trials in the session interleaved four additional flash luminances per condition, which were chosen to lie around the threshold luminance of each condition as detected by the QUEST procedure. These additional flashes had luminances that were ± 1 or ± 2 times a pre-defined luminance increment for a given condition, depending on the detected threshold and earlier pilot data. Specifically, if the detected threshold (according to QUEST) was very low (e.g., no suppression effect), the pre-defined luminance increment was 1 step of luminance (dictated by the luminance resolution of our display; Supplementary Fig. 3a). That is, the four additional flashes were at ± 1 and ± 2 display-determined luminance steps from the detected threshold. If the detected threshold (according to QUEST) was high (e.g., strong suppression), we made the pre-defined luminance increment 2 or 5 display-determined luminance steps (that is, ± 2 and ± 4 display-determined luminance steps or ± 5 and ± 10 display-determined luminance steps, respectively). This allowed fitting the psychometric curves during subsequent data analyses, including measurements from the full dynamic range of perceptual performance. The reasoning behind this approach is as follows: depending on the amount of perceptual saccadic suppression to be expected per condition (e.g., peak suppression during saccades or texture displacements, or very weak suppression during recovery), it is expected that the psychometric curves would be shifted by different amounts from baseline depending on the particular condition (e.g., flash time or coarse versus fine texture). Finally, also note that we only used bright flashes in these particular experiments instead of both bright and dark flashes. In total, we collected 240 trials per condition per subject.

In yet another control experiment for Human Experiments 1 and 2, we mimicked the retinal results of Fig. 4d. Subjects fixated a central fixation spot over a gray background. The background had one of eight luminances (22.4, 30.24, 38.08, 45.92, 53.76, 61.6, 69.44, 77.28 cd m^{-2}). After a random initial fixation duration (similar to Human Experiment 2), the luminance of the background was changed suddenly (in one display frame update) to one of the remaining seven luminances. This meant that across trials, we had seven total levels of contrast change in the background as our visual transient. At one of five different possible times relative to the time of background luminance change (-24 , -12 , 36 , 72 , or 108 ms), a luminance pedestal was flashed briefly, exactly like in Human Experiments 1 and 2. We ensured that the contrast of the flash (relative to the currently displayed background luminance) was always the same across all trials. We also ensured that baseline visibility of the pedestal in the absence of the contrast change was at ceiling performance (see the longest sampled time value in Fig. 5, demonstrating near perfect detection performance for all background luminance steps). Subjects maintained fixation throughout all trials and simply reported the locations of the brief flashes. Subjects performed one session, each, of this experiment, with 1120 trials per session.

In Human Experiment 3 (Fig. 8), the flashes of Human Experiments 1 and 2 were replaced by vertical Gabor gratings having one of five different spatial frequencies (0.41, 0.85, 1.71, 3.42, 4.56, or 6.8 cpd). The contrast of the grating (defined as the difference between maximum and minimum luminance in the grating divided by the sum of the same luminances) was 14.3%. Spatial phase was randomized from trial to trial, and the σ parameter of the Gaussian envelope was 0.49 deg. Also, a virtual monitor of 20 deg diameter was present at display center at the time of Gabor grating flashes. The virtual monitor had a uniform gray luminance equal to the average of the textures used in Human Experiments 1 and 2. Surrounding the virtual monitor, a coarse or fine texture could be visible.

In one block of trials, subjects generated saccades towards display center using the same procedures as in Human Experiment 1. Grating flash times were similar to Human Experiment 1, and the subjects performed 6 sessions each (576 trials per session).

In another block of trials, subjects maintained fixation at display center. In one third of the trials, the virtual monitor and surrounding texture did not move. These trials provided us with “baseline” visual performance (i.e., without saccades or virtual monitor displacements). It was necessary to have these trials because perceptual visibility of different spatial frequencies is not equal due to the well-known human contrast sensitivity function⁷⁰. Therefore, we needed to establish “baseline” grating visibility first and then compare the effects of saccades or saccade-like virtual monitor displacements on such visibility. In the remaining two thirds of the trials, the virtual monitor and surrounding texture initially appeared displaced from display center at a location near one corner of the display and along one of the diagonal directions. After 800–1700 ms, the virtual monitor and surrounding texture were translated rapidly towards display center to simulate visual flow associated with the diagonal saccades of the real-saccade version of the paradigm (the translation parameters were similar to Human Experiment 2). Grating flashes happened 84 ms or 108 ms after virtual monitor and texture displacement. Note that we reduced the number of flash times here because of the larger number of conditions (five different spatial frequencies of the Gabor gratings) that needed to be collected. However, our data were consistent with all other experiments in terms of recovery time courses of suppression (e.g., Figs. 1, 6, 8 and Supplementary Figs. 8–10).

As the initial displaced position of the virtual monitor (and texture) provided a cue to subjects that grating onset was expected soon, and because such a cue was not present in the one third of trials without image motion, we equalized subject

expectations across these conditions by dimming the fixation point to black from the time of image motion onset until 200 ms after flash onset (equal timing was ensured in the one third of trials without image motions, such that the same expectation of grating onset was established by fixation marker dimming). The fixation marker then disappeared, and subjects had to report flash location.

Subjects performed six sessions each of this condition, with 576 trials per session (two subjects performed seven and five sessions each instead of six).

We also repeated the same experiment but with a black surround around the virtual monitor instead of a coarse or fine texture. Note that a black surround is theoretically equivalent to an infinitely coarse surround. We therefore expected results conceptually similar to those with a coarse surround. Also, in this control experiment, we randomly interleaved all trial types together in the same session (fixation with virtual monitor displacement, real saccade, and fixation with neither virtual monitor displacement nor saccade). This allowed us to further confirm that our results from Human Experiment 3 were not influenced by the separate blocking of real saccade trials and virtual monitor displacement trials.

We also repeated Human Experiment 3 to collect full psychometric curves, like we did for Human Experiments 1 and 2 above. In these additional experiments, because of the data-intensive nature of full psychometric curves, we concentrated on the three lowest spatial frequencies of the Gabor gratings. This was sufficient to observe selectivity or lack of selectivity of perceptual suppression as a function of spatial frequency (e.g., Fig. 8). More importantly, these three lowest spatial frequencies were associated with ceiling baseline visibility (Fig. 8), thus simplifying interpretations of any suppression that we would observe. The experiments were the same as Human Experiment 3, except that the contrast of the flashed Gabor grating was varied from trial to trial. We used a similar adaptive procedure to that used in Figs. 2 and 7 to select contrast from trial to trial, in order to optimize finding perceptual thresholds and fitting of psychometric curves (see procedures above). We also used the same online saccade detection algorithm as in the experiments of Fig. 2 to decide on the time of Gabor grating flash onset (see procedures above). For both real and simulated saccade variants of these experiments, we used two times relative to the “saccade” event, one within a period associated with strong perceptual suppression and one at a late time point associated with perceptual recovery (see Figs. 9 and 10).

Retina electrophysiology data analysis and statistics. Low-density MEA recordings were high-pass filtered at a 500 Hz cutoff frequency using a tenth-order Butterworth filter. We extracted spike waveforms and times using thresholding, and we semi-manually sorted spikes using custom software. For high-density MEA recordings, we performed spike sorting by an offline automatic algorithm⁷¹ and assessed the sorted units using UnitBrowser⁷². We judged the quality of all units using inter-spike intervals and spike shape variation. Low-quality units, such as ones with high inter-spike intervals, missing spikes, or contamination, were discarded. All firing rate analyses were based on spike times of individual units.

We first characterized the properties of RGCs. We calculated linear filters in response to full-field Gaussian flicker and binary checkerboard flicker by summing the 500-ms stimulus history before each spike. The linear filters allowed determining cell polarity. Specifically, the amplitude of the first peak of the filter was determined. If the peak was positively deflected, the cell was categorized as an ON cell; if negatively deflected, the cell was an OFF cell. ON cells were later always analyzed with respect to their responses to bright probe flashes in the main experiment, and OFF cells were analyzed with dark probe flashes. We determined the spatial receptive fields of RGCs by calculating the linear filters for each region (checker) defined by the binary checkerboard flickering stimulus. The modulation strength of each linear filter, measured as the s.d. along the 500 ms temporal kernel, is an estimate for how strongly that region drives ganglion cell responses. We fitted the resulting 2D-map of s.d. values with a two-dimensional Gaussian and took the $2\text{-}\sigma$ ellipse (long axis) as the receptive field diameter. For all other figures and analyses, we converted spike times to estimates of firing rate by convolving these times with a Gaussian of $\sigma = 10$ ms standard deviation and amplitude $0.25 \sigma^{-1} e^{1/2}$.

For each RGC, we used responses to full-field contrast steps to calculate an ON-OFF index, a transiency index, and a response latency index. These indices were used to characterize the properties of RGCs (Supplementary Fig. 6) that we included in our analyses. The ON-OFF index was calculated by dividing the difference between ON and OFF step peak response by their sum. The resulting index values ranged between -1 (OFF) and $+1$ (ON) and were then scaled to span between 0 (OFF) and $+1$ (ON). The transiency index was defined as the ratio of the response area within the first 400 ms and the total response area spanning 2000 ms. The resulting index had a value of 1 for pure transient cells. Response latency was calculated as the time from stimulus onset to 90% of peak response. This value was normalized to the maximum response latency in our dataset to create the response latency index.

To quantify retinal “saccadic suppression”, we first determined a “baseline response”, defined as the response to a probe flash ~ 2 s after texture displacement onset (delay between 1967 and 2100 ms, depending on the specific flash times used in a specific experiment). This baseline response was compared to responses of the same cell to the same flash when it occurred at an earlier time (i.e., closer in time to the “saccade”). Usually, the saccade-like texture displacements themselves caused significant neural responses even without flashes (“saccade-response”, e.g., Fig. 3b), and the responses to the flashes were superimposed on these “saccade-responses”

(Fig. 3c). We therefore first isolated the component of the responses caused by the flashes by subtracting the “saccade-responses” from the composite responses.

To get a robust estimate of the response to “saccades” alone (i.e., without any flashes), we averaged spike rate from before “saccade” onset up until the next “saccade” onset for conditions in which no flash was presented, or until just before the flash onset for conditions in which a “post-saccade” flash was presented. This was done for each of the 39 successive “saccades” in a given trial.

We then computed a neural modulation index, ranging from -1 to $+1$. A value of -1 represents complete suppression of flash-induced responses, whereas $+1$ indicates “complete enhancement” of flash-induced responses (that is, there was only a response to a flash after saccades, but not to a flash in isolation). A modulation index of 0 meant no change in flash-induced response relative to the “baseline” response. The modulation index of an RGC for a given flash delay d after “saccade” onset was calculated as $(r_d - r_b)/(r_d + r_b)$ where r_d is the peak firing rate for the flash-component of the response (see above for how we isolated this from the composite “saccade” + flash response) and r_b is the peak firing rate for the baseline flash response (i.e., the same flash but occurring ~ 2 s away from any “saccade”; see above). In all cases, peak firing rate was estimated after averaging responses from all repetitions of a given condition (delay d or baseline) for a given RGC. For ON cells, the modulation index was based only on responses to bright flashes, and for OFF cells, it was based on responses to dark flashes. For some analyses, we also calculated modulation indices of RGCs for each of the 39 individual “saccades” using the same procedure.

In some cells and trials, individual “saccades” from the sequence of 39 were discarded. This happened when the baseline response peak was $<60\%$ of the median baseline response peak across the 39 “saccades” of a given trial. We did this to ensure that our modulation indices were not marred by a numerator and denominator approaching zero (e.g., if both flash and baseline responses were weak). We did, however, re-include sequences in which the peak response to the flash after the “saccade” was above the median baseline response peak (across the 39 “saccades”). This was done in order to re-include sequences (if discarded by the first step) for which the baseline flash response was weak but a flash after “saccades” nonetheless gave a robust response. For example, this could happen if a cell did not respond to a flash in isolation but the “saccade” enhanced the response to a flash following it. Our main results (e.g., Fig. 3) were highly robust to such scenarios.

Finally, to perform statistics, we applied tests at either the individual cell level or at the level of the population. At the individual cell level, we determined whether a given RGC’s modulation index for a probe flash presented at a given delay was significantly different from 0 (i.e., “Is the response of this cell modulated by the “saccade”?”). For this, we performed a one-tailed sign test of the null hypothesis that the 39 individual modulation indices came from a distribution with zero median against the alternative hypothesis that the median was below (for negative modulation index) or above (for positive modulation index) zero. The modulation index was considered significant (i.e., the flash response was modulated by the “saccade”) at $p < 0.05$ if the test had a power $(1 - \beta)$ of at least 0.8 . At the population level, we determined whether the retinal output as a whole was modulated by “saccades”. For this, we performed a two-tailed Wilcoxon signed-rank test of the null hypothesis that the median of the distribution of modulation indices did not differ from 0 . Lastly, we tested whether the modulation index of the population was significantly different across textures. For this, we performed a two-tailed Wilcoxon signed rank test of the null hypothesis that the median of the distribution of modulation indices did not differ across textures. Since our modulation index was based on responses to the brief probe flashes, it could only be computed for cells that did respond to these flash stimuli (mouse: $N = 688$ of 1423 recorded cells; pig: $N = 228$ of 394). Only these cells, showing a measurable baseline flash response, were included in our analyses for retinal “saccadic suppression” (Fig. 3e and Supplementary Fig. 5).

To quantify retinal “saccadic suppression” in our control experiments with structure-free uniform backgrounds and luminance steps in place of textures and texture displacements (Fig. 4d), we used the same analyses and statistical procedures to those described above for the texture displacement paradigm. The only difference was that instead of 39 successive “saccades” in a trial, we now had either 57 or 157 successive full-field luminance steps (depending on experiment setting). Twenty-two of 57 or 66 of 157 steps had a Michelson contrast in the range of ± 0.03 to ± 0.15 and these steps were used to quantify suppression for low-contrast luminance steps. Twenty-four of 57 or 58 of 157 steps had a Michelson contrast in the range of ± 0.20 to ± 0.40 and were used to quantify suppression for high-contrast luminance steps. From the perspective of visual transients across the retina, low-contrast luminance steps are equivalent to fine texture displacements over receptive fields, and high-contrast luminance steps are equivalent to coarse texture displacements. This is simply because of the spatial relationship between receptive field sizes and texture spatial scales: a fine texture presents both dark and bright blobs within individual receptive fields both before and after the texture displacement (resulting in a low-contrast change in luminance over the receptive fields); on the other hand, a coarse texture has dark or bright blobs that are of similar size to the receptive fields (resulting in the potential for a very large contrast change in luminance over the receptive fields after the texture displacement). As shown in Fig. 4d, low and high-contrast luminance steps resulted in the modulation of ganglion cell responses to the probe flashes that was reminiscent of the modulation observed after displacement of fine and coarse textures, respectively

(also validated perceptually in Fig. 5). Similar to the texture displacement paradigm, the modulation index was based on responses to brief probe flashes, and it could therefore only be computed for cells that did respond to these flash stimuli ($N = 376$ of 650 recorded RGCs in mouse). The modulation index for ON RGCs was calculated from responses to bright probe flashes, and that for OFF RGCs was calculated from responses to dark flashes.

Human psychophysics data analysis and statistics. We analyzed eye movements in all trials. We detected saccades using established methods^{39,73}, and we manually inspected all trials to correct for mis-detections. In experiments requiring a saccade (e.g., Fig. 1), we excluded from analysis any trials with premature (before saccade instruction) or late (>500 ms reaction time) saccades. We also rejected all trials in which saccades landed >0.5 deg from the saccade target. In experiments requiring fixation, we excluded from analysis any trials in which a saccade or microsaccade happened anywhere in the interval from 200 ms before to 50 ms after any flash or grating onset.

For experiments with saccades (e.g., Fig. 1), we obtained time courses of perception by calculating, for each trial, the time of flash or grating onset from saccade onset. We then binned these times into 50 ms bins that were moved in 5 ms bin-steps relative to saccade onset. Within each bin, we calculated the proportion of correct trials, and we obtained full time courses of this perceptual measure. We obtained time course curves for each subject individually, and we then averaged the curves for the individual subjects in summary figures. All of our analyses were robust at the individual subject level as well (e.g., Supplementary Fig. 2).

For experiments with simulated saccades (i.e., saccade-like texture displacements), or background luminance steps (Fig. 5), there were discrete flash or grating times relative to “simulated saccade” onset, so no temporal binning was needed. At each flash or grating time, we simply calculated the proportion of correct trials.

When we fitted performance to psychometric curves (e.g., Supplementary Fig. 3a, b), we used the psignifit 4 toolbox⁷⁴, and we used an underlying beta-binomial model. In all psychometric curve fits, we also included lapse parameters among the fitted parameters, in order to account for potential small deviations from either perfect ceiling performance or perfect floor (chance) performance at the extremes of the psychometric curves.

We also used the same toolbox to analyze the variants of Human Experiments 1 and 2 in which we collected full psychometric curves (Figs. 2 and 7). For these experiments, we defined the threshold of an individual subject as the flash luminance level that resulted in correct perceptual performance at a value of 62.5% of the total dynamic range of the subject’s psychometric curve (that is, 62.5% of the dynamic range of the fitted psychometric curve after the inclusion of lapse rates). We then plotted the value of such threshold as a function of flash time relative to real or simulated saccade time.

For some analyses of Human Experiment 3 and its control version, we calculated a “suppression ratio” as a visualization aid (e.g., Fig. 8). This was obtained as follows. For a given spatial frequency grating, we calculated the fraction of correct trials within a given time window (from either simulated or real saccade onset) divided by the fraction of correct trials for the same spatial frequency when there was neither a saccade nor a virtual monitor and texture displacement (i.e., baseline perception of a given spatial frequency). This ratio therefore revealed the effect of suppression independently from the underlying visibility of any given spatial frequency¹⁴. However, note that we also report raw proportions of correct trials in all conditions.

All error bars that we show denote s.e.m. across individual subjects, except where we report individual subject analyses and control analyses. For individual subject performance, error bars denote s.e.m. across trials; for control analyses, error bars denote 95% confidence intervals (e.g., Supplementary Fig. 3a, b) or s.d. (e.g., Supplementary Fig. 3d, f). All error bar definitions are specified in the corresponding figures and/or legends.

To statistically validate if the time courses for perceptual localization performance for saccades across the different background textures (coarse versus fine) differed significantly from each other (e.g., Fig. 1), we used a random permutation test with correction for time clusters of adjoining significant p -values^{37,38}. First, for each time bin, we calculated a test statistic comparing performance for coarse versus fine background textures. This test statistic was the difference between the proportion of correct responses for the different textures. Then, we performed a random permutation with 1000 repetitions for each time bin; that is, we collected all trials of both conditions, within a given time bin, into a single large set, and we randomly assigned measurements as coming from either coarse or fine textures, while at the same time maintaining the relative numbers of observations per time bin for each texture condition. From this resampled data, we calculated the test statistic again, and we repeated this procedure 1000 times. Second, we checked, for each time bin, whether our original test statistic was bigger than 95% of the resampled test statistics (i.e., significant), and we counted the number of adjoining time bins that were significant at this level (i.e. clusters of time bins in which there was a difference between coarse and fine textures). We then repeated this for all 1000 resampled test statistics. The p -value for our original clusters was then calculated as the number of resampled clusters that were bigger or the same size as the original clusters, divided by the total number of repetitions

(1000). This procedure was described in detail elsewhere³⁸. We followed a conservative approach, paying no attention to which bins in the resampled data formed a cluster of time bins. As discussed elsewhere³⁸, our statistical analysis constituted a highly conservative approach to establishing significance of differences between time courses for coarse and fine textures. In Human Experiment 3, we used the same approach to compare time courses of suppression ratio for coarse and fine surround contexts with real saccades.

For Human Experiment 2, we had discrete flash times relative to texture displacement onset. Here, the comparison between coarse and fine textures was tested with a Bonferroni-corrected χ^2 test at corresponding flash times. To compare between real and simulated saccades in Human Experiments 1 and 2, we also ran a Bonferroni-corrected χ^2 test. We only considered time bins in the real saccade data that corresponded to the discrete flash times in the simulated saccade data. A Bonferroni correction was necessary because we tested the same data sets on multiple time bins with the same hypothesis (that there is a difference in time courses).

In Human Experiment 3, we also compared suppression ratios for real and simulated saccades for a given texture surround. We again used a Bonferroni-corrected χ^2 test. This was justified because within a given surround, baseline data were the same for real and simulated saccades. Therefore, the relationship between the proportion of correct localizations and suppression ratio was identical. In contrast, testing suppression ratios between fine and coarse surrounds in the same experiment with a χ^2 test was not applicable because baseline values differed. Therefore, we used instead a random permutation test with 5000 repetitions. To compare the different spatial frequency Gabor gratings in one bin or time stamp, we used the Kruskal–Wallis test.

For the psychometric versions of Human Experiment 3 (Figs. 9 and 10), we used similar analyses on perceptual thresholds to those used in the psychometric versions of Human Experiments 1 and 2 (Figs. 2 and 7).

All analyses were done in MATLAB (The MathWorks Inc).

Reporting summary. Further information on research design is available in the Nature Research Reporting Summary linked to this article.

Data availability

All data presented in this paper are stored and archived on secure institute computers and are available upon reasonable request.

Received: 5 April 2019; Accepted: 30 March 2020;

Published online: 24 April 2020

References

- O'Regan, J. K. & Noë, A. A sensorimotor account of vision and visual consciousness. *Behav. Brain Sci.* **24**, 939–973 (2001).
- Wurtz, R. H. Neuronal mechanisms of visual stability. *Vis. Res.* **48**, 2070–89 (2008).
- Wurtz, R. H., Joiner, W. M. & Berman, R. A. Neuronal mechanisms for visual stability: progress and problems. *Philos. Trans. R. Soc. B Biol. Sci.* **366**, 492–503 (2011).
- Thiele, A., Henning, P., Kubischik, M. & Hoffmann, K. P. Neural mechanisms of saccadic suppression. *Science (80-)* **295**, 2460–2462 (2002).
- Zuber, B. L. & Stark, L. Saccadic suppression: Elevation of visual threshold associated with saccadic eye movements. *Exp. Neurol.* **16**, 65–79 (1966).
- Beeler, G. W. Visual threshold changes resulting from spontaneous saccadic eye movements. *Vis. Res.* **7**, 769–775 (1967).
- Matin, E. Saccadic suppression: a review and an analysis. *Psychol. Bull.* **81**, 899–917 (1974).
- Riggs, L. A. & Manning, K. A. Saccadic suppression under conditions of whiteout. *Invest. Ophthalmol. Vis. Sci.* **23**, 138–143 (1982).
- Volkman, F. C. Human visual suppression. *Vis. Res.* **26**, 1401–1416 (1986).
- Burr, D. C., Morrone, M. C. & Ross, J. Selective suppression of the magnocellular visual pathway during saccadic eye movements. *Nature* **371**, 511–513 (1994).
- Ross, J., Burr, D. C. & Morrone, M. C. Suppression of the magnocellular pathway during saccades. *Behav. Brain Res.* **80**, 1–8 (1996).
- Bremmer, F., Kubischik, M., Hoffmann, K. -P. & Krekelberg, B. Neural dynamics of saccadic suppression. *J. Neurosci.* **29**, 12374–12383 (2009).
- Hafed, Z. M. & Krauzlis, R. J. Microsaccadic suppression of visual bursts in the primate superior colliculus. *J. Neurosci.* **30**, 9542–9547 (2010).
- Chen, C. -Y. & Hafed, Z. M. A neural locus for spatial-frequency specific saccadic suppression in visual-motor neurons of the primate superior colliculus. *J. Neurophysiol.* **117**, 1657–1673 (2017).
- Duffy, F. H. & Lombroso, C. T. Electrophysiological evidence for visual suppression prior to the onset of a voluntary saccadic eye movement. *Nature* **218**, 1074–1075 (1968).
- Diamond, M. R., Ross, J. & Morrone, M. C. Extraretinal control of saccadic suppression. *J. Neurosci.* **20**, 3449–3455 (2000).
- Ross, J., Morrone, M. C., Goldberg, M. E. & Burr, D. C. Changes in visual perception at the time of saccades. *Trends Neurosci.* **24**, 113–121 (2001).
- Gremmler, S. & Lappe, M. Saccadic suppression during voluntary versus reactive saccades. *J. Vis.* **17**, 1–10 (2017).
- Mackay, D. M. Elevation of visual threshold by displacement of retinal image. *Nature* **225**, 90–92 (1970).
- García-Pérez, M. A. & Peli, E. Visual contrast processing is largely unaltered during saccades. *Front. Psychol.* **2**, 1–15 (2011).
- Ilg, U. J. & Hoffmann, K. P. Motion perception during saccades. *Vis. Res.* **33**, 211–220 (1993).
- Campbell, F. W. & Wurtz, R. H. Saccadic omission: why we do not see a grey-out during a saccadic eye movement. *Vis. Res.* **18**, 1297–1303 (1978).
- Mitrani, L., Mateeff, S. & Yakimoff, N. Is saccadic suppression really saccadic? *Vis. Res.* **11**, 1157–1161 (1971).
- Matin, E., Clymer, A. B. & Matin, L. Metacontrast and saccadic suppression. *Science* **178**, 179–182 (1972).
- Mitrani, L., Yakimoff, N. & Mateeff, S. Saccadic suppression in the presence of structured background. *Vis. Res.* **13**, 517–521 (1973).
- Mateeff, S., Yakimoff, N. & Mitrani, L. Some characteristics of the visual masking by moving contours. *Vis. Res.* **16**, 489–492 (1976).
- Brooks, B. A., Impelman, D. M. K. & Lum, J. T. Backward and forward masking associated with saccadic eye movement. *Percept. Psychophys.* **30**, 62–70 (1981).
- Macknik, S. L. & Livingstone, M. S. Neuronal correlates of visibility and invisibility in the primate visual system. *Nat. Neurosci.* **1**, 144–149 (1998).
- Castet, E., Jeanjean, S. & Masson, G. S. 'Saccadic suppression'—no need for an active extra-retinal mechanism. *Trends Neurosci.* **24**, 316–317 (2001).
- Castet, E. Perception of intra-saccadic motion. In *Dynamics of Visual Motion Processing* 141–160 (Springer US, 2010). <https://doi.org/10.1007/978-1-4419-0781-3>
- Krueger, J. & Fischer, B. Strong periphery effect in cat retinal ganglion cells. Excitatory responses in ON- and OFF-center neurons to single grid displacements. *Exp. Brain Res.* **18**, 316–318 (1973).
- Noda, H. & Adey, W. R. Retinal ganglion cells of the cat transfer information on saccadic eye movement and quick target motion. *Brain Res.* **70**, 340–345 (1974).
- Enroth-Cugell, C. & Jakiela, H. G. Suppression of cat retinal ganglion cell responses by moving patterns. *J. Physiol.* **302**, 49–72 (1980).
- Roska, B. & Werblin, F. Rapid global shifts in natural scenes block spiking in specific ganglion cell types. *Nat. Neurosci.* **6**, 600–608 (2003).
- Passaglia, C. L., Freeman, D. K. & Troy, J. B. Effects of remote stimulation on the modulated activity of cat retinal ganglion cells. *J. Neurosci.* **29**, 2467–2476 (2009).
- Dacey, D. M. & Petersen, M. R. Dendritic field size and morphology of midget and parasol ganglion cells of the human retina. *Proc. Natl Acad. Sci.* **89**, 9666–9670 (1992).
- Maris, E. & Oostenveld, R. Nonparametric statistical testing of EEG- and MEG-data. *J. Neurosci. Methods* **164**, 177–190 (2007).
- Bellet, J., Chen, C. -Y. & Hafed, Z. M. Sequential hemifield gating of α - and β -behavioral performance oscillations after microsaccades. *J. Neurophysiol.* **118**, 2789–2805 (2017).
- Chen, C. -Y. & Hafed, Z. M. Postmicrosaccadic enhancement of slow eye movements. *J. Neurosci.* **33**, 5375–5386 (2013).
- Watson, A. B. & Pelli, D. G. Quest: a Bayesian adaptive psychometric method. *Percept. Psychophys.* **33**, 113–120 (1983).
- Robinson, D. L. & Wurtz, R. H. Use of an extraretinal signal by monkey superior colliculus neurons to distinguish real from self-induced stimulus movement. *J. Neurophysiol.* **39**, 852–870 (1976).
- Mayo, J. P. & Sommer, M. A. Neuronal adaptation caused by sequential visual stimulation in the frontal eye field. *J. Neurophysiol.* **100**, 1923–1935 (2008).
- Krock, R. M. & Moore, T. Visual sensitivity of frontal eye field neurons during the preparation of saccadic eye movements. *J. Neurophysiol.* **116**, 2882–2891 (2016).
- Chen, C. -Y., Ignashchenkova, A., Thier, P. & Hafed, Z. M. Neuronal response gain enhancement prior to microsaccades. *Curr. Biol.* **25**, 2065–2074 (2015).
- Breitmeyer, B. G. Visual masking: past accomplishments, present status, future developments. *Adv. Cogn. Psychol.* **3**, 9–20 (2007).
- Castet, E. & Masson, G. S. Motion perception during saccadic eye movements. *Nat. Neurosci.* **3**, 177–83 (2000).
- Ramcharan, E. J., Gnadt, J. W. & Sherman, S. M. The effects of saccadic eye movements on the activity of geniculate relay neurons in the monkey. *Vis. Neurosci.* **18**, 253–258 (2001).

48. Reppas, J. B., Usrey, W. M. & Reid, R. C. Saccadic eye movements modulate visual responses in the lateral geniculate nucleus. *Neuron* **35**, 961–974 (2002).
49. Kleiser, R., Seitz, R. J. & Krekelberg, B. Neural correlates of saccadic suppression in humans. *Curr. Biol.* **14**, 386–390 (2004).
50. Royal, D. W., Sary, G., Schall, J. D. & Casagrande, V. A. Correlates of motor planning and postsaccadic fixation in the macaque monkey lateral geniculate nucleus. *Exp. Brain Res.* **168**, 62–75 (2006).
51. Phongphanphanee, P. et al. Distinct local circuit properties of the superficial and intermediate layers of the rodent superior colliculus. *Eur. J. Neurosci.* **40**, 2329–2343 (2014).
52. Rajkai, C. et al. Transient cortical excitation at the onset of visual fixation. *Cereb. Cortex* **18**, 200–209 (2008).
53. Ibbotson, M. R., Crowder, N. A., Cloherty, S. L., Price, N. S. C. & Mustari, M. J. Saccadic modulation of neural responses: possible roles in saccadic suppression, enhancement, and time compression. *J. Neurosci.* **28**, 10952–60 (2008).
54. Cloherty, S. L., Mustari, M. J., Rosa, M. G. P. & Ibbotson, M. R. Effects of saccades on visual processing in primate MSTd. *Vis. Res.* **50**, 2683–2691 (2010).
55. Ibbotson, M. R. & Cloherty, S. L. Visual perception: saccadic omission-suppression or temporal masking? *Curr. Biol.* **19**, R493–6 (2009).
56. Duhamel, J. R., Colby, C. L. & Goldberg, M. E. The updating of the representation of visual space in parietal cortex by intended eye movements. *Science* **255**, 90–2 (1992).
57. Sommer, M. A. & Wurtz, R. H. Influence of the thalamus on spatial visual processing in frontal cortex. *Nature* **444**, 374–377 (2006).
58. Munch, T. A. et al. Approach sensitivity in the retina processed by a multifunctional neural circuit. *Nat. Neurosci.* **12**, 1308–1316 (2009).
59. Farrow, K. et al. Ambient illumination toggles a neuronal circuit switch in the retina and visual perception at cone threshold. *Neuron* **78**, 325–338 (2013).
60. Tikidji-Hamburyan, A. et al. Retinal output changes qualitatively with every change in ambient illuminance. *Nat. Neurosci.* **18**, 66–74 (2015).
61. Reinhard, K. et al. Step-by-step instructions for retina recordings with perforated multi electrode arrays. *PLoS ONE* **9**, e106148 (2014).
62. Frey, U., Egert, U., Heer, F., Hafizovic, S. & Hierlemann, A. Microelectronic system for high-resolution mapping of extracellular electric fields applied to brain slices. *Biosens. Bioelectron.* **24**, 2191–2198 (2009).
63. Muller, J. et al. High-resolution CMOS MEA platform to study neurons at subcellular, cellular, and network levels. *Lab Chip* **15**, 2767–2780 (2015).
64. Hafed, Z. M. Alteration of visual perception prior to microsaccades. *Neuron* **77**, 775–786 (2013).
65. Grujic, N., Brehm, N., Gloge, C., Zhuo, W. & Hafed, Z. M. Perisaccadic perceptual mislocalization is different for upward saccades. *J. Neurophysiol.* **120**, 3198–3216 (2018).
66. Schwartz, G. W. et al. The spatial structure of a nonlinear receptive field. *Nat. Neurosci.* **15**, 1572–80 (2012).
67. Zhang, Y., Kim, I. -J., Sanes, J. R. & Meister, M. The most numerous ganglion cell type of the mouse retina is a selective feature detector. *Proc. Natl Acad. Sci.* **109**, E2391–E2398 (2012).
68. Sakatani, T. & Isa, T. Quantitative analysis of spontaneous saccade-like rapid eye movements in C57BL/6 mice. *Neurosci. Res.* **58**, 324–331 (2007).
69. Itokazu, T. et al. Streamlined sensory motor communication through cortical reciprocal connectivity in a visually guided eye movement task. *Nat. Commun.* **9**, 338 (2018).
70. Peli, E., Arend, L. E., Young, G. M. & Goldstein, R. B. Contrast sensitivity to patch stimuli: effects of spatial bandwidth and temporal presentation. *Spat. Vis.* **7**, 1–14 (1993).
71. Diggelmann, R., Fiscella, M., Hierlemann, A. & Franke, F. Automatic spike sorting for high-density microelectrode arrays. *J. Neurophysiol.* **120**, 3155–3171 (2018).
72. Idrees, S., Franke, F., Diggelmann, R., Hierlemann, A. & Munch, T. A. UnitBrowser—a tool to evaluate and post-process units sorted by automatic spike sorting algorithms (Abstract). *Front. Neurosci.* **10**, <https://doi.org/10.3389/conf.fnins.2016.93.00054> (2016).
73. Bellet, M. E., Bellet, J., Nienborg, H., Hafed, Z. M. & Berens, P. Human-level saccade detection performance using deep neural networks. *J. Neurophysiol.* **121**, 646–661 (2019).
74. Schutt, H. H., Harmeling, S., Macke, J. H. & Wichmann, F. A. Painfree and accurate Bayesian estimation of psychometric functions for (potentially) overdispersed data. *Vis. Res.* **122**, 105–123 (2016).

Acknowledgements

Andreas Hierlemann provided the HiDens CMOS MEA system and helped establish our high-density MEA recordings. Roland Diggelmann helped in setting up the pipeline (including providing code) for automatic spike sorting of high-density MEA recordings. Our work was supported by funds of the Deutsche Forschungsgemeinschaft (DFG) to the Werner Reichardt Center for Integrative Neuroscience (EXC 307) and to T.A.M. (MU3792/3-1). T.A.M. received support from the Tistou and Charlotte Kerstan Foundation. T.A.M. and Z.M.H. were also supported by an intra-mural funding program (Projekt 2013-05) of the Werner Reichardt Center for Integrative Neuroscience. F.F. was supported by a Swiss National Science Foundation Ambizione grant (PZ00P3_167989), and M.P.B. and Z.M.H. were further funded by the SFB 1233 on “Robust Vision” (DFG) - project number 276693517.

Author contributions

S.I., M.B., T.A.M., Z.M.H. designed the overall study; S.I., M.B., T.A.M., Z.M.H. designed experiments; S.I. performed ex vivo retina experiments; M.B., Z.M.H. performed human psychophysics experiments; S.I., M.B., F.F., T.A.M., Z.M.H. analyzed data; S.I., M.B., F.F., T.A.M., Z.M.H. wrote manuscript.

Competing interests

The authors declare no competing interests.

Additional information

Supplementary information is available for this paper at <https://doi.org/10.1038/s41467-020-15890-w>.

Correspondence and requests for materials should be addressed to T.A.M. or Z.M.H.

Peer review information *Nature Communications* thanks Frank Bremmer and other, anonymous, reviewer(s) for their contributions to the peer review of this work. Peer review reports are available.

Reprints and permission information is available at <http://www.nature.com/reprints>

Publisher’s note Springer Nature remains neutral with regard to jurisdictional claims in published maps and institutional affiliations.



Open Access This article is licensed under a Creative Commons Attribution 4.0 International License, which permits use, sharing, adaptation, distribution and reproduction in any medium or format, as long as you give appropriate credit to the original author(s) and the source, provide a link to the Creative Commons license, and indicate if changes were made. The images or other third party material in this article are included in the article’s Creative Commons license, unless indicated otherwise in a credit line to the material. If material is not included in the article’s Creative Commons license and your intended use is not permitted by statutory regulation or exceeds the permitted use, you will need to obtain permission directly from the copyright holder. To view a copy of this license, visit <http://creativecommons.org/licenses/by/4.0/>.

© The Author(s) 2020

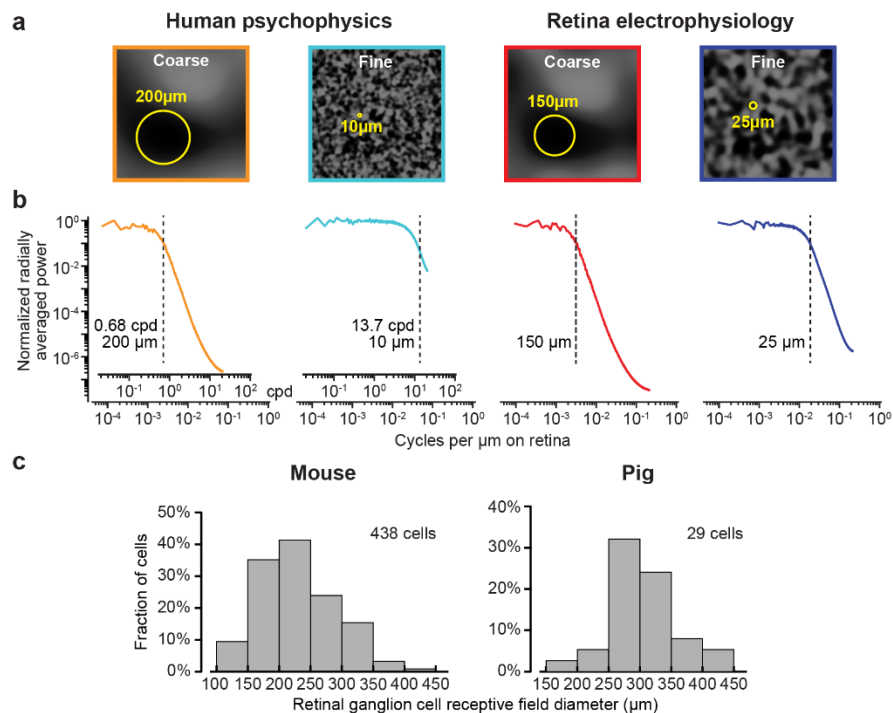
Perceptual saccadic suppression starts in the retina

Idrees†, Baumann†, et al.

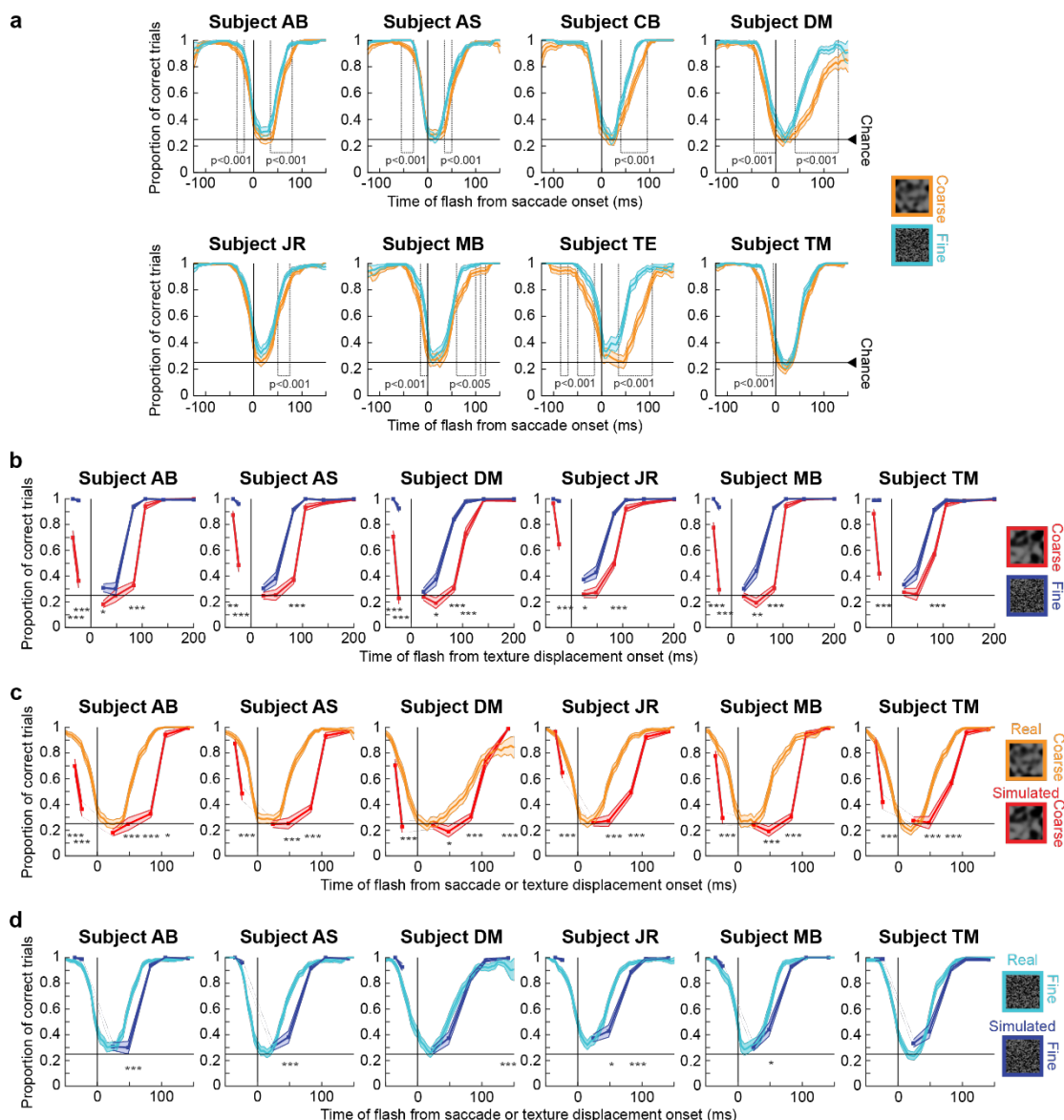
Perceptual saccadic suppression starts in the retina

Saad Idreest†, Matthias P. Baumann†, Felix Franke,
Thomas A. Münch*, and Ziad M. Hafed*

Supplementary information

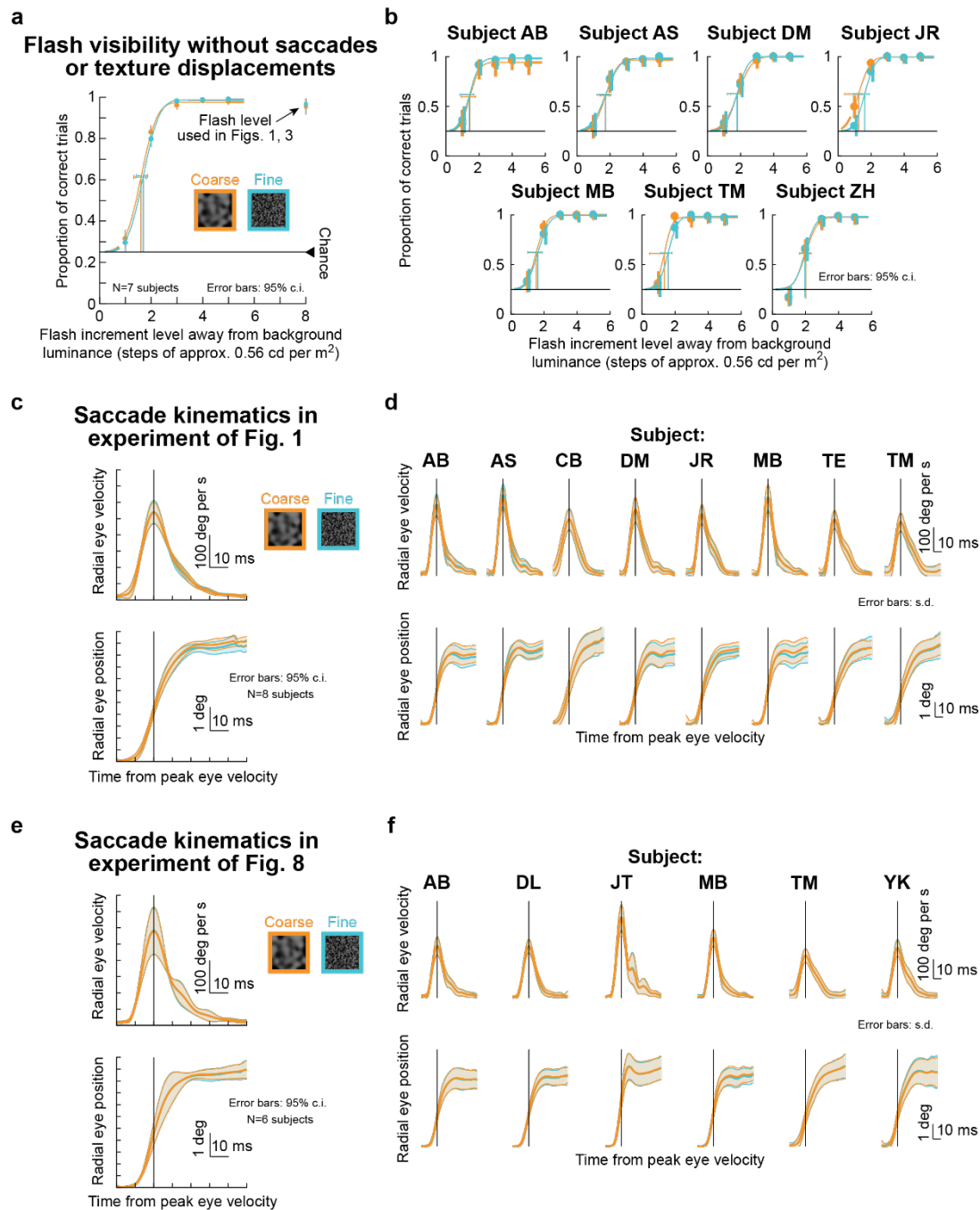


Supplementary Figure 1 Textured backgrounds tailored to receptive field sizes of retinal ganglion cells (coarse) or bipolar cells (fine) in the different species that we studied. (a) We created textures by convolving random binary pixel images with a Gaussian blurring filter. We varied the σ parameter of the Gaussian blurring filter (Methods) to define a so-called spatial scale for the resulting texture (indicated as yellow circles in the examples shown). For each species, we picked the spatial scale to result in dark or bright image blobs that approximated the sizes of either retinal ganglion cell (coarse) or bipolar cell (fine) receptive fields, and we then set σ to half the spatial scale value (Methods). (b) Radially-averaged power spectra for textures like in a, normalized to the maximum average power. Low-pass characteristics in all spatial scales were clear, as expected: less than 5% of the total average power was above the spatial frequency corresponding to the specific spatial scale of a given texture (vertical dashed lines). The inset x-axes in the first two spectra (used for human perceptual experiments) show units of cycles per degree (cpd) in addition to cycles per μ m on the retina. (c) Histograms showing the distributions of receptive field diameters (Methods) in mouse (left) and pig (right) for a subset of retinal ganglion cells that we recorded. Since the distributions were generally similar, we used the same spatial scale parameter for the retinal recordings in both species. Human spatial scale parameters were estimated based on human receptive field diameters from the literature (Methods).



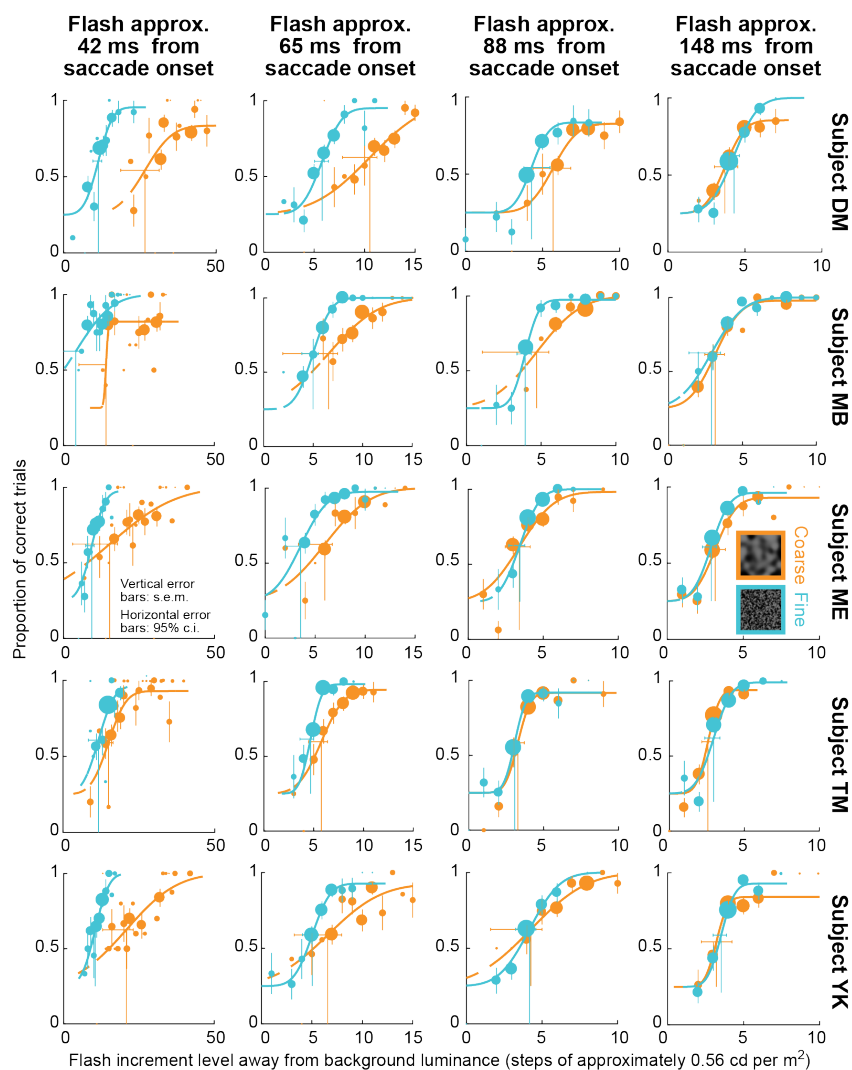
Supplementary Figure 2 Individual subject results from the perceptual experiments of Figs. 1, 6. (a) Identical analyses to Fig. 1d, shown separately for each individual subject. Error bars: s.e.m. across trials. All subjects experienced strong perceptual saccadic suppression, going from near-perfect localization performance to near-chance performance at peak suppression. Moreover, using strict statistical criteria (two-tailed random permutation test; indicated in the figure and described in detail in Methods), all subjects had significant time clusters during which perception was different between saccadic suppression for saccades generated across coarse or fine textures. Also see Fig. 2 and Supplementary Fig. 4. **(b)** Same analyses as in Fig. 6d, but now showing individual subject results when saccades were replaced by saccade-like texture displacements during fixation. All subjects showed longer suppression after coarse texture displacements than after fine texture displacements; all subjects also showed earlier and stronger “pre-saccadic” suppression for coarse textures. Note that this “pre-saccadic” effect is purely visual, since the subjects never made saccades in this condition. Also, note that all subjects who participated in this experiment had also participated in the version with real saccades in **a**. Therefore, whether with or without saccades, perceptual suppression depended on image

statistics. Also see Fig. 7 and Supplementary Fig. 7. **(c, d)** Comparisons of perceptual suppression between real and simulated saccades across coarse **(c)** and fine **(d)** textures, as in Fig. 6e, f but now separating data from individual subjects. Note how even pre-saccadic suppression was prolonged in simulated relative to real saccades (i.e. started earlier in simulated saccades) in the coarse texture condition, which was most effective in causing suppression overall. Error bars: s.e.m. across trials. Asterisks in **b** denote a significant difference between coarse and fine conditions at the indicated flash time (χ^2 tests with Bonferroni corrections; * $p < 0.005$, ** $p < 0.001$, *** $p < 0.0001$). Asterisks in **c, d** denote significant differences (χ^2 tests with Bonferroni corrections; * $p < 0.007$, ** $p < 0.0014$, *** $p < 0.00014$) between real and simulated saccades, comparing perception of a flash at the indicated time delay after simulated saccades to the corresponding time bin (+/- 25 ms) from the real saccade condition.

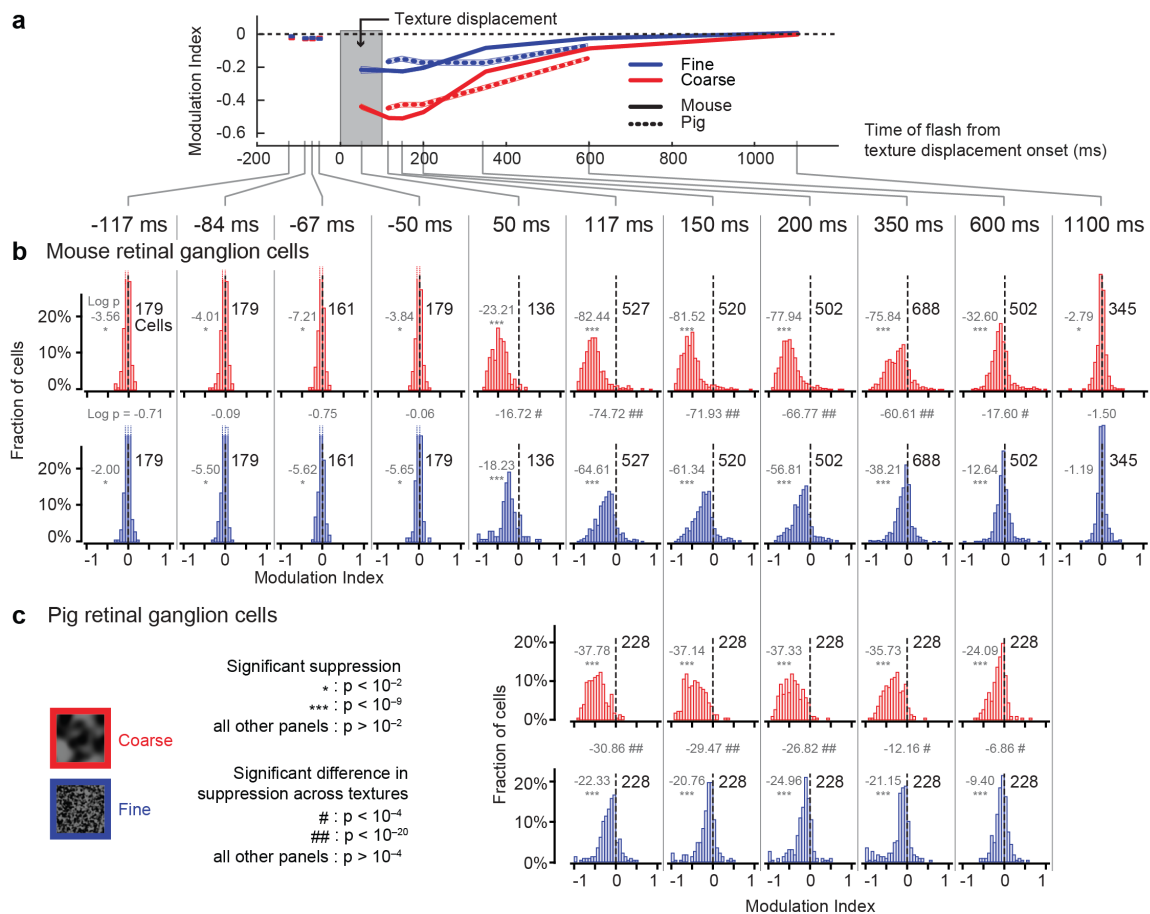


Supplementary Figure 3 Controls for flash visibility and motor variability in our perceptual experiments of Figs. 1, 6, 8. (a) For the same textures as in Figs. 1, 6, we asked subjects to maintain fixation. At a random time, a luminance pedestal appeared as in the main experiments (Figs. 1, 6), but this time, we varied its contrast across trials (Methods). We ensured that no microsaccades occurred near the flash onset time (Methods). Psychometric curves of localization performance (mean across subjects with 95% c.i.; N = 7 subjects) indicate that, at the flash contrast used in Figs. 1, 6 (highlighted by the black arrow), subjects could easily detect flashes during simple fixation. Importantly, flash visibility was identical for coarse or fine textures at all contrasts. Therefore, flash visibility alone (or lack thereof) did not explain the main experiments' results (Figs. 1, 6). The strong perceptual suppression observed in Figs. 1, 6 was instead likely a function of interaction between visual transients associated

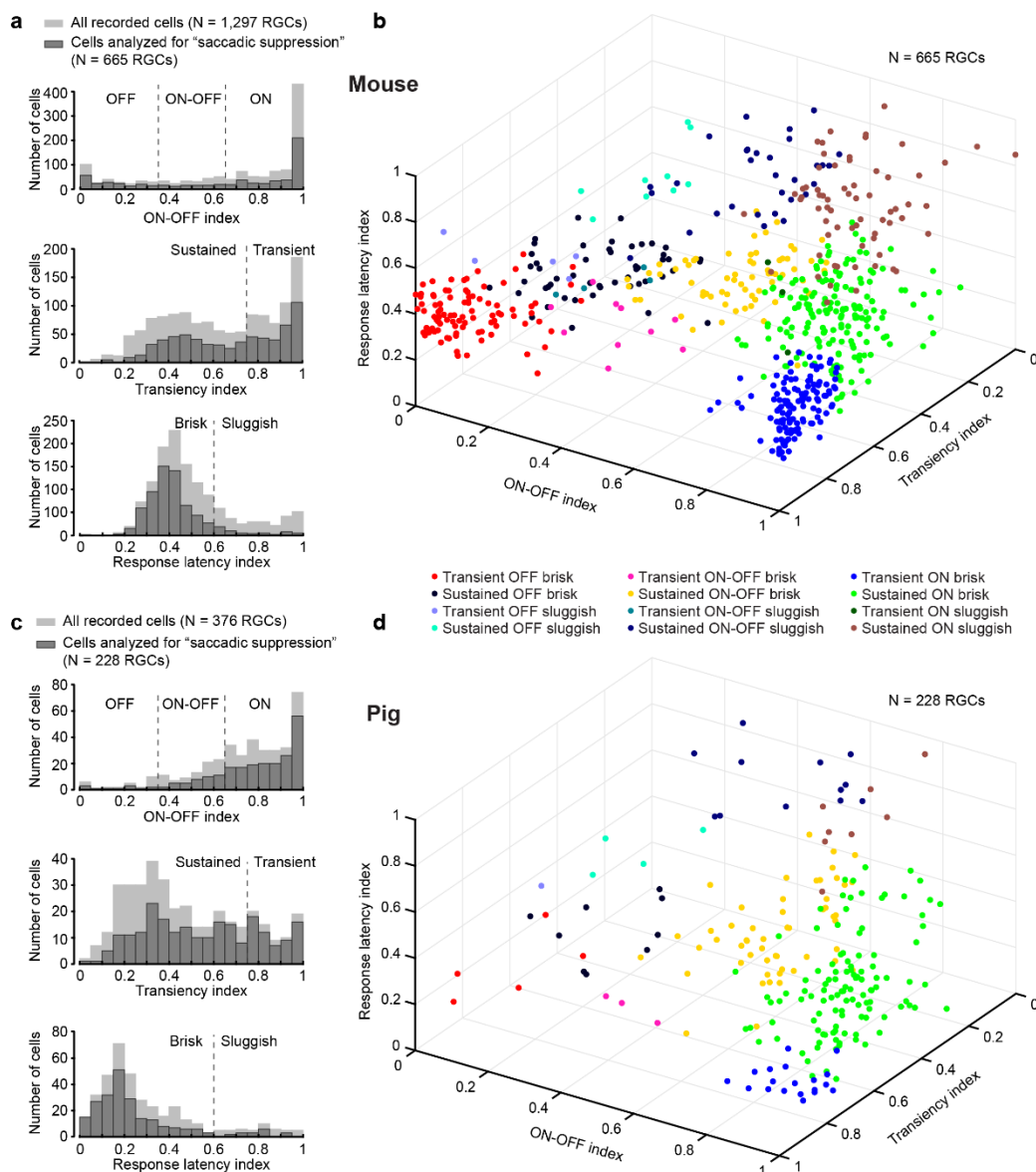
with saccades or texture displacements and the flashes. Also see Figs. 2, 7. **(b)** This idea is further supported by the fact that all individual subjects showed consistent results. All of these subjects had also participated in the experiments of Figs. 1, 6 (with the exception of subject ZH who only performed the control experiment). Psychometric curves were fit using the *psignifit 4 toolbox*¹, and error bars denote 95% confidence intervals centered on the flash levels resulting in threshold perceptual performance (Methods). **(c)** We also checked for potential effects of motor variability on perceptual performance, in order to rule out the possibility that differences in performance between textures (Fig. 1) were due to differences in eye movement kinematics. For the experiments of Fig. 1, we plotted average radial eye velocity (top) and average radial eye position (bottom) across subjects (N = 8 subjects; error bars denote 95% confidence intervals across the individual subjects' curves). There was no effect of background texture on movement kinematics. **(d)** This was also true for each subject individually (mean +/- s.d. across trials). Saccade kinematics were not different when saccades were made across coarse or fine textures. **(e, f)** Same kinematic analyses, but now for the saccades of the experiment of Fig. 8. **(e)** Radial eye velocity and position averaged across subjects (N = 6 subjects; error bars denote 95% confidence intervals across the individual subjects' curves). **(f)** Saccade kinematics for each subject (mean +/- s.d. across trials). Scale bars are defined in their respective panels.



Supplementary Figure 4 Individual subject results from the perceptual experiment of Fig. 2. Each row shows psychometric curves like those shown in Fig. 2a-d, but for a single individual subject. Different rows show results from different subjects. The same conventions as in Fig. 2a-d apply. Here, we also scaled the size of each data point shown by the number of repetitions collected during the experiment. Note that we only show vertical error bars for data points with >10 repetitions, for clarity. Vertical error bars denote s.e.m. across repetitions of a given condition; horizontal error bars indicate 95% confidence intervals for the detection threshold of a given psychometric curve (i.e. the flash contrast resulting in threshold perceptual performance; Methods). Note that the x-axis ranges for the different columns (i.e. different flash times from saccade onset) are different from each other because of the varying amounts of perceptual saccadic suppression that occurred (Figs. 1-2). As can be seen, all subjects showed strong perceptual suppression near the time of saccade onset, with recovery occurring later in time, consistent with Fig. 1. Moreover, all subjects showed stronger perceptual suppression with coarse textures when compared to fine textures, again consistent with Fig. 1.

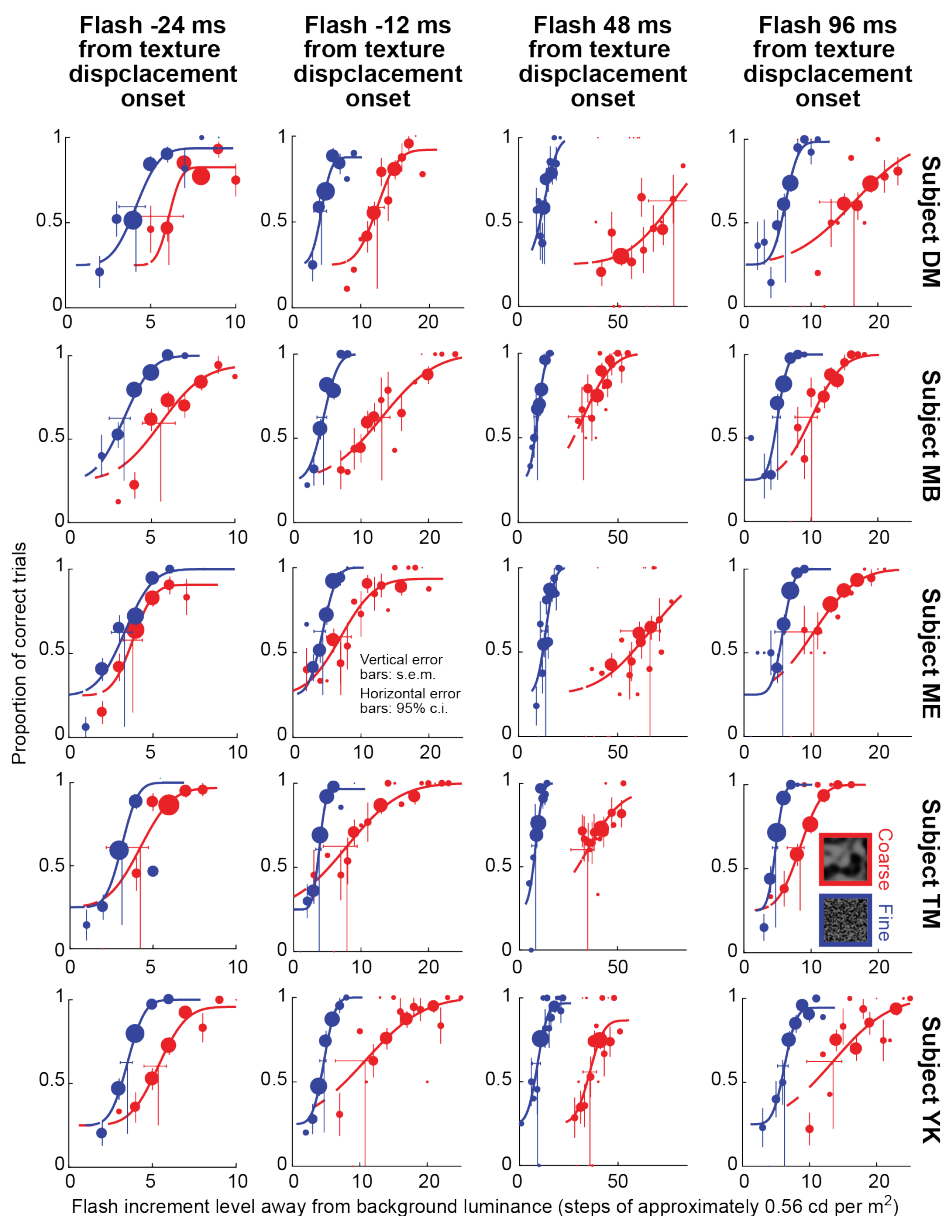


Supplementary Figure 5 Population data detailing the properties of retinal “saccadic suppression”. (a) Replication of Fig. 3e, showing the time courses of retinal “saccadic suppression” in mouse and pig retinae. (b, c) Histograms of modulation indices for mouse (b) and pig (c) RGCs at different flash times relative to texture displacement onset. Red and blue denote coarse and fine textures, respectively. Black numbers in each panel indicate the numbers of RGCs analyzed for each condition; gray numbers next to asterisks in each panel show the logarithm (base 10) of the exact p-value (two-tailed Wilcoxon signed-rank test to determine if the population median was shifted away from 0). Gray numbers next to hashes between coarse (red) and fine (blue) panels show the logarithm (base 10) of the exact p-value comparing suppression indices across the two textures (two-tailed Wilcoxon signed-rank test).

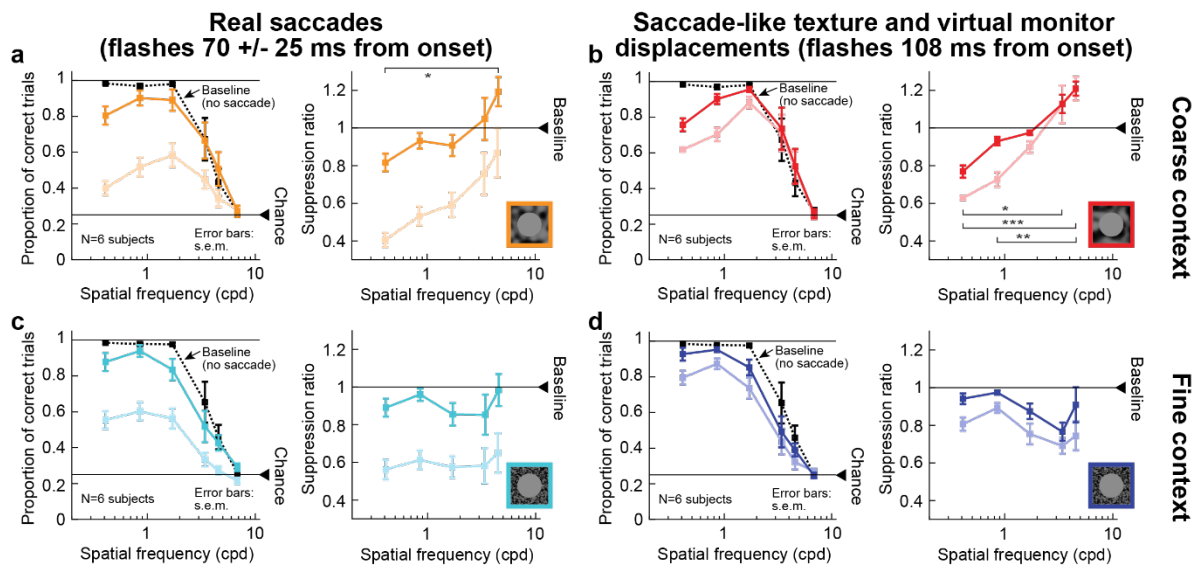


Supplementary Figure 6 Diverse properties of RGCs included in our analysis.

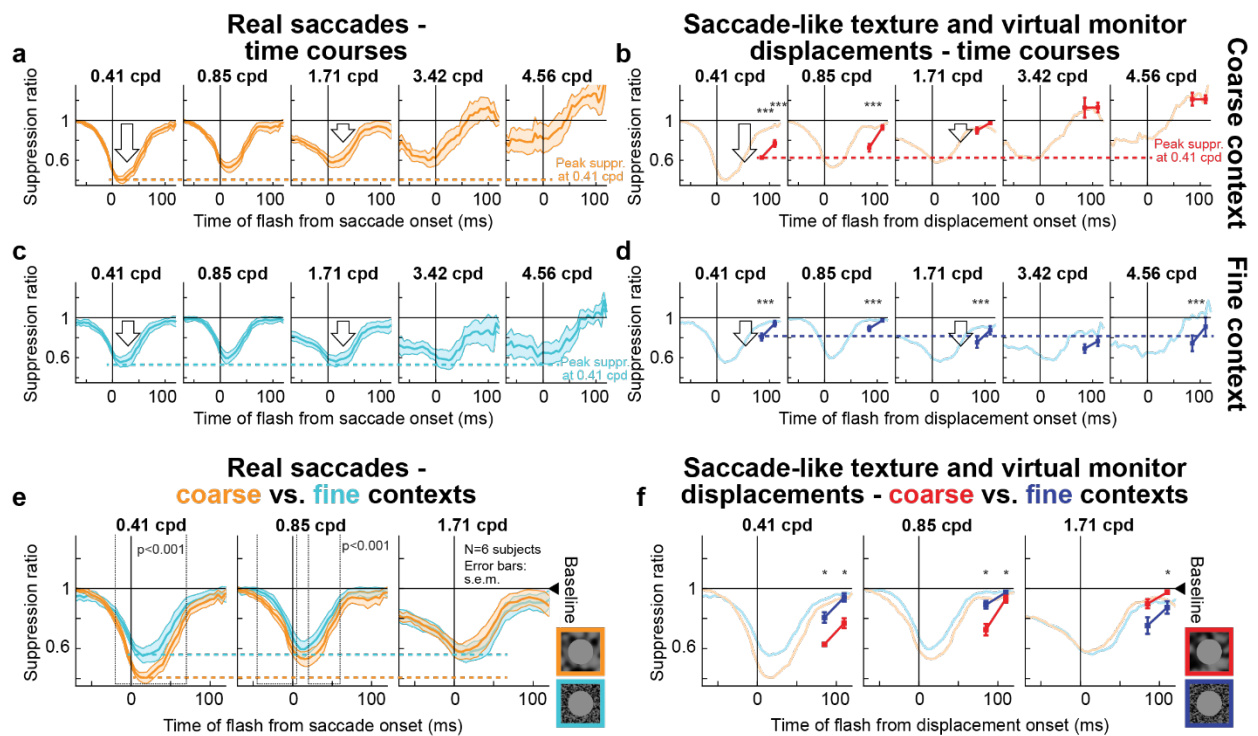
We quantified the response properties of all recorded mouse (a, b) and pig (c, d) RGCs with respect to three neuronal response metrics (see Methods): ON-OFF index, transiency index, and response latency index. Each histogram (a, c) was divided into 2 or 3 groups: RGCs could be OFF, ON-OFF, or ON (top histograms); transient or sustained (middle histograms); and brisk (short response latency) or sluggish (long response latency) (bottom histograms). Combined, this resulted in 12 response categories to which each recorded RGC belonged. The cells that could be analyzed for "saccadic suppression" and for which the response properties could be computed (dark gray histograms) spanned the entire range of response indices exhibited by all recorded cells for which these response properties were analyzed (light gray histograms). The three-dimensional scatter plots (b, d) show the projection of the RGC subsets considered in our analysis for "saccadic suppression" onto the 3 neuronal response indices. The 12 response categories, formed by the combination of histograms in (a, c), can be seen in different colors.



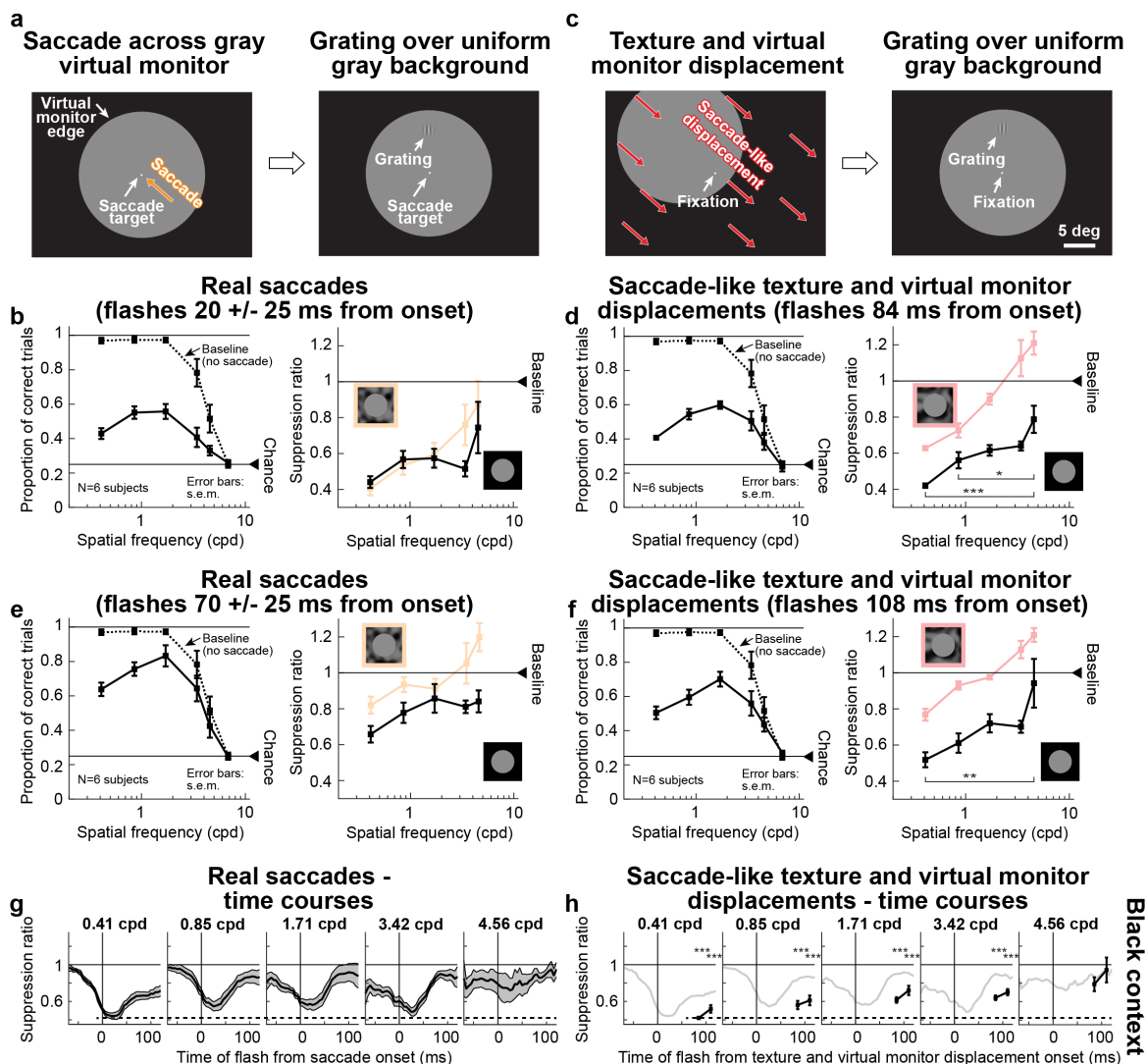
Supplementary Figure 7 Individual subject results from the perceptual experiment of Fig. 7. Same as Supplementary Fig. 4, but now for the experiment of Fig. 7. All subjects showed similar results: there was strong perceptual suppression before and after texture displacements in the absence of saccades, and the suppression effect was stronger when the displaced texture was coarse rather than fine. Note that in this experiment, we added an additional time sample prior to texture displacement onset, in comparison to Fig. 6, in order to demonstrate the robustness of this pre-displacement effect, and also to demonstrate the continuity of perceptual suppression in a time-locked fashion to texture displacement onset (Fig. 6).



Supplementary Figure 8 Recovery, with time, of perceptual suppression with real and simulated saccades in the experiment of Fig. 8. (a) Same analysis as in Fig. 8b, but at a later time point of grating flash onsets relative to saccade onset. Faint curves show the data from Fig. 8b for comparison. At around 70 ms after saccade onset, perceptual recovery from saccadic suppression emerged, but the selectivity of suppression across different spatial frequencies was still present (there was a main effect of spatial frequency on suppression ratio; $\chi^2=11.4$, $p=0.022$, $df=4$, Kruskal-Wallis test; * $p<0.05$, post-hoc pairwise test between the lowest and highest spatial frequencies). All other conventions are as in Fig. 8b). **(b)** Same analysis as in Fig. 8d, but at a later time point of flash onset after virtual monitor and texture displacement. The same observations as in **a** were made: perceptual recovery occurred at the later time point, but selectivity of suppression was still obvious ($\chi^2=25.26$, $p=0.00004$, $df=4$, Kruskal-Wallis test; * $p<0.05$, ** $p<0.01$, *** $p<0.001$ for post-hoc pairwise tests between different indicated pairs of spatial frequencies). The faint curves show the data from Fig. 8d for comparison. Note how this condition of displacements of the virtual monitor and texture surround resulted in longer lasting suppression than with real saccades (also see Supplementary Fig. 9). **(c, d)** Same analyses as in **a** and **b**, but with a fine texture surrounding the virtual monitor (Fig. 8e, f). Error bars in all panels denote s.e.m. All other conventions are as in Fig. 8.



Supplementary Fig. 9 Time courses of perceptual suppression with real and simulated saccades, as well as coarse and fine textures, in the experiment of Fig. 8. (a) Time courses of suppression from Fig. 8a, b with a coarse surround around the virtual monitor. We used similar binning procedures to Fig. 1. Peak suppression was strongest when 0.41 cpd gratings were flashed and progressively weakened for higher spatial frequency gratings (horizontal colored dashed line across panels). (b) With simulated saccade-like virtual monitor and texture displacements, we sampled two grating flash times relative to displacement onset. Recovery at the later time point for each grating spatial frequency was evident. Moreover, selectivity of suppression as a function of grating spatial frequency was evident (horizontal colored dashed line across panels demonstrating the peak suppression for the lowest spatial frequency). The faint curves show time courses from a for comparison. Note how simulated saccades caused longer-lasting suppression than real saccades, exactly as in the experiment of Fig. 6. (c, d) Similar analyses for fine texture surrounds around the virtual monitor. In this case, suppression was the same across all spatial frequencies (horizontal colored dashed lines across panels). In b, d, asterisks denote significant differences in perceptual suppression between the simulated condition and a corresponding time bin in the real condition (***) $p < 0.0001$, χ^2 tests with Bonferroni corrections). (e) For real saccades, and for low spatial frequencies of gratings (i.e. when both coarse and fine surround contexts were associated with strong saccadic suppression), the coarse surround was associated with longer lasting suppression than the fine surround ($p < 0.001$, two-tailed random permutation test). This is consistent with the results of Fig. 1 when saccades were generated across full-screen textures. (f) This texture-dependence was also true with simulated saccades (* $p < 0.05$, two-tailed random permutation test comparing coarse and fine textures at a given grating flash time). In all panels: $N = 6$ subjects; and error bars denote s.e.m. All other conventions are as in Figs. 1, 6, 8.



Supplementary Fig. 10 Replicating the results of Fig. 8 but with black surrounds around a uniform gray display. (a) We repeated the same experiment as in Fig. 8a but this time using a black surround around the virtual monitor, as we might normally do in experiments on saccadic suppression^{2,3}. Note that a black (or white) surround is theoretically equivalent to an infinitely coarse surround; hence, we expected observations more similar to Fig. 8a-d (i.e. selectivity of suppression for low spatial frequencies) than Fig. 8e, f. (b) Similar suppression selectivity for low spatial frequencies occurred with real saccades as in Fig. 8b (faint curves replicate that data for comparison). (c) Same experiment as in Fig. 8c, but with a black surround. (d) Selectivity of suppression for low spatial frequencies was even more evident with simulated saccades (effect of spatial frequency on suppression ratio during simulated saccades: $\chi^2=18.84$, $p=0.0008$, $df=4$, Kruskal-Wallis test; * $p<0.05$, *** $p<0.001$ for post-hoc pairwise tests between the highest spatial frequency and either the lowest or second lowest spatial frequency). Faint curves show results from Fig. 8d for comparison. (e, f) Similar analyses at a later time point, identical to Supplementary Fig. 8. There was recovery for both real (e) and simulated (f) saccades (effect of spatial frequency on suppression ratio during simulated saccades: $\chi^2=15.12$, $p=0.0045$, $df=4$, Kruskal-Wallis test; ** $p<0.01$ for post-hoc pairwise comparisons between individual spatial frequencies). Faint colored curves show data from Supplementary Fig. 8a, b at

the same time points for easier comparison. Note that with black surrounds, suppression strength was larger overall than with either coarse or fine texture surrounds (as if the black surround was indeed an extension of the coarseness of the texture). **(g, h)** Full time courses of suppression as in Supplementary Fig. 9. All error bars denote s.e.m., and all conventions are similar to Fig. 8 and Supplementary Figs. 8, 9. In **h** asterisks denote significant differences in perceptual suppression between the simulated condition and a corresponding time bin in the real condition, both with a black background (***) $p < 0.001$, two-tailed random permutation test).

- 1 Schutt, H. H., Harmeling, S., Macke, J. H. & Wichmann, F. A. Painfree and accurate Bayesian estimation of psychometric functions for (potentially) overdispersed data. *Vision Res* **122**, 105-123 (2016).
- 2 Hafed, Z. M. & Krauzlis, R. J. Microsaccadic suppression of visual bursts in the primate superior colliculus. *J Neurosci* **30**, 9542-9547 (2010).
- 3 Chen, C. Y. & Hafed, Z. M. A neural locus for spatial-frequency specific saccadic suppression in visual-motor neurons of the primate superior colliculus. *J Neurophysiol* **117**, 1657-1673 (2017).

Chapter 2

Suppression without inhibition: A novel mechanism in the retina accounts for saccadic suppression

Saad Idrees, Matthias P. Baumann, Maria M. Korympidou, Timm Schubert, Alexandra Kling, Katrin Franke, Ziad M. Hafed, Felix Franke, Thomas A. Münch

(Submitted)

<https://doi.org/10.1101/2020.08.21.261198>

Suppression without inhibition: A novel mechanism in the retina accounts for saccadic suppression

Saad Idrees^{1,2}, Matthias-Philipp Baumann¹, Maria M. Korympidou^{1,2,3},
Timm Schubert^{1,3}, Alexandra Kling⁴, Katrin Franke^{3,5}, Ziad M. Hafed¹,
Felix Franke^{6,7,8*}, Thomas A. Münch^{1,3*}

¹Werner Reichardt Centre for Integrative Neuroscience, University of Tübingen, 72076 Tübingen, Germany

²International Max Planck Research School, University of Tübingen, 72074 Tübingen, Germany

³Institute for Ophthalmic Research, University of Tübingen, 72076 Tübingen, Germany

⁴Department of Neurosurgery, Stanford School of Medicine, Stanford, CA 94305, USA

⁵Bernstein Center for Computational Neuroscience, University of Tübingen, 72076 Tübingen, Germany

⁶Bio Engineering Laboratory, ETH Zürich, 4058 Basel, Switzerland

⁷Institute of Molecular and Clinical Ophthalmology Basel, 4031 Basel, Switzerland

⁸Faculty of Science, University of Basel, 4056 Basel, Switzerland

*Correspondence: felfranke@googlemail.com (F.F.), thomas.muench@gmail.com (T.A.M.)

Abstract

Visual perception remains stable across saccadic eye movements, despite the concurrent strongly disruptive visual flow. This stability is partially associated with a reduction in visual sensitivity, known as saccadic suppression, which already starts in the retina with reduced ganglion cell sensitivity. However, the retinal circuit mechanisms giving rise to such suppression remain unknown. Here, we describe these mechanisms using electrophysiology in mouse, pig, and macaque retina, 2-photon calcium imaging, computational modeling, and human psychophysics. We find a novel retinal processing motif underlying retinal saccadic suppression, “dynamic reversal suppression”, which is triggered by sequential stimuli containing contrast reversals. This motif does not involve inhibition but relies on nonlinear transformation of the inherently slow responses of cone photoreceptors by downstream retinal pathways. Two further components of suppression are present in ON ganglion cells and originate in the cells’ receptive field surround, highlighting a novel disparity between ON and OFF ganglion cells. Our results are relevant for any sequential stimulation encountered frequently in naturalistic scenarios.

Keywords: retina, ganglion cell, cone photoreceptor, saccadic suppression, computational model, sequential stimuli, rapid image shifts, perception, dynamic vision, visual processing

Introduction

Vision appears as a continuous and coherent process. This is a striking achievement of the visual system, considering that the visual flow across the retina is not continuous, but governed by frequent and sudden changes, irregularities, and disruptions. As a consequence of this active vision, i.e. the process of active exploration of the visual environment, the meaningful images falling onto the retina are only brief snapshots of the world, interrupted by blinks and rapid motion. The most prominent cause for such disruptions are eye movements. Saccades, for example, are critical for efficiently sampling the visual world (Schütz et al., 2011; Tatler et al., 2010; Yarbus, 1967), which is particularly true for species in which high visual resolution is limited to a small fraction of the overall visual space, such as the foveal region in primates. On the other hand, as a result of saccades, the number of photons falling onto a given area of the retina can change by several orders of magnitude within tens of milliseconds, causing sudden and frequent visual transients of local intensity across the entire retina. From the perspective of the retina, saccades are therefore equivalent to robust visual stimuli, and they are a powerful model for a very profound question of visual neuroscience: How does the visual system extract robust information from the “meaningful” snapshots of the world, in the face of frequent, strong, and disruptive other input?

Perceptually, saccadic disruptions are minimized by reducing the sensitivity of the visual system to new input around the time of saccades - a phenomenon known as saccadic suppression. While this phenomenon has been extensively characterized over the past few decades (Beeler, 1967; Bremmer et al., 2009; Idrees et al., 2020; Krekelberg, 2010; Matin, 1974; Volkmann, 1986; Wurtz, 2008; Zuber and Stark, 1966), its underlying mechanisms still remain unclear. Several electrophysiological studies have shown neural correlates of saccadic suppression throughout the visual system, namely a modulation of neural activity and/or sensitivity around the time of saccades (Bremmer et al., 2009; Chen and Hafed, 2017; Hafed and Krauzlis, 2010; Ibbotson et al., 2008; Kleiser et al., 2004; Krekelberg, 2010; Wurtz, 2008). These observations have often been interpreted to be caused by active suppressive signals originating from (pre-) motor areas, such as corollary discharge signals related to the saccadic eye movement command (Bremmer et al., 2009; Diamond et al., 2000; Duffy and

Lombroso, 1968; Ross et al., 2001; Zuber and Stark, 1966). Most studies investigating the mechanisms of saccadic suppression have therefore focused on cortical or subcortical neuronal recordings and/or on behavioral measures of perceptual state, largely neglecting the consequence of visual processing in early visual pathways, for example in the retina.

The retina is an independent signal processing “front end” in the visual system, before visual information is sent along the optic nerve to higher brain areas. Consequently, image processing triggered by visual transients, such as those that naturally occur during active vision, including saccades, could potentially lead to altered retinal output. Retinal signal processing could therefore contribute to perceptual saccadic suppression. Some studies have investigated how the retina processes information in the context of spatio-temporal dynamics that occur during natural visual behavior (Appleby and Manookin, 2019; Baccus et al., 2008; Berry et al., 1999; Chen et al., 2013; Fried et al., 2002; Garvert and Gollisch, 2013; Geffen et al., 2007; Gollisch, 2013; Münch et al., 2009; Tikidji-Hamburyan et al., 2015; Wei, 2018; Zaghloul et al., 2007; Zhang et al., 2012), including saccades (Amthor et al., 2005; Barlow et al., 1977; Enroth-Cugell and Jakiela, 1980; Krishnamoorthy et al., 2017; Krueger and Fischer, 1973; Noda and Adey, 1974; Passaglia et al., 2009; Roska and Werblin, 2003). A retinal neural correlate of perceptual saccadic suppression has recently been shown by a previous study from our labs (Idrees et al., 2020). There, we showed that the retinal output is indeed altered by saccade-like image shifts. In most mouse and pig retinal ganglion cells (RGCs) that we recorded from, responses to brief probe flashes were suppressed when preceded by saccade-like image displacements across the retina. This retinal saccadic suppression had properties consistent with the perceptual suppression of probe flashes reported by human subjects using similar images, and following either real or simulated saccades. In fact, we already observed elementary properties of perceptual saccadic suppression, such as its dependency on background scene statistics, at the level of the output of the retina, providing strong evidence of a retinal mechanism directly contributing to perceptual saccadic suppression.

In this study, we describe such a mechanism. We experimentally mimicked the visual flow resulting from saccades and recorded the neural activity of the output neurons of the retina (RGCs) from ex vivo retinae of mice, pigs, and macaque monkeys. We found

that retinal saccadic suppression was the result of multiple mechanisms. The major component originated from a novel visual processing motif within an RGC's receptive field center, which we call "dynamic reversal suppression". Dynamic reversal suppression does not depend on any inhibitory signals; it results from a combination of inherent response properties of cone photoreceptors and non-linear processing of cone output by downstream pathways in the retina. Two further components of suppression originated from beyond the RGC's receptive field center, only one of them driven by GABAergic inhibition. Interestingly, these two additional components were observed primarily in ON RGCs, highlighting a novel disparity between ON and OFF type RGCs. Perhaps one of the most intriguing outcomes of this study, also consistent with observations of perception (Idrees et al., 2020), is that the suppressive effects observed in RGCs are not exclusively triggered by saccades, but occur for many scenarios involving sequential visual stimulation, which are ever-present during natural vision. Therefore, while the results described here are crucial for understanding the mechanisms of saccadic suppression, they also elucidate more general mechanisms of retinal signal processing across any time-varying visual input over short time scales (10 ms to 1 s).

Results

Experimental Approach

We measured the modulation of retinal ganglion cell (RGC) output following saccade-like changes of the visual input with a variety of different light stimulation strategies (Fig. S1). The basic experimental paradigm was similar to that described in (Idrees et al., 2020). Briefly, we recorded spiking activity of RGCs in isolated ex vivo mouse retinae using both high-density and low-density multi-electrode arrays (MEAs). Each retina was exposed to a background texture having one of several possible spatial scales that defined its spatial spectrum ("fine" to "coarse", Methods, Fig. S2). We simulated saccade-like image displacements by rapidly translating the texture globally across the retina (Methods; Fig. 1a). Most RGCs responded robustly to such saccade-like texture displacements (see Fig. 1b for responses of example ON and OFF RGCs). At different times relative to the saccade-like texture displacements ("saccades" from now on), we presented a brief probe flash (Fig. 1c). We then

analyzed how the response (spike rate of the RGC) to this probe flash was influenced by the preceding saccade, by comparing it to the response to the flash presented in isolation (baseline). To quantify RGC response modulation, we calculated a modulation index (Methods) as follows: we first isolated the flash-induced response component by subtracting the saccade-only response (e.g., Fig. 1b) from the response to the composite saccade-flash stimulus (e.g., Fig. 1c). Based on this flash-induced response component (Fig. 1d), we calculated the modulation index as $(r_d - r_b)/(r_d + r_b)$. Here, r_d is the peak response to the probe flash presented with a delay d relative to saccade onset, and r_b is the baseline (peak response to the flash presented ~ 2 s after the saccade). This modulation index is negative when flash-induced responses are suppressed (Fig. 1d shows, on the horizontal dashed line, the modulation index for the responses at each flash-time). In yet further recordings we applied various manipulations to this base paradigm to probe for the mechanisms underlying modulation of RGC responses following saccades. To generalize our findings across other species, we also performed similar analyses of pig and macaque RGC data.

Similarities and differences in retinal saccadic suppression across ON and OFF type RGCs

Suppression was robust across most RGCs that we recorded from, consistent with what we reported previously (Idrees et al., 2020). Here, we more closely inspected functionally different RGCs. Specifically, throughout this study, we divided RGCs into ON and OFF types, i.e. into RGCs responding best to light increments or decrements, respectively (Methods). We always quantified the modulation index defined above for ON RGCs based on their responses to bright probe flashes and for OFF RGCs based on their responses to dark probe flashes (Fig. 1c, d). Flash responses following a saccade were suppressed in both ON and OFF RGCs, as seen in Fig. 1d for example cells. Fig. 1e shows the temporal profile of the mean population modulation index, and Fig. S3 the underlying population data. Suppression was consistently stronger for coarser background textures (Figs. 1e, S3), for both ON and OFF RGCs. This is consistent with (Idrees et al., 2020), where we showed that this dependency on the texture can be explained by the distinct statistics of luminance and contrast changes when coarse or fine textures move across the RGCs' receptive fields. However, a striking difference existed in suppression recovery times: OFF RGCs recovered by

~350 ms after saccade onset, whereas ON RGCs recovered only by ~1 s. Similar results were obtained under scotopic conditions for coarse textures, while suppression for fine textures was very weak (Fig. S4; all other mouse retina data was recorded at mesopic conditions). In general, the presence of post-saccadic suppression of probe flash responses in both ON and OFF type RGCs suggests a common mechanistic theme across these cell types (Idrees et al., 2020). On the other hand, the different recovery times indicate either additional suppressive mechanisms in ON RGCs or additional recovery mechanisms in OFF RGCs.

Spatial origin of retinal saccadic suppression

Global component of suppression

To probe the mechanisms underlying suppression and its differences across ON and OFF type RGCs, we first examined the spatial origin of suppression. We hypothesized that suppression of flash responses was caused by circuits detecting rapid global shifts across the retina. Typically, these circuits include a lateral network of interneurons, communicating with RGCs even from beyond their classical center-surround receptive field (i.e., from their periphery, or far surround) (Lin and Masland, 2006; Roska and Werblin, 2003). To test whether suppression was caused by such circuits, we modified the spatial layout of the paradigm: we placed a square mask of $1000 \times 1000 \mu\text{m}^2$ (Fig. 2a, right) to restrict the saccades to the periphery of an RGC's receptive field. Similar to the previous experiments, the probe flash was either a dark or bright flash presented over the entire retina, including the masked region. Figure 2b shows the mean population modulation indices of ON RGCs (top) and OFF RGCs (bottom) from these experiments (Fig. S5 depicts the underlying population data and shows responses of representative ON and OFF RGCs from these experiments). In OFF RGCs, responses to full-field probe flashes were no longer suppressed when saccades were restricted to the periphery. The responses of ON RGCs, on the other hand, were still suppressed in this condition. The resulting suppression was however weaker and shorter-lived (recovered by 350 ms) than with full-field saccades. These observations (Figs. 2b, S5c) were robust across ON and OFF RGCs whose receptive fields were completely contained within the mask (Fig. S5b).

We will refer to this component of suppression in ON RGCs, which originates from the periphery, as the “global component” from now on. Such spatially far-reaching inhibition is often mediated through GABAergic wide-field amacrine cells. We tested this hypothesis by blocking GABA_A receptors. Indeed, in the periphery saccade condition, the modulation index for most ON RGCs was around 0 in the presence of the GABA_A receptor antagonist SR-95531 (Fig. 2b, S5d). These results suggest that this short-lived global component of suppression is caused by inhibition via GABAergic amacrine cells, perhaps similar to the polyaxonal amacrine cells described previously (Baccus et al., 2008; Ölveczky et al., 2003; Roska and Werblin, 2003). Thus, while suppression is indeed partially caused by circuits detecting global changes across the retina, those circuits seem to act predominantly on ON RGCs, and even there, they only account for a fraction of the total suppression observed with full-field saccades (without mask), which lasts longer. Other, probably more local sources of suppression must exist that account for most of the suppression in ON RGCs and all of the suppression in OFF RGCs.

Local components of suppression

To understand the more local components of suppression, we used different analyses and manipulations of the main experimental paradigm. As we will see below, the more local components can be subdivided into a “central” and a “surround” component. First, we eliminated the global component, by repeating our normal full-field saccade paradigm in the presence of GABA receptor blockers. The suppression profile of both ON and OFF RGCs was only weakly affected upon blocking GABA_{A,C} receptors (5 μ M SR-95531 and 100 μ M Picrotoxin; Fig. 2c, S6a). Since the GABA-block eliminates the global component of suppression, the remaining more local components did not seem to rely on GABAergic inhibition. Also, this suggests that the local components dominate retinal saccadic suppression under full-field conditions. We then also blocked glycine receptors (1 μ M of Strychnine; Fig. 2d, S6b) to test if the local components of suppression were caused by local inhibition via glycinergic pathways. Here again, the suppression profiles of both ON and OFF RGCs were only weakly affected upon blocking glycine receptors in combination with blocking GABA_{A,C} receptors. Therefore, inhibitory synaptic interactions are not the major mechanism behind the local components, which dominate suppression of RGCs.

Next, we tested whether these local components originated from within the receptive field center. For this, we modified the spatial layout of our paradigm to exclude saccades from the very center of the receptive field. Simply reducing the size of our mask would have severely decreased the number of simultaneously recorded cells located inside the mask, and we therefore resorted to a different strategy: saccades and flashes were presented in small square regions spread across the retina, separated by gaps kept at mean luminance (“checkerboard mask”, Fig. 2e). In one condition (Fig. 2e, left), we presented saccades and flashes in all regions of the checkerboard mask; in the other condition (Fig. 2e, right), saccades and flashes were presented in alternate regions. With this second arrangement, saccades were excluded from at most $\sim 300 \times 300 \mu\text{m}^2$ of a cell’s receptive field center, even if that cell was perfectly centered on a non-saccade region. Flashes were presented in the set of regions that included the square region covering the receptive field center of the analyzed RGC (Fig. S7a).

Probe flash responses following saccades were suppressed in both ON and OFF RGCs when the saccade and flash were presented in all regions (Fig. 2f, thick lines; Fig. S7c; see Fig. S7b for example cells), consistent with the suppression observed after full-field saccades (Figs. 1, S3). When saccades were excluded from the receptive field center, and were presented in alternate regions to the flash, the flash responses were no longer suppressed in OFF RGCs (Fig. 2f, bottom, thin line), even though these cells showed spiking responses to saccades themselves (Fig. S7b). In fact, flash responses were even enhanced. This suggests that the local component of suppression in OFF RGCs arises fully from within the receptive field center (“central component”). This highly localized origin of suppression in OFF RGCs was further confirmed by additional analysis of the large mask experiments (see Figs. S7d, e). In ON RGCs, on the other hand, suppression persisted (Fig. 2f, top; Fig. S7c), even though a loss in suppression was apparent for flashes presented immediately after the saccade, at 117 and 150 ms (marked with an arrow in Fig. 2f). This suggests that in ON RGCs, part of the early suppression originates from the “central component”. The leftover suppression during these early time points might be explained by the global component of suppression, described above (Fig. 2b, S5c), which should also be triggered under this experimental setting. However, since the global component also

recovers quickly (by 350 ms, Fig. 2b, S5c), the persisting suppression at the later time points (350 ms and beyond) needs to originate from yet another source beyond the receptive field center. We call this the “surround component”, and it may originate from the ON RGCs’ immediate surround, which also experiences the saccade under this experimental setting. Therefore, in ON RGCs, the local component of suppression can be divided into a central and a surround spatial component.

Summary of retinal saccadic suppression spatial origins

In summary, our data suggests that retinal saccadic suppression is mediated by at least three components with distinct spatial origins and temporal properties (Fig. 3): a central, surround, and global component. Suppression in OFF RGCs is mediated exclusively by the central component, which originates from the cell’s receptive field center and is characterized by fast onset and fast recovery (by 350 ms after saccade onset). In ON RGCs, we most directly observed the global component (Figs. 2b, S5a). It extends into the periphery and its timing is similar to the central component in OFF RGCs. Only this global component is affected by blocking GABA receptors (Figs. 2b, S5b). During full-field saccades, removing this component by blocking GABA receptors has little effect on the overall suppression (Figs. 2c, 2d, S7), suggesting a more dominant role of the remaining components. The central component in ON RGCs can only be observed by the loss in suppression for early flashes when saccades are excluded from the receptive field center (marked with an arrow in Fig. 2f, top). Its full duration and time course are obscured by the concurrently acting global and surround components. However, given the identical pharmacological dependencies and spatial origins, it is plausible that the central component is symmetric across ON and OFF RGCs with a common underlying mechanism. Therefore, the longer suppression in ON RGCs can neither be attributed to the central nor global components. It likely originates from the immediate surround of the receptive field. This surround component is long lasting (recovers by ~1s) and has a slow onset (Figs. 2f, S3).

Suppression is triggered by interaction between consecutive stimuli of opposite polarity

We previously showed (Idrees et al., 2020) that retinal and perceptual saccadic suppression not only occur after texture displacements, but also after instantaneous

texture jumps and structure-free uniform luminance steps. These observations suggested that saccadic suppression is the consequence of rather general mechanisms in which the response to a second stimulus (here: probe flash) gets suppressed by a previous visual transient (caused by saccades or luminance steps). In the following, we apply additional analysis to the luminance-step paradigm (Fig. S1b) dataset of (Idrees et al., 2020), to investigate how the polarity and strength of the visual transients affect the suppression of ON and OFF RGCs.

Similar to all previous experiments, we analyzed the modulation index of ON and OFF RGCs separately, using bright probe flashes to analyze ON RGCs and dark probe flashes for OFF RGCs. Consistent with the suppression after texture displacements (Figs. 1e, S3), responses to flashes after luminance steps were strongly suppressed in both ON and OFF RGCs, and ON RGC suppression outlasted suppression in OFF RGCs (Fig. 4a, S8a). The two seemingly different experimental paradigms may therefore trigger similar mechanisms in the retina.

We hypothesized that the response to a luminance step might strongly activate RGCs, so that the response to a subsequent probe flash would drive the cells into adaptation or saturation, effectively resulting in suppressed flash responses. At least for the local components of suppression, this could be a viable mechanism as suppression is not caused by inhibitory synaptic interactions. If this was indeed the case, then positive-contrast luminance steps would suppress responses to bright flashes in ON RGCs, and negative-contrast luminance steps would suppress responses to dark flashes in OFF RGCs. To test this, we separately analyzed the effects of positive- and negative-contrast luminance steps on probe flash responses (Fig. 4b). Surprisingly, the resulting effects were contrary to our adaptation/saturation hypothesis: the responses of ON RGCs to bright probe flashes were only weakly suppressed after positive-contrast luminance steps (Fig. 4b, left), but strongly suppressed following negative-contrast luminance steps (Fig. 4b, right). Similarly, responses of OFF RGCs to dark probe flashes were weakly suppressed by negative-contrast luminance steps (Fig. 4b, right), but strongly suppressed by positive-contrast luminance steps (Fig. 4b, left). Fig. S8 shows the underlying population data for these experiments, and Figs. S9a, b show the spiking response of a representative ON and OFF RGC, respectively. While ON RGCs did show a small component of suppression in support

of our adaptation/saturation hypothesis (Fig. 4b left panel, see Fig. S9a left column and Fig. S10a for a detailed analysis), the dominant suppressive effect in both ON and OFF RGCs was caused by luminance steps with the opposite contrast as the subsequent flash.

Such crossover style of suppression would be consistent with mechanisms involving crossover inhibition via amacrine cells (Werblin, 2010), where activation of OFF pathways (here: by the negative-contrast luminance step) would inhibit responses in the ON pathway (here: to the bright probe flash) and vice versa. However, consistent with our earlier experiments (Fig. 2c, d), suppression in ON RGCs still persisted upon blocking GABA_{A,C} and glycine receptors (5 μ M SR-95531, 100 μ M Picrotoxin and 1 μ M Strychnine) (Fig. 4c). We could not calculate a modulation index for OFF RGCs under these conditions because they did not respond to brief probe flashes in the presence of the pharmacological agents, and therefore the modulation index was mathematically undefined. However, in our texture displacement experiments, the same pharmacological agents (Fig. 2d) had no substantial effect on OFF RGC suppression. The crossover-style suppression observed in Fig. 4b was therefore unlikely to be caused by classical crossover inhibition pathways involving amacrine cells and GABA_{A,C} or glycine receptors.

Central component of suppression results from cone response kinetics and nonlinearities in downstream retinal pathways

So far, our experiments suggest that suppression in OFF RGCs (1) is mediated solely by the central component of suppression that originates in the receptive field center (Figs. 2e, S7b-e), (2) is predominantly triggered by the interaction between consecutive stimuli with opposite polarity (Figs. 4b, S8b), and (3) is not caused by inhibitory amacrine cells (Figs. 2c, 2d, S6). Similar conclusions can be drawn for the central component of suppression in ON RGCs. Together, these results restrict the possible cellular substrates for this central suppressive mechanism to the feed-forward pathway in the retina, namely photoreceptors - bipolar cells - RGCs. We wondered whether opposite-polarity stimulus-stimulus interactions could already modulate the responses of photoreceptors themselves. For this, we recorded the output of cones with an intensity-based glutamate-sensitive fluorescent reporter (iGluSnFR) (Marvin

et al., 2013; Szatko et al., 2020), predominantly expressed in horizontal cells postsynaptic to cone terminals (Methods). We presented a shortened version of the luminance step paradigm in which a homogeneous background alternated between a brighter and darker gray value (Fig. S1c) to induce positive-contrast (+0.4 Michelson contrast) and negative-contrast (-0.4 Michelson contrast) luminance steps. Dark or bright probe flashes (100 ms duration, -0.33 or +0.33 Michelson contrast, respectively) followed the luminance steps at different delays (50, 250, and 2000 ms), with the flash at 2000 ms serving as baseline.

The luminance steps caused sustained changes in the cones' glutamate output (Fig. 5a). The transient responses to the probe flashes were superimposed on these glutamate modulations (Fig. 5b). This superposition was mostly linear and did not indicate nonlinear effects such as adaptation or saturation. Therefore, when we isolated the flash responses by subtracting the step responses, the resulting peak flash responses were only weakly affected by the preceding luminance step (Fig. 5c). Thus, at the level of the cone output (Fig. 5b), there was hardly any suppression when only considering the peak of the probe flash responses (Fig. 5c). How does the suppression observed at the level of RGC output arise from effectively linear cone responses? The answer lies in other properties of the cone response, such as its kinetics, which will be captured by downstream retinal pathways.

To demonstrate this, we used a previously published phenomenological model of retinal processing. In the model (Drinnenberg et al., 2018), RGC responses are described by passing a "light stimulus" to model photoreceptors, feeding their output through a set of linear-nonlinear filters to describe the processing in different bipolar pathways (Methods), and eventually converting these filter outputs into RGC spiking. Here, as the first step of analysis, we fitted the parameters of the model cone to reflect our measured data of cone output. The model faithfully explained the observed cone responses (Fig. S11) and gave us the opportunity to calculate cone responses to flashes presented at additional time points. This modeled cone output to step-flash combinations was fed into the model bipolar cells, finally yielding model RGC responses (Fig. 6). In the model, different RGC types can be described by varying the bipolar cell filter properties. We first investigated transient RGC responses (Fig 6a-c) and calculated a modulation index (Fig. 6d) comparable with the modulation index of

our real RGC data. As a control, we also passed the raw cone output data, instead of the fitted cone model, to the model bipolar cells and found qualitatively the same results (Fig. S12).

The model's ON and OFF RGCs (Fig. 6d) showed crossover-style suppression that was consistent with the suppression of real RGCs under similar luminance step experiments (Fig. 4b): the model's ON RGC showed strong suppression to the bright flashes presented immediately after the negative-contrast luminance step (Fig. 6d, right), while flashes after the positive-contrast luminance step were only weakly affected (Fig. 6d, left). Suppression recovered by 200 ms, consistent with the recovery time for the central component of suppression in real RGCs. Similarly, the model's OFF RGC showed strong suppression of its response to dark flashes presented immediately after the positive-contrast luminance step (Fig. 6d, left); suppression was absent in OFF RGC when the dark flash was presented later or after a negative-contrast luminance step (Fig. 6d). The markers on the curves in Fig. 6d correspond to the time points when the flashes were presented to the cones in the experiments depicted in Fig. 5. Model RGC responses to step-flash combinations and flash-induced responses at these time points are shown in Fig. 6a-c.

What mechanism within the model led to the emergence of the suppressive effect in RGC responses, despite the mostly linear response superposition at the cone output? In the model, the bipolar cells have transient filter properties and are driven predominantly by the instantaneous rate of change in the cone output, i.e. its derivative, rather than by the absolute cone output. The response to a probe flash presented immediately after an opposite-contrast luminance step (50 ms) occurred during the initial phase (ramp) of the cone response to the luminance step (Fig. 5b, columns 2 and 3). This causes a much smaller rate of change in cone output and therefore drives the downstream bipolar cells only weakly, resulting in weak or even completely suppressed model RGC responses (Fig. 6c, columns 2 and 3). On the other hand, flashes presented during the steady state phase of the luminance step response (250 ms and 2000 ms in Fig. 5b, columns 2 and 3), or flashes presented immediately after (50 ms) a same-contrast luminance step (Fig. 5b, columns 1 and 4) caused larger instantaneous changes in the cone output, and therefore resulted in

relatively stronger spiking (250 ms and 2000 ms in Fig. 6c; 50 ms in Fig. 6c, columns 1 and 4).

If suppression observed at RGC output did indeed result from the weaker rate of change in the cone output, less transient RGCs should show weaker suppression because they reflect the absolute cone output signal more faithfully. To test this, we varied the linear-nonlinear filter of the model bipolar cell to make the retinal pathway less transient (Methods). Indeed, the resulting crossover-style suppression was weaker in model RGCs with less transient response properties, indicated by the negative modulation index slope in Fig. 6e; seen in the ON RGC suppression after negative-contrast steps (blue lines in row 2) and OFF RGC suppression after positive-contrast steps (red lines in row 1); columns represent different time points sampled. Curious if this effect was also present in our real RGC data, we re-analyzed the data of Fig. 4 and evaluated suppression as a function of RGC transiency (Methods). The result was congruent with the model prediction: suppression was weaker in less transient (more sustained) cells (Fig. 6f).

The analyses above suggest that the central component of retinal saccadic suppression does not have a single site of origin. Instead, it appears to emerge from the relatively slow kinetics of cone responses (such that flash responses ride on the initial rising/falling phase of the cone's step response), combined with temporal properties and nonlinearities of downstream retinal pathways. The downstream pathways shape the exact strength and time course of RGC suppression. We term this novel retinal processing motif “dynamic reversal suppression”: “dynamic” because of the necessarily tight temporal link between responses to the two consecutive stimuli; and “reversal” because the response to an event gets suppressed when it reverses the cone output triggered by the first stimulus.

Generalization to other species

Retinal saccadic suppression, at least its central component, was triggered by stimulus-stimulus interactions (Figs. 4, 6, S8), governed by general retinal signal processing, without the need for any specialized “saccadic suppression” circuit. It is likely that such general processing is conserved across species. Indeed, we observed

quantitatively similar retinal saccadic suppression in pig ON and OFF RGCs (Fig. S13), including the dependency on background texture statistics. Interestingly, like in mouse, OFF RGCs in pig retina also recovered faster than ON RGCs, suggesting that the surround component of suppression was also present in pig ON RGCs. In an additional experiment, we also recorded the activity of RGCs from an ex vivo macaque retina while subjecting it to a shorter version of the luminance step paradigm (Fig. S1b) with fewer conditions than in the original paradigm. Our results (Fig. 7) indicate that macaque RGC responses to probe flashes, following luminance steps, are suppressed in a way similar to mouse retina. However, more data will be required to determine the population trend and for characterizing the dictionary of response modulations in macaque retina.

Downstream visual areas may modulate retinal saccadic suppression

Given the similarities we previously described between retinal and perceptual saccadic suppression (Idrees et al., 2020), it was tempting to test whether the crossover style of suppression, observed in the retina (Fig. 4b), was also reflected in perception. We therefore conducted human psychophysics experiments where we asked human subjects ($N = 5$) to maintain saccade-free fixation, while we simply changed the luminance of the homogenous background to a brighter (0.3 to 0.56 Michelson contrast) or darker (-0.3 to -0.56 Michelson contrast) background (Fig. 8a; Methods). At random times relative to the luminance step, we presented a dark (-0.033 Michelson contrast) or bright probe flash (+0.033 Michelson contrast), at one of four locations in the subjects' field of view. At trial end, the subjects were asked to localize the probe flash.

Irrespective of the step \rightarrow flash combination, subjects were strongly impaired in their ability to localize the probe flashes presented around the time of the luminance step (Fig. 8b). Most interesting in this context was the combination of negative-contrast luminance steps with dark probe flashes. In mouse retina, even though few OFF RGCs did show weak suppression to this combination (Fig. S8b, inverted histograms in row 2), this effect was virtually absent at the population level (Fig. 4b, right panel). In human perception, however, this combination led to strong suppression (Fig. 8b, right panel). We cannot exclude that stronger retinal suppression to this specific

combination might be present under different light or stimulus conditions. Another possibility is that it might be more pronounced in the retina of humans and other primate species (Fig. 7). Nonetheless, visual mechanisms of suppression certainly exist in higher visual brain areas (Idrees et al., 2020). Perceptual suppression after same-contrast stimulus combinations may arise from processing in these higher visual brain areas, which may modulate and complement retinal saccadic suppression to achieve robust effects at the perceptual level.

Discussion

For most RGCs that we recorded, responses to brief probe flashes were strongly suppressed when presented after saccade-like texture displacements across the retina. In fact, similar suppression occurred when texture displacements were replaced by sudden uniform changes in background luminance, suggesting that suppression was caused by rather generic mechanisms, triggered by visual transients across the retina, rather than specialized suppression circuits that react to image motion. We found that the suppression strength depended on four main factors: (1) strength of the visual transients, governed by the statistics of the background texture or the contrast of the luminance step; (2) elapsed time following the visual transient; (3) RGC polarity (ON vs. OFF RGCs); and (4) RGC response properties (RGC transiency). Stronger visual changes, elicited either by coarser textures or larger luminance step contrasts, caused stronger suppression, peaking approximately 50 ms after the stimulus offset (Figs. 1e, 4). The recovery times depended on RGC polarity: OFF RGCs recovered by 250 - 350 ms whereas suppression in ON RGCs lasted for up to 1 s (Figs. 1e, 4). The suppression was stronger in more transient RGCs (Fig. 6e, f). We identified at least three components of retinal saccadic suppression, with distinct spatial origins, defined as central, surround, and global components (Fig. 3). These components were mediated by different underlying mechanisms.

The central component was the only source of suppression in OFF RGCs, and the dominant source in ON RGCs for time points immediately after a full-field saccade or luminance step. This component was short-lived (~250-350 ms) and originated from a cell's receptive field center. It was triggered by opposite-polarity stimulus-stimulus interactions, which naturally occur during saccades and other forms of sequential

visual stimulation. The relatively slow temporal dynamics of the cone photoreceptor responses to two opposite-polarity consecutive stimuli were the basis for subsequent non-linear processing, ultimately suppressing RGC response to the second stimulus. Therefore, the central component of suppression cannot be pinpointed to one specific site but seems to be an emergent property. We call this novel processing motif “dynamic reversal suppression”. Such a mechanism, where the cone response itself remains linear, but nonetheless forms the basis for subsequent nonlinear response modulation, is clearly different from adaptation (Clark et al., 2013) or desensitization (Baylor and Hodgkin, 1974) mechanisms within the cones, which would evoke nonlinear responses of the cones themselves.

The suppressive mechanism of the central component also suggests that perceptual saccadic suppression is derived, at least in part, from the inherent response properties of photoreceptors, the very first cell in the visual processing cascade. In fact, this early implementation could also explain why we observed suppression in most RGCs we recorded from (Figs. S3, S8, S13), covering a wide spectrum of response properties and therefore presumably many RGC cell types (see Supplementary Fig. 6 of Idrees et al., 2020). Still, our results suggest that the suppression initiated at the level of cone photoreceptors is translated differently by the different parallel pathways in the retina, leading to variability in response suppression at the ganglion cell level (such as the stronger suppression in more transient RGCs, Fig. 6e, f). Further cell type classification will be required to relate the degree of modulation with pathway specificity. The type and degree of modulation might also differ across species, even though we see qualitatively similar suppression in mouse, pig, and macaque RGCs.

ON RGC sensitivity, in addition to this central component, is suppressed by two more components. First, the global component is a fast but short-lived (~250-350 ms) component, caused by inhibition via GABAergic wide field amacrine cells, triggered by global image changes and carried to the RGC from as far as the cell’s periphery (Figs. 2b, S5). This likely belongs to the same class of circuits that suppresses RGC responses to global motion (Baccus et al., 2008; Roska and Werblin, 2003). These circuits were previously suggested to suppress motion awareness during saccades, a phenomenon known as saccadic omission. As indicated by our results, such circuits also contribute towards suppressing RGC sensitivity even after the motion is

completed (i.e. saccadic suppression). However, since their influence is masked by more local components of suppression during full-field saccades (Fig. 2c, 2d, S6), they are unlikely to account for perceptual saccadic suppression. The global suppressive component mediated by GABAergic inhibition is nevertheless a mechanism to process global visual changes, in addition to the several others (Wei, 2018). It may, for example, play a role in perceptual modulations during smooth pursuit eye movements (Schütz et al., 2011). Here, the central component of suppression will not be triggered in RGCs whose receptive field centers are locked to the tracked object; but these RGCs will still be suppressed by the global component.

The second additional component is the surround component. It seems to act with a delay of ~200 ms and can last for up to 1000 ms. The spatial origins of this component are not very well understood, but our data indicate that it presumably arises from the immediate surround of a cell's receptive field. Additionally, similar to the central component, it does not rely on GABA_{A,C} or glycine receptors (Fig. 2c, 2d, S6), but the exact mechanisms remain to be explored. Possible mechanisms could involve negative feedback of horizontal cells onto the cones (Drinnenberg et al., 2018; Kemmler et al., 2014). This slower component most likely contributes to the longer recovery times observed in ON cells. Interestingly, visual masking in cat LGN also lasts longer in ON versus OFF cells (Schiller, 1968), which may be a consequence of the effects we describe here in the retina. While this surround component plays an important role in shaping RGC and downstream neural responses following a visual transient, its contribution to perceptual saccadic suppression can also be disputed. This is because, during real saccades, eye-movement related signals (e.g., corollary discharge) shorten the duration of suppression caused by visual mechanisms (Idrees et al., 2020), such that the long-lasting surround component may not critically shape perception. Yet another additional component of suppression, based on saturation-like mechanisms (Fig. 4b left, S10a), was found only in ON RGCs. It is possible that this component originates at the level of bipolar cells, especially because response saturation has been observed predominantly in ON bipolar cells but not in OFF bipolar cells (Schreyer and Gollisch, 2020). In summary, while Fig. 3 summarizes the three spatial components of suppression and their temporal properties, these components in turn can have further sub-components.

Irrespective of which components of retinal saccadic suppression contribute towards perceptual saccadic suppression, our results show that retinal responses to stimuli following visual transients are modulated concurrently by several mechanisms (Fig. 3). Additional mechanisms might exist under different stimulus conditions. From the perspective of retinal visual feature processing, this would be consistent with how multiple mechanisms concurrently process other visual features in the retina, such as motion (Wei, 2018). The retinal suppression that we studied likely contributes to several other visual phenomena, such as visual masking (Breitmeyer, 2007) or neural adaptation with successive stimuli (Mayo and Sommer, 2008). The similarities between the observations there and the suppression that we observed in the retina suggest that the retina may be a common neural substrate for these seemingly different types of perceptual phenomena, unifying their underlying mechanisms. The retinal processing described here may also contribute towards specialized visual-motor tasks. For example, while threading a needle, microsaccades will jitter the needle and its background across the retina. RGCs exposed to the background will experience stronger visual transients than RGCs exposed to the needle. As a result, RGCs 'seeing' the background might show suppressed responses following microsaccades, perceptually blurring out the background. This relative enhancement of the fixated object by background suppression could be valuable for visual tasks such as object recognition.

It is remarkable that an elementary property of retinal suppression, i.e. its dependence on the scene statistics (Fig. 1e), is clearly preserved all the way to perception (Idrees et al., 2020). However, retinal suppression alone cannot explain all perceptual effects of saccadic suppression. For example, suppression before a saccade (or a luminance step) is observed perceptually (even in the absence of eye movements, Fig. 8), but not in the retinal output (Idrees et al., 2020). Similarly, not all properties of retinal suppression were preserved in perception. The crossover style of suppression observed in the retinal output of mice (Fig. 4b) was not observed perceptually in humans (Fig. 8). The more far-reaching perceptual suppression may be the result of additional processing beyond the retina (Shapley and Enroth-Cugell, 1984). Alternatively, our results may not capture the full array of retinal processing. For one, our stimulus conditions in mouse retina experiments may not have been

comprehensive enough to capture all retinal suppressive effects. Further, the retinal output of humans and other primate species (Fig. 7) might differ from mouse retina in this respect.

Retinal suppression is only one way that the retina alters its output during dynamic vision. Other forms certainly co-exist, such as brief changes in RGC polarity following peripheral shifts (Geffen et al., 2007) or sensitization of some RGC types following a change in background luminance (Appleby and Manookin, 2019). These and several other studies (Amthor et al., 2005; Barlow et al., 1977; Enroth-Cugell and Jakiela, 1980; Krishnamoorthy et al., 2017; Noda and Adey, 1974; Passaglia et al., 2009; Roska and Werblin, 2003), together with ours, demonstrate the complex image processing capabilities in the retina to facilitate downstream visual processing for the ultimate service of perception during natural vision. Looking forward, the detailed characterization of retinal output provided here paves the way to investigate the visual features that the retina encodes during dynamic vision. Moreover, it also paves the way to investigate the interactions between retinal and extra-retinal (visual and non-visual) mechanisms of saccadic suppression, to further our understanding of how the visual system maintains stability in the face of constant disruptions.

Acknowledgements

We thank Elisabeth Gustafsson for providing technical support; Andreas Hierlemann for providing the HiDens CMOS MEA system and helping establish our high-density MEA recordings; Roland Diggelmann for helping in setting up the pipeline (including providing code) for automatic spike sorting of high-density MEA recordings; Martin Schenk at the Department of Experimental Surgery, Tübingen, for providing us domestic pig eyes. Our work was supported by funds of the Deutsche Forschungsgemeinschaft (DFG) to the Werner Reichardt Center for Integrative Neuroscience (EXC 307) and to TAM (MU3792/1-1 and MU3792/3-1). TAM received support from the Tistou and Charlotte Kerstan Foundation. SI, TAM and ZMH were also supported by an intra-mural funding program (Project 2013-05) of the Werner Reichardt Center for Integrative Neuroscience. FF was supported by a Swiss National Science Foundation Ambizione grant (PZ00P3_167989) and Swiss National Science Foundation Eccellenza grant (PCEFP3_187001). MPB and ZMH were further funded

by the SFB 1233 on “Robust Vision” (DFG, project number 276693517). KF was supported by the Bundesministerium für Bildung und Forschung (BMBF, 01GQ1002) and the Max Planck Gesellschaft (MPG, M.FE.A.KYBE0004).

Author contributions

TAM conceptualized the study; SI and TAM designed the overall study; FF developed and supervised computational modeling; SI, MPB, AK, KF, ZMH, FF and TAM designed experiments; SI performed ex vivo mouse and pig retina experiments; AK performed ex vivo macaque retina experiment; MPB performed human psychophysics experiments; KF performed viral injections; MK performed cone imaging experiments; SI and FF implemented computational model; All authors analyzed and interpreted the data and wrote the manuscript.

Declaration of interests

The authors declare no competing interests.

Data availability

All data presented in this paper are stored and archived on secure institute computers and are available upon reasonable request.

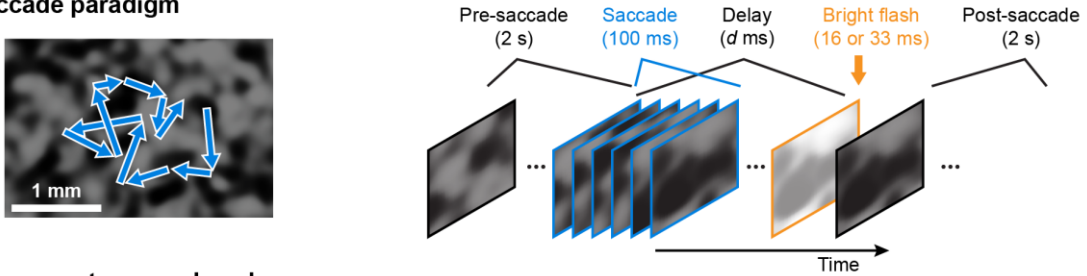
Code availability

All code used for analysis and computational modeling is available upon reasonable request.

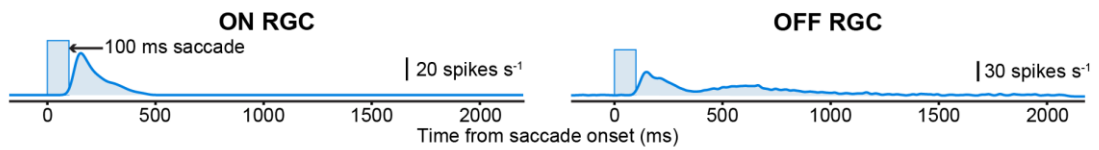
Figures

Figure 1

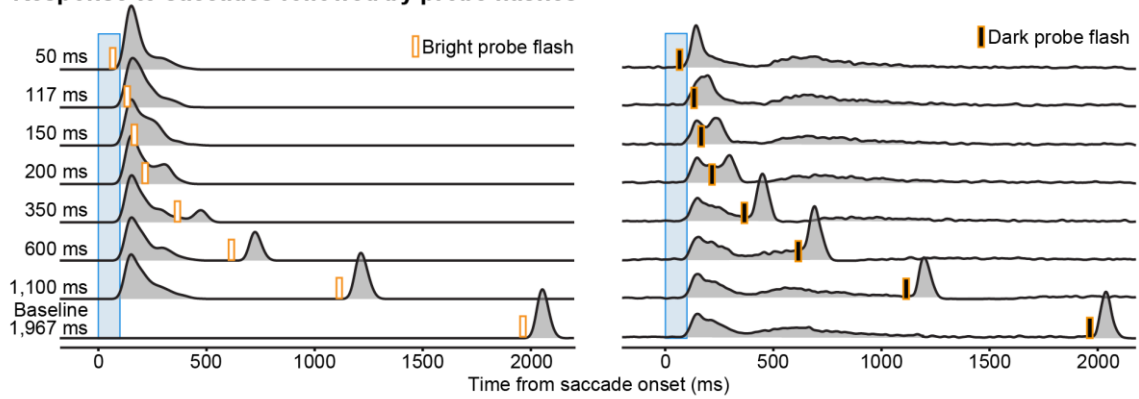
a Saccade paradigm



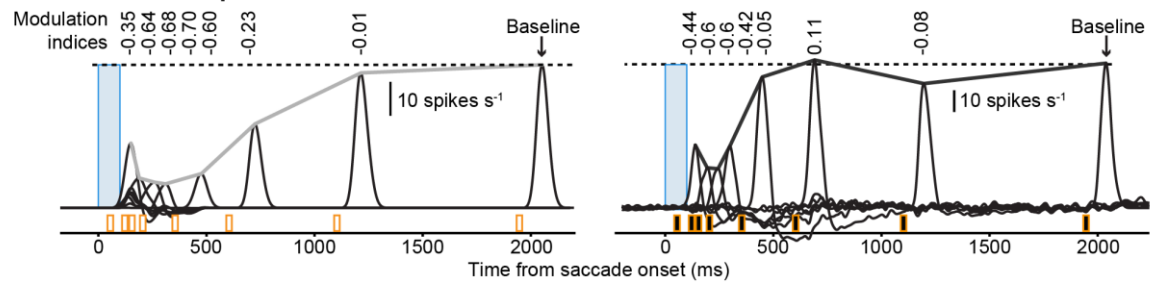
b Response to saccades-alone



c Response to saccades followed by probe flashes



d Flash-induced responses



e Modulation index (population)

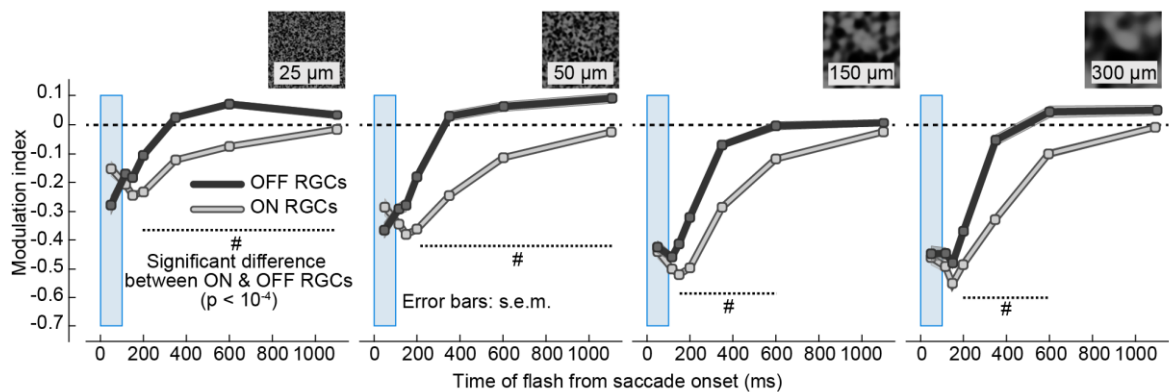


Figure 1 Similarities and differences in retinal saccadic suppression across ON and OFF RGCs.

a. RGC action potentials were recorded from ex vivo retinae placed on multielectrode arrays. Saccades were mimicked by displacing a texture projected onto the retina (blue arrows in left panel indicate texture displacement paths). The texture remained static for 2 s and was then displaced over 100 ms (blue outlines) followed by a brief probe flash (here bright probe flash is depicted, orange outline). Each trial consisted of 39 such successive saccade-flash sequences (Fig. S1a).

b,c. Average activity (firing rate) of an example ON RGC (left column) and OFF RGC (right column) to 39 saccade sequences not followed by a probe flash (**b**), and to 39 saccade sequences followed by probe flashes at different delays after saccade onset (**c**). Blue window: timing of saccades; orange markers: timing of probe flashes.

d. Isolated flash-induced responses (firing rate) of the same RGCs obtained by subtracting responses to saccades-alone (**b**) from responses to saccades followed by probe flashes (**c**). Lines connecting the response peaks highlight the time courses of retinal saccadic suppression relative to baseline flash-induced responses. Numbers above each response peak represent the modulation index which quantifies how much the probe flash response is modulated by the preceding saccade (Methods, negative modulation indices correspond to suppressed flash-induced responses).

e. Population modulation index (mean \pm s.e.m.) of ON (light gray) and OFF (dark gray) RGCs, for different background textures with different spatial scales (left to right: fine to coarse). The number of ON and OFF RGCs in the population varied between 68 and 574 for different flash times and textures (see Fig. S3 for exact numbers and relevant statistics). Hash symbols: significant modulation difference between ON and OFF RGCs ($p < 10^{-4}$, two-tailed Wilcoxon rank-sum test).

Figure 2

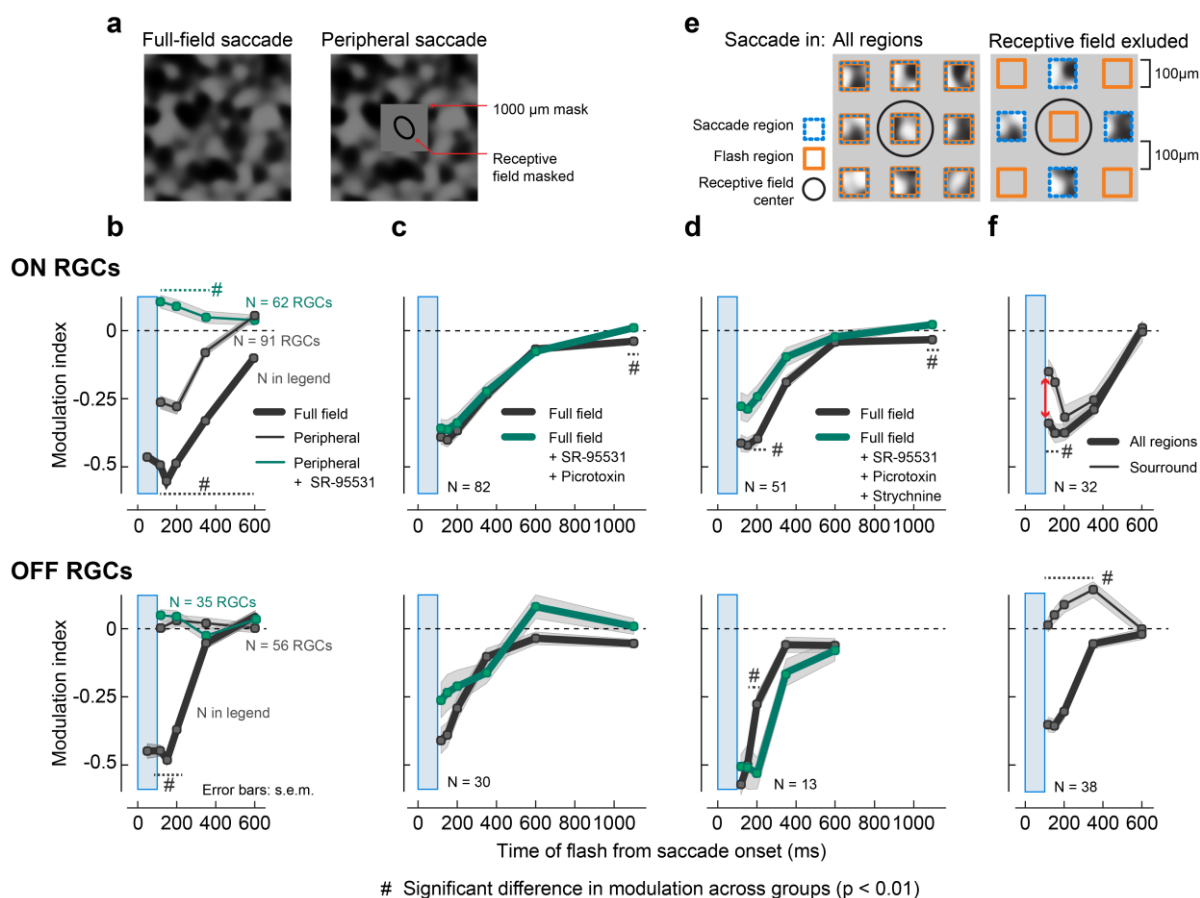


Figure 2 Spatial origins of retinal saccadic suppression.

a. Spatial layout of the visual stimulation paradigm used in experiments to probe the global component of suppression. Saccades were presented either full-field (left; same as in Fig. 1) or in the periphery (right), where a $1000 \times 1000 \mu\text{m}^2$ mask (intensity: mean luminance of texture) covered at least $2\text{-}\sigma$ of the 2D Gaussian fit to the RGC receptive fields (Fig. S5b).

b. Population modulation index (mean \pm s.e.m.) of ON (top) and OFF (bottom) RGCs for full-field saccades condition (thick gray lines, same as Fig. 1e rightmost panel; N = 68 to 574 RGCs (see Fig. S3 for exact numbers)); periphery saccades condition (thin gray lines; N = 91 ON RGCs, N = 56 OFF RGCs); and periphery saccades condition in the presence of GABA_A receptor blocker ($5\mu\text{M}$ SR-95531; green lines; N = 62 ON RGCs, N = 35 OFF RGCs). Blue window shows the timing of the saccade. In these experiments, we used a coarse background texture ($300 \mu\text{m}$ spatial scale). Timing of probe flashes: 50 and 150 (only for full-field saccade), 117, 200, 350, 600 and 2100 ms (baseline) after saccade onset.

c,d. Population modulation index (mean \pm s.e.m.) of ON (top) and OFF (bottom) RGCs for full-field saccades without any pharmacological agents (gray lines; N = 82 ON RGCs, N = 30 OFF RGCs) and with GABA_{A,C} receptor blockers $5 \mu\text{M}$ SR-95531 + $100 \mu\text{M}$ Picrotoxin (**c**; green lines), and for a subset of RGCs where we additionally

blocked glycine receptors using 1 μM Strychnine (**d**; green lines; $N = 51$ ON RGCs, $N = 13$ OFF RGCs). In these experiments, we used a coarse background texture (150 μm spatial scale). Probe flashes were presented at 117 ms, 150, 200, 350, 600, 1100 and 2100 (baseline) after saccade onset.

e. Spatial layout of the visual stimulation paradigm used in experiments to probe local components of suppression. Saccades and flashes were presented in $100 \times 100 \mu\text{m}^2$ square regions, separated by 100 μm gaps with mean overall luminance. **Left:** Saccades and flashes were presented in all regions. **Right:** Saccades and flashes were presented in alternate regions; only cells with receptive fields (RFs) in the non-saccade regions (orange) were analyzed (black ellipse: $1-\sigma$ of the 2D Gaussian fit to an example RGC receptive field). Consequently, saccades were excluded from at most $\sim 300 \times 300 \mu\text{m}^2$ of a cell's RF center. In these experiments, we used a coarse background texture (150 μm spatial scale).

f. Population modulation index (mean \pm s.e.m.) of ON (top; $N = 32$) and OFF (bottom; $N = 38$) RGCs for saccades and flashes in all regions (thick lines) or saccades excluded from RGC RF center (thin lines). Red arrow indicates significant loss in suppression in ON RGCs for early flashes at 117 and 150 ms upon excluding saccades from RF center ($p = 0.0016$ and $p = 0.002$ respectively; two-tailed Wilcoxon rank-sum test).

In all panels, hash symbols indicate statistically significant difference between groups ($p < 0.01$, two-tailed Wilcoxon rank-sum test).

Figure 3

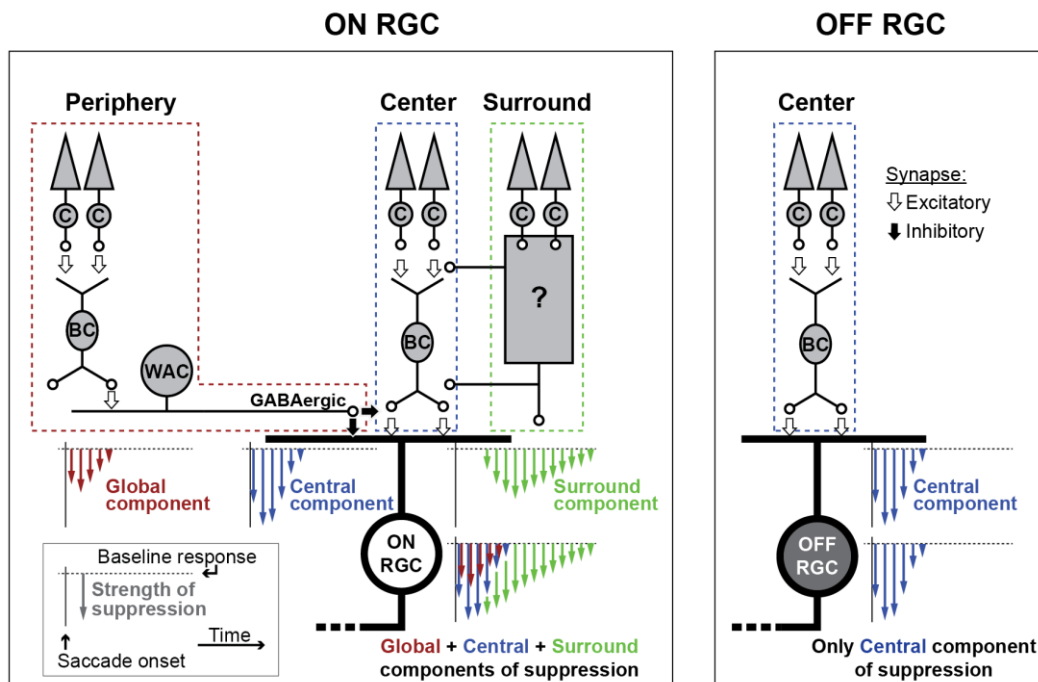


Figure 3 Schematic summarizing the spatial origins of retinal saccadic suppression.

Saccadic suppression in OFF RGCs (right) is mediated primarily by the central component of suppression (blue) that originates from the cells' receptive field center. ON RGCs (left) get suppressed from two additional components: First, the fast but short-lived global component (red), mediated by GABAergic inhibition, that originates from as far as the cells' periphery. This global component has a similar temporal profile as the central component. It is however weaker than the central component and acts in parallel to it, indicated by the red arrows parallel to blue arrows in the total suppression schematic. Second, the delayed but long-lasting surround component (green), which might originate from the cell's immediate surround. The central component and surround component do not depend on classical GABAergic or glycinergic inhibitory pathways. The differences in the suppression recovery time in ON and OFF RGCs was mainly due to this surround component acting on ON RGCs. Inset shows the legend for arrow schematics. Length of the arrows represent suppression strength; spread of the arrows show the temporal profile of suppression.

Figure 4

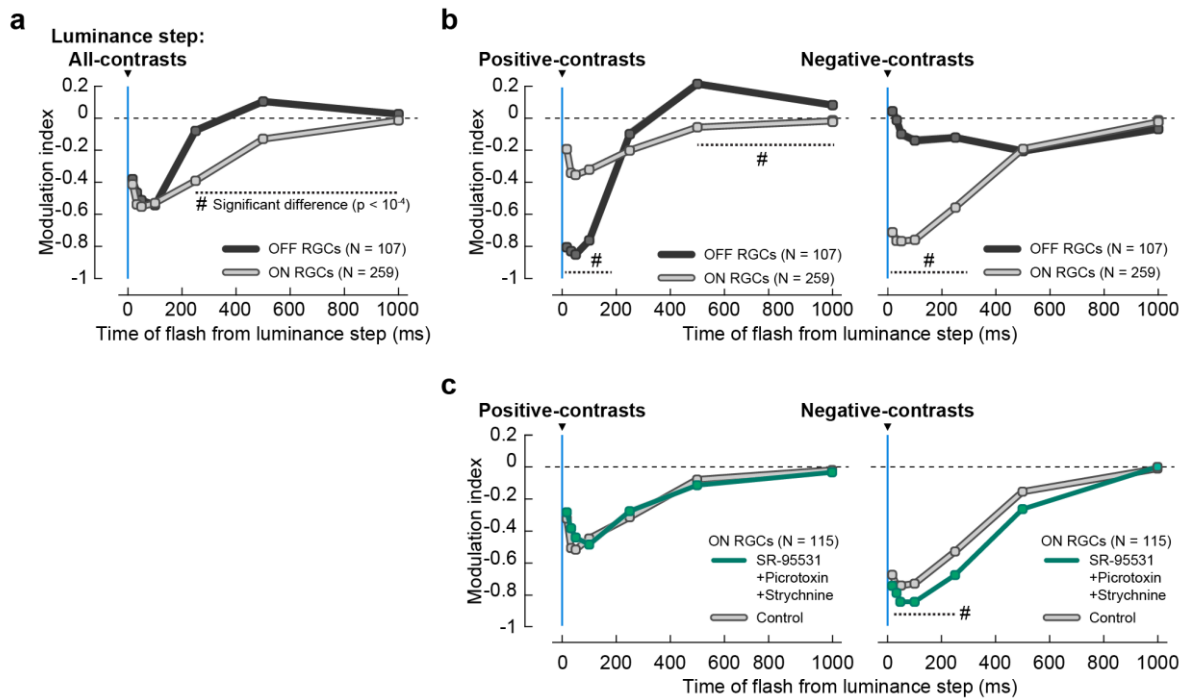


Figure 4 Suppression following luminance steps.

a. Population modulation index (mean \pm s.e.m.) of ON (light gray, N = 259) and OFF (dark gray, N = 107) RGCs for probe flashes following luminance steps (blue line). Modulation index for each RGC was based on its average response to 56 or 156 luminance step sequences (Fig. S1b) spanning a contrast range of -0.5 to +0.5 Michelson contrast (Methods). Probe flashes were presented at 17 ms, 33, 50, 100, 250, 500, 1000 and 2000 (baseline) after luminance steps. Probe flash responses were suppressed in both ON and OFF RGCs, with similar time course and recovery as in the saccade paradigm with textures (Fig. 1e). Error bars are not visible due to small s.e.m.

b. Same as in **a**, except that the modulation index for each RGC was separately based on average responses to probe flashes after positive-contrast luminance steps (left panel; +0.03 to +0.5 Michelson contrast), and after negative-contrast luminance steps (right panel; -0.03 to -0.5 Michelson contrast). Underlying population data is shown in Fig. S8.

c. Same as in **b**, for a subset of ON RGCs (N = 115) in control conditions (light gray lines) and with GABA_{A,C} and glycine receptors blocked (green lines; cocktail of 5 μ M SR-95531, 100 μ M Picrotoxin and 1 μ M Strychnine). Hash symbol: significant difference between modulation of ON and OFF RGCs in **a** or between ON RGCs without and with pharmacological blockers in **c** ($p < 10^{-4}$, two-tailed Wilcoxon rank-sum test).

Figure 5

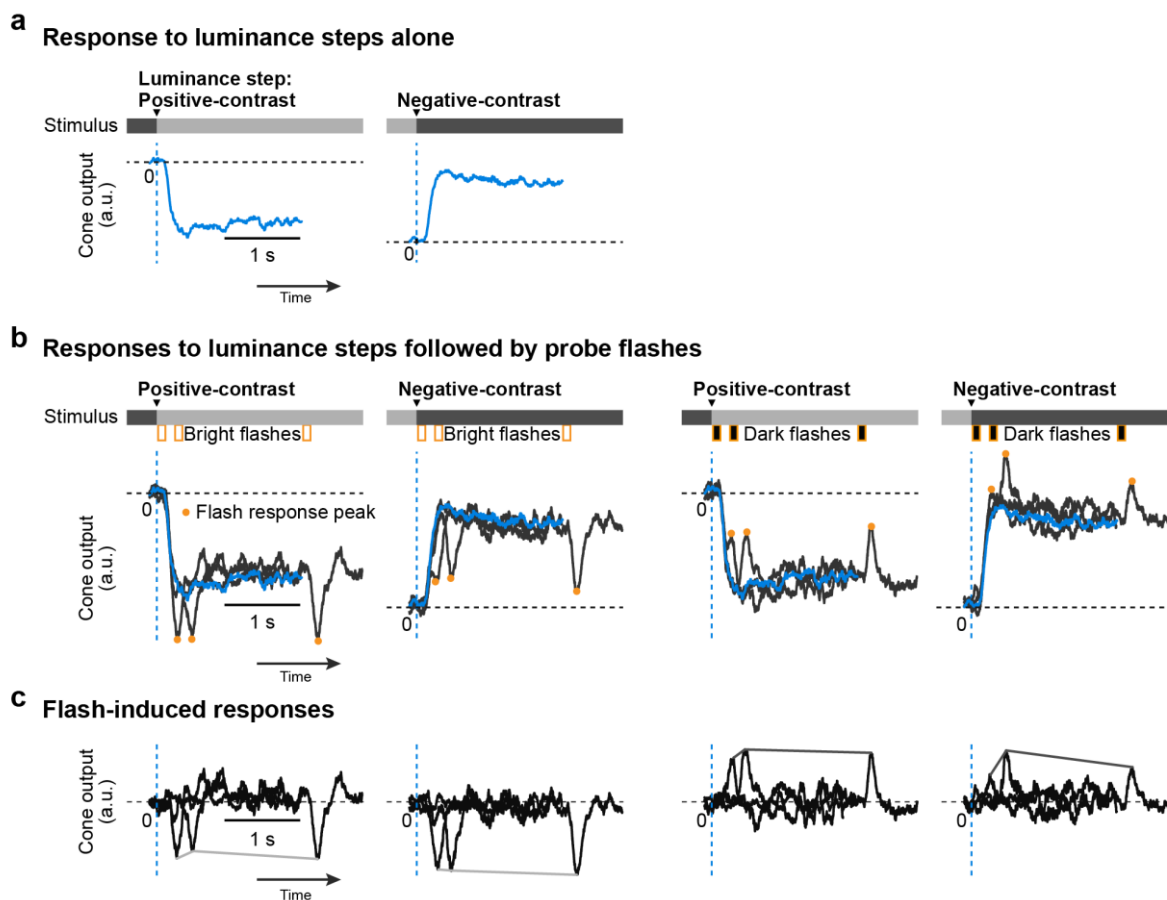


Figure 5 Cone output in response to probe flashes following luminance steps.

a,b. Cone responses (baseline normalized iGluSnFR indicator fluorescence signal) to positive- and negative-contrast (+0.4 and -0.4 on Michelson scale) luminance steps alone (**a**) and to luminance steps followed by probe flashes at 17, 250 and 2000 ms (orange bars below the intensity bar shows timing of probe flashes) (**b**). Probe flashes were either bright or dark (+0.33 or -0.33 Michelson contrast respectively; 100 ms long). In **b**, responses to step-alone (blue) and individual step → flash pairs (dark gray) are overlaid. Dashed blue lines: timing of luminance step; orange circles: peak cone response to flashes; horizontal dashed line: cone level prior to the luminance step.

c. Flash-induced responses, isolated by subtracting luminance step alone responses (blue) from individual composite luminance step-probe flash responses (dark gray) in **b**. Lines connecting the response peaks highlight the time courses of suppression relative to baseline flash-induced (2000 ms) responses.

Figure 6

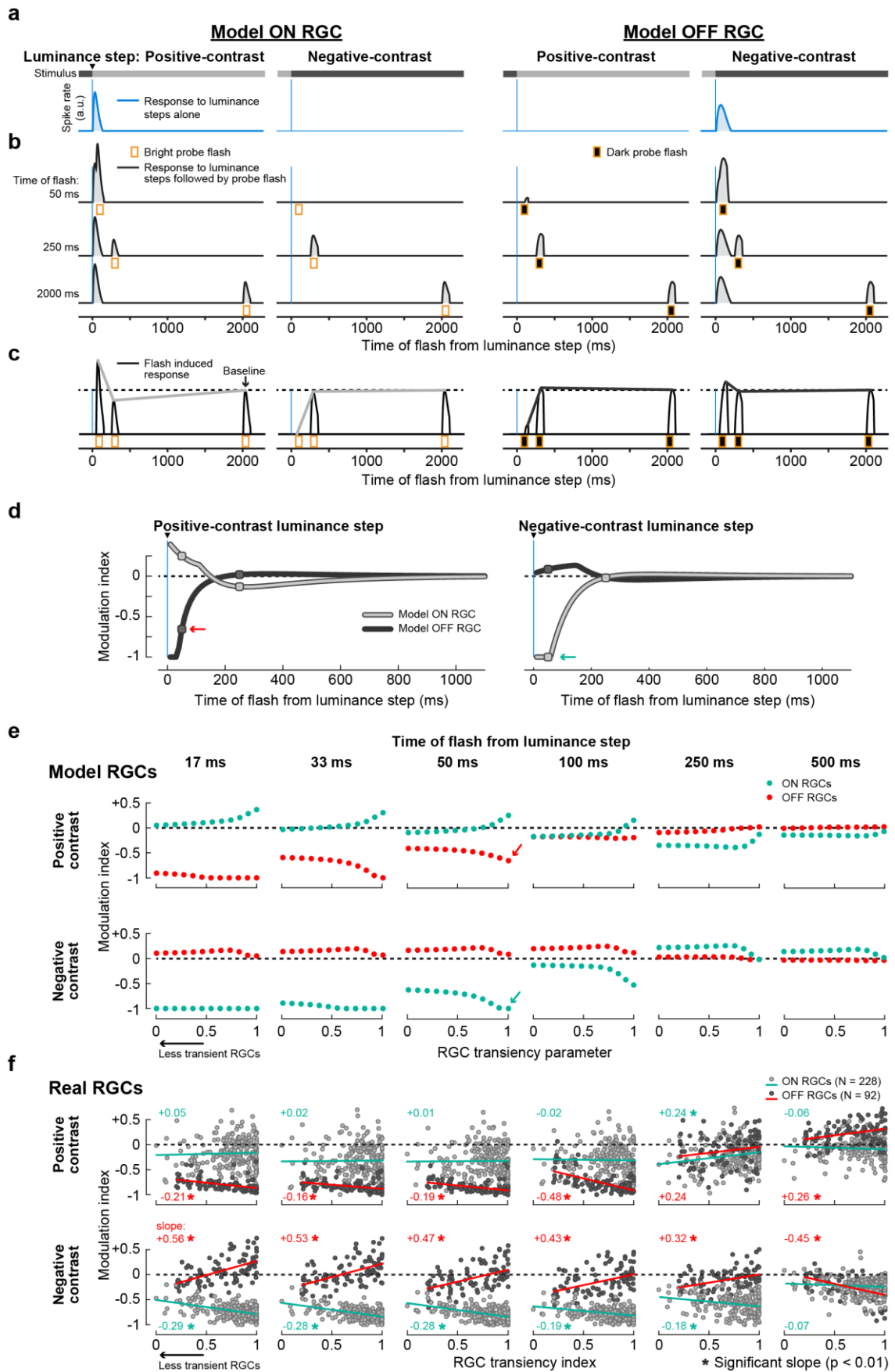


Figure 6 Model RGC responses to probe flashes following luminance steps.

a,b. Spiking response of model ON (columns 1-2) and OFF (columns 3-4) RGCs to luminance steps alone (**a**, blue) and to luminance steps followed by probe flashes (**b**, black) at 50, 250 and 2000 ms (different rows; analogous to real RGCs in Fig. 1b, c). Luminance steps are depicted by intensity bars in **a**. First column in each cell type: responses following a positive-contrast luminance step; second column: responses following a negative-contrast luminance step. Vertical blue lines: timing of luminance step; orange bars: timing of probe flashes. Note the ON RGC and OFF RGC did not spike in response to negative-contrast (column 2) and positive-contrast (column 3) luminance steps respectively.

c. Flash-induced responses, after subtracting **a** from **b**, overlaid to show the modulation of probe flash responses at different times (analogous to real RGCs in Fig. 1d). Lines connecting the response peaks highlight the time courses of suppression relative to baseline flash-induced responses (2000 ms).

d. Modulation indices for probe flashes in ON (light gray) and OFF model RGCs (dark gray), following positive-contrast (left panel) and negative-contrast (right panel) luminance steps. Modulation indices were calculated based on model responses to probe flashes presented at 10 ms intervals after luminance steps, and baseline as response to a flash at 2000 ms. Circle markers indicate modulation indices based on probe flashes at 50 and 250 ms shown in **b**, **c**. Cyan and red arrows highlight the suppression of opposite-contrast flashes at 50 ms in ON and OFF RGCs, respectively.

e. Modulation indices of model ON (cyan) and OFF (red) RGCs plotted as a function of RGC transiency. Individual panels correspond to different flash times (chosen from real-RGC recordings, Fig. 4) after positive-contrast (top row) and negative-contrast (bottom row) luminance steps. In **a-d**, transiency parameter was set to 1. Arrows highlight the same data as in **d**.

f. Same as in **e** but for real ON (light gray circles; $N = 228$; cyan line: linear regression fit) and OFF RGCs (dark gray circles; $N = 92$; red line: linear regression fit). These RGCs are a subset of the population data shown in Fig. 4b for which we could compute a transiency index (Methods). Consistent with model predictions, suppression after negative-contrast steps was weaker in less transient ON RGCs (bottom row, blue regression line has negative slope) and, after positive-contrast steps, suppression was weaker in less transient OFF RGCs (top row, red regression line has negative slope). Numbers in each panel indicate the slope of the fits and asterisk symbol indicates statistically significant slope (slope $\neq 0$, $p < 0.01$, two-tailed t-test).

Fig. S12 shows model RGC responses based on real cone data of Fig. 5 instead of model cone responses.

Figure 7

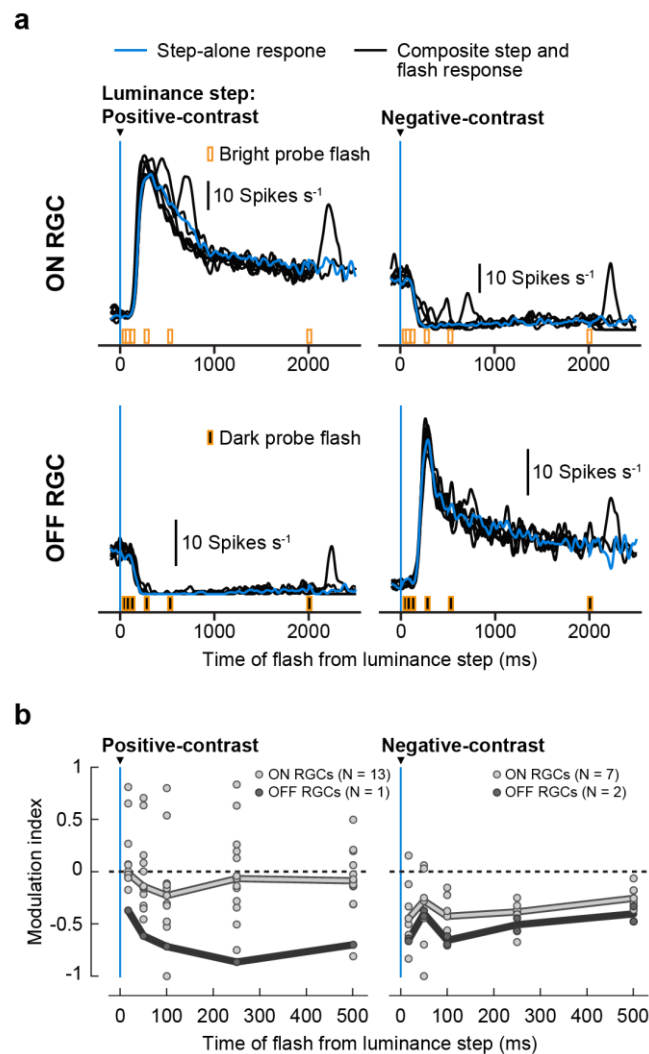


Figure 7 Retinal saccadic suppression in Macaque RGCs.

a. Average activity of an example macaque ON RGC (top) and OFF RGC (bottom) to positive-contrast (left column) and negative-contrast (right column) luminance steps alone (blue traces) and luminance steps followed by probe flashes (black traces). ON RGCs were analyzed for bright probe flashes and OFF RGCs for dark probe flashes. Responses were averaged across the different positive-contrast (0.05 to 0.5 Michelson contrast, N = 10 sequences) and negative-contrast luminance steps (-0.05 to -0.5 Michelson contrast, N = 10 sequences).

b. Median modulation index (thick lines) of macaque ON (light gray) and OFF (dark gray) RGCs for probe flashes presented after positive-contrast (left panel; N = 13 ON RGCs, N = 1 OFF RGC) and negative-contrast luminance steps (right panel; N = 7 ON RGCs, N = 2 OFF RGC). Circles represent modulation indices of individual RGCs. This experiment was performed under scotopic light conditions.

Figure 8

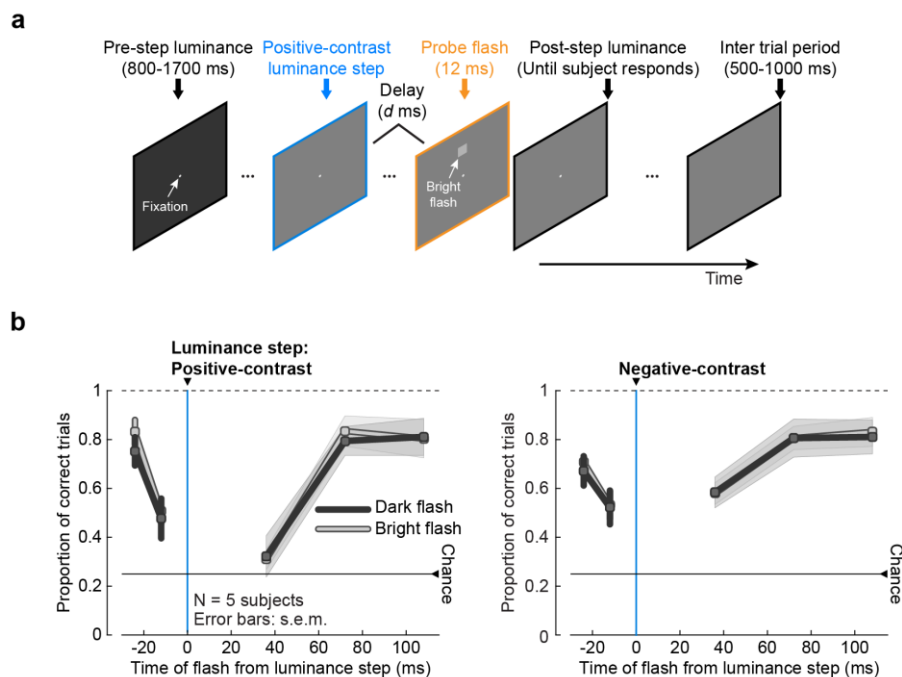


Figure 8 Perceptual suppression following luminance steps.

a. Example visual task trial. Subjects fixated a small spot on a uniform background with a set luminance (pre-step luminance) for a random duration (800-1700 ms). Background luminance then increased (like shown here) or decreased (positive or negative-contrast luminance step, respectively). At one of 5 times relative to the luminance step (-24, -12, 36, 72, or 108 ms), a luminance pedestal (probe flash, 147.8 x 147.8 min arc) was applied for ~12 ms at one of four locations relative to the fixation spot: 7 deg above (shown here), below, to the right, or to the left. The probe flash was brighter (shown here) or darker than the current screen luminance. The background remained at the post-step luminance until the subject responded with the perceived location of the flash, plus an additional 500-1000 ms but without the fixation spot, allowing the subject to relax. The current luminance was the pre-step luminance of the consecutive trial.

b. Performance of human subjects (mean \pm s.e.m., N = 5 subjects), to correctly localize a dark (dark gray) or a bright (light gray) probe flash presented at different times relative to positive-contrast (left panel) and negative-contrast (right panel) luminance steps (blue line). Each subject's responses were averaged across the different positive-contrast (0.3 to 0.56 Michelson contrast) and negative-contrast (-0.3 to -0.56 Michelson contrast) luminance steps. Perceptual performance was reduced around the time of luminance steps, reflecting suppression, irrespective of the combination of luminance step polarity and flash polarity. There were no statistically significant differences in suppression of dark and bright probe flashes (two-tailed Wilcoxon rank-sum test). Note that in the right panel, the suppression profile for bright probe flashes almost completely overlaps the suppression profile of dark probe flashes.

METHODS

Experimental model and subject details

Animals

We performed electrophysiological experiments on ex vivo mouse, pig and macaque retinae; and imaging experiments on ex vivo mouse retinae.

Mouse and pig ex vivo retinae experiments were performed in Tübingen, in accordance with German and European regulations, and animal experiments were approved by the Regierungspräsidium Tübingen. Macaque ex vivo retina experiment was performed at Stanford University. Eyes were removed from a terminally anesthetized macaque rhesus monkey used by other laboratories in the course of their experiments, in accordance with the Institutional Animal Care and Use Committee guidelines of Stanford University.

For mouse retina electrophysiology, we used 47 retinae from 15 male and 30 female *PV-Cre x Thy-S-Y* mice (*B6;129P2-Pvalb^{tm1(cre)Arbr/J} × C57BL/6-tg (ThystopYFPJS)*), 3-12 months old, which are functionally wild type (Farrow et al., 2013; Münch et al., 2009; Tikidji-Hamburyan et al., 2015). Additionally, we recorded the cone output from 4 retinae obtained from two C57BL/6 male mice, 9 to 10 weeks old. We housed mice on a 12/12 h light/dark cycle, in ambient temperatures between 20-22 °C and humidity levels of 40%.

We also replicated experiments on 9 pig retinae obtained from domestic female pigs after they had been sacrificed during independent studies at the Department of Experimental Surgery at the Medical Faculty of the University of Tübingen. Pigs were anesthetized using atropine, azaperone, benzodiazepine (midazolam), and ketamine, and then sacrificed with embutramide (T61). Before embutramide administration, heparin was injected.

One experiment was conducted with a retina extracted from a macaque rhesus monkey.

Humans

Human psychophysics experiments were performed in Tübingen. Human subjects provided written, informed consent, and they were paid 10 Euros per session of 60 minutes each, for three sessions. Human experiments were approved by ethics committees at the Medical Faculty of Tübingen University, and they were in accordance with the Declaration of Helsinki.

In total, we collected data from 5 subjects (24-29 years old; one female).

Experimental setup

Retina electrophysiology (mouse and pig): procedure and laboratory setup

Mice were dark adapted for 4-16 h before experiments. We then sacrificed them under dim red light, removed the eyes, and placed eyecups in Ringer solution (in mM: 110 NaCl, 2.5 KCl, 1 CaCl₂, 1.6 MgCl₂, 10 D-glucose, and 22 NaHCO₃) bubbled with 5% CO₂ and 95% O₂. We removed the retina from the pigment epithelium and sclera while in Ringer solution.

Pigs were dark-adapted for 15-20 min before sacrifice. Immediately after veterinary-confirmed sacrifice, the eyes were enucleated under dim red light, and the cornea, lens, and vitreous were removed. Eyecups were kept in CO₂-independent culture medium (Gibco) and protected from light. We transported eyecups to our laboratory and cut pieces from mid-peripheral or peripheral retinae. Only those retinae which showed ganglion cell responses to light stimuli were used in our experiments.

We recorded mouse and pig retinal ganglion cell (RGC) activity using either low- or high-density multi-electrode arrays (MEAs). The low-density setup consisted of a perforated 60-electrode MEA (60pMEA200/30ir-Ti-gt, Multichannel Systems (MCS), Reutlingen, Germany) having a square grid arrangement and 200 μ m inter-electrode distance. We whole mounted an isolated retina on a nitrocellulose filter (Millipore) with a central 2 x 2 mm hole. The mounted retina was placed with the RGC side down into the recording chamber, and good electrode contact was achieved by negative pressure through the MEA perforation. We superfused the tissue with Ringer solution at 30-34 °C during recordings, and we recorded extracellular activity at 25 kHz using

a USB-MEA-system (USB-MEA 1060, Multichannel Systems) or a memory-card based system (MEA1060, Multichannel Systems). Data was acquired using MC Rack version 4.6.2 (Multichannel Systems). A detailed step-by-step approach is provided in (Reinhard et al., 2014).

The high-density MEA setup consisted of either a HiDens CMOS MEA (Frey et al., 2009) (developed by the lab of Andreas Hierlemann, Basel, Switzerland) or a MaxOne system (Müller et al., 2015) (Maxwell Biosystems, Basel, Switzerland). The HiDens CMOS MEA featured 11,011 metal electrodes with inter-electrode (center-to-center) spacing of 18 μm placed in a honeycomb pattern over an area of 2 x 1.75 mm. Any combination of 126 electrodes could be selected for simultaneous recording. The MaxOne MEA featured 26,400 metal electrodes with center-to-center spacing of 17.5 μm in a grid-like arrangement over an area of 3.85 x 2.1 mm. In this system, up to 1024 electrodes could be selected for simultaneous recordings. For each experiment, a piece of isolated retina covering almost the entire electrode array was cut and placed RGC-side down in the recording chamber. We achieved good electrode contact by applying pressure on the photoreceptor side of the retina by carefully lowering a transparent permeable membrane (Corning Transwell polyester membrane, 10 μm thick, 0.4 μm pore diameter) with the aid of a micromanipulator. The membrane was drilled with 200 μm holes, with center-center distance of 400 μm , to improve access of the Ringer solution to the retina. We recorded extracellular activity at 20 kHz using FPGA signal processing hardware. In the case of the HiDens CMOS MEA, data were acquired using custom data acquisition software, called MEA 1k Scope (developed by the lab of Andreas Hierlemann, Basel, Switzerland). In the case of the MaxOne MEA, data were acquired using MaxLab software provided by Maxwell Biosystems, Basel, Switzerland.

In total, we performed 59 recordings, 47 from mouse and 12 from pig retinae. 24 of the 59 recordings were done using low-density MEAs. Once a basic experimental protocol was established, we shifted to HiDens CMOS MEA providing much higher throughput. 12 experiments were done using this setup. We upgraded to the MaxOne MEA for even higher throughput and did 23 recordings using this setup. A subset of the data collected from 32 of the 59 recordings (20 from mouse and 12 from pig

retinae), was also used in our previous study (Idrees et al., 2020). Here, we show further in-depth analysis of that data.

We presented light stimuli to the retinal piece that was placed on the MEA using a DLP projector running at 60 Hz (Acer K11 for low-density MEA experiments and Lightcrafter 4500 from EKB Technologies Ltd. with internal red, green and blue light-emitting diodes, for high-density MEA experiments). 60 Hz is above the flicker fusion frequency of both mouse and pig retinae; therefore, the framerate of these projectors was adequate for our purposes. The Acer K11 projector had a resolution of 800 x 600 pixels covering 3 x 2.25 mm on the retinal surface. Lightcrafter 4500 had a resolution of 1280 x 800 pixels, extending 3.072 x 1.92 mm on the retinal surface. We focused images onto the photoreceptors using a condenser (low-density MEA recordings, illumination from below) or a 5x objective (high-density MEAs, illumination from above). In each case, the light path contained a shutter and two motorized filter wheels with a set of neutral density (ND) filters (Thorlabs NE10B-A to NE50B-A), having optical densities from 1 (ND1) to 5 (ND5). The filters allowed us to adjust the absolute light level of the stimulation.

We measured the spectral intensity profile (in $\mu\text{W cm}^{-2} \text{nm}^{-1}$) of our light stimuli with a calibrated USB2000+ spectrophotometer (Ocean Optics) and converted the physical intensity into a biological equivalent of photoisomerizations per rod photoreceptor per second ($R^*\text{rod}^{-1}\text{s}^{-1}$), as described before (Tikidji-Hamburyan et al., 2015). Light intensities of the projector output covered a range of 3 log units (i.e. 1000-fold difference between black and white pixels, over an 8-bit range). We linearized the projector output, and we used only grayscale images of limited contrast, spanning at most the range from 0 to 120 in the 8-bit range of the projector (see stimulus description below for details). Absolute light intensities were set to the mesopic level, where a stimulus intensity of '30' in our 8-bit DLP projector scale (0-255) corresponded to 225 to 1000 $R^*\text{rod}^{-1}\text{s}^{-1}$, depending on the experimental rig used for the experiment (i.e. different DLP projectors and MEAs). We pooled all data from the different rigs as separate individual analyses from the individual setups revealed no effects of recording conditions in the different setups. For experiments of Fig. S4, we also recorded at scotopic light levels where a stimulus intensity of '30', corresponded to 23 $R^*\text{rod}^{-1}\text{s}^{-1}$ at scotopic level.

Retina electrophysiology (macaque): procedure and laboratory setup

In one experiment, we recorded the activity of macaque retinal ganglion cells. For this experiment we used a high-density MEA, as described previously (Chichilnisky and Baylor, 1999; Field et al., 2007). Following enucleation, the anterior portion of the eye and vitreous were removed. The eye was stored in a dark container in oxygenated Ames' solution (Sigma, St. Louis, MO) at 33°C, pH 7.4. Under infrared illumination, a small piece of retina approximately 1x1 mm, from a retinal region with eccentricity around 12 mm (4.0-17mm temporal equivalent eccentricity; (Chichilnisky and Kalmar, 2002)), was dissected and placed ganglion cell side down on a MEA for recording. The retina pigment epithelium remained attached during the recording; the retina was perfused with oxygenated Ames' solution. A custom planar large-scale MEA (Field et al., 2007; Litke et al., 2004) with a hexagonal outline of 519 electrodes at 30 μm pitch was used. Recorded voltages were band-pass filtered, amplified, and digitized at 20 kHz using custom electronics (Litke et al., 2004). Spike sorting process was described previously (Field et al., 2007).

Visual stimulation was performed with the optically reduced image of a gamma-corrected OLED microdisplay (eMagin) refreshing at 60.35 Hz focused on the photoreceptor outer segments. The visual stimulus was delivered through the mostly-transparent electrode array. The power of each display primary was measured at the preparation with a calibrated photodiode (UDT Instruments). At the mean background illumination level, the photoisomerization rates for the rods and the L, M, and S cones were approximately 29, 9, 9, and 2 $\text{P}^*\text{receptor}^{-1}\text{s}^{-1}$, respectively (see Li et al., 2014), placing the retina in scotopic regime.

Retina electrophysiology: pharmacology

In several MEA experiments, we used pharmacological agents to block specific receptors in the mouse retina. To block GABA_A receptors selectively, we used 5 μM SR-95531 (gabazine, an antagonist of GABA_A receptors; Sigma). To block both GABA_A and GABA_C receptors, we used 100 μM picrotoxin (an antagonist of GABA_A and GABA_C receptors; Sigma). To block glycine receptors, we used 1 μM Strychnine (antagonist of Glycine receptors).

We first prepared a 1000x stock solution of these pharmacological blockers as follows: SR-95531 was dissolved in water at a concentration of 5 mM; picrotoxin was dissolved in DMSO at a concentration of 100 mM; Strychnine was dissolved in Chloroform at a concentration of 1mM. During the experiments, we pipetted the stock solution to the Ringer solution in a 1:1000 ratio. Wash-in was performed for 20 min.

Cone photoreceptors imaging: procedure and laboratory setup

To record the output of cone photoreceptors in the mouse retina, we measured the glutamate release using an intensity based glutamate-sensitive fluorescent reporter, iGluSnFR (Marvin et al., 2013) expressed in horizontal cell processes post-synaptic to cone terminals, using a viral approach. We recorded the cone output from 4 retinæ obtained from two C57BL/6 male mice, 9 to 10 weeks old. Below, we reproduce the methods, previously described in Szatko et al (Szatko et al., 2020).

We dark-adapted the mice for ≥ 1 h before the experiments. They were then anaesthetized using isoflurane (Baxter) and sacrificed by cervical dislocation. The eyes were enucleated and hemisected in carboxygenated (95% O₂ and 5% CO₂) artificial cerebrospinal fluid (ACSF) solution containing (in mM): 125 NaCl, 2.5 KCl, 2 CaCl₂, 1 MgCl₂, 1.25 NaH₂PO₄, 26 NaHCO₃, 20 glucose, and 0.5 L-glutamine (pH 7.4). We then moved the tissue to the recording chamber where it was continuously perfused with carboxygenated ACSF at ~ 36 °C. In these experiments, ACSF contained ~ 0.1 μ M Sulforhodamine-101 (SR101, Invitrogen) to reveal blood vessels and any damaged cells in the red fluorescence channel (Euler et al., 2019). All procedures were carried out under very dim red (>650 nm) light.

iGluSnFR was expressed in the retina by viral transduction of AAV2.7m8.hSyn.iGluSnFR, generated in the Dalkara lab (Institut de la Vision) as described in (Dalkara et al., 2013; Khabou et al., 2016). The iGluSnFR plasmid construct was provided by J. Marvin and L. Looger (Janelia Research Campus, USA). A volume of 1 μ L of the viral construct was injected into the vitreous humour of the mice, anaesthetized with 10% Ketamine (Bela-Pharm GmbH & Co. KG) and 2% xylazine (Rompun, Bayer Vital GmbH) in 0.9% NaCl (Fresenius). For the injections, we used a micromanipulator (World Precision Instruments) and a Hamilton injection

system (syringe: 7634-01, needles: 207434, point style 3, length 51 mm, Hamilton Messtechnik GmbH). Imaging experiments were performed 3-4 weeks after injection. In the outer retina, iGluSnFR was predominantly expressed in horizontal cells. As the expression tended to be weaker in the central retina, most scan fields were acquired in the medial to peripheral ventral or dorsal retina.

To record the iGluSnFR signal, we used a MOM-type two-photon microscope setup (designed by W. Denk, MPI, Heidelberg; purchased from Sutter Instruments / Science Products). The design and procedures have been previously described in (Euler et al., 2009, 2019). In brief, the system was equipped with a mode-locked Ti:Sapphire laser (MaiTai-HP DeepSee, Newport Spectra-Physics), two fluorescence detection channels for iGluSnFR (HQ 510/84, AHF/Chroma) and SR101 (HQ 630/60, AHF), and a water immersion objective (W Plan-Apochromat 20x /1.0 DIC M27, Zeiss). The laser was tuned to 927 nm for imaging iGluSnFR. For image acquisition, we used custom made software (ScanM by M. Müller and T. Euler) running under IGOR Pro 6.3 for Windows (Wavemetrics), taking time-lapsed 128 x 128 pixel image scans at 3.9 Hz in the outer plexiform layer (OPL).

For light stimulation in cone imaging experiments, we used the Lightcrafter (LCr; DPM-E4500UVBGMKII), a DLP projector from EKB Technologies Ltd. with internal UV and green light-emitting diodes (LEDs). The light from the DLP projector was focused through the objective. To optimize spectral separation of mouse M- and S- opsins, LEDs were band-pass filtered (390/576 Dualband, F59-003, AHF/Chroma). LEDs of the DLP projector were synchronized with the microscope's scan retrace. Stimulus intensity (as isomerization rate, $P^*_{\text{cone}} \cdot \text{s}^{-1}$) was calibrated to range from ~500 (black image) to ~20,000 for M- and S-opsins. In addition, a steady illumination component of $\sim 10^4 P^*_{\text{cone}} \cdot \text{s}^{-1}$ was present during the recordings because of two-photon excitation of photopigments. The overall light intensity falling on to the retina was therefore in the low photopic regime. The light stimulus was centered to the recording field before every experiment. For all experiments, the retinal tissue was kept at a constant mean stimulator intensity level for at least 15 s after the laser scanning started and before stimuli were presented.

Human psychophysics: laboratory setup

We used a similar laboratory setup as described previously (Idrees et al., 2020). Briefly, subjects sat in a dark room 57 cm in front of a CRT monitor (85 Hz refresh rate; 41 pixels per deg resolution) spanning 34.1 x 25.6 deg (horizontal x vertical). Head fixation was achieved with a custom head, forehead, and chin rest (Hafed, 2013), and we tracked eye movements of the left eye at 1 kHz using a video-based eye tracker (EyeLink 1000, SR Research Ltd, Canada). Gray backgrounds in the luminance step experiment (Fig. 8) were always presented at an average luminance of 49.84 cd m⁻², and the monitor was linearized (8-bit resolution) such that equal luminance increments and decrements for luminance steps were possible around this average. In total, we collected data from 5 subjects (24-29 years old; one female). A subset of the data from 4 subjects was used in our previous study (Idrees et al., 2020). Here, we perform novel analyses of the complete dataset, in addition to one new subject.

Visual stimuli: Retina electrophysiology (Figs. 1-4, 7, S3-S10, S13)

In retina electrophysiology experiments, we used two broad visual stimulation paradigms: a saccade (texture displacements) paradigm (Fig. S1a), and a luminance step paradigm (Fig. S1b), described in detail below. In different experiments we used different spatial and/or pharmacological manipulations of these two paradigms.

Saccade (texture displacements) paradigm

Background textures

We created background textures (Fig. S2a) by convolving a random binary (i.e. white or black) pixel image with a two-dimensional Gaussian blurring filter (Schwartz et al., 2012) defined by the kernel

$$G(x, y) = e^{-\frac{(x^2+y^2)}{2\sigma^2}} \quad (\text{Equation 1})$$

The parameter σ of the kernel influenced the amount of blurring. This resulted in textures having effectively low-pass spectral content (Fig. S2b) with a cutoff frequency depending on σ . For easier interpretation, we define the spectral content of these textures by a spatial scale. Intuitively, the spatial scale approximates the size of the

smallest dark and bright image blobs of the texture (Fig. S2a). Quantitatively, the spatial scale is defined as the $2*\sigma$ parameter of the Gaussian blurring filter. We generated textures with four different spatial scales: 25, 50, 150 and 300 μm , that resulted in dark and bright image blobs approximating a range of receptive field sizes between bipolar cells (texture with spatial scale 25 μm , see (Zhang et al., 2012)) and RGCs (textures with spatial scale 150 and 300 μm). In other words, coarser textures matched the resolution of RGCs, and finer textures matched the resolution of one processing stage earlier, the retinal bipolar cells. Calculating power spectra for the textures (Fig. S2b) confirmed that the spatial scale and hence the cutoff frequencies were consistent with this design aim. In different experiments, we used textures of all or a subset of the different spatial scales.

We normalized the pixel intensities in the textures to have uniform variations in luminance around a given mean. We used pixel intensities (from our 8-bit resolution scale) ranging from 0 to 60 around a mean of 30, or ranging from 30 to 90 around a mean of 60 (see sub-section *Saccades and probe flashes* for when each paradigm was used).

Saccades and probe flashes

To simulate saccades in our ex vivo retina electrophysiology experiments, we displaced the texture across the retina in 6 display frames (100 ms at 60 Hz refresh rate). For easier readability, we usually refer to these saccade-like texture displacements as “saccades”. The textures were displaced in each frame by a constant distance along a linear trajectory. While each “saccade” lasted 100 ms, displacement direction was varied randomly for each “saccade” (uniformly distributed across all possible directions), and “saccade” amplitude could range from 310 μm to 930 μm (corresponding to a velocity range of 3100-9300 $\mu\text{m s}^{-1}$ on the retinal surface). In visual degrees, this corresponds to a velocity range of 100-300 deg s^{-1} and displacement range of 10-30 deg in mice, well in the range of observed mouse saccade amplitudes (Sakatani and Isa, 2007). Similar to primates, mice also have oculomotor behavior, even under cortical control (Itokazu et al., 2018). For example, they make, on average, 7.5 saccade-like rapid eye movements per minute when their head is fixed (Sakatani and Isa, 2007) (humans make several saccades per second).

We used the same retinal displacement range of 310 μm to 930 μm for pig retinae. To the best of our knowledge, pig oculomotor behavior has not been documented in the literature. However, with their larger eyeball sizes, our translations of the retinal image would correspond to slower saccades (e.g. small saccades in humans and monkeys), which are also associated with saccadic suppression. Moreover, retinal “saccadic suppression” is not critically dependent on the details of movement kinematics, as it is triggered by visual transients (Fig. 4, also see Figs. 4, 5 in Idrees et al., 2020).

Each trial consisted of successive sequences (Fig. 1a, S1a) that combined a “saccade” with a probe flash, as follows: there was first a “pre-saccade” fixation of 2 seconds, where the texture remained static over the retina, then a 100 ms “saccade”, followed by “post-saccade” fixation where the texture again remained static over the retina but now with a shifted texture. At a certain time from “saccade” onset (delay d , range: 50 ms to 2100 ms), we presented a probe flash (see below). Following the probe flash, the texture remained static at the post-saccade fixation position for another 2 seconds before the next saccade of the successive sequence occurred. The post-probe-flash fixation of one sequence was therefore also the pre-saccade fixation of the next sequence. This way the texture remained visible during the entire trial, being translated during saccades of the successive sequences. In a single trial, 39 such sequences occurred. In each successive sequence, the direction and amplitude of the saccade was pseudo-randomly determined by the range of allowed saccade amplitudes and directions. The texture always landed at unique locations within a trial. The end result was that, within a single trial, RGCs experienced a wide spectrum of saccade amplitudes, directions and contrasts across these 39 saccades. As such, by analyzing the average effects of the 39 saccades on RGC responses to probe flashes, we captured a wide range of saccade-induced kinematics and luminance changes over the RGC receptive fields.

In most cases, the probe flash had a duration of 2 frames (~ 33 ms). We used 1 frame (~ 16 ms) in a subset of earlier experiments (mouse: 709 of 1616 cells; pig: 116 of 228 cells). Results were pooled across these paradigms as the effects were indistinguishable. The probe flash was a full-screen positive (“bright”) or negative (“dark”) stimulus transient.

Bright or dark probe flashes could happen in two different ways across our experiments. The results were indistinguishable between the two ways, so we pooled results across them. Briefly, in one manipulation, the probe flash replaced the texture with a homogeneous bright (pixel intensity of 60 in our 8-bit projectors) or dark (pixel intensity of 0) full-screen (in these experiments, the textures themselves had intensities ranging from 0 to 60 pixel intensity; see *Background textures* above). This way, the flash contrast from the underlying background luminance was variable across space (e.g. a bright flash on a bright portion of a texture had lower contrast from the underlying texture than the same flash over a dark portion of the texture). In the second manipulation, the bright and dark flashes were simply luminance increments or decrements (by pixel values of 30 on our 8-bit projectors) over the existing textures. This way, spatial contrast relationships in the background textures were maintained. In these experiments, the textures themselves had a range of 30-90 pixel intensities and a mean pixel value of 60 (on our 8-bit projectors). Out of the 1616 RGCs that we analyzed for saccadic suppression across all experiments where texture displacements were used as saccades (irrespective of the spatial or pharmacological manipulations), 1129 RGCs experienced such probe flashes, whereas the rest (487 RGCs) experienced the homogenous probe flash. For pig retina recordings, we always used the homogenous framework. However, in the subset of pig experiments where the 2-frame probe flash was employed (112 of 228 RGCs), we used a high-contrast probe flash such that a bright flash would be achieved by first going to 0 in the first frame of the flash then going to 60 (on our 8-bit projectors) in the next frame (and vice versa for a dark flash). Again, all data were pooled across these different paradigms because their outcomes were indistinguishable.

The number of trials required during a physiology experiment depended on the number of conditions that we ran on a specific day. For example, testing 7 different flash delays required 15 trials (7 with bright probe flashes, 7 with dark probe flashes, and 1 without probes). In a given experiment, we always interleaved all the conditions; that is, in any one of the 15 necessary trials, each of the 39 saccades could be followed by a bright or a dark probe at any of the 7 delays, or no probe flash at all (Fig. S1a shows schematic of one such trial). Moreover, we repeated the total number of conditions (e.g. the interleaved 15 trials) 4 times per session, and we averaged responses across

those repetitions. Since one trial typically lasted for 2 minutes, the example of 15 trials repeated 4 times lasted for approximately 2 hours. This was usually combined with additional conditions (e.g. other background texture scales). Therefore, the total number of saccades shown in any given experiment could be computed by $\# \text{trials} \times 39 \text{ saccades per trial} \times \# \text{textures} \times \# \text{repetitions}$. A typical experiment lasted 10-12 hours. If the combination of conditions would have required even longer recordings in a given experiment, we reduced the number of conditions (e.g. we presented flashes at fewer delays, or used fewer texture scales).

Full-field saccades

In the full-field saccades experiments, saccades and probe flashes occurred over the entire retina. This was our main experimental paradigm that we used for characterizing how saccades modulate RGC responses to probe flashes. This paradigm was also used as a control in experiments in which we applied different spatial or pharmacological manipulations of this paradigm to probe for the spatial origins and mechanisms of saccadic suppression. Further, results from this paradigm served as a baseline standard across different experimental rigs. This paradigm was used in a total of 32 retinal recordings (32 retinae from 30 mice). In different recordings, we used a subset of the texture scales and probe flash delays. This explains the different values of N seen for different conditions in, for example, Figs. 1e, S3. However, to ensure comparison, some conditions always overlapped across different recordings. This paradigm was also used in 12 recordings with retinae from 6 pigs.

Periphery saccades (global component of suppression)

In this manipulation, we restricted saccades to the RGC's receptive fields periphery (i.e. its far surround). This spatial manipulation was used to investigate the spatial origins of the global component of suppression (Figs. 2a-b, S5). We performed 13 recordings (13 retinae from 13 mice) with this paradigm, always with the high-density multielectrode array system (MaxOne by MaxWell), as it provided a large electrode area ($\sim 2 \times 4 \text{ mm}^2$) for the retina to be placed on. The recording region was typically either a high density block of electrodes (inter-electrode spacing: $\sim 17.5 \mu\text{m}$) or a block with one-electrode spacing (inter-electrode spacing: $\sim 35 \mu\text{m}$). The recording region was selected close to the center of the electrode array. We centered a large square mask ($1000 \times 1000 \mu\text{m}^2$) over the recording region to restrict the texture and saccade

presentation to the periphery of RGC receptive fields (Fig. S5b). The mask had a homogenous intensity corresponding to the mean luminance of the texture. At different times relative to texture displacements, full-field probe flashes were presented, similar to experiments with full-field texture displacements. The intensity of each pixel of the stimulus (both the mask and the texture regions) was adjusted for the probe flashes, either decreased or increased by a pixel value of 30 (on our 8-bit projectors) for dark and bright probe flashes, respectively. In all periphery saccade experiments, we used probe flash duration of ~33 ms, and a coarse texture background of spatial scale 300 μm .

Checkerboard mask paradigm (local component of suppression)

In this spatial manipulation we presented saccades and flashes in small square regions spread equidistantly over the entire retina. Each square region measured 100 x 100 μm^2 , separated from adjacent squares by an edge-edge gap of 100 μm . The gap was kept at mean luminance throughout the experiment. Saccades and flashes could either be presented in all the regions (similar to full-field saccades, except for the gap), or in alternate regions (Fig. 2e, S7a), arranged like in a checkerboard. This paradigm was used to investigate the origins of the local component of suppression (Figs. 2f, S7a-c). We performed 4 recordings (4 retinae from 3 mice) with this paradigm, always with the low density MCS MEA rig. In all experiments with this spatial manipulation, we used probe flash duration of ~17 ms, and a coarse texture background of spatial scale of 150 μm .

Luminance step paradigm

In this paradigm (Fig. S1b), we used no textures at all. The screen was always a homogenous gray field, and the visual event of a "saccade" was replaced by an instantaneous step to a different gray value. The gray backgrounds had intensities between 30 and 90 (on our 8-bit projector). The instantaneous step in intensity caused either a positive contrast luminance step (in the range of +0.03 to +0.50 Michelson contrast) or a negative contrast luminance step (-0.03 to -0.50 Michelson contrast). This paradigm was used to characterize the stimulus-stimulus interactions that ultimately trigger retinal saccadic suppression (Figs. 4, 7, S8-10). We performed a total of 4 recordings (4 retinae from 4 mice) with this paradigm, always with the high density MaxOne MEA rig. A trial consisted of either 56 or 156 successive sequences

(Fig. S1b) that each combined a luminance step with a probe flash, as follows: there was first a “pre-step” fixation of 2 seconds where the retina was exposed to a fixed gray level (analogous to “pre-saccade” fixation in texture displacements), then an instantaneous switch to “post-step” fixation (analogous to “post-saccade”). At a certain time from the luminance step (delay: 17, 33, 50, 100, 250, 500, 1000 or 2000 ms), we presented a 2-frame (~33 ms) dark (-0.33 Michelson contrast) or bright (+0.33 Michelson contrast) probe flash. Some sequences contained no probe flash, the next luminance step then happened 4 seconds after the previous one. In a given experiment, we had 17 trials representing the 17 conditions: 8 flash delays x 2 probe flash polarities + 1 condition with no probe flash. Similar to the saccade paradigm, we always interleaved all conditions; that is, in any one of the 17 necessary trials, each luminance step could be followed by a bright or a dark probe at any of the 8 delays, or no probe flash. Moreover, we repeated the 17 trials at least 4 times.

A shorter version of this paradigm was used in our macaque retina recording (Fig. 7). Here, a trial consisted of 20 successive sequences. The 20 luminance steps induced contrasts in the range -0.5 to +0.5. Flashes of ~33 ms were presented with a delay of 17, 50, 100, 250, 500 and 2000 ms after the luminance step.

Other stimuli

Finally, we used other stimuli unrelated to the main experiments to help us characterize RGC properties (e.g. response polarity, latency, transiency, and spatial receptive fields). These stimuli had the same mean intensities and intensity ranges as the textures or luminance steps used in each experiment. Below, we describe these stimuli for the condition in which the texture intensities ranged from 0 to 60 pixel intensity (represented as grayscale RGB values in the units of our 8-bit projects). In experiments in which the textures ranged in intensity from 30 to 90, or the luminance step experiment, all intensities reported below were shifted upward by 30. (1) Full-field contrast steps. ON steps: stepping from 0 to 30 (+1 Michelson contrast) and from 30 to 60 (+0.33) for 2 s. OFF steps: stepping from 60 to 30 (-0.33) and from 30 to 0 (-1) for 2 s. (2) Full-field Gaussian flicker, 1 minute. Screen brightness was updated every frame and was drawn from a Gaussian distribution with mean 30 and standard deviation 9. This stimulus was used to calculate linear filters representing the temporal receptive fields of RGCs through reverse correlation (spike-triggered averaging of the

stimulus history). (3) Binary checkerboard flicker, 10-15 minutes. The screen was divided into a checkerboard pattern; each checker either covered an area of $55 \times 55 \mu\text{m}$, $60 \times 60 \mu\text{m}$, or $65 \times 65 \mu\text{m}$ depending on the recording rig. The intensity of each checker was updated independently from the other checkers and randomly switched between 10 and 50 or 0 and 120. This stimulus also allowed us to calculate linear filters representing the spatial receptive fields of RGCs.

Visual stimuli: Cone photoreceptors imaging (Figs. 5, 6)

For cone imaging experiments, we used a minimalistic version of the luminance step paradigm used in retina electrophysiology. A homogeneous background alternated between a darker (pixel intensity 50 on 8-bit projector) and brighter gray value (pixel intensity 120 on 8-bit projector); the transitions between these two background values represented positive and negative contrast of 0.4 Michelson contrast. At various times after the luminance step (50, 250, and 2000 ms) we presented a probe flash (100 ms duration, +0.33 or -0.33 Michelson contrast). The probe flash at 2000 ms served as the baseline. The next background transition always happened 2 s after the preceding probe flash. The combination of the two luminance steps and the two probe flash polarities yielded a total of four combinations: negative-contrast luminance step followed by dark flash; negative-contrast luminance step followed by bright flash; positive-contrast luminance step followed by dark flash; and positive-contrast luminance step followed by bright flash. A single trial (Fig. S1c) was composed of the four step-flash combinations occurring three times (for the three delays with which the flash was presented); and the negative- and positive-contrast luminance step without a flash. Within a trial, these conditions were randomized. A trial was repeated three times. The luminance steps and the flashes were presented within a $700 \mu\text{m}$ disc region centered over the scan field.

Visual stimuli: Human psychophysics (Fig. 8)

In the human psychophysics experiment (Fig. 8), we mimicked the retinal luminance step experiments of Fig. 4. The paradigm (Fig. 8a) was similar to the one described in (Idrees et al., 2020). Subjects fixated a central fixation spot over a gray background that remained there for the entire duration of a trial. The background had one of 8

luminances (22.4, 30.24, 38.08, 45.92, 53.76, 61.6, 69.44, 77.28 cd m^{-2}). After a random initial fixation duration (800-1700 ms after fixation spot onset), the luminance of the background was changed suddenly (in one display frame update) to one of the remaining 7 luminances, inducing a positive-contrast luminance step or a negative-contrast luminance step. In our analysis, we used the luminance steps that induced contrasts in the range +0.3 to +0.56 Michelson contrast and -0.3 to -0.56 Michelson contrast. At one of 5 different possible times relative to the time of the luminance step (-24, -12, 36, 72, or 108 ms), a luminance pedestal (probe flash) was applied briefly for one display frame (~ 12 ms) at one of four locations relative to display center (7 deg above, below, to the right of, or to the left of center). Note that because the display was rasterized (that is, drawn by the computer graphics board from the top left corner in rows of pixels), the exact flash time and duration depended on the location of the flash on the display (but in a manner like other psychophysical experiments studying the same phenomenon, and also in a manner that is unlikely to affect our results). The luminance pedestal consisted of a square of 147.8×147.8 min arc, in which we added or subtracted a value to represent bright and dark probe flashes. We ensured that the contrast of the flash (relative to the currently displayed background luminance) was always the same across all trials: +0.033 for a bright flash, and -0.033 for a dark flash. Following each trial, the fixation spot was removed from the background to allow the subjects to relax. This inter trial period lasted for 500-1000 ms. The next trial happened consecutively, in a way that the current luminance of the background was used as the pre-step luminance. Subjects maintained fixation throughout all trials (except the inter trial period) and simply reported the locations of the brief flashes. Each subject performed 3 sessions, with 1120 trials per session.

Data Analysis

Data analysis: Retina electrophysiology

MEA recordings preprocessing

Low-density MEA recordings were high-pass filtered at a 500 Hz cutoff frequency using a tenth-order Butterworth filter. We extracted spike waveforms and times using thresholding, and we semi-manually sorted spikes using custom software. For high-density MEA recordings, we performed spike sorting by an offline automatic

algorithm (Diggelmann et al., 2018) and assessed the sorted units using a custom developed tool, the UnitBrowser (Idrees et al., 2016). We judged the quality of all units using inter-spike intervals and spike shape variation. Low quality units, such as ones with high inter-spike intervals, missing spikes, or contamination, were discarded. All firing rate analyses were based on spike times of individual units. In total, we extracted 3,510 high quality units after the spike sorting (referred to as RGCs from now on), from recordings of mouse retina. From pig retina recordings, we extracted 376 RGCs and from macaque retina we extracted 57 RGCs after the spike sorting. However, as we mention below, only a subset of these could be analyzed for saccadic suppression.

RGCs characterization: Receptive fields, ON-OFF index, Transiency index

We first characterized the properties of RGCs. We calculated linear filters in response to full-field Gaussian flicker and binary checkerboard flicker by summing the 500-ms stimulus history before each spike. The linear filters allowed determining cell polarity. Specifically, the amplitude of the first peak of the filter was used: If the peak was positively deflected, the cell was categorized as an ON cell; if negatively deflected, the cell was an OFF cell. ON cells were later always analyzed with respect to their responses to bright probe flashes, and OFF cells were analyzed with dark probe flashes. We determined the spatial receptive fields of RGCs by calculating the linear filters for each region (checker) defined by the binary checkerboard flickering stimulus. The modulation strength of each linear filter, measured as the standard deviation (s.d.) along the 500 ms temporal kernel, is an estimate for how strongly that region drives ganglion cell responses. We fitted the resulting 2D-map of s.d. values with a two dimensional Gaussian and took the $2\text{-}\sigma$ ellipse (long axis) as the receptive field diameter. For all other figures and analyses, we converted spike times to estimates of firing rate by convolving these times with a Gaussian of $\sigma = 10$ ms standard deviation and amplitude $0.25 \sigma^{-1} e^{1/2}$.

For each RGC, we used responses to full-field contrast steps to calculate an ON-OFF index, a transiency index, and a response latency index. These indices were used to characterize the properties of RGCs that we included in our analyses. The ON-OFF index was calculated by dividing the difference between ON and OFF step peak response by their sum. The resulting index values ranged between -1 (OFF) and +1 (ON) and were then scaled to span between 0 (OFF) and +1 (ON). The transiency

index was defined as the ratio of the response area within the first 400 ms and the total response area spanning 2000 ms. The resulting index had a value of 1 for pure transient cells. Response latency was calculated as the time from stimulus onset to 90% of peak response. This value was normalized to the maximum response latency in our dataset to create the response latency index.

Modulation index

To quantify retinal saccadic suppression, we first determined a baseline response, defined as the response to a probe flash approximately 2 s after texture displacement onset or 2 s after luminance step (delay between 1967 to 2100 ms, depending on the specific flash times used in a specific experiment). This baseline response was compared to responses of the same cell to the same flash when it occurred at an earlier time (i.e. closer in time to the “saccade”). Usually, the saccade-like texture displacements themselves caused significant neural responses (saccade-alone response, e.g. Fig. 1b), and the responses to the flashes were superimposed on these “saccade-responses”. We therefore first isolated the component of the responses caused by the flashes by subtracting the saccade-alone responses from the composite saccade and flash responses. We refer to this isolated component as the flash-induced responses.

To get a robust estimate of the response to saccades-alone (i.e. without any flashes), we averaged spike rate from before saccade onset up until the next saccade onset for conditions in which no flash was presented, or until just before the flash onset for conditions in which a post-saccade flash was presented. This was done for each of the 39 successive saccades in a given trial.

We then computed a neural modulation index, ranging from -1 to +1. A value of -1 represents complete suppression of flash-induced responses, whereas +1 indicates “complete enhancement” of flash-induced responses (that is, there was only a response to a flash after saccades, but not to a flash in isolation). A modulation index of 0 meant no change in flash-induced response relative to the “baseline” response. The modulation index of an RGC for a given flash delay d after saccade onset was calculated as $(r_d - r_b)/(r_d + r_b)$ where r_d is the peak firing rate for the flash-component of the response (see above for how we isolated this from the composite saccade+flash

response) and r_b is the peak firing rate for the baseline flash response (i.e. the same flash but occurring ~ 2 s away from any “saccade”; see above). In all cases, peak firing rate was estimated after averaging responses from all repetitions of a given condition (delay d or baseline) for a given RGC, across all saccades. For ON cells, the modulation index was based only on responses to bright flashes, and for OFF cells, it was based on responses to dark flashes. To quantify the modulation at a population level, we averaged the modulation indices of the individual RGCs in that population. For some analyses, we also calculated modulation indices of RGCs for each of the 39 individual “saccades” using the same procedure.

In some cells, individual saccades from the sequence of 39 were discarded. For example, imagine that “saccade No 3” gets discarded. This would happen when the baseline response strength (response to the probe flash with 2 s delay) after saccade No 3 is weak (specifically: peak amplitude less than 60% of the median of all 39 baseline response strengths). We did this to ensure that our modulation indices were not marred by a denominator approaching zero (e.g. if both flash and baseline responses were weak). We did, however, re-include some sequences. For example, if the probe flash with delay 100 ms after saccade No 3 triggered a strong response (specifically: peak amplitude larger than the median baseline response peak across the 39 saccades), then saccade No 3 would be re-included for the condition “100 ms delay”. This was done in order to re-include sequences (if discarded by the first step) for which the baseline flash response was weak but a flash after saccades nonetheless gave a robust response. For example, this could happen if a cell did not respond to the baseline flash but the saccade enhanced the response to a flash following it.

Finally, to perform statistics, we applied tests both at the level of individual cells and at the level of the population. At the individual cell level, we determined whether the modulation index for a probe flash presented at a certain delay was significantly different from 0 (i.e. “Is the response of this cell modulated by the ‘saccade’?”). For this, we performed a one-tailed sign test of the null hypothesis that the 39 individual modulation indices (or its subset in case weak sequences were discarded, as described above) came from a distribution with zero median. The alternative hypothesis was that the median was below (for negative modulation index) or above (for positive modulation index) zero. The modulation index was considered significant

(i.e. the flash response was modulated by the saccade) at $p < 0.05$. However, we did not consider cells significantly modulated if the test had a power ($1-\beta$) smaller than 0.8, which could happen if we previously had to exclude too many sequences ($N \leq 39$). At the population level, we determined whether the retinal output as a whole was modulated by saccades. For this, we performed a two-tailed Wilcoxon signed rank test of the null hypothesis that the median of the distribution of modulation indices did not differ from 0. Lastly, we tested whether the population modulation index was significantly different across populations of ON and OFF RGCs or across different paradigms. For this, we performed a two-tailed Wilcoxon rank-sum test of the null hypothesis that the median of the distribution of modulation indices did not differ across the two populations being tested.

Since the modulation index was based on responses to the brief probe flashes, it could only be computed for RGCs that did respond to these brief flash stimuli. In our analysis, we included all such RGCs. Of the spike sorted RGCs across all paradigms, we included: 2002 of 3510 in mice; 228 of 376 in pigs; and 15 of 57 in macaque.

Saccade (texture displacement) paradigm

Full-field saccades

We analyzed 1010 mouse RGCs (633 ON; 377 OFF) and 228 pig RGCs (197 ON; 31 OFF) for saccadic suppression using the full-field version of the saccade paradigm. A subset of data from 688 of the 1010 mouse RGCs and a subset of data from all the 228 pig RGCs was presented previously (Idrees et al., 2020). Here, we perform novel analyses on the complete datasets from the RGCs recorded previously, in addition to analyzing the newly recorded RGCs. For each RGC, we quantified the modulation index for a full-field probe flash presented at different times from saccade onset.

A subset of these RGCs were also tested for saccadic suppression while blocking GABAergic and glycinergic inhibition. For 82 ON and 30 OFF RGCs, we had a direct comparison with and without GABA_{A,C} blockers (5 μ M SR-9553 + 100 μ M Picrotoxin) (Fig. 2c, S6a). For 51 ON and 13 OFF RGCs, we had a direct comparison with and without GABA_{A,C} blockers in addition to glycine blocker (1 μ M Strychnine; Fig. 2d, S6b).

In yet another subset of RGCs (72 ON; 49 OFF), we also analyzed saccadic suppression at scotopic light level (Fig. S4), which was 1 log unit dimmer than the light level at which all other recordings were performed. For these cells, we had a direct comparison of responses at scotopic and mesopic levels.

Periphery saccades (global component of suppression)

For each recorded RGC, we computed a masking factor (post hoc) to quantify how well its receptive field was covered by the 1000 x 1000 μm^2 mask. We first determined the spatial receptive field center of each RGC (described above in *RGCs characterization*). The masking factor was defined as the multiple of σ of the two dimensional Gaussian fit for which the ellipse just touched the mask boundary (Fig. S7d). Cells with receptive field centers within the mask were defined to have a positive masking factor while those lying outside were given a negative masking factor. The magnitude of the factor increased with distance from the edge of the mask. This way, cells for which the mask covered their receptive field centers and immediate surround had masking factors > 2 (these were the cells included in analysis shown in Figs. 2b, S5); cells with a mask covering only the receptive field center had masking factors between 1 and 1.5. Cells located close to the mask's edge, with masking factors between -1 to +1, had their receptive field centers partially exposed to the saccade. Finally, cells lying outside the mask where the receptive field center always experienced saccades had masking factors < -1 . A total of 642 RGCs (401 ON; 241 OFF) from 13 experiments were recorded with this spatial layout of the saccade paradigm. Cells for which clear receptive fields could not be calculated were excluded from any further analysis. The exact number of cells for different conditions within this paradigm are reported in the results section. For each RGC, we calculated the modulation index for flashes presented at different times from saccade onset, in the same manner as described under the heading *Modulation index*. Fig. S7e shows the modulation index of individual RGCs as a function of its masking factor. Only a subset of RGCs with masking factors in the range -3 to +5 were included in this analysis. The median modulation index was calculated by taking the median of modulation indices of RGCs within a 1.2 masking factor window, sampled at intervals of 0.1 (running median).

In a subset of these experiments, we analyzed the effects of blocking GABAergic inhibition (using 5 μ M SR-95531) on the modulation of probe flash responses in RGCs with masking factors > 2 , i.e. with receptive field centers and immediate surround effectively masked. This included 62 ON RGCs and 35 OFF RGCs with robust responses to brief probe flashes with the pharmacological agent; only these RGCs were analyzed for saccadic suppression under the presence of SR-95531 (Fig. 2b). In a subset of these RGCs (29 ON; 25 OFF), we had a direct comparison of modulation indices with the control condition, i.e. periphery saccades in the absence of SR-95531 (Fig. S5d).

Checkerboard mask regions saccades

In experiments where we investigated the local component of suppression (Figs. 2e-f, S7b, c), we had three stimulus presentation settings (Fig. S7a): (1) saccade and flash presented in all squares regions; (2, 3) saccades and flashes in alternate regions of a hypothetical binary checkerboard. For each recorded RGC we calculated the modulation index for the following two scenarios: saccades and flashes in all regions (Fig. S7a presentation setting 1); and saccades excluded from the receptive field center (Fig. S7a presentation setting 1 or 2 depending on the RGCs spatial position relative to the presentation area). For this, we first calculated the spatial receptive field center (see heading *RGCs characterization*; receptive field center was defined as the $1-\sigma$ ellipse of the 2D Gaussian fit) for each RGC. We then calculated the Euclidean distance between the receptive field center and the closest flash region for both presentation settings 2 and 3. For further analysis, we used the presentation setting with the shortest distance between a flash region and the receptive field center. In case this flash region is perfectly centered over the receptive field center, saccades will be excluded from a region of at most 300 μ m diameter centered over the receptive field center. In most cases, the RGCs were indeed well centered within a flash region since the center of each region coincided with electrodes in the low density MEA. Nonetheless, for each RGC we calculated the intersection between its receptive field area and saccade regions in pixels (where each pixel corresponded to 3.75 μ m on the retinal surface). RGCs for which more than 15% of their receptive field area intersected with the saccade regions were excluded from

further analysis. In the end, a total of 51 RGCs (32 ON; 38 OFF) from 4 retinal recordings were used for further analysis of saccadic suppression.

Luminance step paradigm

To quantify retinal “saccadic suppression” with the luminance-step paradigm (Fig. 4, Fig. 7), we used the same analyses and statistical procedures to those described above for the saccade (texture displacement) paradigm. The only difference was that instead of 39 successive sequences in a trial, we now had either 56 or 156 successive sequences (or 20 in case of macaque retina experiment), spanning a contrast range of ± 0.03 to ± 0.5 Michelson contrast. Similar to the texture displacement paradigms, the modulation index was based on responses to brief probe flashes (~33 ms flash duration), and it could therefore only be computed for cells that did respond to these flash stimuli (N = 366 of 668 spike sorted RGCs from 4 mouse retinal recordings; N = 15 of 57 spike sorted RGCs from a macaque retina). The modulation index for ON RGCs (N = 259 mouse RGCs; N = 13 macaque RGCs) was calculated from responses to bright probe flashes, and that for OFF RGCs (N = 107 mouse RGCs; N = 2 macaque RGCs) was calculated from responses to dark flashes. A subset of data from all mouse RGCs was presented previously (Idrees et al., 2020). Here, we perform novel analyses on the complete dataset of the same RGCs.

In a subset of luminance step experiments (2 mouse retinal recordings), we analyzed the effects of blocking GABAergic and glycinergic inhibition on the modulation of probe flash responses. 115 ON RGCs showed robust responses to the brief probe flashes with and without the pharmacological blockers. However, none of the OFF RGCs responded robustly to the baseline probe flash in the presence of pharmacological blockers and therefore OFF RGCs were excluded in quantification of saccadic suppression in the presence of pharmacological blockers.

We also analyzed if the modulation of flash-induced responses depended on the strength of the response to the preceding luminance step. This analysis was done to establish whether suppression of flash responses resulted from saccade-induced saturation or adaptation of ganglion cell responses (Fig. S10). For each RGC, we calculated an association index which quantified the monotonic relationship between response to the luminance step and response to subsequent flashes. We first binned

the responses across the 56 or 156 step-flash sequences (Fig. S1b) based on the contrast induced by the luminance step in each sequence. Bin width was set to 0.025 Michelson contrast. Then, within each bin, we averaged the responses to luminance steps alone (Fig. S9a, b, top row) and to luminance steps followed by probe flashes. For each probe flash delay and contrast bin, we quantified the strength of the response induced by the luminance step preceding each probe flash (we integrated the average response to the luminance steps followed by probe flashes, up until the response to that probe flash). The modulation index was calculated as usual. We then calculated the Spearman's rank correlation coefficient (R) between the modulation index and the response strength induced by the luminance step, across all the contrast bins. This can be visualized from the insets in Fig. S9. For ease in interpretation of the results, we termed the resulting correlation coefficient as the association index. Intuitively, this association index describes the monotonic relationship between the step response strength and the strength of suppression and can be interpreted as follows: the larger the magnitude of the association index, the stronger is the monotonic relation between the two quantities. A negative value indicates that stronger step responses are associated with decreasing (more negative) modulation indices (i.e. weaker flash responses \rightarrow suppression). A positive value indicates that stronger step responses are associated with increasing modulation indices (i.e. stronger flash responses \rightarrow less suppression or even enhancement). In the example cell of Fig. S9a, the association index has large negative values for flashes immediately after the positive luminance step, suggesting that a stronger step response is indeed strongly correlated with stronger suppression of subsequent flashes. A robust calculation of association index was only possible for luminance steps that activated the RGC (i.e. positive-contrast luminance steps in ON RGCs, negative-contrast luminance steps in OFF RGCs). Fig. S10 shows the association index for each RGC and flash time as a function of the cell's modulation index.

In Fig. 6f, we plot modulation index as a function of RGC transiency index (see heading *RGCs characterization* for details on transiency index). The RGCs shown in this sub-figure were a subset of the RGCs analyzed with the luminance step paradigm for which we could also compute a transiency index. The relation between RGC transiency and modulation index for each condition was modeled using a linear

regression least-squares fit through the ON and OFF RGC population. To determine if the slope of the resulting line was statistically significant non-zero, we conducted a t-test of this slope.

Data analysis: Cone photoreceptors

Quantifying cone responses

We analyzed data from 11 scan fields recorded from four retinae (2 mice). Each scan field was 128 x 128 pixels, which on the retinal surface was 94 x 94 μm^2 , 110 x 110 μm^2 , or 132 x 132 μm^2 , depending on the zoom factor used. In each scan field, we identified regions of interest (ROIs) as a group of neighboring pixels with correlated fluorescence signals in time. Only ROIs with diameters corresponding to the cone axon terminal diameter (3-7 μm) were considered for further analysis. The output signal of the ROIs (baseline normalized iGluSnFR indicator fluorescence signal), represented the changes in glutamate release at the cone terminals. A total of 931 ROIs were extracted from the 11 scan fields. Identifying the ROIs and extracting their output signal were automated using custom IGOR Pro scripts.

Within a scan field, each ROI was sampled every 256 ms (3.9 Hz sampling rate). This interval was greater than the duration of probe flashes (100 ms) in these experiments. Therefore, the measured signal of many ROIs might not capture the peak response to the probe flashes. A conventional upsampling method, such as interpolation, could also underestimate the peak response in this case. However, since all ROIs (within and across scan fields) experienced the same visual stimulus (Fig. S1c), but were sampled at different points in time, we temporally ‘stitched’ the output from these ROIs. The resulting signal had a sampling interval of 2 ms, where the signal in a specific time bin was computed from ROIs sampled within that specific time window. In this ‘stitching’ approach, we first baseline-adjusted the output signal of each ROI for a trial by subtracting the baseline activity (calculated as the average ROI output across 1 s epoch prior to the first luminance step in the trial). Then, for each 2-ms time bin, we averaged the response across those ROIs that were sampled within that time window. This resulted in an output vector of the same duration as the trial but with a sampling interval of 2 ms. The output vector was empty for time bins where no ROIs were sampled. We therefore convolved this output vector with a moving average filter of

size 80 ms to fill in the empty time bins and to also smooth out the stitching boundaries (boundaries between time bins filled with output from different ROIs). This method gave a much better temporal resolution than conventional upsampling techniques, robustly capturing the peak for the 100 ms duration probe flash, as shown in Fig. 5b.

The ‘stitched’ signal was then cut into snippets that captured the relevant responses to our stimulus (e.g. step followed by probe flash). For this, we used stimulation trigger signals that marked the presentation of each luminance step. Each snippet was then baseline-adjusted by subtracting the average response over 800 ms prior to the luminance step. This way the output signal was 0 prior to a luminance step (Fig. 5). The output was averaged across the three repetitions of the trial. The normalized and averaged snippets represented the cone response to a particular stimulus sequence (for example Fig. 5a) and were used to fit parameters for model cones as described in the next section.

RGC model

To describe cone responses (Fig. 5) and RGC responses (Fig. 7) to our luminance step paradigm, we used a phenomenological model of the retina, previously published in Drinnenberg et al., 2018.

The original model related light intensity to retinal ganglion spiking activity by three layers of processing: first, the “light stimulus” was passed to model cone photoreceptors. Their activity was modulated by negative feedback from model horizontal cells. Second, the output of the model cones was passed to six inner retina pathways describing retinal processing by three different ON and three different OFF bipolar cells (fast, intermediate and slow pathways). Third, the output from the model pathways were then fed into model RGCs to yield RGC spiking activity. This cascade modeled RGC spiking in response to the “light stimulus” passed to model cones.

The cone responses were describes as

$$r(t) = \frac{\alpha_c y(t)}{[1 + \beta_c z(t)]} - h(t) \quad (\text{Equation 2})$$

where

$$r(t) = V(t) - V_{dark} \quad (\text{Equation 3})$$

$V(t)$ and V_{dark} were the instantaneous and dark membrane potentials of the cone, respectively, $h(t)$ was the feedback signal from the horizontal cell, and α_c and β_c were numerical factors. The time-varying functions $y(t)$ and $z(t)$, were related to light input through linear convolution, as

$$y(t) = \int_{-\infty}^t dt' K_y(t - t') I(t') \quad (\text{Equation 4})$$

$$z(t) = \int_{-\infty}^t dt' K_z(t - t') I(t') \quad (\text{Equation 5})$$

where $I(t)$ was the incident light intensity (or, more precisely, R^*/s). The kernels describing the cone response were given by

$$K_y(t) = \frac{t}{\tau_y} \frac{e^{-\frac{t}{\tau_y}}}{\tau_y} \quad (\text{Equation 6})$$

and

$$K_z(t) = \gamma K_y(t) + (1 - \gamma) \frac{t}{\tau_z} \frac{e^{-\frac{t}{\tau_z}}}{\tau_z} \quad (\text{Equation 7})$$

where τ_z was larger than τ_y , and $0 \leq \gamma \leq 1$ ensured proper normalization. Note that $\int_0^{\infty} dt' K_y(t - t') = 1$ for all filters. The response of the horizontal cell was described by

$$h(t) = \alpha_c \int_{-\infty}^t dt' K_h(t - t') r(t') \quad (\text{Equation 8})$$

with

$$K_h(t) = \frac{t}{\tau_h} \frac{e^{-\frac{t}{\tau_h}}}{\tau_h} \quad (\text{Equation 9})$$

Here, instead of the cone model parameters used in the published model (Drinnenberg et al., 2018), we re-fitted the parameters of the model cone to reflect our measured data of cone output (Fig. 5b) which yielded faithful fits (Fig. S12) to our experimentally measured cone responses.

All the parameters of the outer retina component (Equations 2 and 8) of our circuit model were fit once to cone responses (Fig. 5b, S11) and then kept unchanged for all simulations reported in Fig. 6. The fitted values are given as follows (original values (Drinnenberg et al., 2018) are reported in brackets):

$$\alpha_c = -3.342 * 10^{-5} (-9.602 * 10^{-6}), \beta_c = -1.273 * 10^{-6} (-1.148 * 10^{-5}), \gamma = 0.842 (0.764), \alpha_h = 0.016 (0.177), \tau_y = 48.98 \text{ ms} (50.64), \tau_z = 200 \text{ ms} (576.9), \tau_h = 1.232 * 10^3 \text{ ms} (371).$$

The small α_h suggested that in our cone recordings, horizontal cell feedback had only a minor effect.

In (Drinnenberg et al., 2018) three different retinal pathways were modelled according to

$$b_{p,k}(t) = \left[-1^k \left(\int_{-\infty}^t dt' K_p(t-t')V(t') - \theta_{p,k} \right) \right] \quad (\text{Equation 10})$$

where $p = 1,2,3$ labeled the pathway based on its response properties (1 = fast, 2 = intermediate, 3 = slow), $k = 0$ for OFF pathways and $k = 1$ for ON pathways.

$$[x] = \begin{cases} 0, & x < 0 \\ x, & x \geq 0 \end{cases} \quad (\text{Equation 11})$$

was a thresholding non-linearity, and $\theta_{p,k}$ acted as a threshold.

The main difference between the pathways was the temporal characteristics of the filters K_p . In the current study we wanted to smoothly vary the transiency of the model ganglion cells. To this end, we based our bipolar pathway on the fast bipolar pathway ($p = 1$) and modified its temporal characteristics to make it less transient. K_1 represented a high-pass filter which took the derivative of the cone potential on the order of 1 ms. We obtained K_1 by convolving the high-pass filter of the form

$$G(t) = \sin\left(\frac{\pi t}{\mu}\right) \frac{1}{\sqrt{2\pi\sigma}} e^{-\frac{1}{2}\left(\frac{t-\mu}{\sigma}\right)^2}, \text{ with } \mu = 3 \text{ ms}, \sigma = 1 \text{ ms} \quad (\text{Equation 12})$$

with an exponential function.

$$K_1(t) = \int_{-\infty}^t dt' \left(e^{-\frac{t-t'}{\tau_d}} \right) G(t') \quad (\text{Equation 13})$$

Higher values of the time constant, τ_d , of the exponential function decreased the pathway transiency. We set $\tau_d = 0.5$ as the default transient pathway (Fig. 6a-d). The ‘transiency parameter’ shown in In Fig. 6e was obtained by normalizing $15 \geq \tau_d \geq 0.5$ in the range 0 to 1, with 0 being less transient. In the original model (Drinnenberg et al., 2018), $K_1(t) = G(t)$.

The threshold $\theta_{1,k}$ was set to $-1^k \cdot 0.1$.

$b_{1,k}(t)$, the output of fast inner retina models was used as the input to the model RGCs used in this study. The spiking rate of the model RGC was obtained as the thresholded input and a temporally coarse version of the input’s derivative,

$$R_{1,k}(t) = \left[(1 - \alpha) b_{1,k}(t) + \alpha \left(\int_{-\infty}^t dt' K(t - t') b_{1,k}(t') \right) - \theta \right] \quad (\text{Equation 14})$$

where $K(t)$ was a biphasic filter similar in its form to $G(t)$. The threshold, θ , was a multiple of the peak response to any given input. We used the same parameters for the inner retina component as the ones described in the published model (Drinnenberg et al., 2018):

- (i) *Transient OFF*, $R_{1,0}(t)$: $\alpha = 0$, $\theta = 0$;
- (ii) *Transient ON*, $R_{1,1}(t)$: $\alpha = 0$, $\theta = 0$;

All simulations were computed with a 1 ms sampling interval.

Using the above cascade, we calculated model RGC’s spike rate in response to the recorded cone output when subjected to “luminance steps alone” and “luminance

steps followed by probe flash” stimuli (Fig. 6a, b). Similar to real RGC analysis, we calculated the “flash-induced responses” (Fig. 6c) by subtracting “response to luminance steps alone” (Fig. 6a) from “response to luminance steps followed by probe flash” (Fig. 6b). We then calculated the modulation index also in the same way as for the real RGCs: $(r_d - r_b)/(r_d + r_b)$ where r_d was the peak spiking rate of the flash-induced response for the flash presented with delay d from the luminance step, and r_b was the peak firing rate for the baseline flash-induced response (flash at 2000 ms).

As a control, we replaced the model cone responses with the experimentally acquired cone responses (Fig. 5) thus forming a hybrid model. Before passing the cone response to the downstream model pathways, we passed it through a low pass filter to further smooth the fluctuations at the stitching boundaries in order to avoid discontinuities in calculation of its temporal derivative. For this smoothing, we convolved the cone output with a moving average filter of size 40 ms. Here, the model ON RGC responses (Fig. S12a, b, columns 1-2) were calculated using the cone responses to bright probe flashes (Fig. 5a, b, columns 1-2), and OFF RGC responses (Fig. S12a, b, columns 3-4) were calculated using cone responses to dark probe flashes (Fig. 5a, b, columns 3-4). The resulting hybrid model RGC responses (Fig. S12) were consistent with the pure model responses shown in Fig. 6.

Data analysis: Human psychophysics

We analyzed eye movements in all trials and detected saccades using established methods (Chen and Hafed, 2013). We excluded from analysis trials in which a saccade or microsaccade happened anywhere in the interval from 200 ms before to 50 ms after a probe flash. At each flash time, we calculated the proportion of correct trials to obtain time courses of this perceptual measure. We obtained time course curves for each subject individually, and then averaged it across trials and different contrasts of the luminance steps. Reduced proportion of correct trials at any flash time indicated perceptual saccadic suppression. A subset of data from 4 of the 5 subjects was used in our previous study (Idrees et al., 2020). Here we perform novel analyses of the complete dataset.

We applied a two-tailed Wilcoxon rank-sum test to determine if the suppression after luminance steps differed across bright and dark probe flashes.

All data analyses were performed in MATLAB (The MathWorks Inc).

References

- Amthor, F.R., Tootle, J.S., and Gawne, T.J. (2005). Retinal ganglion cell coding in simulated active vision. *Vis. Neurosci.* 22, 789–806.
- Appleby, T.R., and Manookin, M.B. (2019). Neural sensitization improves encoding fidelity in the primate retina. *Nat. Commun.* 10, 1–15.
- Baccus, S.A., Olveczky, B.P., Manu, M., and Meister, M. (2008). A Retinal Circuit That Computes Object Motion. *J. Neurosci.* 28, 6807–6817.
- Barlow, H.B., Derrington, A.M., Harris, L.R., and Lennie, P. (1977). The effects of remote retinal stimulation on the responses of cat retinal ganglion cells. *J. Physiol.* 269, 177–194.
- Baylor, D.A., and Hodgkin, A.L. (1974). Changes in time scale and sensitivity in turtle photoreceptors. *J. Physiol.* 242, 729–758.
- Beeler, G.W. (1967). Visual threshold changes resulting from spontaneous saccadic eye movements. *Vision Res.* 7, 769–775.
- Berry, M., Brivanlou, I., Jordan, T., and Meister, M. (1999). Anticipation of moving stimuli by the retina. *Nature* 398.
- Breitmeyer, B. (2007). Visual masking: Past accomplishments, present status, future developments. *Adv. Cogn. Psychol.* 3, 9–20.
- Bremmer, F., Kubischik, M., Hoffmann, K.P., and Krekelberg, B. (2009). Neural dynamics of saccadic suppression. *J. Neurosci.* 29, 12374–12383.
- Chen, C.-Y., and Hafed, Z.M. (2013). Postmicrosaccadic enhancement of slow eye movements. *J. Neurosci.* 33, 5375–5386.
- Chen, C.-Y., and Hafed, Z.M. (2017). A neural locus for spatial-frequency specific saccadic suppression in visual-motor neurons of the primate superior colliculus. *J. Neurophysiol.* 117, 1657–1673.
- Chen, E.Y., Marre, O., Fisher, C., Schwartz, G., Levy, J., da Silveira, R.A., and Berry, M.J. (2013). Alert response to motion onset in the retina. *J. Neurosci.* 33,

120–132.

Chichilnisky, E.J., and Baylor, D.A. (1999). Receptive-field microstructure of blue-yellow ganglion cells in primate retina. *Nat. Neurosci.* 2, 889–893.

Chichilnisky, E.J., and Kalmar, R.S. (2002). Functional asymmetries in ON and OFF ganglion cells of primate retina. *J. Neurosci.* 22, 2737–2747.

Clark, D.A., Benichou, R., Meister, M., and Azeredo da Silveira, R. (2013). Dynamical Adaptation in Photoreceptors. *PLoS Comput. Biol.* 9.

Dalkara, D., Byrne, L.C., Klimczak, R.R., Visel, M., Yin, L., Merigan, W.H., Flannery, J.G., and Schaffer, D. V. (2013). In vivo-directed evolution of a new adeno-associated virus for therapeutic outer retinal gene delivery from the vitreous. *Sci. Transl. Med.* 5.

Diamond, M.R., Ross, J., and Morrone, M.C. (2000). Extraretinal control of saccadic suppression. *J. Neurosci.* 20, 3449–3455.

Diggelmann, R., Fiscella, M., Hierlemann, A., and Franke, F. (2018). Automatic spike sorting for high-density microelectrode arrays. *J. Neurophysiol.* 120, 3155–3171.

Drinnenberg, A., Franke, F., Morikawa, R.K., Jüttner, J., Hillier, D., Hantz, P., Hierlemann, A., Azeredo da Silveira, R., and Roska, B. (2018). How Diverse Retinal Functions Arise from Feedback at the First Visual Synapse. *Neuron* 1–18.

Duffy, F.H., and Lombroso, C.T. (1968). Electrophysiological evidence for visual suppression prior to the onset of a voluntary saccadic eye movement. *Nature* 218, 1074–1075.

Enroth-Cugell, C., and Jakiela, H.G. (1980). Suppression of cat retinal ganglion cell responses by moving patterns. *J. Physiol.* 302, 49–72.

Euler, T., Hausselt, S.E., Margolis, D.J., Breuninger, T., Castell, X., Detwiler, P.B., and Denk, W. (2009). Eyecup scope—optical recordings of light stimulus-evoked fluorescence signals in the retina. *Pflügers Arch. - Eur. J. Physiol.* 457, 1393–1414.

Euler, T., Franke, K., and Baden, T. (2019). Studying a light sensor with light: Multiphoton imaging in the retina. *Neuromethods* 148, 225–250.

Farrow, K., Teixeira, M., Szikra, T., Viney, T.J., Balint, K., Yonehara, K., and Roska, B. (2013). Ambient illumination toggles a neuronal circuit switch in the retina and visual perception at cone threshold. *Neuron* 78, 325–338.

Field, G.D., Sher, A., Gauthier, J.L., Greschner, M., Shlens, J., Litke, A.M., and Chichilnisky, E.J. (2007). Spatial properties and functional organization of small bistratified ganglion cells in primate retina. *J. Neurosci.* 27, 13261–13272.

Frey, U., Egert, U., Heer, F., Hafizovic, S., and Hierlemann, A. (2009). Microelectronic system for high-resolution mapping of extracellular electric fields applied to brain slices. *Biosens. Bioelectron.* 24, 2191–2198.

Fried, S., Münch, T., and Werblin, F. (2002). Mechanisms and circuitry underlying directional selectivity in the retina. *Nature* 411–414.

Garvert, M.M., and Gollisch, T. (2013). Local and global contrast adaptation in retinal ganglion cells. *Neuron* 77, 915–928.

Geffen, M.N., De Vries, S.E.J., and Meister, M. (2007). Retinal ganglion cells can rapidly change polarity from off to on. *PLoS Biol.* 5, 0640–0650.

Gollisch, T. (2013). Features and functions of nonlinear spatial integration by retinal ganglion cells. *J. Physiol. Paris* 107, 338–348.

Hafed, Z.M. (2013). Alteration of Visual Perception prior to Microsaccades. *Neuron* 77, 775–786.

Hafed, Z.M., and Krauzlis, R.J. (2010). Microsaccadic suppression of visual bursts in the primate superior colliculus. *J. Neurosci.* 30, 9542–9547.

Ibbotson, M.R., Crowder, N.A., Cloherty, S.L., Price, N.S.C., and Mustari, M.J. (2008). Saccadic modulation of neural responses: possible roles in saccadic suppression, enhancement, and time compression. *J. Neurosci.* 28, 10952–10960.

Idrees, S., Franke, F., Diggelmann, R., Hierlemann, A., and Münch, T.A. (2016). UnitBrowser - A tool to evaluate and post-process units sorted by automatic spike sorting algorithms. *Front. Neurosci.* 10.

Idrees, S., Baumann, M.P., Franke, F., Münch, T.A., and Hafed, Z.M. (2020).

- Perceptual saccadic suppression starts in the retina. *Nat. Commun.* *11*, 1977.
- Itokazu, T., Hasegawa, M., Kimura, R., Osaki, H., Albrecht, U.-R., Sohya, K., Chakrabarti, S., Itoh, H., Ito, T., Sato, T.K., et al. (2018). Streamlined sensory motor communication through cortical reciprocal connectivity in a visually guided eye movement task. *Nat. Commun.* *9*, 338.
- Kemmler, R., Schultz, K., Dedek, K., Euler, T., and Schubert, T. (2014). Differential regulation of cone calcium signals by different horizontal cell feedback mechanisms in the mouse retina. *J. Neurosci.* *34*, 11826–11843.
- Khabou, H., Desrosiers, M., Winckler, C., Fouquet, S., Auregan, G., Bemelmans, A.P., Sahel, J.A., and Dalkara, D. (2016). Insight into the mechanisms of enhanced retinal transduction by the engineered AAV2 capsid variant -7m8. *Biotechnol. Bioeng.* *113*, 2712–2724.
- Kleiser, R., Seitz, R.J., and Krekelberg, B. (2004). Neural correlates of saccadic suppression in humans. *Curr. Biol.* *14*, 386–390.
- Krekelberg, B. (2010). Saccadic suppression. *Curr. Biol.* *20*, R228–R229.
- Krishnamoorthy, V., Weick, M., and Gollisch, T. (2017). Sensitivity to image recurrence across eye-movement-like image transitions through local serial inhibition in the retina. *Elife* e22431.
- Krueger, J., and Fischer, B. (1973). Strong periphery effect in cat retinal ganglion cells. Excitatory responses in ON- and OFF-center neurones to single grid displacements. *Exp. Brain Res.* *18*, 316–318.
- Li, P.H., Field, G.D., Greschner, M., Ahn, D., Gunning, D.E., Mathieson, K., Sher, A., Litke, A.M., and Chichilnisky, E.J. (2014). Retinal Representation of the Elementary Visual Signal. *Neuron* *81*, 130–139.
- Lin, B., and Masland, R.H. (2006). Populations of wide-field amacrine cells in the mouse retina. *J. Comp. Neurol.* *499*, 797–809.
- Litke, A.M., Bezayiff, N., Chichilnisky, E.J., Cunningham, W., Dabrowski, W., Grillo, A. a., Grivich, M., Grybos, P., Hottowy, P., Kachiguine, S., et al. (2004). What does

the eye tell the brain?: Development of a system for the large-scale recording of retinal output activity. *IEEE Trans. Nucl. Sci.* *51*, 1434–1440.

Marvin, J.S., Borghuis, B.G., Tian, L., Cichon, J., Harnett, M.T., Akerboom, J., Gordus, A., Renninger, S.L., Chen, T.W., Bargmann, C.I., et al. (2013). An optimized fluorescent probe for visualizing glutamate neurotransmission. *Nat. Methods* *10*, 162–170.

Matin, E. (1974). Saccadic suppression: a review and an analysis. *Psychol. Bull.* *81*, 899–917.

Mayo, J.P., and Sommer, M.A. (2008). Neuronal Adaptation Caused by Sequential Visual Stimulation in the Frontal Eye Field. *J. Neurophysiol.* *100*, 1923–1935.

Müller, J., Ballini, M., Livi, P., Chen, Y., Radivojevic, M., Shadmani, A., Viswam, V., Jones, I.L., Fiscella, M., Diggelmann, R., et al. (2015). High-resolution CMOS MEA platform to study neurons at subcellular, cellular, and network levels. *Lab Chip* *15*, 2767–2780.

Münch, T.A., da Silveira, R.A., Siegert, S., Viney, T.J., Awatramani, G.B., and Roska, B. (2009). Approach sensitivity in the retina processed by a multifunctional neural circuit. *Nat. Neurosci.* *12*, 1308–1316.

Noda, H., and Adey, W.R. (1974). Excitability Changes in Cat Lateral Geniculate Cells during Saccadic Eye Movements. *Science* (80-.). *183*, 543–545.

Ölveczky, B.P., Baccus, S.A., and Meister, M. (2003). Segregation of object and background motion in the retina. *Nature* *423*, 401–408.

Passaglia, C.L., Freeman, D.K., and Troy, J.B. (2009). Effects of remote stimulation on the modulated activity of cat retinal ganglion cells. *J. Neurosci.* *29*, 2467–2476.

Reinhard, K., Tikidji-Hamburyan, A., Seitter, H., Idrees, S., Mutter, M., Benkner, B., and Münch, T.A. (2014). Step-By-Step instructions for retina recordings with perforated multi electrode arrays. *PLoS One* *9*, e106148.

Roska, B., and Werblin, F. (2003). Rapid global shifts in natural scenes block spiking in specific ganglion cell types. *Nat. Neurosci.* *6*, 600–608.

- Ross, J., Morrone, M.C., Goldberg, M.E., and Burr, D.C. (2001). Changes in visual perception at the time of saccades. *Trends Neurosci.* *24*, 113–121.
- Sakatani, T., and Isa, T. (2007). Quantitative analysis of spontaneous saccade-like rapid eye movements in C57BL/6 mice. *Neurosci. Res.* *58*, 324–331.
- Schiller, P.H. (1968). Single unit analysis of backward visual masking and metacontrast in the cat lateral geniculate nucleus. *Vision Res.* *8*, 855–866.
- Schreyer, H.M., and Gollisch, T. (2020). Nonlinearities in retinal bipolar cells shape the encoding of artificial and natural stimuli. *BioRxiv* 1–40.
- Schütz, A., Braun, D., and Gegenfurtner, K. (2011). Eye movements and perception: A selective review. *J. Vis.* *11*, 1–30.
- Schwartz, G.W., Okawa, H., Dunn, F. a, Morgan, J.L., Kerschensteiner, D., Wong, R.O., and Rieke, F. (2012). The spatial structure of a nonlinear receptive field. *Nat. Neurosci.* *15*, 1572–1580.
- Shapley, R., and Enroth-Cugell, C. (1984). Chapter 9 Visual adaptation and retinal gain controls. *Prog. Retin. Res.* *3*, 263–346.
- Szatko, K.P., Korympidou, M.M., Ran, Y., Berens, P., Dalkara, D., Schubert, T., Euler, T., and Franke, K. (2020). Neural circuits in the mouse retina support color vision in the upper visual field. *Nat. Commun.* *11*, 3481.
- Tatler, B.W., Wade, N.J., Kwan, H., Findlay, J.M., and Velichkovsky, B.M. (2010). Yarbus, Eye Movements, and Vision. *Iperception.* *1*, 7–27.
- Tikidji-Hamburyan, A., Reinhard, K., Seitter, H., Hovhannisyan, A., Procyk, C.A., Allen, A.E., Schenk, M., Lucas, R.J., and Münch, T.A. (2015). Retinal output changes qualitatively with every change in ambient illuminance. *Nat. Neurosci.* *18*, 66–74.
- Volkman, F.C. (1986). Human visual suppression. *Vision Res.* *26*, 1401–1416.
- Wei, W. (2018). Neural mechanisms of motion processing in the mammalian retina. *Annu. Rev. Vis. Sci.* *4*, 165–192.

Werblin, F. (2010). Six different roles for crossover inhibition in the retina: correcting the nonlinearities of synaptic transmission. *Vis. Neurosci.* 27, 1–8.

Wurtz, R.H. (2008). Neuronal mechanisms of visual stability. *Vision Res.* 48, 2070–2089.

Yarbus, A.L. (1967). *Eye Movements and Vision* (Boston, MA: Springer US).

Zaghloul, K.A., Manookin, M.B., Borghuis, B.G., Boahen, K., and Demb, J.B. (2007). Functional circuitry for peripheral suppression in Mammalian Y-type retinal ganglion cells. *J Neurophysiol* 97, 4327–4340.

Zhang, Y., Kim, I.-J., Sanes, J.R., and Meister, M. (2012). The most numerous ganglion cell type of the mouse retina is a selective feature detector. *Proc. Natl. Acad. Sci.* 109, E2391–E2398.

Zuber, B.L., and Stark, L. (1966). Saccadic suppression: Elevation of visual threshold associated with saccadic eye movements. *Exp. Neurol.* 16, 65–79.

Supplementary Figures

Figure S1

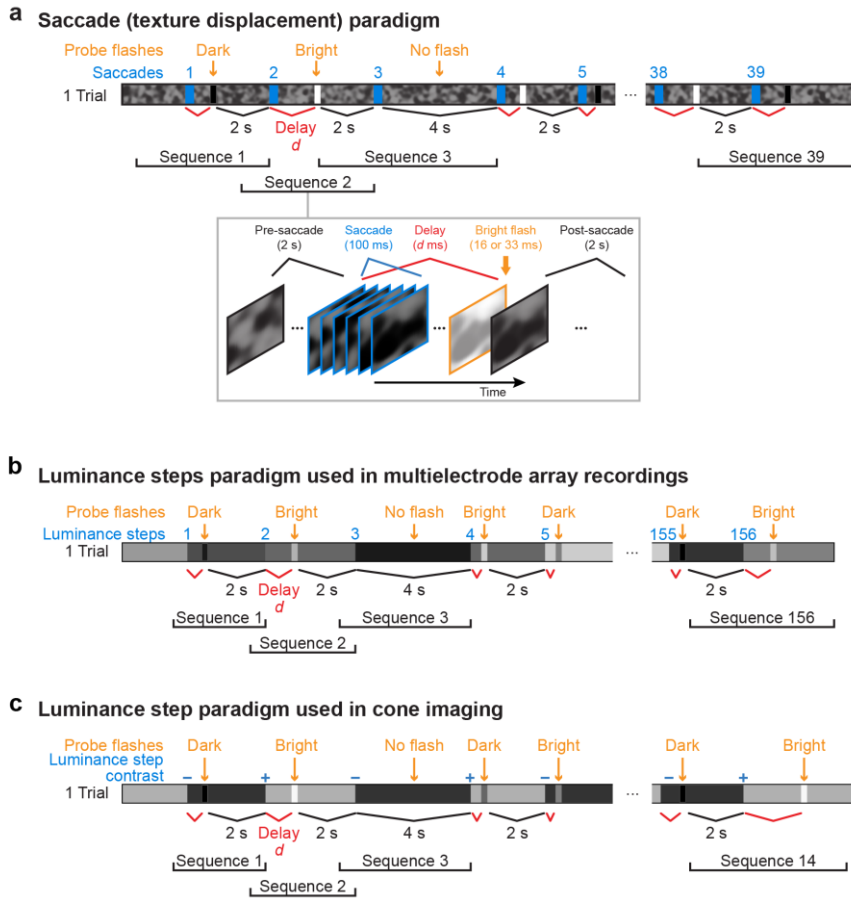


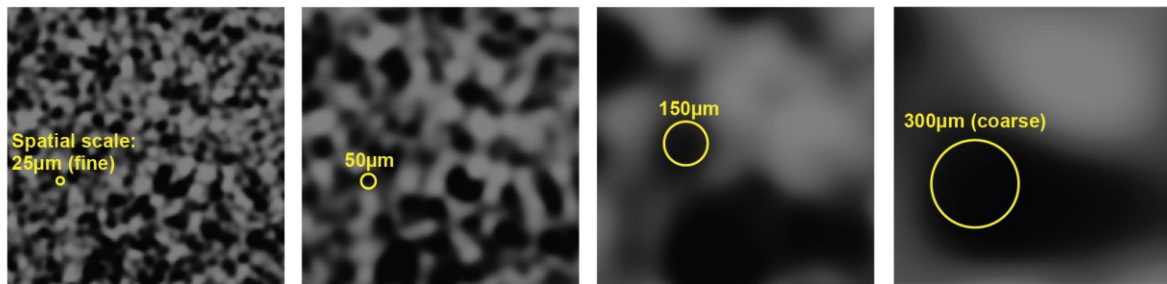
Figure S1 Stimulation paradigms.

a. Example trial of the temporal sequence of saccades and probe flashes. A trial started with turning on the texture over the retina. To mimic saccades (blue windows), the texture was displaced for 6 consecutive frames (100 ms) to a new position relative to the retina. After a certain delay d , a dark or bright probe flash (~ 16 or 33 ms) was presented, followed by 2 s post-flash time. A saccade-flash pair, along with pre- and post-saccade durations, formed one sequence (illustrated in detail below Sequence 2). The post-flash time of one sequence was the pre-flash time of the next sequence. A single trial consisted of 39 such sequences. In some sequences, no flash was presented after the saccade (saccade-only sequence). Here, the next saccade occurred 4 s after the previous saccade. The delay and the flash polarity were both randomized within a trial. In different trials, the saccades always remained the same but the order of delay and flash polarity changed. Each trial lasted for 2-4 minutes, and the number of trials needed depended on the number of conditions that were tested in an experiment. For example, to test 7 different probe-flash delays, 15 trials would be required: 7 trials for bright flashes, 7 trials for dark flashes, and 1 trial for no-flash condition. The pseudo-randomization within and across trials was designed in a way that a single condition (for example bright flash 150 ms after saccade onset), happened once after each of the 39 saccades.

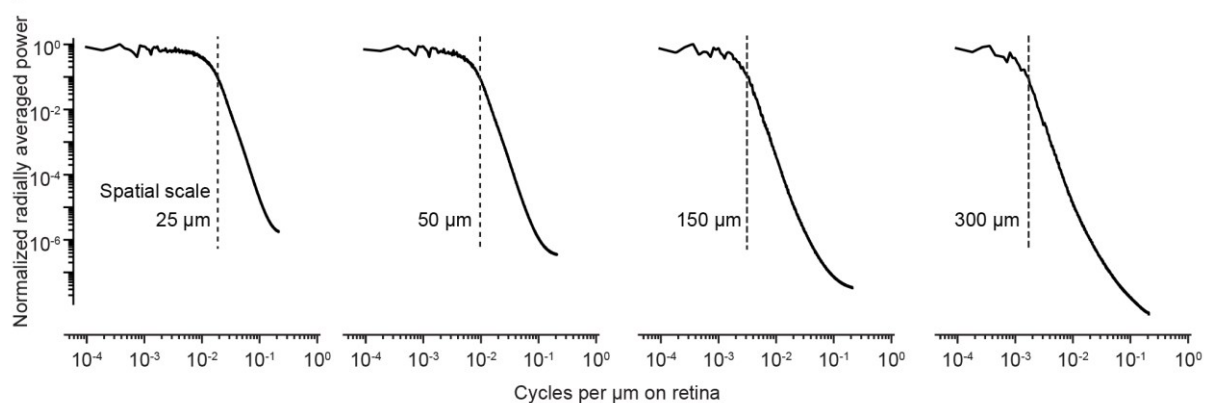
- b.** Example trial of the luminance step paradigm. Here, the texture was replaced by a uniform gray background and saccades were represented by sudden increases or decreases in the background's luminance. In a single trial, 56 or 156 sequences occurred. In macaque RGC experiments, only 20 sequences occurred in a single trial. The luminance steps in a trial had different contrasts, spanning a range of -0.5 to +0.5 on the Michelson scale. Randomization was done similar to the saccade paradigm described in **a**. Each trial lasted for 3-7 minutes, and the number of trials needed depended on the number of conditions that were tested in an experiment.
- c.** Shortened luminance step paradigm used in cone imaging experiments. The luminance of a uniform 700 μm disc centered over the imaging field alternated between a bright and a dark intensity. The transitions caused positive- and negative-contrast luminance steps over the imaging field (+0.4 and -0.4 Michelson contrast). Dark (-0.33 Michelson contrast) or bright (+0.33) probe flashes (100 ms) occurred 50, 250 and 2000 ms after the step. A single trial consisted of 14 sequences: 2 contrast polarity x 2 flash polarity x 3 delays + 2 no flash conditions, and lasted ~45 s. Conditions were randomized within this trial.

Figure S2

a



b

**Figure S2 Textured backgrounds.**

a. Textures were created by convolving random binary pixel images with a Gaussian blurring filter. We varied the σ parameter of the Gaussian blurring filter to define a so-called spatial scale for the resulting texture (indicated as yellow circles). σ was set to half the spatial scale value. The fine (25 μm) and coarse (150 - 300 μm) spatial scales were picked to result in dark or bright image blobs that approximated the sizes of bipolar cell and ganglion cell receptive fields respectively.

b. Radially-averaged power spectra for textures like in **a**, normalized to the maximum average power. Low-pass characteristics in all spatial scales were clear: less than 5% of the total average power was above the spatial frequency corresponding to the specific spatial scale of a given texture (vertical dashed lines).

Figure S3

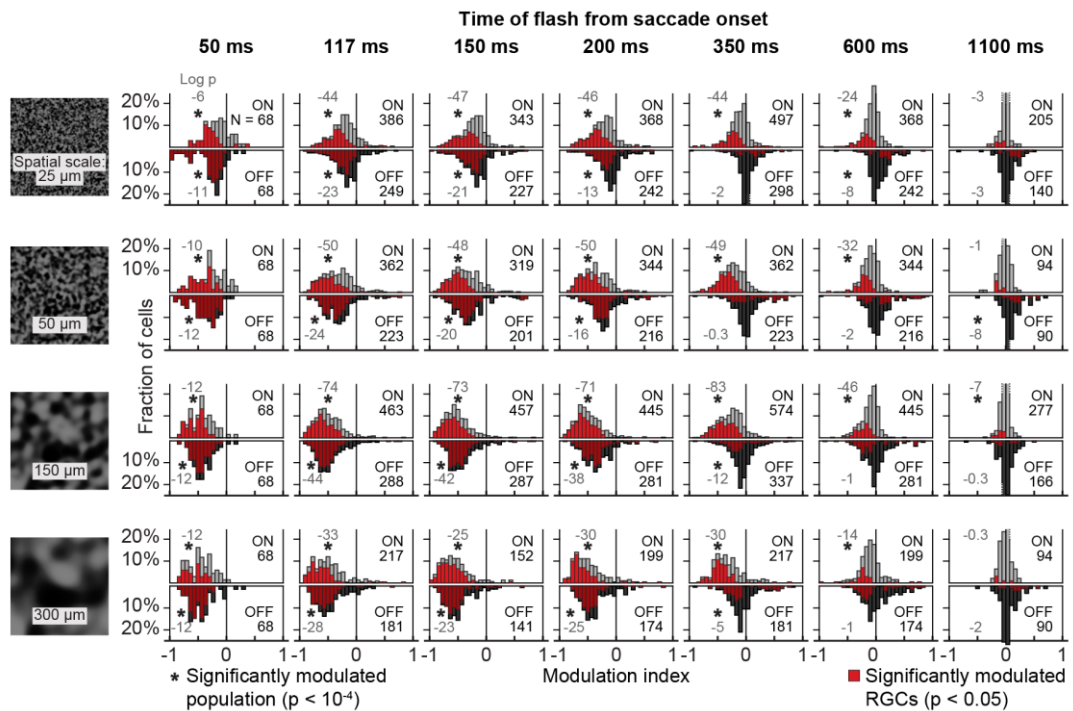


Figure S3 Histograms of modulation indices of ON and OFF RGCs. Histograms of modulation indices for all analyzed RGCs at different flash times relative to saccade onset (columns). Rows correspond to background textures of different spatial scales. Upright histograms (light bars) are for ON RGCs and inverted histograms (dark bars) are for OFF RGCs. These histograms show the underlying distribution for the mean modulation indices shown in Fig. 1e. Red bars indicate RGCs that are statistically significantly modulated (modulation index > 0 or < 0 , $p < 0.05$, one-tailed sign test). Black numbers on the right in each panel indicate the number N of ON and OFF RGCs analyzed for that condition; gray numbers on the left in each panel are the logarithm (base 10) of the exact p -value (two-tailed Wilcoxon signed-rank test) to determine if the population median was shifted away from 0. Additionally, the asterisks show the significance level at $p < 0.001$.

Figure S4

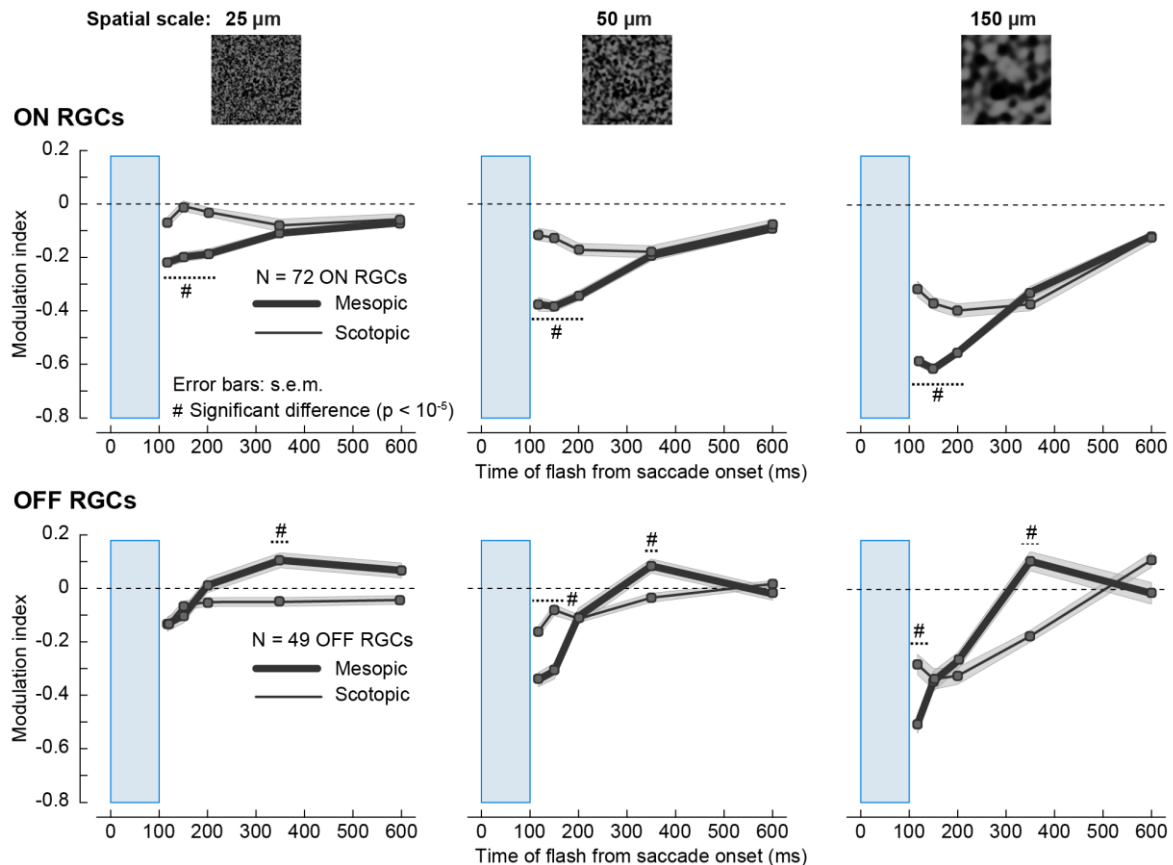
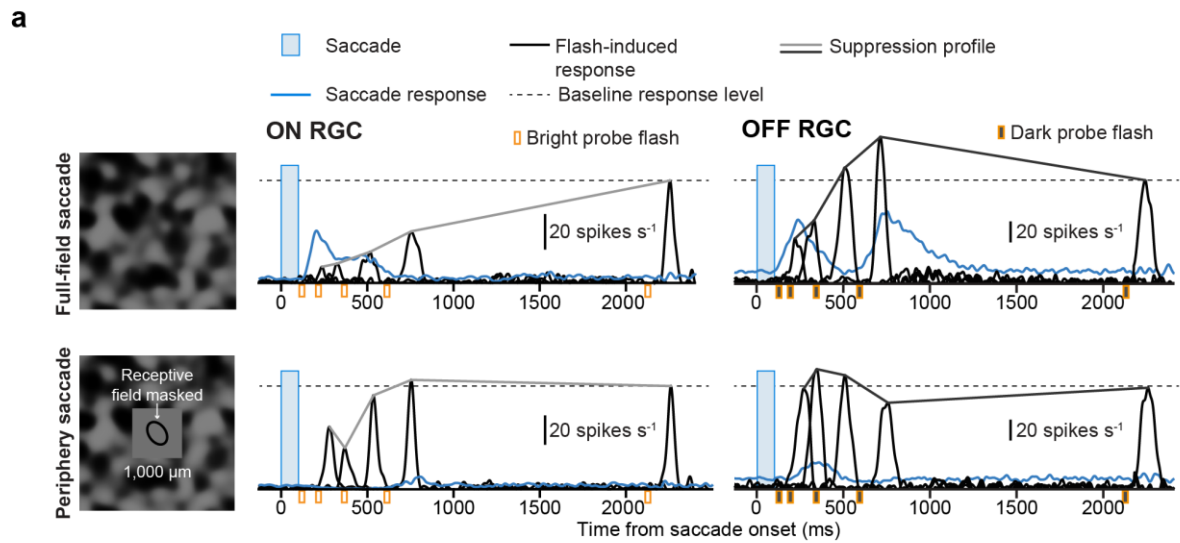
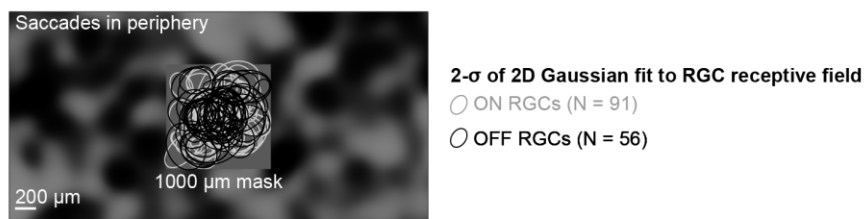


Figure S4 Retinal saccadic suppression at scotopic light levels. Population modulation index (mean \pm s.e.m.) across ON (top; N = 72) and OFF (bottom; N = 49) RGCs at mesopic light levels (thick lines; mean absolute light intensity: $225 \text{ R}^* \text{rod}^{-1} \text{s}^{-1}$) and scotopic light levels (thin lines; mean absolute light intensity: $23 \text{ R}^* \text{rod}^{-1} \text{s}^{-1}$). Columns are for different spatial scales of the background texture. Mouse and pig RGC data shown in all other figures is from mesopic light levels. Suppression in both ON and OFF RGCs was weaker at scotopic light level. Blue window: timing of the saccade. Probe flashes were presented after saccade onset at 117, 150, 200, 350, 600 and 2100 ms. Hash symbols: statistically significant difference in modulation across mesopic and scotopic light levels ($p < 10^{-5}$, two-tailed Wilcoxon rank-sum test). Suppression at later time points (> 300 ms, presumably originating from the surround component, see Figs. 2, 3) was not different between mesopic and scotopic conditions in ON RGCs, and tended to be even slightly stronger in OFF RGCs. Suppression at early time points (< 250 ms, likely dominated by the central component, see Figs. 2, 3) was much less pronounced at scotopic conditions.

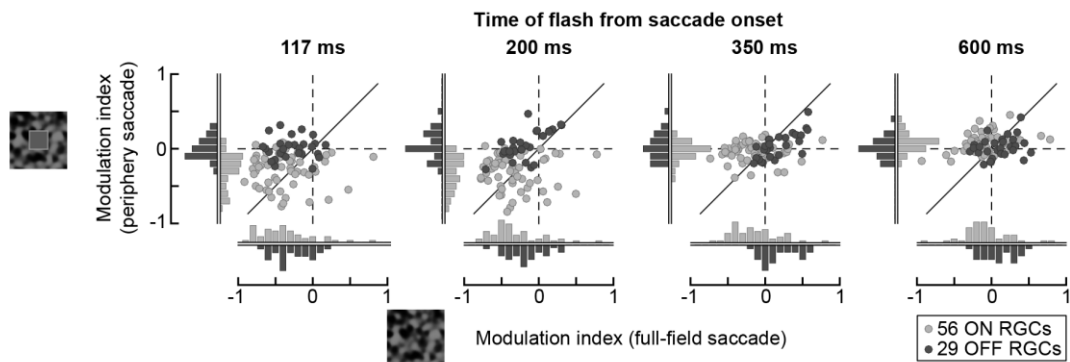
Figure S5



b Relative position of RGCs included in panels c, d and Fig. 2b



c Modulation index across full-field saccades and periphery saccades



d Modulation index across periphery saccades with and without GABA_A receptors blocker

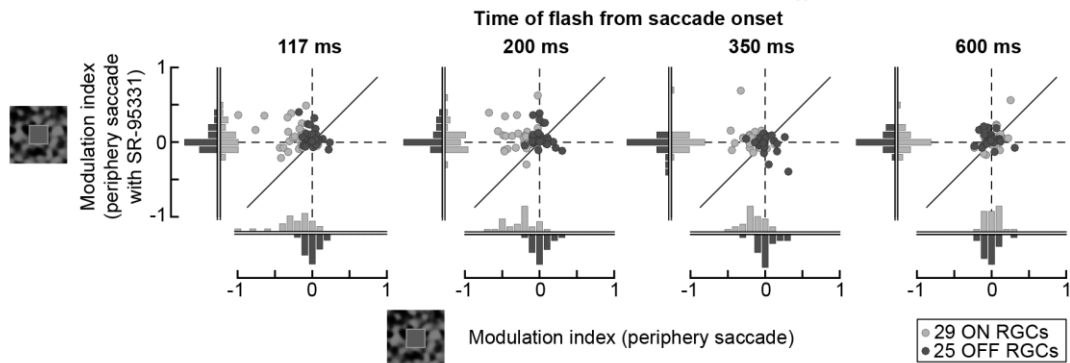


Figure S5 Extended data figure for global component of suppression (Fig. 2a-b).

a. Activity (firing rate) of example ON and OFF RGCs to full-field saccades (top; same paradigm as in Fig. 1; background texture here had a spatial scale of 300 μm) and during periphery saccades condition (bottom), where a 1000 x 1000 μm^2 gray square mask (intensity: mean luminance of texture) restricted saccades to RGC receptive field periphery ($>2\text{-}\sigma$ of the 2D Gaussian fit to the receptive field). Blue lines: average saccade-alone responses (N = 39 sequences). Black lines: average flash-induced responses (composite saccade and flash responses minus saccade-alone response). Blue windows: timing of saccades; orange markers: timing of the probe flashes; dashed lines: baseline response level (response to flash at 2100 ms). Periphery saccades revealed a global component of suppression in the ON RGC, which was weaker and short-lived (recovered by 350 ms) than full-field saccades. The OFF RGC was no longer suppressed with periphery saccades. Lines connecting the response peaks highlight the time courses of retinal saccadic suppression relative to baseline flash-induced responses.

b. Schematic showing position of the RGCs relative to the 1000 μm mask that were included in the analysis of **c**, **d**, Fig. 2b. These RGCs had at least $2\text{-}\sigma$ of the 2D Gaussian fit to their receptive fields covered by the mask, shown here by bright and dark ellipses for ON (N = 91) and OFF (N = 56) RGCs, respectively. Saccades were restricted to outside of the mask, i.e. periphery of RGCs receptive fields.

c. Modulation indices of ON RGCs (light gray circles; N = 56) and OFF RGCs (dark gray circles; N = 29) across full-field saccades (x-axis) and periphery saccades (y-axis), at different flash times relative to saccade onset (columns). Oblique lines are the unity lines between the two conditions and the dashed lines correspond to zero modulation. Distribution of modulation indices for the two conditions are projected onto their respective axes (light gray bars for ON RGCs and dark gray bars for OFF RGCs). The modulation index of most OFF RGCs was close to 0 in the periphery saccades condition, for all flash times, suggesting they were not suppressed by the global component of suppression, originating from the receptive field periphery. ON RGCs were still suppressed, although they recovered by 350 ms, which was quicker than after full-field saccades.

d. Modulation indices of ON (N = 29) and OFF (N = 25) RGCs across periphery saccades without (x-axis) and with GABAA receptor blocker (y-axis; 5 μM SR-95531). With GABAA receptors blocked, modulation indices of ON RGCs were around 0, suggesting that the global component of suppression was mediated through GABAergic pathways. OFF RGCs remain unaffected.

Figure S6

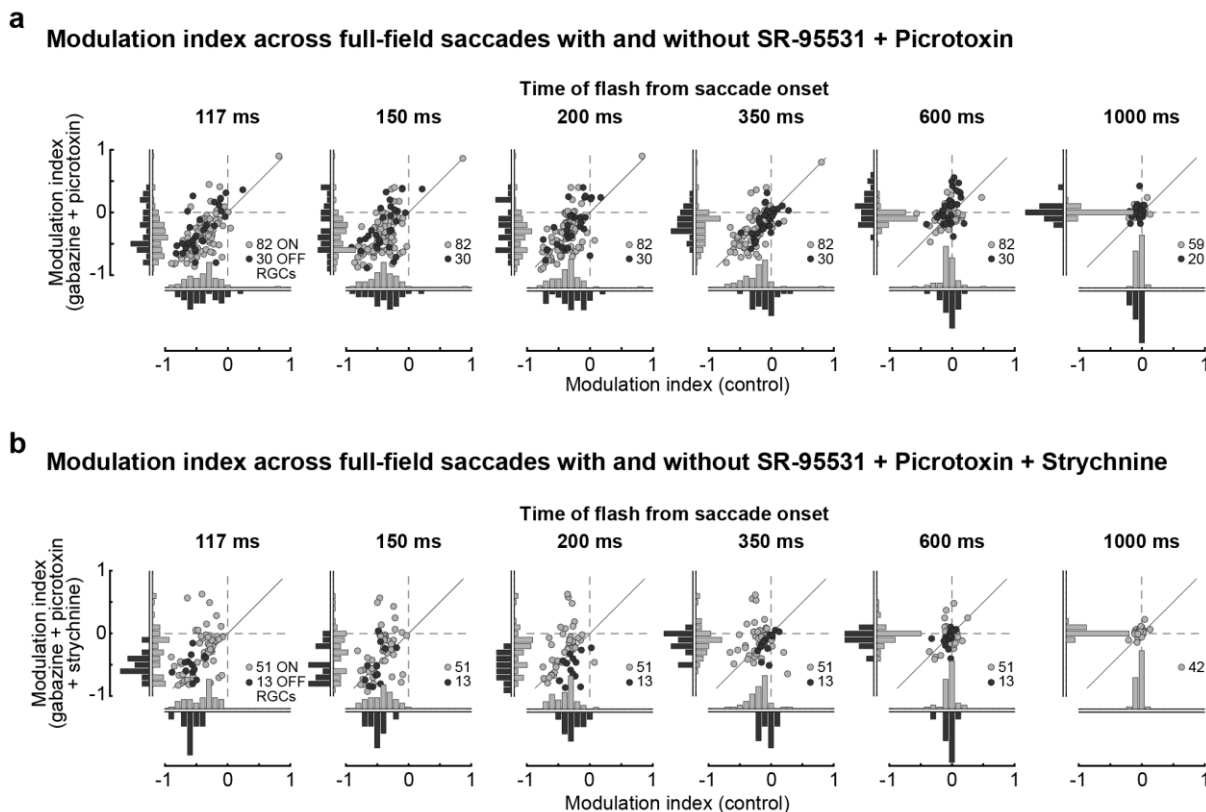


Figure S6 Population data underlying pharmacology experiments of Fig. 2c, d.

a. Modulation indices of ON RGCs (light gray circles; $N = 59$) and OFF RGCs (dark gray circles; $N = 20$) across full-field saccades in control conditions (x-axis) and with GABA_{A,C} receptors blockers (y-axis; $5 \mu\text{M}$ SR-95531 + $100 \mu\text{M}$ Picrotoxin), at different flash times relative to saccade onset (columns). Oblique lines are the unity lines between the two conditions and the dashed lines correspond to zero modulation. Distribution of modulation indices for the two conditions are projected onto their respective axes (light gray bars for ON RGCs and dark gray bars for OFF RGCs). While the modulation index of individual cells showed small changes across the conditions, in general, the population was mostly concentrated around the unity line.

b. Same as in **a**, except that glycine receptors ($1 \mu\text{M}$ Strychnine) were also blocked in addition to GABA_{A,C} receptors. No OFF RGCs were recorded in experiments which included flashes at 1000 ms.

Figure S7

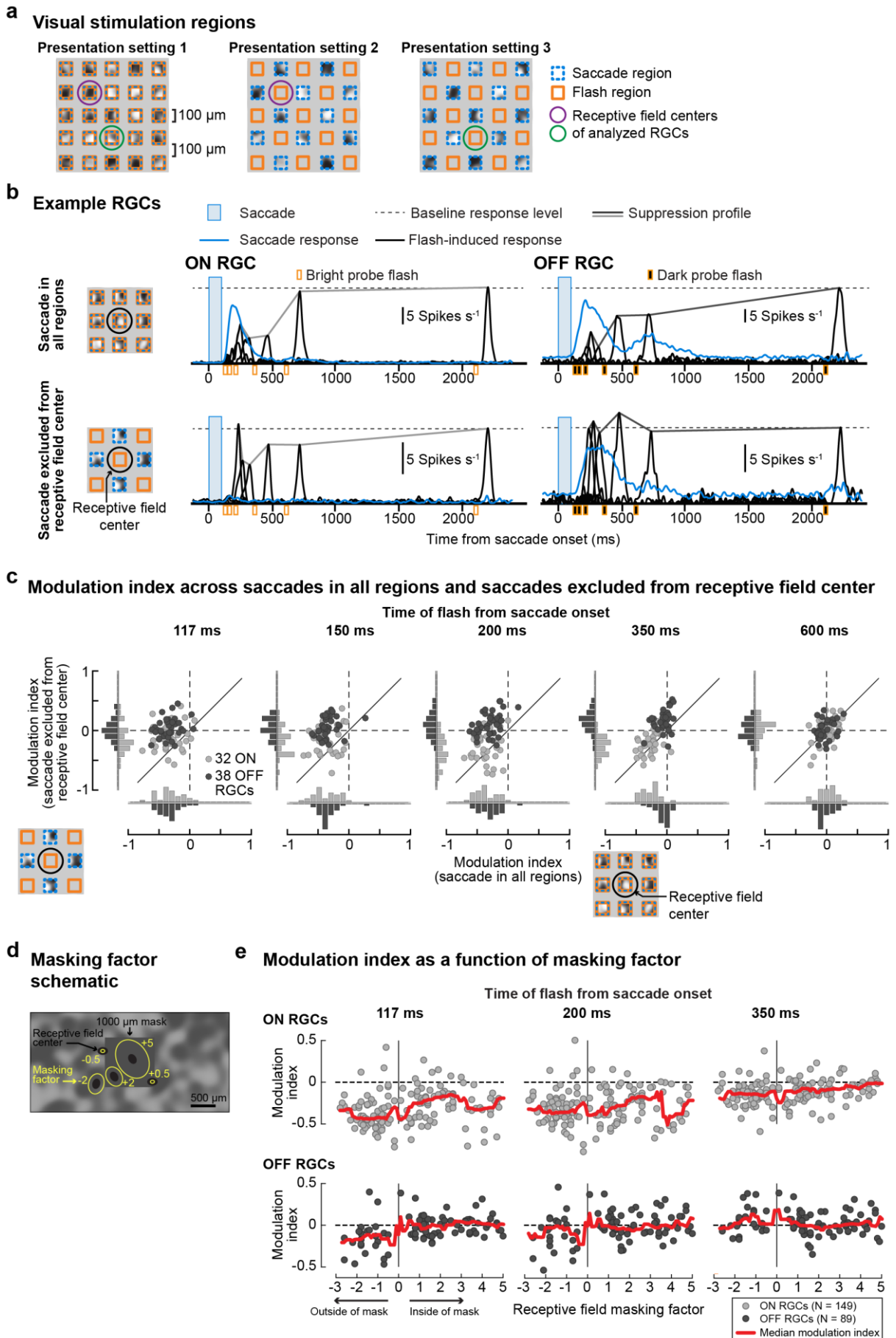


Figure S7 Extended data figure for the local component of suppression (Fig. 2e)

a. Schematic of the visual stimulation settings used in the checkerboard-mask paradigm. In setting 1, saccades and flashes were presented in all square regions of size $100 \times 100 \mu\text{m}^2$ separated by a gap of $100 \mu\text{m}$. Throughout an experiment, the gap's intensity remained at mean luminance of the saccade background texture. In setting 2 and 3, saccades and flashes were presented in alternate sets of square regions. For quantifying modulation when saccades were excluded from the receptive field center, setting 2 was used for an RGC with position indicated by the purple circle and setting 3 was used for an RGC with position indicated by the blue circle.

b. Activity (firing rate) of example ON and OFF RGCs to the condition where saccades and flashes were presented in all regions (top), and where saccades and flashes were presented in alternate regions (bottom). In these experiments, we used a coarse background texture ($150 \mu\text{m}$ spatial scale). Blue lines: average saccade-alone responses ($N = 39$ sequences). Black lines: average flash-induced responses (composite saccade and flash responses minus saccade-alone response). Blue windows: timing of saccades; orange markers: timing of the probe flashes; dashed lines: baseline response level (response to flash at 2100 ms). Lines connecting the response peaks highlight the time courses of retinal saccadic suppression relative to baseline flash-induced responses.

c. Modulation indices of ON RGCs (light gray circles; $N = 32$) and OFF RGCs (dark gray circles; $N = 38$) across saccades and flashes presented in all square regions of a checkerboard mask (x-axis) and saccades and flashes presented in alternate regions of the checkerboard mask where saccades were excluded from the receptive field center of the analyzed RGC (y-axis), at different flash times relative to saccade onset (columns). Oblique lines are the unity lines between the two conditions and the dashed lines correspond to zero modulation. Distribution of modulation indices for the two conditions are projected onto their respective axes (light gray bars for ON RGCs and dark gray bars for OFF RGCs). -

d. A masking factor was computed for each RGC recorded under the periphery saccades protocol (Fig. 2a). This factor was defined as the multiple of σ of the 2D Gaussian fit of a cell's receptive field center (black filled ellipses) for which the ellipse just touched the mask boundary (yellow ellipses). Positive masking factor: cells with receptive field centers within the mask; negative factor: cells with receptive field centers outside the mask. The magnitude of the factor increased with distance of the receptive field from the edge of the mask. Only RGCs with masking factors > 2 were included in the analysis of global component of suppression (Fig. 2b, S5).

e. Modulation indices of ON RGCs (top; light circles; $N = 149$) and OFF RGCs (bottom; dark circles; $N = 89$) plotted as a function of receptive field masking factor at different flash times relative to saccade onset (columns). Red lines indicate the running median modulation index (Methods). In OFF RGCs with more than half of their receptive fields covered by the mask (masking factor > 0), only weak or no suppression of flash responses was observed. However, when more than half of the receptive field of OFF RGCs was exposed to the saccade, even marginally (masking factors between 0 and -1), flash responses were suppressed. This confirms the findings of Fig. 2f and

S7c, that there is a narrow spatial window centered on the receptive field center of OFF RGCs, which, when stimulated with a saccade and a subsequent flash, suppresses the response to the flash.

Figure S8

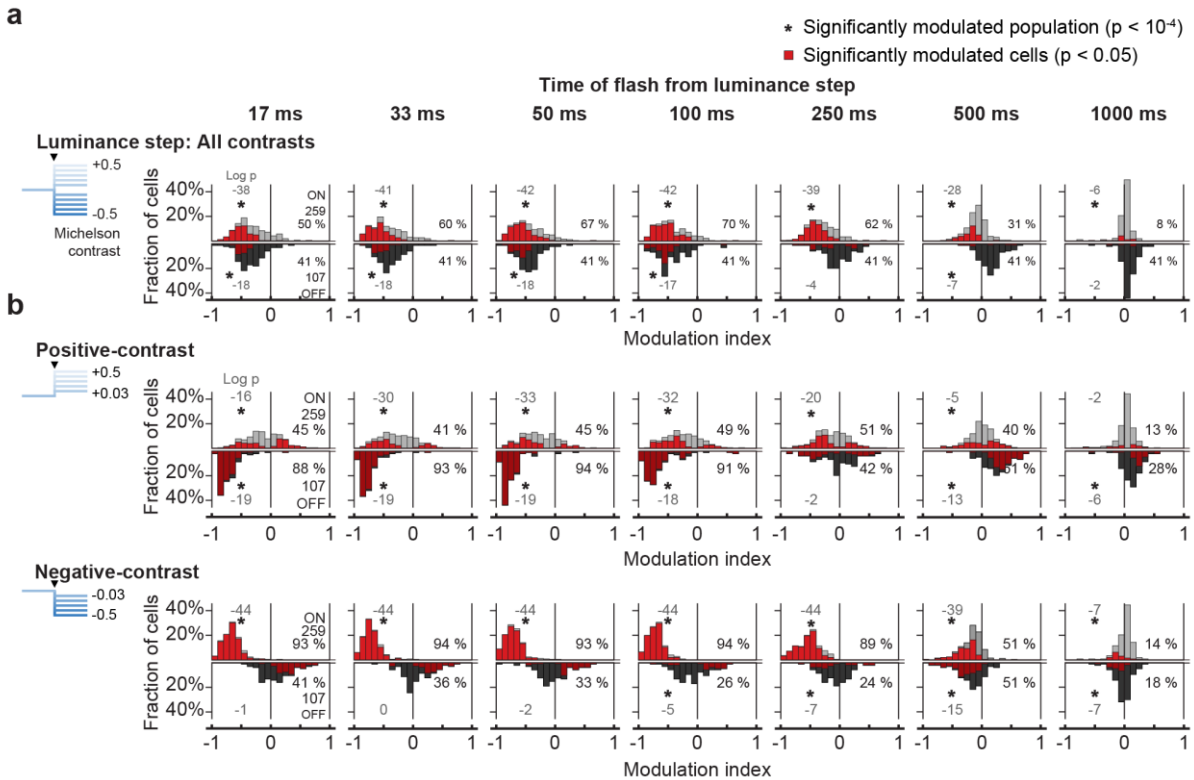
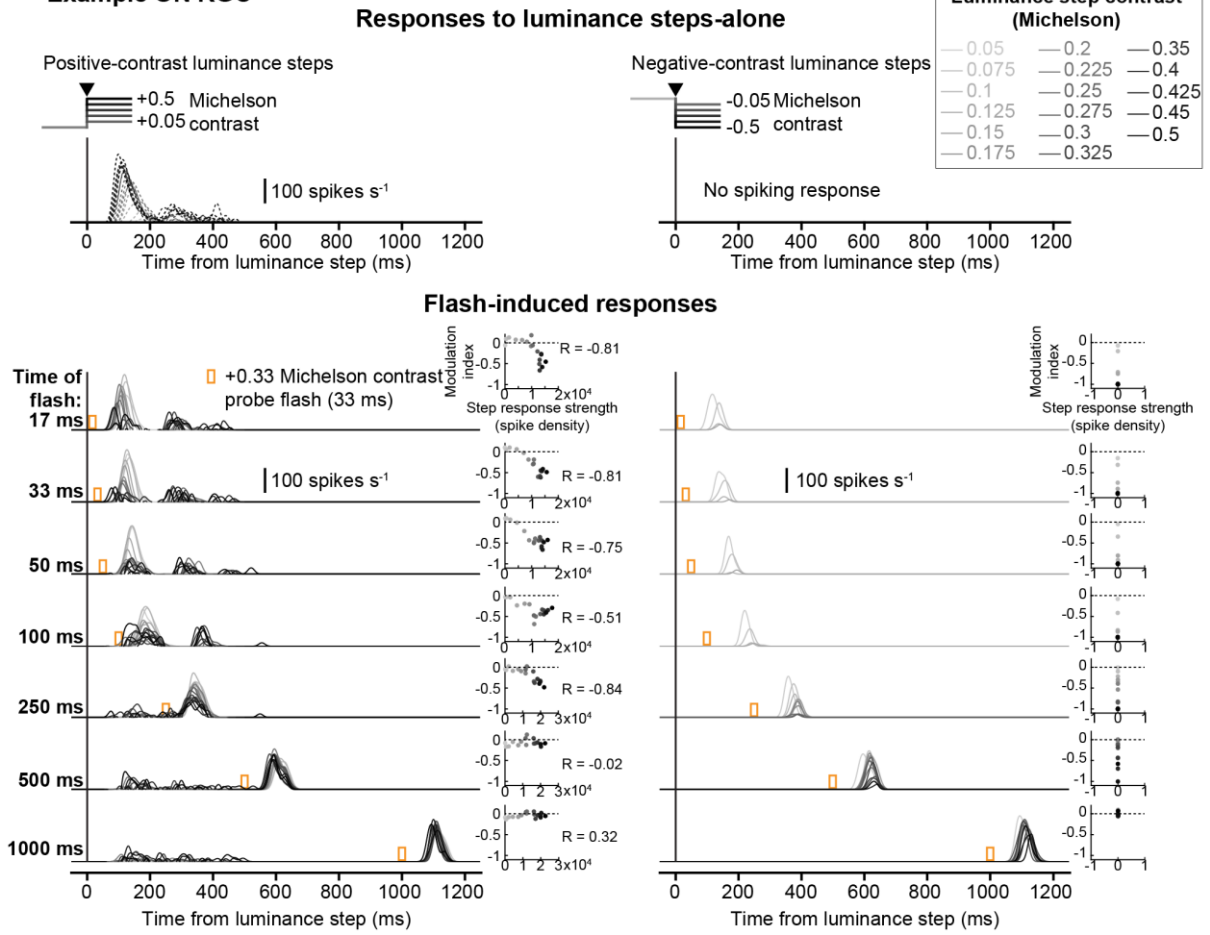


Figure S8 Population data underlying luminance step experiments of Fig. 4. Histograms of modulation indices for all analyzed RGCs. Modulation index for each RGC was based on responses averaged across all luminance steps collectively (**a**; -0.5 to +0.5 Michelson contrast; $N = 56$ or 156 sequences), or across all positive-contrast ($N = 28$ or 78 sequences) and all negative-contrast ($N = 28$ or 78 sequences) luminance steps separately (**b**). Upright histograms (light gray bars) are for ON RGCs ($N = 259$) and inverted histograms (dark gray) are for OFF RGCs ($N = 107$). Red bars indicate the RGCs with statistically significant modulation (modulation index < 0 or > 0 , $p < 0.05$, one-tailed sign test). Columns show modulation at different flash times relative to luminance steps. These histograms show the underlying distribution for the mean population modulation indices shown in Fig. 4. The percentage values on the right in each panel indicate the percentage of RGCs significantly modulated in that condition. Gray value on the left in each panel is the logarithm (base 10) of the exact p-value (two-tailed Wilcoxon signed-rank test) to determine if the population median was shifted away from 0. Additionally, the asterisks indicate significance level $p < 0.0001$.

Figure S9

a Example ON RGC



b Example OFF RGC

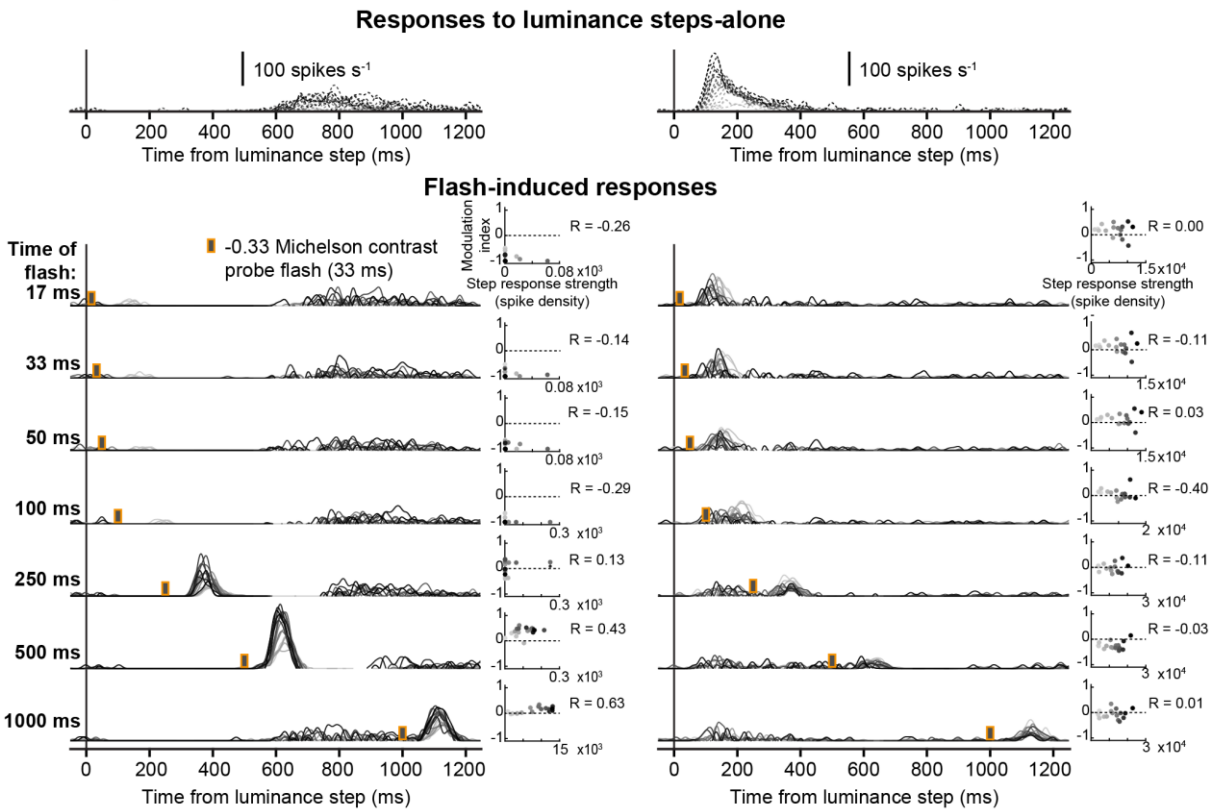


Figure S9 Example cells showing suppression of flash responses following luminance steps.

a. Average activity of an example ON RGC to positive-contrast (left column) and negative contrast (right column) luminance steps. Top row: luminance steps alone (dotted lines). Other rows: flash-induced responses (solid lines; different rows represent flashes presented with different delays), obtained by subtracting responses to the isolated luminance step from responses to the composite luminance step and bright flash stimulus. Responses to the different luminance step → flash sequences ($N = 56$ or 156 ; Fig. S1b) were first binned according to the contrast induced by the luminance step (17 bins; 0.05 to 0.5 absolute Michelson contrast range). Responses were then averaged within each bin, as shown here. Darker lines represent responses after stronger-contrast luminance steps. Orange bars indicate time of probe flash after the step (+0.33 Michelson contrast; 33 ms long). After positive-contrast luminance steps (left column), the RGC responded relatively strongly to flashes presented after weak luminance steps (lighter lines). However, responses to flashes presented 17-100 ms after strong luminance steps were suppressed, as indicated by the reduced amplitude or even absence of dark traces in these panels. The scatter plots towards the right show the dependency of flash-induced response modulation (y-axis; modulation index, Methods) on the luminance-step response strength (x-axis; Methods). In general, stronger positive-contrast luminance steps (darker circles) induced stronger responses to luminance-steps themselves (darker dots are further right), and also caused stronger suppression of flash-induced responses for flashes presented 17-250 ms after the step (darker dots are further down). This monotonic relation between flash response modulation index and luminance step response strength was quantified by calculating the Spearman correlation, R , which we refer to as the association index (AI). The larger its magnitude, the stronger is the monotonic relation between the two quantities. A negative AI value indicates a negative monotonic relation such that stronger luminance step responses are associated with decreasing (more negative) modulation indices (i.e. weaker flash responses → stronger suppression); a positive AI value indicates that stronger luminance step responses are associated with increasing modulation indices (i.e. stronger flash responses → less suppression or even enhancement). The example ON RGC showed no spiking responses to negative-contrast luminance steps (right column), and therefore the association index was undefined. Nonetheless, stronger-contrast luminance steps caused stronger suppression, noted by the absence of dark response lines for flashes presented up to 100 ms after the step.

b. Same as in **a**, but for an example OFF RGC where probe flashes were dark (-0.33 Michelson contrast). Dark flash responses were strongly suppressed after a positive-contrast luminance step (17-100 ms; left column), irrespective of the step contrast. Responses were enhanced around 500 ms with stronger contrasts inducing stronger enhancement (note the positive AI). Responses to flashes presented after a negative-contrast luminance step (right column) were not suppressed.

Figure S10

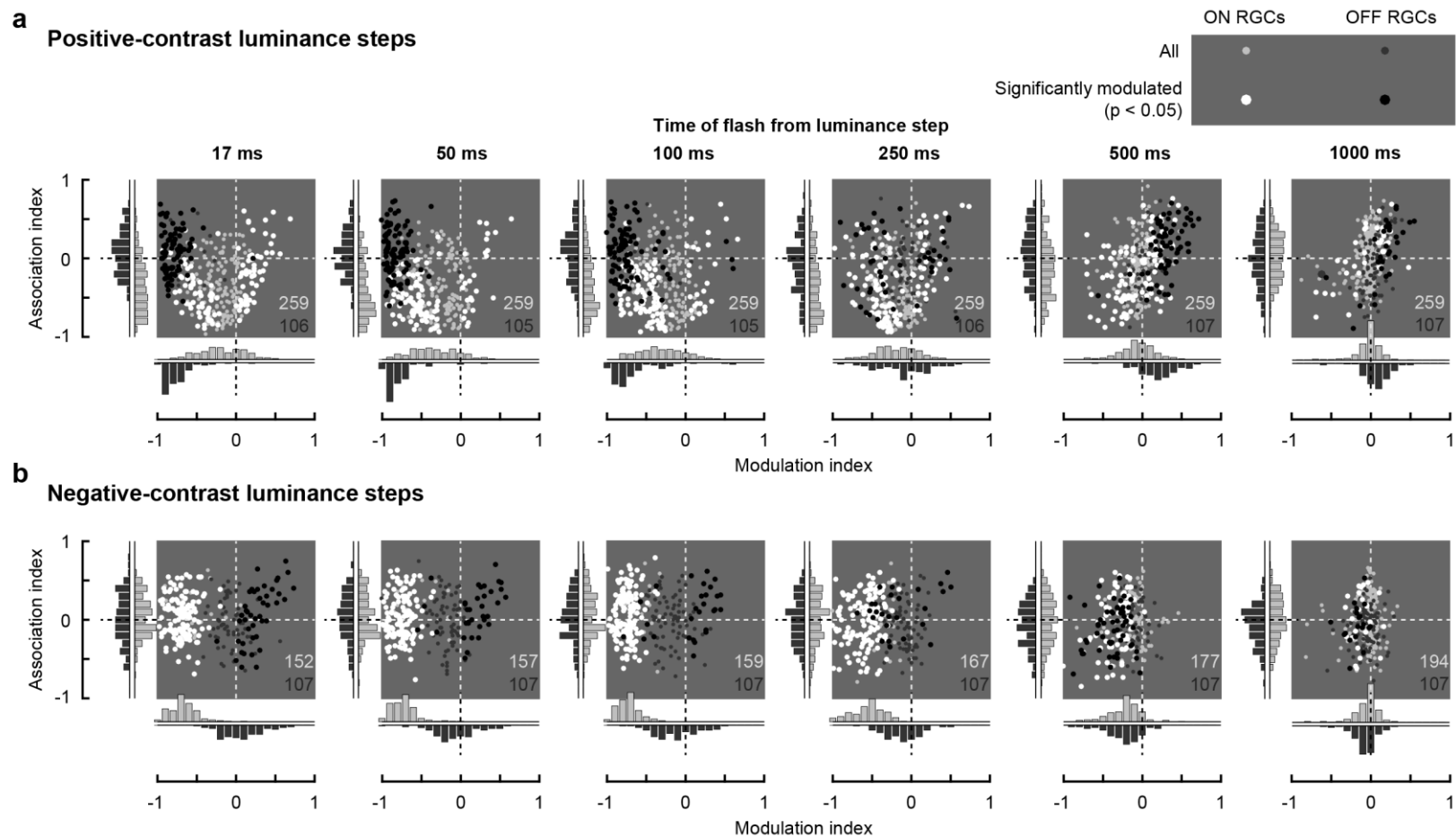


Figure S10 Indication of suppression through a saturation-like mechanism in ON RGCs. Scatter plots showing association index (AI, y-axis) of ON and OFF RGCs as a function of their modulation index (x-axis), at different flash times after positive-contrast (**a**) and negative-contrast luminance steps (**b**). See Legend of Fig. S9 and Methods for an explanation of the association index. These RGCs are a subset of cells in Fig. 4, S8. Light gray and dark gray circles are all ON and OFF RGCs respectively; white and black circles are

the significantly modulated ON and OFF RGCs ($p < 0.05$, one-tailed sign test) respectively. Dashed lines represent no modulation (vertical) and no association (horizontal). Distribution of the indices for all RGCs are projected onto the relevant x- and y-axes (light gray bars for ON RGCs and Dark gray bars for OFF RGCs). After a positive-contrast luminance step (**a**), many ON RGCs are suppressed (negative modulation index, although not as strongly as after a negative-contrast step) and have a negative association index (see example ON RGC in Fig. S9a). Such ON RGCs are located in the lower-left quadrants of the scatter plots in **a**. In these RGCs, suppression of flash responses increased monotonically (i.e. the modulation index decreased), with increasing response to the preceding luminance steps. This is consistent with an adaptation/saturation mechanism, where the response to a positive-contrast luminance step might strongly activate ON RGCs, so that the response to a subsequent probe flash would drive the cells into adaptation or saturation, effectively resulting in suppressed flash responses. Note that there are no OFF RGCs with similar properties, as, in general, they were not suppressed by negative-contrast luminance steps; they would occupy the lower left quadrant in the scatter plots in **b**.

Figure S11

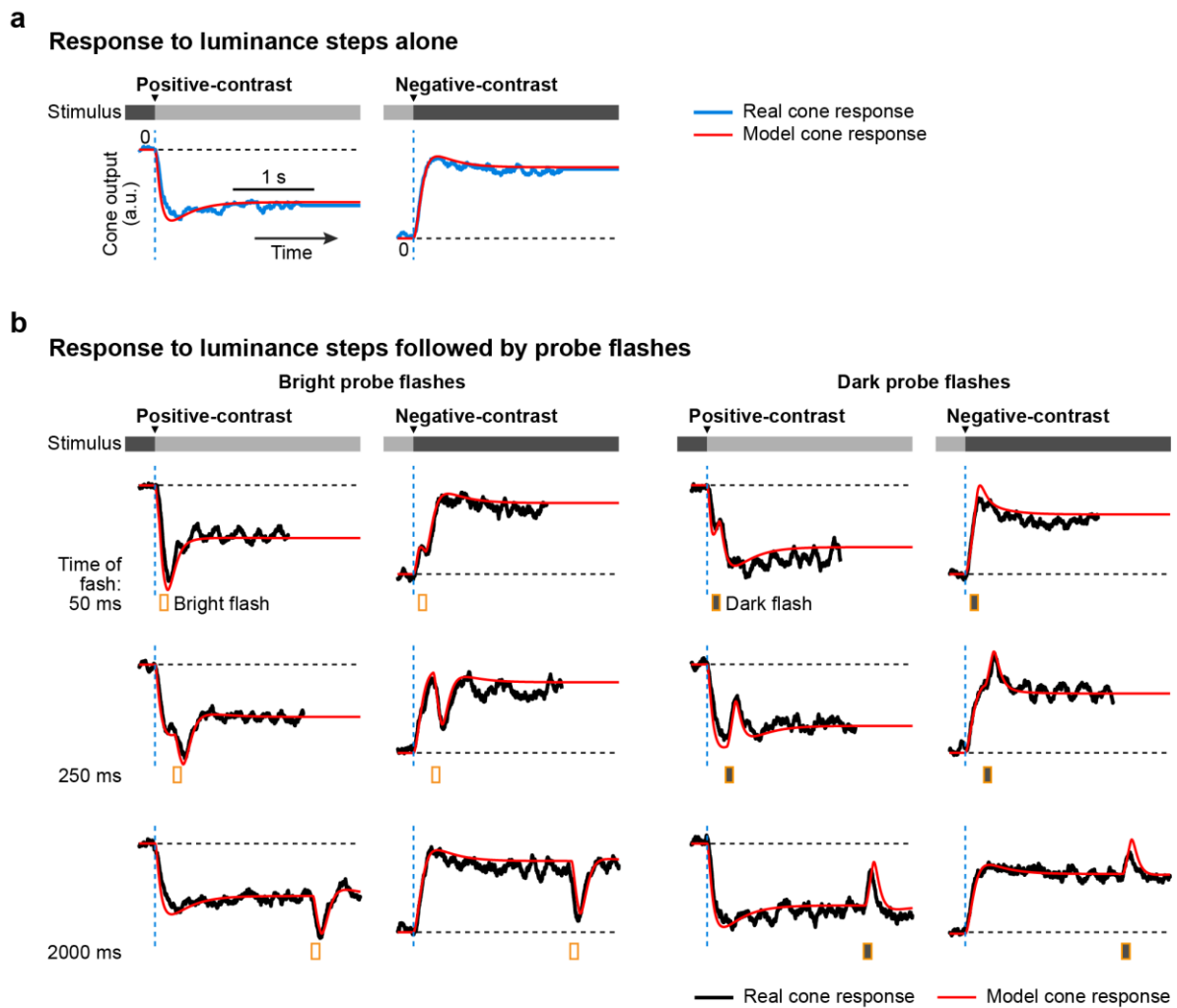


Figure S11 Model fit to cone responses of Fig. 5.

a,b. Cone responses to positive-contrast and negative-contrast (+0.4 and -0.4 on Michelson scale) luminance steps alone (**a**) and to luminance steps followed by probe flashes at 17, 250 and 2000 ms (**b**). Probe flashes were either bright or dark (+0.33 or -0.33 Michelson contrast respectively; 100 ms long). Orange markers show the timing of probe flashes. Real cone responses (blue/black; normalized $\Delta F/F$ of the iGluSnFR indicator signal; same as Fig. 5a-b) and model cone responses (red) are overlaid. Dashed blue lines: timing of luminance step; horizontal dashed line: cone level prior to the luminance step.

Figure S12

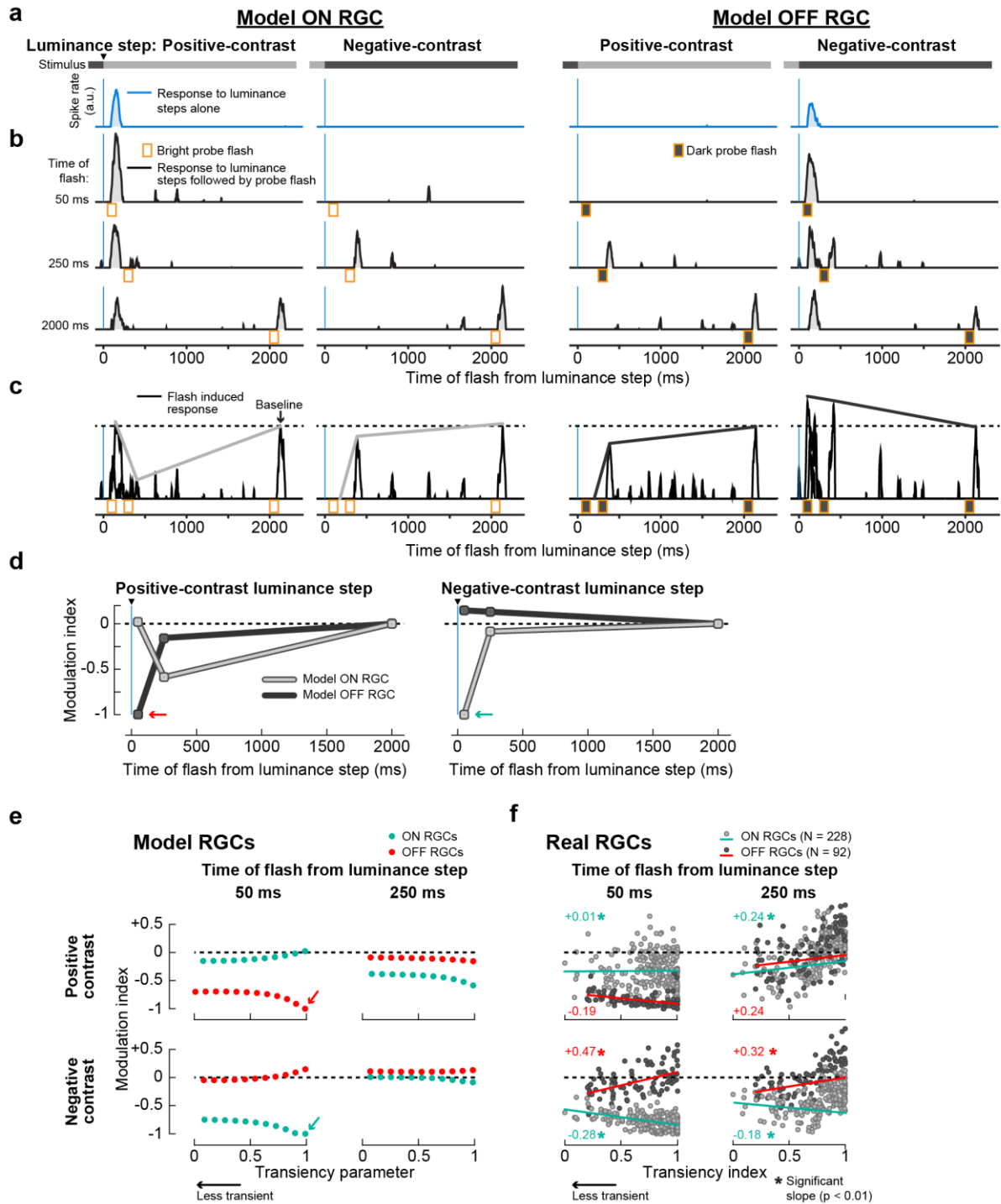


Figure S12 Model RGC responses based on real cone data of Fig. 5.

a,b. Spiking response of model ON (columns 1-2) and OFF (columns 3-4) RGCs to luminance steps alone (**a**, blue) and to luminance steps followed by probe flashes (**b**, black). First column in each cell type: responses following a positive-contrast luminance step; second column: responses following a negative-contrast luminance step. Instead of model cone output like in Fig. 6, we used acquired cone responses (Fig. 5) to RGC responses. Horizontal intensity bar below each trace illustrates the underlying visual stimuli. Vertical blue lines: timing of luminance step; orange bars: timing of probe flashes.

- c.** Flash-induced responses, after subtracting **a** from **b**, overlaid to show the modulation of probe flash responses at different times (analogous to real RGCs in Fig. 1d). Response to flash presented 50 ms after the step was strongly suppressed in ON RGC when presented after the negative-contrast step and strongly suppressed in OFF RGC when presented after the positive-contrast step, consistent with the cross-over style of suppression observed in real RGC data of Fig. 4, or in pure RGC models of Fig. 6.
- d.** Modulation indices for probe flashes in ON (light gray) and OFF model RGCs (dark gray), following negative-contrast (left panel) and positive-contrast (right panel) luminance steps. Cyan and red arrows highlight the suppression of opposite-contrast flashes at 50 ms in ON and OFF RGCs, respectively.
- e.** Modulation indices of model ON (cyan) and OFF (red) RGCs plotted as a function of RGC transiency. Individual panels correspond to different flash times (chosen from real-RGC recordings, Fig. 4) after positive-contrast (top row) and negative-contrast (bottom row) luminance steps. In **a-d**, transiency parameter was set to 1. Arrows highlight the same data as in **d**.
- f.** Replica of Fig. 6f but with relevant time points only. Modulation indices of real ON RGCs (light gray circles; $N = 228$; cyan line: linear regression fit) and OFF RGCs (dark gray circles; $N = 92$; red line: linear regression fit) plotted as a function of RGC transiency index (Methods). These RGCs are a subset of the population data shown in Fig. 4b for which we could compute a transiency index. Columns correspond to flashes presented at different times after positive-contrast (top row) and negative-contrast (bottom row) luminance steps. Suppression was stronger in more transient ON and OFF RGCs after negative- and positive-contrast steps respectively, indicated by the negative slope of the linear fits. Numbers in each panel indicate the slope of the fits and asterisk symbol indicates statistically significant slope (slope $\neq 0$, $p < 0.01$, two-tailed t-test).

Figure S13

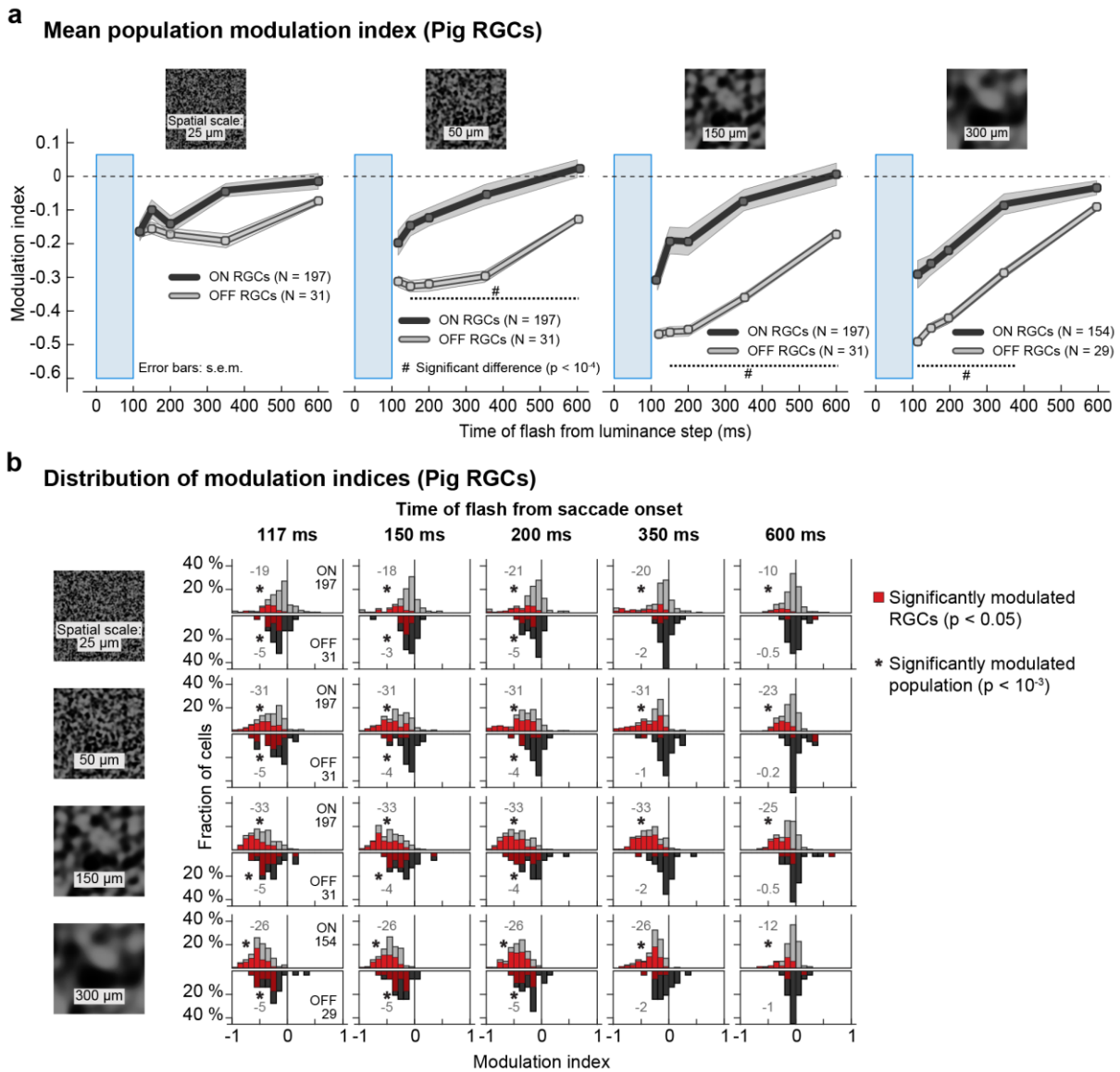


Figure S13 Saccadic suppression in pig retina.

a. Population modulation index (mean \pm s.e.m.) across ON (light gray) and OFF (dark gray) RGCs, for different spatial scales of the background texture (columns). OFF RGCs recovered from suppression by 350 ms whereas ON RGCs recovered by 1 s. Suppression in both ON and OFF RGCs increased with the spatial scale of the background texture. These observations were consistent with observations from mouse RGCs (Fig. 1e, S3). Blue windows: timing of saccades. Probe flashes were presented at 117, 150, 200, 350, 600, and 2100 (baseline) ms after saccade onset. Population modulation index was based on average across 197 ON and 31 OFF RGCs for spatial scales 25, 50, 150 μ m; and 154 ON and 29 OFF RGCs for 300 μ m. Hash symbols: significant difference in modulation between ON and OFF RGCs ($p < 10^{-4}$, two-tailed Wilcoxon rank-sum test).

b. Histograms of modulation index for all analyzed pig RGCs at different flash times relative to saccade onset (columns). Rows are for background textures with different spatial scales. Upright histograms (light gray bars) are for ON RGCs and inverted histograms (dark gray) are for OFF RGCs. Red bars highlight the RGCs with

modulation index significantly different from 0 ($p < 0.05$, one-tailed sign test). Black numbers in each panel of the first column indicate the number of RGCs analyzed for that background texture. Gray numbers on the left in each panel show the logarithm (base 10) of the exact p-value (two-tailed Wilcoxon signed-rank test) to determine if the population median was shifted away from 0. Additionally, the asterisks indicate the significance at $p < 0.001$.

Acknowledgements

I'm grateful to Thomas Münch, my doctoral advisor, who taught me how to be a good scientist and instilled in me research skills. I'm thankful for the many opportunities he provided and for letting me grow at my own pace. I'm also grateful to Ziad Hafed, my second advisor, who mentored and supported me as one of his own students. He was a great source of motivation and was always there to guide me.

I was lucky to have great colleagues who helped me integrate in the lab very quickly and supported me throughout the years. I'm especially thankful to Katja who taught me with great patience all the experimental techniques and for always being there to discuss my project. I'm also thankful to Hartwig and Marion for teaching me a lot of the lab work, helping me with my project, and supporting me till the end; Elli who not only helped me in the lab but took care of me as my lab mother; Boris for always backing up my shenanigans; Natalia and Anahit for making the lab environment lively. I'm also thankful to friends from the neighboring labs for their continuous support.

I'm thankful all those who directly contributed towards my thesis. Matthias-Philipp Baumann's contributions lifted the project significantly. Felix Franke provided great support and valuable feedback throughout the project, and trained me in computational modelling techniques. Timm Schubert and Katrin Franke were always there to discuss various aspects of the project.

I'm grateful to Anil Bharath, my master's supervisor, who introduced me to scientific research and in the first place encouraged me to pursue a doctorate.

Reaching this stage would not have been possible without the unconditional love and support of my family. My father's wisdom and my mother's love kept me balanced, during highs and lows. I'm also thankful to my sisters for their support, love and believing in me.

I'm grateful to Araceli. As a wife, her love and support gave me the strength I needed to reach the finish line. As a fellow scientist, the challenging discussions with her and her reviews of my scientific writings among many other things, have shaped me into a better scientist. I'm thankful to all my Tübingen friends, many of whom have now moved on. They made my time enjoyable; gave me the strength and helped me get by different phases throughout my PhD. They will always remain family to me. I'm also thankful to my long-distance old friends who have always been there in life for me, whenever I needed them.

In loving memory of Mubashir Niaz – a mentor and a friend, who realized my potential early on and encouraged me to pursue research.